Modeling, Experimentation, and Control of Autotrophic Nitrogen Removal in Granular Sludge Systems

Vangsgaard, Anna Katrine; Sin, Gürkan; Gernaey, Krist V.; Smets, Barth F.

Publication date:
2013

Document Version
Publisher's PDF, also known as Version of record

Modeling, Experimentation, and Control of Autotrophic Nitrogen Removal in Granular Sludge Systems

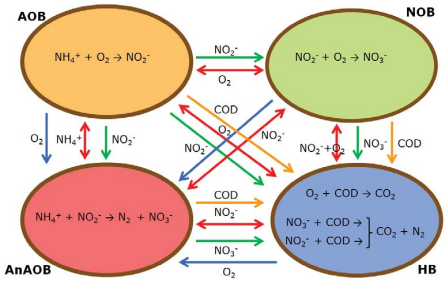

Anna Katrine Vangsgaard
Ph.D. Thesis
September 2013

DTU Chemical Engineering
Department of Chemical and Biochemical Engineering

Modeling, Experimentation, and Control of Autotrophic Nitrogen Removal in Granular Sludge Systems

Ph.D. Thesis

Anna Katrine Vangsgaard

September 2013

Computer Aided Process Engineering Center

Department of Chemical & Biochemical Engineering

Technical University of Denmark

Kongens Lyngby, Denmark

CAPEC

Address: Computer Aided Process Engineering Center
Department of Chemical and Biochemical Engineering
Technical University of Denmark
Building 229
DK-2800 Kgs. Lyngby
Denmark
Phone: +45 4525 2800
Fax: +45 4588 4588
Web: www.capec.kt.dtu.dk

Print: J&R Frydenberg A/S
København
October 2013

ISBN: 978-87-93054-12-7

Preface

This thesis is submitted as partial fulfillment of the requirements for the Doctor of Philosophy (Ph.D.) degree at the Technical University of Denmark (DTU). The work presented has been carried out at the Department of Chemical & Biochemical Engineering at the Computer Aided Process Engineering Center (CAPEC) and at the Department of Environmental Engineering from September 2010 to August 2013 under the guidance of Associate Professor Gürkan Sin as main supervisor as well as Professor Krist V. Gernaey and Professor Barth F. Smets (DTU Environment) as co-supervisors.

For financial support I thank the Danish Strategic Research Council for funding through the Centre for Design of Microbial Communities in Membrane Bioreactors (EcoDesign-MBR) (DSF no. 09-067230) and the Technical University of Denmark.

I have the pleasure to acknowledge numerous people who have contributed directly and indirectly to the development of this project:

I would like to start by expressing my special gratitude to my supervisors Gürkan Sin, Krist V. Gernaey and Barth F. Smets for their support, inspiring ideas, discussion and enthusiasm for the project.

I would also like to thank fellow Ph.D. student A. Gizem Mutlu for great collaboration and discussions in- and outside the lab. Without her, many obstacles would not have been overcome. I would also like to express my gratitude to researcher Miguel Mauricio-Iglesias who has supplied invaluable ideas, support, time, and discussions throughout my Ph.D. project. I thank the co-workers at DTU Environment. Especially thanks to Christina, Chen, Carlos, Carles, and Bent for help and assistance in the lab. Also many thanks to all of my co-workers in CAPEC, with whom I have had many great times, at and outside of DTU.

Finally, I would like to thank both my friends and my Danish, Italian, and Norwegian family for the great support they have given and the patience they have shown me during the last three years.

Kongens Lyngby, August 2013

Anna Katrine Vangsgaard

Abstract

Complete autotrophic nitrogen removal (CANR) is a novel process that can increase the treatment capacity for wastewaters containing high concentrations of nitrogen and low organic carbon to nitrogen ratios, through an increase of the volumetric removal rate by approximately five times. This process is convenient for treating anaerobic digester liquor, landfill leachate, or special industrial wastewaters, because costs related to the need for aeration and carbon addition are lowered by 60% and 100%, respectively, compared to conventional nitrification-denitrification treatment. Energy and capital costs can further be reduced by intensifying the process and performing it in a single reactor, where all processes take place simultaneously, e.g. in a granular sludge reactor, which was studied in this project. This process intensification means on the other hand an increased complexity from an operation and control perspective, due to the smaller number of actuators available.

In this work, an integrated modeling and experimental approach was used to improve the understanding of the process, and subsequently use this understanding to design novel control strategies, providing alternatives to the current ones available. First, simulation studies showed that the best removal efficiency was almost linearly dependent on the volumetric oxygen to nitrogen loading ratio. This finding among others, along with experimental results from start-up of lab-scale reactors, served as the basis for development of three single-loop control strategies, having oxygen supply as the actuator and removal efficiency as the controlled variable. These were investigated through simulations of an experimentally calibrated and validated model. A feedforward-feedback control strategy was found to be the most versatile towards the disturbances at the expense of slightly slower dynamic responses and additional complexity of the control structure. The functionality of this strategy was tested experimentally in a lab-scale reactor, where it showed the ability to reject disturbances in the incoming ammonium concentrations. However, during high ammonium loadings, when the capacity of the present sludge was reached, an oscillatory response was observed. Proper tuning of the controller is therefore of essential importance.

In this thesis, it was demonstrated that proactive use of model simulations, in an integrated methodology with experimentation, resulted in improved process understanding and novel control ideas. This will contribute to moving this promising technology from a case-by-case ad hoc approach to a more systematic knowledge based approach.

Resumé på dansk

Fuldstændig autotrof kvælstoffjernelse er en relativ ny proces, som kan øge behandlingskapaciteten for spildevand, der indeholder høje koncentrationer af kvælstof og lave mængder organisk kulstof i forhold til kvælstof. Denne proces er velegnet til behandling rejektvand fra rådnetank brugt i biogasanlæg, perkolat fra affaldsdeponier eller andre specielle typer af spildevand fra industrien, fordi omkostningerne forbundet med beluftning og tilførsel af ekstern kulstof bliver sænket med henholdsvis 60% og 100%, sammenlignet med den konventionelle behandling bestående af nitrifikation og denitrifikation. Energi- og kapitalomkostninger kan reduceres yderligere ved at intensivere processen og udføre den i en enkelt reaktor, hvor alle processer foregår samtidig. Et eksempel på en intensiveret proces er en bioreaktor med granulater, hvilket blev undersøgt i dette projekt. Denne procesintensivering betyder samtidig en øget kompleksitet med hensyn til drift og regulering, på grund af en reducering i antallet af reguleringshåndtag til rådighed.

I dette arbejde blev en integreret tilgang bestående af både modellering og eksperimentelle forsøg brugt til at forbedre forståelsen af processen. Efterfølgende blev denne forståelse brugt til at designe nye reguleringsstrategier, hvorved alternativer til de nuværende blev udarbejdet. Matematiske modelsimuleringer viste, at den bedste fjernelseseffektivitet er lineært afhængig af forholdet mellem ilt- og kvælstof*tilførslen*. Sammen med eksperimentelle erfaringer fra opstart af laboratorie-skala reaktorerne, tjente dette som grundlag for udviklingen af tre single-loop reguleringsstrategier, som har ilttilførsel gennem beluftning som aktuator og effektiviteten af kvælstoffjernelsen som reguleret variabel. Disse tre reguleringsstrategier blev grundigt testet igennem modelsimuleringer foretaget med en eksperimentelt kalibreret og valideret procesmodel. En feedforward-feedback strategi viste sig at være den mest alsidige mod forstyrrelser på bekostning af lidt langsommere dynamiske respons og en lidt mere kompleks reguleringsstruktur. Anvendeligheden af denne strategi blev testet eksperimentelt i en laboratorie-skala reaktor, hvor evnen til at afvise forstyrrelser i de indkommende ammoniumkoncentrationer blev bekræftet. Reaktorslammets maksimum kapacitet blev nået ved høje ammoniumbelastninger, hvilket resulterede i et oscillerende, ikke-stabilt respons. Korrekt justering af reguleringen er derfor af afgørende betydning.

Dette bidrag vil, igennem både modelsimuleringer og eksperimenter, hjælpe med til at tage anvendelsen af denne lovende teknologi i retning af en mere systematisk, videnbaseret, standard fuldskalaimplementering igennem de præsenterede resultater og de udviklede reguleringsstrategier.

Nomenclature

Abbreviations

AE	Algebraic equation
AnAOB	Anaerobic ammonium oxidizing bacteria (anammox bacteria)
ANR	Autotrophic nitrogen removal
AOB	Ammonium oxidizing bacteria
ASM	Activated sludge model
BNR	Biological nitrogen removal
BOD	Biological oxygen demand
BSM	Benchmark simulation model
CANON	Complete autotrophic nitrogen removal over nitrite
CANR	Complete autotrophic nitrogen removal
CFD	Computational fluid dynamics
COD	Chemical oxygen demand
CS	Control strategy
CSTR	Continuously stirred tank reactor
CV	Controlled variable
DO	Dissolved oxygen
EBPR	Enhanced biological phosphorus removal
EPS	Extracellular polymeric substance
ER	Exchange ratio
GAO	Glycogen accumulating organism
GHG	Green house gas
HB	Heterotrophic bacteria
HRT	Hydraulic retention time
IAE	Integral absolute error
IMC	Internal model control
ISE	Ion selective electrode
LHS	Latin hypercube sampling
MABR	Membrane aerated biofilm reactor
MBBR	Moving bed biofilm reactor
MBR	Membrane bioreactor
MC	Monte Carlo
MF	Membership function
MFC	Mass flow controller
MPC	Model predictive control
MTBL	Mass transfer boundary layer
MV	Manipulated variable
N	Nitrogen
NDF	Numerical differentiation formula
NOB	Nitrite oxidizing bacteria
ODE	Ordinary differential equation
OLAND	Oxygen-limited autotrophic nitrification-denitrification

ORP	Oxidation reduction potential
P	Proportional
PAO	Phosphor accumulating organism
PBM	Population balance model
PDE	Partial differential equation
PI	Proportional-integral
PSD	Particle size distribution
RBC	Rotating biological contactor
RMSE	Root-mean-square error
rpm	Rotations per minute
SBR	Sequencing batch reactor
SHARON	Single reactor system for high activity ammonium removal over nitrite
SNAP	Single-stage nitrogen removal using anammox and partial nitritation
SRC	Standardized regression coefficient
SRT	Sludge/solids retention time
SVI	Sludge volume index
TAN	Total ammonium nitrogen
TIC	Total inorganic carbon
TN	Total nitrogen
TNN	Total nitrite nitrogen
TSS	Total suspended solids
TV	Total variance
VSS	Volatile suspended solids
WSSE	Weighted sum of squared errors
WWT	Wastewater treatment
WWTP	Wastewater treatment plant

Symbols

A	Area
$A_{biofilm}$	Total biofilm area
b	Decay rate
C_i	Concentration of compound i
$D_{bio,i}$	Diffusivity of compound i in a biofilm matrix
D_i	Diffusivity of compound i in water
e	Error or offset
E_{Amm}	Ammonium removal efficiency
E_{Tot}	Total nitrogen removal efficiency – in percent
f	Ratio between biofilm and water diffusivities
f_i	Inert content in biomass
f_{redox}	Number of redox transitions within one SBR cycle
i_{NXB}	Nitrogen content in active biomass
i_{NXI}	Nitrogen content in inert biomass

j_i	Flux of compound i
J	Janus coefficient
K_C	Proportional controller gain
k_i	Mass transfer coefficient
k_H	Hydrolysis rate constant
k_La	Volumetric mass transfer coefficient
K_S / K_i	Affinity (half saturation)/inhibition constant
K_X	Hydrolysis half saturation constant
L	Biofilm thickness
L_B	Mass transfer boundary layer thickness
L_{NH4}	Volumetric ammonium loading
L_{O2}	Volumetric oxygen loading
M_i	Mass of compound i
n	Number of discretized points in biofilm, unless otherwise stated
n_{cal}	Number of experimental observations for calibration
n_{val}	Number of experimental observations for validation
Q	Flow rate
r_i	Reaction rate for compound i
r_{gran}	Radius of the granules
R_{AmmTot}	Ammonium removed over total nitrogen removed
R_{NitAmm}	Nitrite produced over ammonium removed
R_{NatTot}	Nitrate produced over total nitrogen removed
R_{on}	Fraction of an SBR cycle, which is being aerated
RO	Volumetric oxygen loading rate over ammonium loading rate
RT	Total nitrogen removal efficiency - fraction
S_i	Concentration of soluble compound i
t	Time
t_{aer}	Length of time that aeration is turned on during a cycle
t_{cycle}	Length of an SBR cycle
t_{off}	Length of a non-aerated phase
t_{on}	Length of an aerated phase
u_D	Biofilm detachment velocity
u_F	Biofilm growth velocity
u_L	Biofilm net growth velocity
V	Volume
$V_{reactor}$	Reactor volume
X_i	Concentration of particulate compound i
Y	Growth yield
y_{meas}	Observed output
y_{model}	Model output
y_{reg}	Linearly regressed model output
z	Radial distance
z_{max}	Maximum granule radius
Z^+	Background charge

Subscripts

bio	Occurring or present in the biofilm
bulk	Occurring or present in the bulk liquid
end	At the end of an SBR cycle
g	SBR cycle number
h	Process number
i	Compound i, unless otherwise stated
in	Influent entering the reactor
k	Location in biofilm
out	Effluent leaving the reactor
sat	Saturation concentration
sp	Set point
start	At the beginning of an SBR cycle
∞	Steady state value

Greek symbols

β	Standardized regression coefficient
φ	Non-settled fraction of free cells in bulk liquid
η_{HB}	Anoxic inactivation coefficient
θ	Parameter value or biofilm porosity
μ	Mean value
μ_{max}	Maximum specific growth rate
ρ	Biomass density
ρ_h	Process rate of process h
σ	Standard deviation
τ_C	Closed loop time constant
τ_I	Integral time
ν	Stoichiometric coefficient
υ_s	Superficial gas velocity

Contents

PART I – Introduction, Experimentation, and Modeling

In part I, the topic of autotrophic nitrogen removal is introduced from a general perspective along with an introduction to the tools used to investigate and achieve these goals. The issues and challenges associated to the development and application of such a technology, and the specific objectives of this PhD thesis are presented along with a general introduction to the subject in chapter 1, followed by an introduction to the experimental laboratory setup along with a description of all experimental methods and analyses used (chapter 2). Then, a detailed description of the model and the methodology used for its construction and derivation is given in chapter 3.

1 Introduction

Water is an essential resource to sustain life. With the growing population and rise in population density, the importance of managing water resources properly, by among others, ensuring clean water, is rapidly increasing. Along with intensive farming and the development of artificial fertilizer production, nitrogen pollution has been observed in increasing amounts in rivers, lakes, oceans, and ground water aquifers over the last couple of decades. The legislation – e.g. in Europe, the Water Framework Directive (Directive 2000/60/EC) – therefore requires removal or conversion of certain compounds that are present in wastewater as a consequence of anthropogenic activity. These include organic compounds containing carbon (C), but also nutrients such as, nitrogen (N), and phosphorus (P), which cause eutrophication of receiving water bodies, and micropollutants, such as heavy metals, pharmaceuticals, and other xenobiotic compounds, which are of increasing concern as a risk towards human health and the natural ecosystem.

Nitrogen is one of the most critical pollutants, because it can be found in significant quantities in most types of wastewater, it causes eutrophication, and especially nitrate and nitrite are toxic toward most invertebrates and vertebrates in high concentrations. Nitrogen can therefore pose a threat to the health status of the natural ecosystem and the drinking water quality if it reaches aquifers or other water bodies used as drinking water sources. A number of treatment methods for nutrient removal has been developed and applied in wastewater treatment (WWT). Especially biological treatment processes were developed in the 1970s and 1980s, with the development of the bio-N and the bio-P processes (Tchobanoglous et al., 2003). In Denmark, many wastewater treatment plants (WWTPs) started to employ biological nutrient removal in the late 1970s and early 1980s by means of the BIO-DENITRO and the BIO-DENIPHO processes (Henze Christensen, 1975; Bundgaard et al., 1989).

Lately, climate change and its causes and consequences have been given major attention, and thus focus has been on reduction of energy consumption and greenhouse gas production. Also within wastewater treatment technology there is a call for energy efficiency and lowering of greenhouse gas production. A significant cost in conventional wastewater treatment is the cost of aeration, in particular the energy used in supplying sufficient air, either through surface aeration equipments or by using compressors to supply air through bubble diffusers. Up to 50% of the total electricity consumption of an entire WWTP employing biological nitrogen removal is due to aeration (Ingildsen et al., 2002). By combining partial nitrification with the relatively

newly discovered anaerobic ammonium oxidation process, complete autotrophic nitrogen removal (CANR) can be obtained, which has proven to be a low cost and energy efficient way of treating wastewater with high nitrogen concentrations and low organic carbon to nitrogen ratios. Examples of such wastewaters are the side-stream wastewater produced after dewatering of digested waste sludge, landfill leachate or special industrial wastewaters.

Although this is a promising technology, it has shown to be difficult to operate in a stable manner in pilot- and full-scale plants (Joss et al., 2011). A more detailed understanding of its complex nature, and the development of effective control and operational strategies for stable operation, is therefore needed to realize the full potential and facilitate successful transfer of this promising technology to industrial practice.

1.1 Autotrophic nitrogen removal - what, why, and where?

1.1.1 What is autotrophic nitrogen removal?

Nitrification

Nitrogen appears in wastewater in reduced form, either as ammonium (NH_4^+) or organically bound nitrogen (Tchobanoglous et al., 2003). Traditionally, nitrogen removal consists of nitrification, which is most often followed by the denitrification process (Figure 1.1 and 1.2).

Nitrification is an autotrophic process, which means that carbon for cell synthesis is acquired from inorganic compounds. The process is conducted in two steps. First, ammonium is converted to nitrite (eq. 1.1) over hydroxylamine (NH_2OH) by ammonium oxidizing bacteria (AOB), which mainly belong to the bacterial species *Nitrosomonas* (Jetten et al., 2001). Oxidation of ammonium to nitrite uses approximately 1.5 mole O_2 as electron acceptor per mole ammonium, which is converted. The process is also termed partial nitrification or nitritation. Nitritation is followed by nitratation, in which nitrite is oxidized to nitrate (NO_3^-) (eq. 1.2) by nitrite oxidizing bacteria (NOB), which often belong to the bacterial species *Nitrobacter* or *Nitrospira* (Downing and Nerenberg, 2008). In this process oxygen is also used as electron acceptor, however here approximately 0.5 mole of O_2 is used to oxidize 1 mole of nitrite to

nitrate. The simplified (1.1-1.2) and complete (1.3-1.4) reaction stoichiometries involved in the two processes conducted by AOB and NOB are presented below:

$$NH_4^+ + 1.5\ O_2 \rightarrow NO_2^- + 2\ H^+ + H_2O \quad (1.1)$$

$$NO_2^- + 0.5\ O_2 \rightarrow NO_3^- \quad (1.2)$$

$$NH_4^+ + 1.382\ O_2 + 1.982\ HCO_3^- \rightarrow$$
$$0.982\ NO_2^- + 0.018\ C_5H_7NO_2 + 1.891\ H_2CO_3 + 1.036\ H_2O \quad (1.3)$$

$$NO_2^-\ 0.0051\ NH_4^+ + 0.473\ O_2 + 0.0051\ HCO_3^- + 0.0204\ H_2CO_3 \rightarrow$$
$$NO_3^- + 0.0051\ C_5H_8NO_2 + 0.0123\ H_2O \quad (1.4)$$

In a WWTP, biological nitrification takes place in aerated activated sludge tanks (indicated in Figure 1.2B).

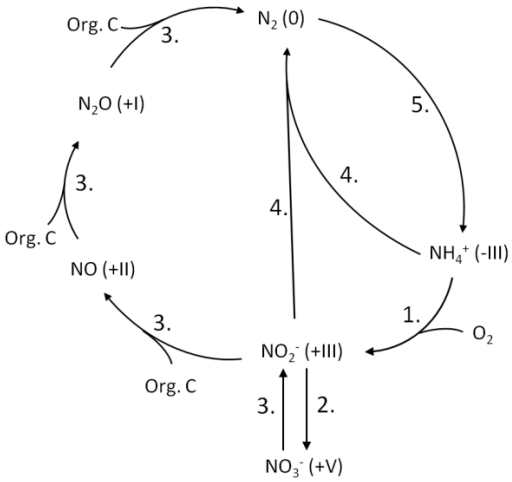

Figure 1.1 The inorganic nitrogen cycle. 1. Nitritation, 2. Nitratation, 3. Denitrification, 4. Anammox, 5. N fixation. The numbers in between the parentheses behind the compounds indicate the oxidation state of the nitrogen atom.

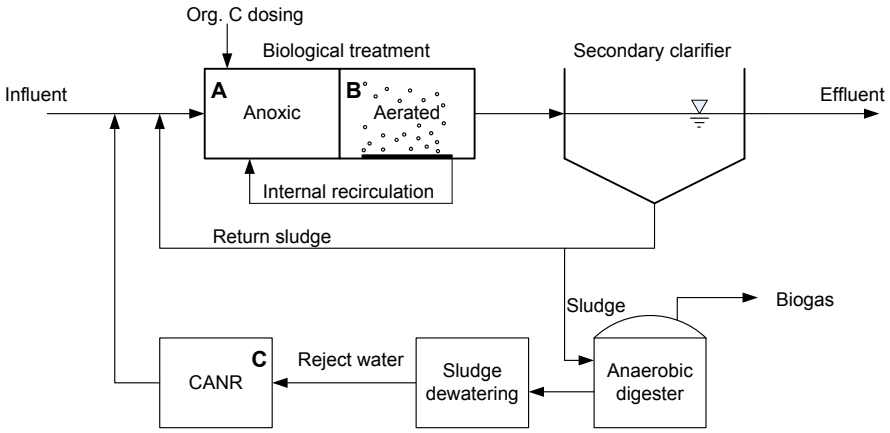

Figure 1.2 Schematic diagram of a typical wastewater treatment plant (WWTP) with biological nitrogen removal (BNR), sludge digestion, and side-stream treatment. A) Anoxic denitrification tank, B) Aerobic nitrification tank, and C) CANR of the sludge digester liquor.

The rates, at which AOB and NOB convert nitrogen, are influenced by many different environmental factors. Manipulation of these factors has been sought to control the relative abundance of the microbial groups in a mixed culture community. Temperature, hydraulic retention time (HRT), sludge retention time (SRT), pH and alkalinity, inhibiting compounds, and substrate concentrations are among the most important factors (Gujer, 2010).

The HRT control concept uses the fact that at high temperatures (above 15-20^{o}C) AOB have a higher specific growth rate than NOB, whereas the opposite is true at low temperatures (Hellinga et al., 1998). The difference in specific growth rates can be utilized by choosing a sufficiently low SRT to wash out NOB from the system, while retaining AOB in the system (Pollice et al., 2002). This can relatively easily be done in continuously operated suspended sludge systems, where there is no biomass retention and the SRT is equal to the HRT. However this strategy becomes more difficult to administer in attached growth, sedimentation, or membrane based systems in which solids, and thus the bacteria, are retained to a higher degree in the system.

pH directly affects nitrification as it determines the relative distribution of the nitrogen species' concentrations in the medium due to chemical acid-base equilibria. In addition, the nitrification process itself affects the pH of the medium, because protons are produced when ammonium is oxidized to nitrite (eq. 1.1). The speciation of the true substrates of the nitrogen compounds for AOB and NOB has been a point of discussion for a while, with Anthonisen et al. (1976) proposing

the unionized forms (ammonia (NH_3) and nitrous acid (HNO_2)) as the true substrates. pH can also affect the concentration of inhibiting compounds. Many different concentrations have been reported, and the speciation is also important in case of substrate or product inhibition (Anthonisen et al. 1976; Wiesmann, 1994).

Another important factor affecting nitrification is the dissolved oxygen (DO) concentration. Even though many different values, within a significant range of variation, have been reported for the oxygen half saturation constants for both AOB and NOB (Wiesmann, 1994; Brockmann et al., 2008; Lackner and Smets, 2012), there is a general trend that the half saturation constant of AOB is lower compared to that of NOB. This means that at low DO concentrations, AOB will have a competitive advantage over NOB. As a consequence many studies (Picioreanu et al., 1997; Bernet et al., 2001; Chen et al., 2001; Downing and Nerenberg, 2008; Pambrun et al., 2008 to name a few) have focused on controlling the DO concentration as a tool for obtaining partial nitrification (i.e. nitritation without nitratation or nitrite accumulation).

Denitrification

In conventional treatment systems, the nitrification is typically followed by denitrification, where nitrate is reduced eventually to nitrogen gas (N_2) by heterotrophic bacteria (HB) (see Figure 1.1). The process occurs under anoxic conditions and with organic carbon as electron donor. This process takes place in multiple steps with several intermediates (eq. 1.5). A broad range of HB exists, some of which have the ability to completely reduce nitrate to nitrogen gas, whereas others are specialized in a specific step of the process.

$$NO_3^- \rightarrow NO_2^- \rightarrow NO \rightarrow N_2O \rightarrow N_2 \qquad (1.5)$$

Different configurations of nitrification-denitrification can be implemented in the biological treatment train at a WWTP. One common configuration is an anoxic tank followed by an aerated tank with an internal recirculation stream carrying nitrate from the aerobic tank back to the anoxic tank, where the nitrate is denitrified (see Figure 1.2A+B).

Depending on the wastewater composition, it might be necessary to supply external organic carbon to the anoxic stage in order to ensure complete denitrification (Tchobanoglous et al., 2003).

A detailed understanding of the denitrification mechanism, the substrate preference and competition, and the bacteria involved remains somewhat unclear due to the complexity of the

process (Sin et al., 2008c). Since heterotrophic activity is not the focus of this study, the reader is referred to the reviews of Peng and Zhu (2006) and Sin et al. (2008c) for discussion of the status of the understanding, operation, and control of this process.

Anaerobic ammonium oxidation (Anammox)

In the anammox process, ammonium is oxidized by using nitrite as electron acceptor, to form nitrogen gas and a bit of nitrate. This process is performed by anaerobic ammonium oxidizing bacteria (AnAOB). A simplified (1.6) and a complete (1.7) version of the process stoichiometry is given below:

$$NH_4^+ + NO_2^- \rightarrow N_2 + 2\ H_2O \quad (1.6)$$

$$NH_4^+ + 1.124\ NO_2^-\ 0.014\ HCO_3^- + 0.121\ H_2CO_3 \rightarrow$$
$$0.987\ N_2 + 0.138\ NO_3^- + 0.270\ C_5H_8N_{0.5}O_2 + 2.185\ H_2O \quad (1.7)$$

As can be seen in equation 1.7, in practice, the stoichiometry of ammonium to nitrite is 1 to 1.12. Most of the nitrogen is converted to N_2, but about 6-7% of the converted nitrogen can be found as nitrate, and the rest is incorporated in new biomass that is produced during growth.

The possible existence of AnAOB was first mentioned in the article “Two lithotrophs missing in nature” (Broda, 1977), but was not proved existing until the 1990s (Mulder et al., 1995; van de Graaf et al., 1995). Most of the identified AnAOB belong to the bacterial division *Planctomycetales* (Kuenen, 2008). AnAOB have a characteristic bright red color, which is related to their high production of cytochrome C (Jetten et al., 1999). Since the discovery of the AnAOB, almost two decades ago, they have been found to be present in many WWTPs around the world and in natural redox-stratified ecosystems, such as in sea sediments. It is estimated that up to 35% of the natural nitrogen turnover in the marine environment is through the anammox process (Dalsgaard et al., 2003). Thus, this process is of great significance both in engineered systems, as well as in the natural nitrogen cycle.

AnAOB are extremely slow growing with a doubling time of approximately 11 days (Strous et al., 1998). They are very sensitive toward certain compounds and are inhibited by oxygen and nitrite (Strous et al., 1999). Since the process is catalyzed by an obligate anoxic microorganism, oxygen has an inhibiting effect on AnAOB already at a concentration of 0.2 mg O_2 L^{-1} (Jung et al., 2007). However, it has been found that AnAOB can recover their activity after exposure to low oxygen

concentrations (Strous et al., 1997; Egli et al., 2001), thus the inhibition is probably somewhat reversible.

Complete autotrophic nitrogen removal (CANR) is the combination of aerobic (eq. 1.1) and anaerobic (eq. 1.6) ammonium oxidation (see eq. 1.8), and can therefore be described by the simplified version below:

$$2NH_4^+ + 1.5O_2 \rightarrow N_2 + 2H^+ + 3H_2O \quad (1.8)$$

1.1.2 Why use complete autotrophic nitrogen removal?

As the name gives away, the CANR process is completely autotrophic, which means that the microorganisms assimilate inorganic compounds as their carbon source. Since only 53% of the influent ammonium has to be converted to nitrite to obtain CANR, the oxygen requirement is 1.83 g O_2 (g N)$^{-1}$ as opposed to 4.30 g O_2 (g N)$^{-1}$, which is required for complete nitrification (see Table 1.1). The organic carbon requirement, measured as chemical oxygen demand (COD), for N removal is 8.67 g COD (g N removed)$^{-1}$ in complete nitrification-denitrification, whereas it is 0 g COD (g N removed)$^{-1}$ in CANR. This is an advantage, because organic carbon, e.g. in the form of methanol, often is added in conventional treatment to reach complete denitrification of nitrate (Tchobanoglous et al., 2003), and thus comprises an extra operational cost. Also the sludge production is reduced significantly from 4.27 g biosolids (g N removed)$^{-1}$ in the nitrification-denitrification process to 0.14 g biosolids (g N removed)$^{-1}$ in CANR. This is due to the relatively low biomass yield of the AOB and AnAOB (Strous et al., 1999) compared to the yield of heterotrophic denitrifiers (Henze et al., 2000). As can be seen in Table 1.1, the shortcut nitrification-denitrification is superior to complete nitrification-denitrification with respect to oxygen consumption, organic carbon requirement, and sludge production. However, the CANR is still significantly more efficient than the short-cut pathway.

Table 1.1 Comparison of substrate requirements and sludge production for conventional nitrification-denitrification, shortcut nitrification-denitrification, and CANR, when considering the stoichiometries given in eq.s1.3, 1.4, and 1.7.

	Complete nitrification - denitrification	**Shortcut nitrification - denitrification**	**Complete autotrophic N removal**
Oxygen requirement (g O_2/g N)	4.30	3.22	1.83
Org. carbon requirement (g COD/g N)	8.67	5.18	0.00
Sludge production (g VSS/g N)	4.27	2.59	0.14

In mixed culture systems, such as biological WWT systems, other bacterial groups are competing with the ammonium oxidizers. In particular, NOB, which are competing with AOB for oxygen and with AnAOB for nitrite. HB, utilizing organic compounds originating from decay processes, can also be competing for oxygen with AOB and NOB, and for nitrite with AnAOB, but can also use nitrate as electron acceptor. Finally, AOB and AnAOB can compete with each other for ammonium (see Figure 1.3).

To add to the complexity, there are also some microbial groups that utilize substrates that are inhibiting for others, while some are growing on decay products originating from other microbial groups. A complicated network of interactions thus exists within the nitrogen converting microbial community (Figure 1.3).

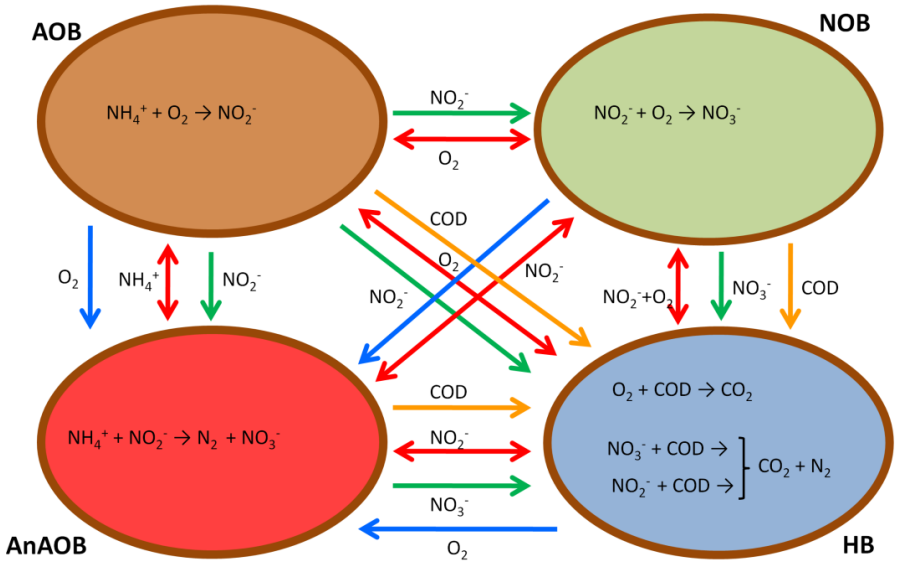

Figure 1.3 Interactions between microbial groups involved in N conversion in WWT. Green arrows: substrate dependency, red arrows: substrate competition, blue arrows: inhibition removal, orange arrows: decay products used as substrates.

1.1.3 Where to use CANR?

As CANR is a very suited process to treat wastewater streams with high nitrogen concentrations and low C/N ratios, it is mainly employed in side-stream treatment, such as for example treatment of reject water from sludge digestion (Figure 1.2C). Currently, efforts are being put

into expanding the application to main-stream municipal wastewater treatment as well (Hu et al., 2013).

Since CANR consists of processes carried out by two different microbial groups (AOB and AnAOB), it can be realized either in a two-stage system, where the two processes take place in separate reactors, or in a single-stage system where the reactor contains both organisms (see Figure 1.4). In the two-stage configuration, the optimal substrate concentration ratio for the anammox process (1 NH_4^+:1.12 NO_2^-) is obtained by partial aerobic ammonium oxidation in a reactor separated from the anammox process reactor. The single-stage configuration can only be realized if different oxic (both aerobic and anoxic) conditions can be obtained within the same reactor, e.g. by having a redox stratification governed by biofilm or granule formation of the bacteria (see Figure 1.5). Alternatively, the oxic conditions can be time-segregated, e.g. through intermittent or periodic aeration.

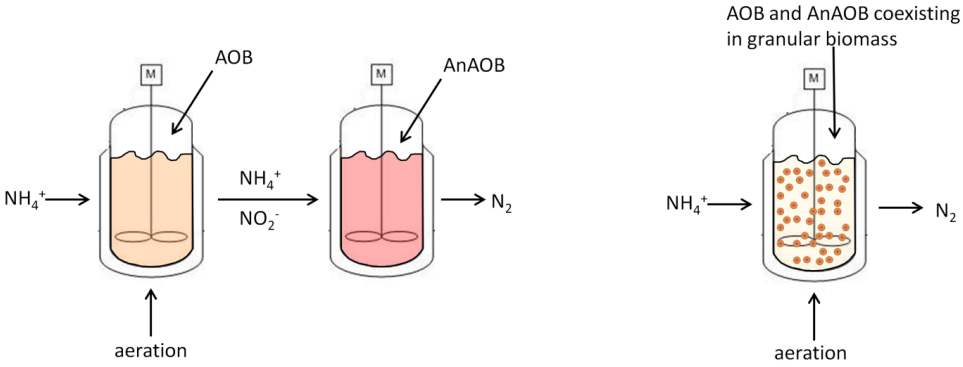

Figure 1.4 Reactor configurations. Left: Two-stage configuration, right: example of a single-stage configuration.

The first full-scale implementation of CANR was the SHARON-Anammox two-stage process (van Dongen et al., 2001; van Kempen et al., 2001), which was started up during 2002-2004 (van der Star et al., 2007). In the SHARON (Single reactor High activity Ammonia Removal over Nitrite) process, nitrite is produced from ammonium. Partial nitrification is assured by running the process at high temperature and low SRT. The reactor is configured as a chemostat, which is a continuously stirred tank reactor (CSTR) with no biomass retention, and the SRT is thus equal to the HRT. When the SHARON process was first developed, it was used to treat reject water from an anaerobic sludge digester to a degree where it could be recycled back into the main wastewater stream to be conventionally treated by denitrification (Hellinga et al., 1998). As the anaerobic digester effluent usually contains high concentrations of ammonium and low

biodegradable organic carbon concentrations, nitrogen removal was obtained by converting most of the ammonium to nitrite and subsequently reducing it to nitrogen gas by addition of methanol for denitrification. However, it was later discovered that the effluent from the SHARON process makes up a good influent composition for the anammox process (van Dongen et al., 2001).

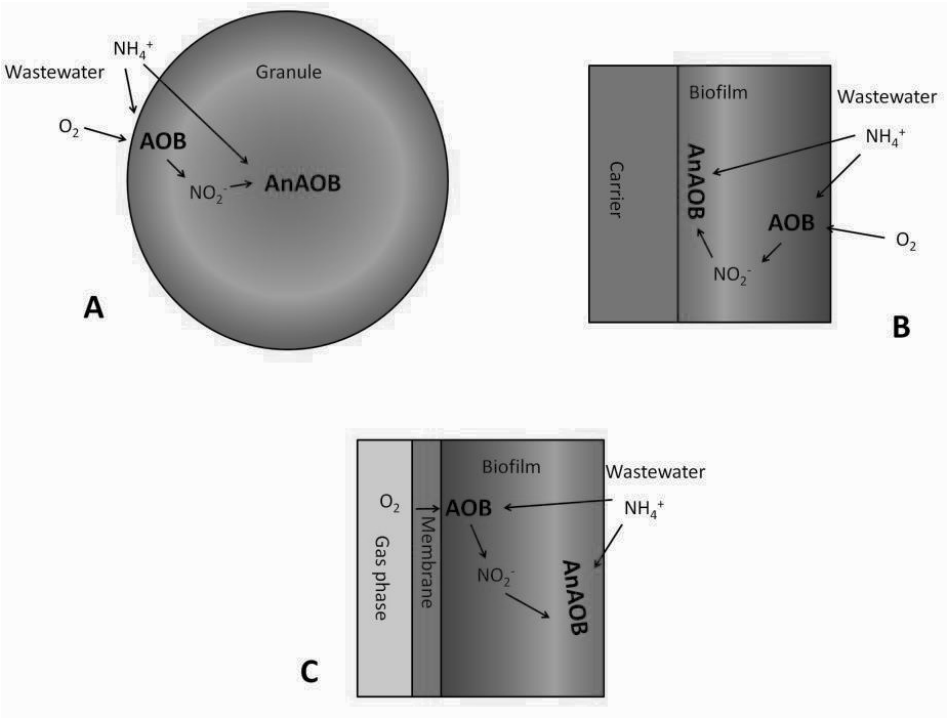

Figure 1.5 Idealized spatial location of bacterial groups in different single-stage biofilm systems. A) Granular biomass, B) Carrier based biofilm system, C) MABR system.

Among the first reported successful single-stage process was the OLAND (Oxygen-Limited Autotrophic Nitrification-Denitrification) process (Kuai and Verstraete, 1998). Since then, several single-stage configurations have been introduced, among them the CANON (Completely Autotrophic Nitrogen-removal Over Nitrite) process (Third et al., 2001; Sliekers et al., 2002), the SNAP (Single-stage Nitrogen removal using Anammox and Partial nitritation) process (Furukawa et al., 2006), where the biomass is immobilized onto acryl fiber material in a fixed film configuration (Figure 1.5B), in moving bed biofilm reactors (MBBRs), where the biomass is attached onto specially designed plastic carriers (Helmer et al., 2001), e.g. the ANITAMox

process (Christensson et al., 2011) (Figure 1.5B), in membrane aerated biofilm reactor (MABR) systems, where the membrane acts as both substratum for the biofilm and oxygen supply source (Figure 1.5C) (Pellicer-Nacher et al., 2010), in a rotating biological contactor (RBC) (Siegrist et al., 1998; Pynaert et al., 2003), where the biomass is immobilized onto rotating discs, which are alternating in contact with the bulk liquid and the oxygen containing atmosphere (Figure 1.5B), or in an sequencing batch reactor (SBR) (Strous et al., 1998) with sludge or granules (Figure 1.5A) containing both microbial groups, e.g. the DEMON® process (Wett, 2006) or as in the study by Vlaeminck et al. (2009), where detailed microbial analysis was made.

The obvious advantage of the single-stage configuration, over the two-stage configuration, is that it has a lower reactor footprint and a lower capital cost. Also, operational costs are lower, because only one reactor, and its associated equipment, instead of two, has to be maintained. By having two bacterial communities within one reactor, AOB-produced nitrite can be utilized immediately by AnAOB, whereby nitrite build-up and inhibitions associated with it, are avoided. However, operating the system in such a way, that optimal conditions for both the aerobic partial nitritation and for the anaerobic anammox process are ensured, is easier in the two-stage system, since both reactors can be controlled independently of each other. Higher removal rates can therefore likely be obtained in a two-stage configuration than in the single-stage.

Currently, approximately 40 full-scale CANR implementations are operated for the treatment of a range of different types of nitrogen-rich wastewaters (Hu et al., 2013) and the number is constantly growing. The majority of these are single-stage implementations (Vlaeminck et al., 2012), and it seems that the industry believes this to be the best suited solution for their needs.

1.2 Mathematical modeling of biological WWT

Mathematical models can serve as useful tools to help understand and elucidate governing mechanisms and interactions in process systems, such as wastewater treatment plants. Also, they can help to improve and reduce the time needed for plant and reactor design, controller construction, and process optimization. Moreover, they can be used to evaluate alternative options of plant or reactor layouts and operational strategies for a smaller cost than experimental testing.

In order to facilitate and enhance the model construction and use in biological wastewater treatment, the IAWPRC (now IWA) formed a task group dedicated to provide a modeling

platform in 1983. The model developed by a South African research group (Dold et al., 1980) served as their starting point. The task group's work resulted in a model for a single-sludge treatment system performing COD oxidation, nitrification, and denitrification (Grady et al., 1986). The model was evaluated and revised later by Henze et al. (1987) resulting in the first version of the activated sludge model no. 1 (ASM1). The model is based on a mechanistic interpretation of the behavior of the microbial groups catalyzing the process reactions considered in the system, as well as detailed characterization of influent wastewater composition with respect to different fractions of COD and nitrogen. The task group later on expanded the ASM1 by incorporating additional phenomena and concepts. This resulted in the ASM2d, which contains enhanced biological phosphorus removal (EBPR) combined with denitrification (Henze et al., 1999) and the ASM3, which includes the concept of internal compound storage by the heterotrophs (Gujer et al., 1999). Since then, numerous activated sludge models have been developed and evaluated, addressing different levels of detail, such as the two step nitrification and denitrification, metabolic models for phosphorus accumulating organisms (PAOs) and glycogen accumulating organisms (GAOs), and biofilm models, to mention a few. This prompted Gujer (2006) to declare a moratorium on model development activity and urge the community to rather start using and applying the models than further develop new ones, yet the development has been and still is continuing.

Below, further introduction to biofilm modeling and modeling of CANR is presented.

1.2.1 Mathematical modeling of biofilm systems

The difference between the activated sludge type models and biofilm models is that space is introduced as an independent variable in biofilm models, and gradients of substrate concentrations and often gradients within the microbial compositions are considered in biofilm systems. This entails that mass transfer phenomena are accounted for explicitly in biofilm models. The microbial kinetic parameter (e.g. half saturation constant) values in biofilm models are thus only describing the microbial metabolism, and not accounting for the effects of mass transfer limitation, which they otherwise do in traditional activated sludge models.

The first biofilm models were describing a steady-state, one-dimensional (1-D), flat-sheet geometry with a uniform distribution of a single microbial species and a single substrate and were focusing on the substrate flux and concentration profile (Rittmann and McCarty, 1980). Since then, the model complexity has increased such that the palette of biofilm models now

contains: dynamic, multi-species and multi-substrate models (Wanner and Gujer, 1986), multi-dimensional models (Picioreanu et al., 1998) describing the structure and morphology of the biofilms, individual based models (Kreft et al., 2001; Lardon et al., 2011) in which individual cells are considered, and hybrid models (Alpkvist et al., 2006), where the extracellular polymeric substance (EPS) matrix and individual cells are modeled. The increase in model complexity goes hand in hand with the increase in available tools for experimental observation of the biofilms (Wanner et al., 2006) such as *in situ* hybridization techniques, microsensors, and advanced microscopy such as confocal laser scanning microscopy, as well as with the increase in available computational power.

1.2.2 Mathematical modeling of CANR systems

Modeling of CANR can be done either as modeling of two separate processes in a two-stage configuration (nitrification and anammox) or as a simultaneous process, which is carried out by means of multi-species biofilm models.

Two-stage CANR modeling

For the first approach, many studies have modeled two-step nitrification and investigated how to stimulate and achieve partial nitrification, i.e. promote AOB growth and suppress NOB growth. Picioreanu et al. (1997) investigated the effect of oxygen concentration in a nitrifying biofilm reactor, Hellinga et al. (1999) modeled a SHARON reactor for process design calculations at a full-scale plant, Wyffels et al. (2004) and Pambrun et al. (2006) modeled nitrification in a membrane bioreactor (MBR) and in an SBR, respectively, both with the objective of obtaining optimal operational conditions for partial nitrification, while Bernet et al. (2005) constructed a steady-state biofilm model with homogenous AOB and NOB distribution in order to design a control system ensuring nitrite accumulation.

The study of Dapena-Mora et al. (2004) modeled an anaerobic SBR by extending the ASM1 with AnAOB growth and decay processes and investigated the interaction between AnAOB and HB. The same was investigated by Ni et al. (2012) in a 1-D flat-sheet biofilm model. Both concluded that HB will be present in significant (although low) amounts despite the absence of organic carbon in the reactor feeds.

Single-stage CANR modeling

The study of Koch et al. (2000) was amongst the first to mathematically describe a single-stage CANR configuration by modeling a biofilm based RBC removing nitrogen without organic carbon supply. Under the operational conditions investigated it was found that diffusion of nitrite to the anoxic AnAOB containing parts of the biofilm was the limiting process for nitrogen removal in the system. Later, the effect of temperature, influent ammonium concentration, and influent flow rate (Hao et al., 2002b), plus bulk oxygen concentration and biofilm thickness (Hao et al., 2002a) were investigated by modeling of the CANON process as a 1-D flat-sheet biofilm. It should be noted that both the model of Koch et al. (2000) and the model of Hao et al. (2002a&b) did not consider the presence of HB and did not explicitly include external mass transfer resistance. However, the study of Hao et al. (2004) investigated the impact of HB presence in the biofilm in cases where biodegradable organic carbon was present in the influent. This was extended by the study of Lackner et al. (2008) which looked into the effect of HB and COD in co-diffusion and counter-diffusion biofilm systems performing CANR. The counter-diffusion system being an MABR, in which the oxygen was supplied through a membrane acting as biofilm substratum. The MABR configuration for CANR was first modeled by Terada et al. (2007). The study found that the surface loading ratio of ammonium to oxygen was determining the performance of the N removal.

The latest development within modeling of single-stage CANR is the modeling of granular sludge reactors (Volcke et al., 2010). Both the effect of average granule size (Volcke et al., 2010) and the distribution of granule sizes (Volcke et al., 2012) have been investigated. The results show that bigger granules are less efficient but more robust than smaller ones, and that modeling of a single average granule size might give a different result than modeling of a distribution of granule sizes, which is a more accurate representation of reality. However, external mass transfer resistance has not been considered in these granule investigations either, hence the interpretation of the results will be limited by this assumption.

1.3 Control of biological WWT processes

The objective of WWT is to supply the best possible (at least within the legislative demands) effluent quality at the lowest possible energy and resource utilization costs. However, also of tremendous importance is the ability to handle and reject disturbances. In obtaining these goals, control and automation play an essential role (Olsson, 2012). Control systems and strategies are

often acting on flow and concentrations – process variables that can relatively easily be observed – but it is important to keep in mind that these affect the microbial composition of the biomass performing the treatment. Control strategies can thus, apart from enhancing effluent quality, also be used actively in optimizing microbial properties or in limiting the growth of unwanted microbial groups (Olsson, 2012). An example of such is the suppression of NOB growth through control of the pH in the system or through SRT control.

Early nitrogen removal controllers focused on controlling the DO, which has proven effective in reducing the effluent concentrations (Nielsen et al., 1981). Since then, more advanced strategies have been developed along with the utilization of more sophisticated sensor equipment, such as on-line nutrient sensors. In the study of Ingildsen et al. (2002) a feedforward controller, based on on-line ammonium signals, was tested in a full-scale WWTP and it was found that 5-15% of energy for aeration could be saved. The study of Vrecko et al. (2006) presented a feedforward-feedback controller to improve aeration consumption. Intermittent aeration based on on-line nitrogen sensors has also resulted in improved nitrogen removing performance (Kaelin et al., 2008). In the study of Lemaire et al. (2008) pH signals, along with DO, were utilized to construct an automated switching off of the aeration in an SBR system achieving short-cut nitrification-denitrification via nitrite. A SHARON reactor removing nitrogen via short-cut nitrification-denitrification was operated with and optimized by a fuzzy logic control strategy based on pH and oxygen reduction potential (ORP) measurements (Claros et al., 2012).

For CANR, the study of Volcke et al. (2006a) investigated a number of control strategies for the SHARON process in a two-stage configuration based on DO and/or pH signals. A strategy, in which the DO set point was set by a master controller keeping the nitrite to ammonium ratio (cascade control) combined with a pH controller, was proposed as a result of this study, in order to produce a good influent quality for a subsequent anammox reactor. Valverde-Perez et al. (2012) extended this study to also include a control loop on the anammox reactor, which was cascaded onto the set point of the nitrite to ammonium ratio in the SHARON reactor and was based on effluent concentration measurements from the anammox reactor.

As for the single-stage CANR systems, the DEMON® process developed by Wett (2007) made use of on-line pH measurements to control the intermittent aeration in a full-scale SBR implementation with a long feeding phase. The pH set point was derived from the oxygen transfer efficiency, and during this operation the DO was kept between 0.25-0.35 mg O_2 L^{-1} in the aerated phases. Intermittent aeration was also tested both in a suspended sludge system (Joss et al., 2011; Jardin and Hennerkes, 2012) and in a carrier based system (Zubrowska-Sudol

et al., 2011). The first study found little difference in performance, but claimed that continuously aerated systems are easier to observe and control, Jardin and Hennerkes (2012) found that the control of aeration length and control of frequency of switching between oxic and anoxic conditions were essential for suppression of NOB growth, while the latter study found that the length of aeration time impacted the removal efficiency. In the ANITAMox plant, DO is also the controlled variable, but here the nitrate produced over the ammonium removed is used to deduce the value of the DO set point (Christensson et al., 2013). In a lab-scale study of a fixed filter performing CANR, Kwak et al. (2012) showed that tight control on the oxygen to nitrogen volumetric loading ratio resulted in a good nitrogen removal performance.

1.4 Issues and challenges

The challenges related to CANR can be divided into 1) start-up, 2) scale-up, and 3) operation. Below, the issues related to these three challenges are highlighted.

Since AnAOB have very slow growth rates, starting up reactors utilizing this process has proved challenging and time consuming (Strous et al., 1998; Wett, 2006; van der Star et al. 2007; Joss et al., 2009). This makes the systems very sensitive towards biomass retention, and in cases using sedimentation, sludge flocculation or granulation problems can upset the system performance due to washout of AnAOB (van der Star et al., 2007; Joss et al., 2009).

Mass transfer phenomena play a role in CANR performance, which means that proper design, operation and control for process scale-up is not straightforward. This, together with the slow growing biomass and its sensitivity towards biomass retention, emphasizes the importance of a systematic development of a scale-up methodology.

Microbial competition for substrates and for space, especially in single-stage systems, has posed an obstacle for well-functioning CANR (Fux et al., 2004). Inhibitions of involved microorganisms, e.g. by substrates and/or products, especially oxygen inhibition of AnAOB, make the systems very sensitive towards influent composition (which is often complex in full-scale implementations (van der Star et al., 2007)) and towards operating conditions. As a consequence of these issues, pilot- and full-scale systems have shown instability and loss of microbial activity (Joss et al., 2011; Jardin and Hennerkes, 2012).

Intensification of the process, by running it as a single-stage configuration, makes it difficult to observe and operate an already complex biological system. Multiple biological processes are

occurring simultaneously, while at the same time mass transfer limitation might play an important role. In addition to this, fewer actuators are available in the intensified system. The tradeoff between reduction of footprint/energy consumption and actuator availability is often an issue in intensified systems (Nikacevic et al., 2012). All these things together underline the importance of formulating and testing indicators and strategies, which can be used to diagnose and control the status of the system. Establishing operational guidelines and robust control strategies is therefore highly needed (van Hulle et al., 2010; Vlaeminck et al., 2012).

Development of control in wastewater treatment systems, including the CANR process, whether it is for side-stream treatment or industrial nitrogen-rich wastewater applications, is usually done by previous process experiences and past insights and observations. A systematic analysis of the controllability and generation of control ideas and strategies, especially linking regulatory control to the control objective, is lacking and does therefore need to be addressed.

Addressing the above mentioned issues solely through the execution of an experimental campaign is expensive and time consuming. Hence, model-based or model-supported systematic studies are needed to facilitate and speed up such investigations. By first conducting simulation analysis, subsequent experimental testing can be guided and more targeted than in pure experimental studies.

In this work the issue of ensuring optimal and stable operation is tackled using a systematic approach that uses modeling, experimental work, and control studies in a complementary and integrated manner. The knowledge obtained from this work is expected to realize the full potential of this promising technology in industrial practice of wastewater treatment.

1.5 Objectives of the PhD project

On the basis of the status and the challenges related to complete autotrophic nitrogen removal presented above, this PhD project has been formulated aiming at gaining further insight into the CANR process by applying a systematic and generic methodology, combining modeling and experimental analyses (see Figure 1.6), and to use the derived knowledge and insights to optimize and control the operation of this process in granular based sequencing batch reactors.

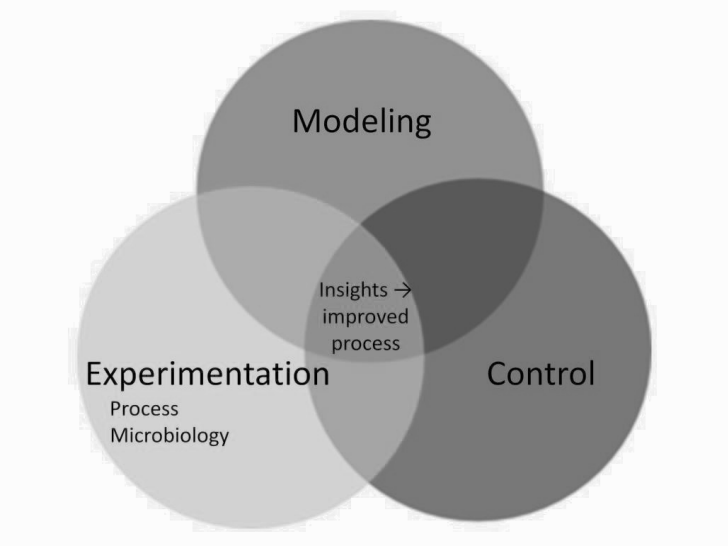

Figure 1.6 Research methodology of the PhD project.

In particular the research methodology addresses the following questions:

Process understanding:

- What are the most important parameter(s), mechanism(s), and interactions affecting nitrogen removal in these systems?
- Which parameters are of highest importance under different sets of operating conditions?
- Which operating conditions are the optimal ones?

Control and optimization:

- Can a model accurately capture process performance?

- Which possible actuators are available for controlling the system?
- How are these paired with controlled variables for achieving the best possible control strategy?
- Can the performance be stabilized and/or improved through automated control?
- And can the effect of this control strategy be validated experimentally?

The research scope of the PhD project is summarized in the methodology shown in Figure 1.6 and in the graphical abstract in Figure 1.7. As indicated in the graphical abstract, the research aims at closing the cycle of modeling and experimentation in a complementary manner going from model development, simulation analysis, calibration and validation, to control strategy generation and design, testing, evaluation and experimental validation (Figure 1.7). The output of the research cycle is expected to deliver improved process understanding and novel ideas for stable and optimized operation of the CANR process.

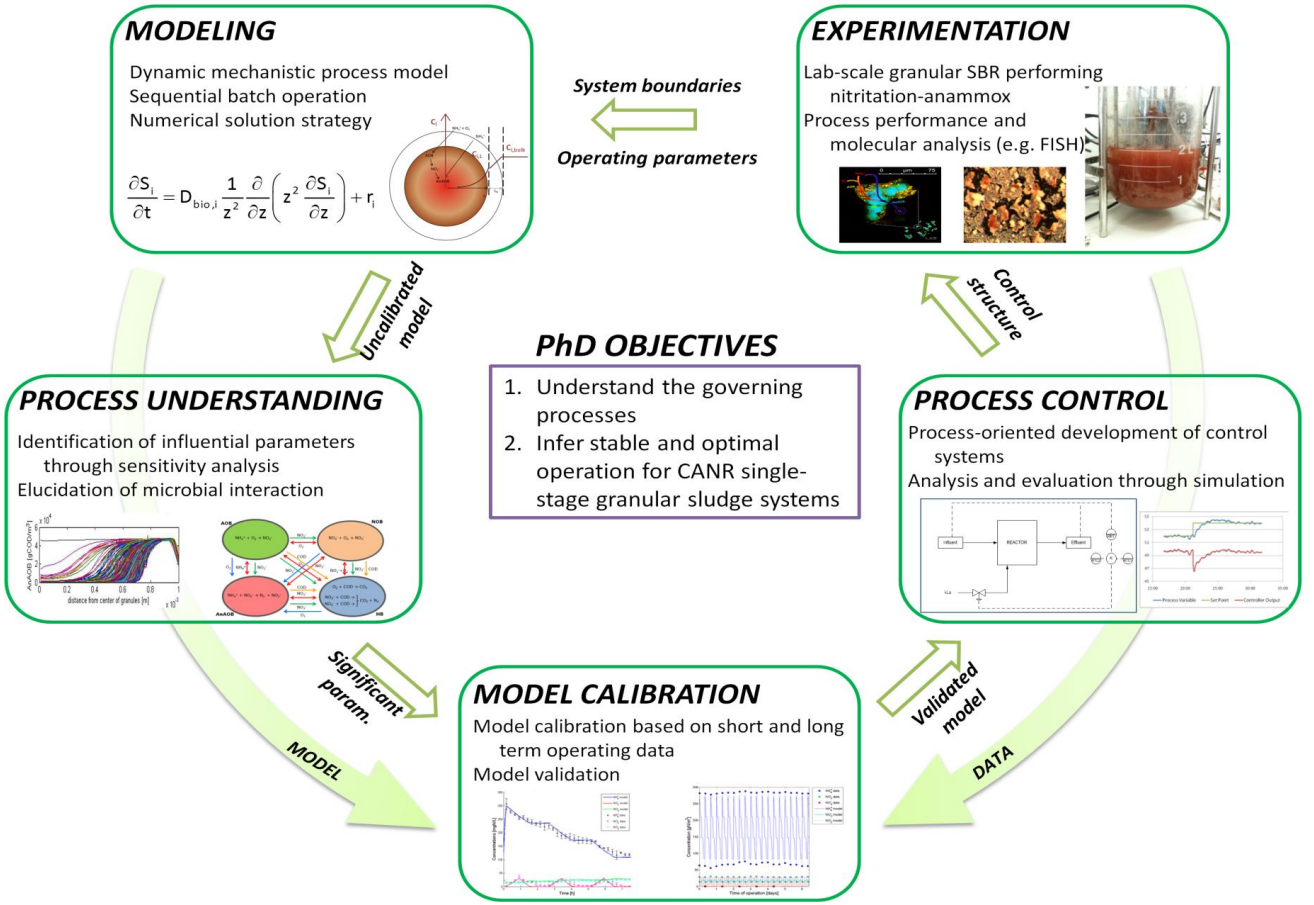

Figure 1.7 Graphical abstract of the PhD project. The overall objectives are present in the center, and these are achieved through utilizing mathematical modeling tools, practical experimentation, and process control theory.

1.6 Structure of PhD thesis

The thesis is divided into 4 parts consisting of 9 chapters. The first part contains introduction, and a description of the experimentation and modeling. The first and current chapter gives a general introduction to the autotrophic nitrogen removal topic and the background, motivation, and objectives of the project are presented. Chapter 2 contains a description of the experimental setup and chapter 3 contains the mathematical model used to describe the system along with the methodology used to construct this model. Parts of the mathematical model described in chapter 3 have been published as a paper in *Bioresource Technology*. Part II contains simulation and scenario studies, which investigate the importance of microbial kinetics versus mass transfer through global sensitivity analysis in chapter 4 and the effect of including pH as a state variable in the model in chapter 5. Parts of chapter 4 consist of the article published in *Bioresource Technology* and chapter 5 is based on an article published in *Water Science and Technology*. In part III, the knowledge from the previous chapters is used to control and optimize the operation and performance of the system. In order to do this, a validated model was needed and this was obtained by following a customized calibration and validation methodology, which is presented in chapter 6. This chapter is based on an article published in *Journal of Chemical Technology and Biotechnology*. Subsequently, in chapter 7, ideas for control strategies were generated through a process oriented approach. These were tested and evaluated through exhaustive simulations studies with the validated model developed in the previous chapter. Chapter 7 is based on a published conference proceedings paper from the *ESCAPE23* conference, but has been extended in the dissertation and has been submitted as a full paper to the journal *Computers and Chemical Engineering*. The most promising control strategy from chapter 7 was implemented experimentally for validation in the lab-scale reactors, and this work is presented in chapter 8. This chapter comprises material used in a research article in preparation. In the final chapter, the general conclusions obtained from the PhD project are given and future works and perspectives are discussed. In appendix A1 a full list of journal publications and conference contributions resulting from activities within this PhD project can be found.

In Figure 1.6 and 1.7 the links and dependencies between the different tools, developments, and objectives are illustrated.

2 Experimental setup

Two reactors (denominated SBR1 and SBR2) were run in parallel for approximately 26 months. They were operated to obtain granular biomass which performed complete autotrophic nitrogen removal. They were started up in May 2011 using an ammonium oxidation bacteria enriched inoculum (see below). SBR2 has been running since then, while SBR1 had to be reinoculated in October 2011 due to an unrecoverable upset in the operation.

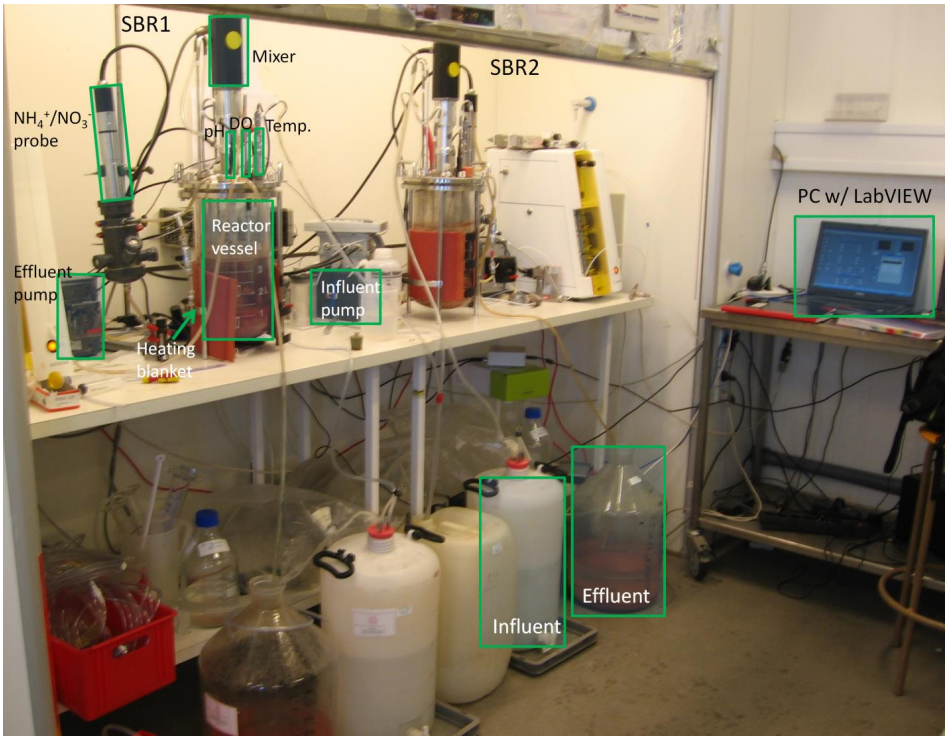

Figure 2.1 The experimental laboratory scale setup with the two parallel reactors.

2.1 Reactors

2.1.1 Physical layout

The reactor vessels were modified 4 L fermentors of the model Biostat A Plus (Sartorius, Melsungen, Germany), which have a cylindrical geometry with a diameter of 16 cm and a height of 25 cm. Each vessel was mixed by mechanical stirring (Rushton impeller), which was built into

the fermentors (Figure 2.1 and 2.2). Other equipment originally belonging to the fermentors were an electrical heating jacket for temperature control, a ring-shaped bottom aeration line in steel, an OxyFerm FDA DO sensor, an EasyFerm plus K8 325 pH sensor (both Hamilton, Bonaduz, Switzerland), and a Pt-100 temperature sensor (Sartorius, Melsungen, Germany). In order to construct a functioning SBR, external influent and effluent peristaltic pumps (Watson-Marlow, Wilmington, MA, USA) were added to the setup. Aeration was provided using compressed air from a central line available in the laboratory, and regulated by an external EL-FLOW mass flow controller (Bronkhorst, Ruurlo, The Netherlands). A sensor containing both an ammonium and a nitrate ion selective electrode (Varion, WTW, Weilheim, Germany) was placed in a separate probe chamber connected to the effluent line (Figure 2.2).

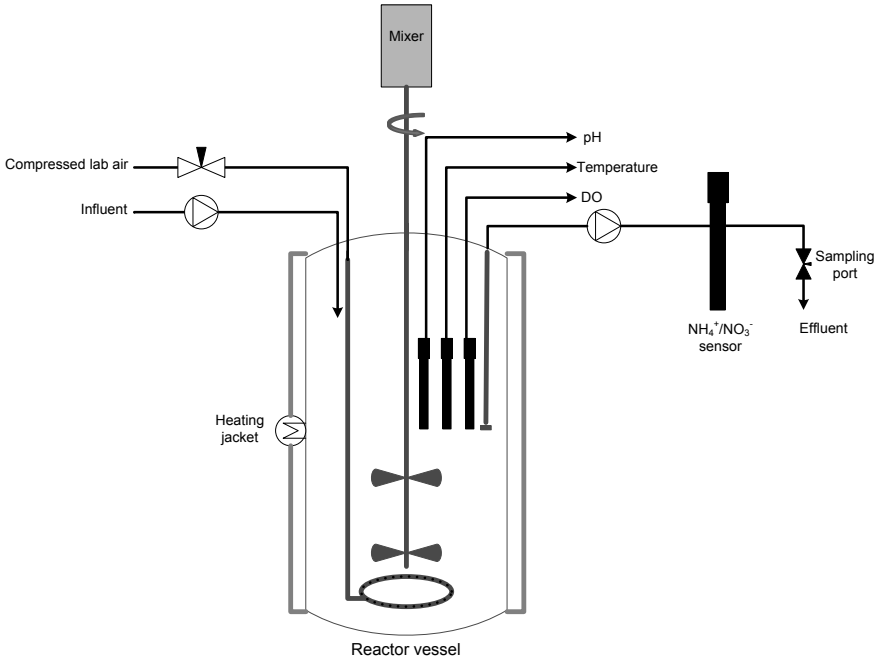

Figure 2.2 Schematic illustration of SBR with equipment.

All of the equipment was operated through a tailor-made software routine programmed in LabVIEW (National Instruments, Austin, USA), which was also used for data acquisition, monitoring, control and data storage purposes. The equipment built into the Sartorius fermentor was connected to LabVIEW through an OPC server acting as a data socket and the external equipment were connected through a solid state relay and a NI USB-6008 DAQ device (National Instruments, Austin, USA).

2.1.2 Inoculum

The reactors were seeded with sludge from AnoxKaldnes' ANITAMox "BioFarm" plant located at Sjölunda WWTP in Malmö, Sweden. The "BioFarm" plant is a full-scale MBBR performing autotrophic nitrogen removal treating anaerobic sludge digester liquor. The biomass was manually removed from the carriers obtained from the plant, and was subsequently used as inoculum for the reactors. The reactors were inoculated within a week after the carriers were collected, and they were stored in a nitrate solution prior to reactor inoculation.

2.1.3 Substrate – synthetic wastewater

A synthetic wastewater was fed to the reactor, which was based on demineralized water and contained NH_4HCO_3 (N source, C source, and alkalinity) and $NaHCO_3$ (C source and alkalinity). The ammonium and with it the bicarbonate concentration changed over time as described in the "operation history" below. The bicarbonate to ammonium molar concentration ratio varied between 1.27 and 1.48. Trace elements solutions based on van de Graaf et al. (1996) were also added to the feed, and the final concentrations in the feed were: 169.7 mg KH_2PO_4 L^{-1}, 751.1 mg $MgSO_4 \cdot 7H_2O$ L^{-1}, 451.6 mg $CaCl_2 \cdot 2H_2O$ L^{-1}, 20.0 mg EDTA L^{-1}, 5.00 mg $FeSO_4 \cdot 7H_2O$ L^{-1}, 0.43 mg $ZnSO_4 \cdot 7H_2O$ L^{-1}, 0.24 mg $CoCl_2 \cdot 6H_2O$ L^{-1}, 0.99 mg $MnCl_2 \cdot 4H_2O$ L^{-1}, 0.25 mg $CuSO_4 \cdot 5H_2O$ L^{-1}, 0.22 mg $NaMoO_4 \cdot 2H_2O$ L^{-1}, 0.19 mg $NiCl_2 \cdot 6H_2O$ L^{-1}, 0.21 mg $NaSeO_4 \cdot 10H_2O$ L^{-1}. In order to avoid precipitation issues, six different stock solutions were made. The substrate solution was prepared by diluting the stock solutions appropriately into 25 L bottles. In order to avoid oxygen supply through the influent and avoid microbial growth in the influent bottles, the substrate was sparged with N_2 gas for 20 minutes immediately after preparation. The substrate feed was prepared twice per week.

2.1.4 "Default" reactor operation

The operating temperature was controlled at 30°C, the pH was kept at 7.5±0.5, and the vessel was mixed by mechanical stirring at 80 rpm combined with intermittent or continuous bubble aeration.

The influent to the reactor contained 500 mg total ammonium nitrogen (TAN) L^{-1}. The reactor was operated with a cycle length of 8 hours and an exchange ratio of 50%, which resulted in an HRT of 16 hours, and a volumetric N loading rate of 750 mg N L^{-1} d^{-1}. The 8 hour cycle was distributed in a 10 minute fill phase, a 447 minute reaction phase, a 3 minute settling phase, a 10 minute draw phase, and a 10 minute idle phase (Figure 2.3). During the aerated phases the air flow was approximately 0.5-1.0 L min^{-1}.

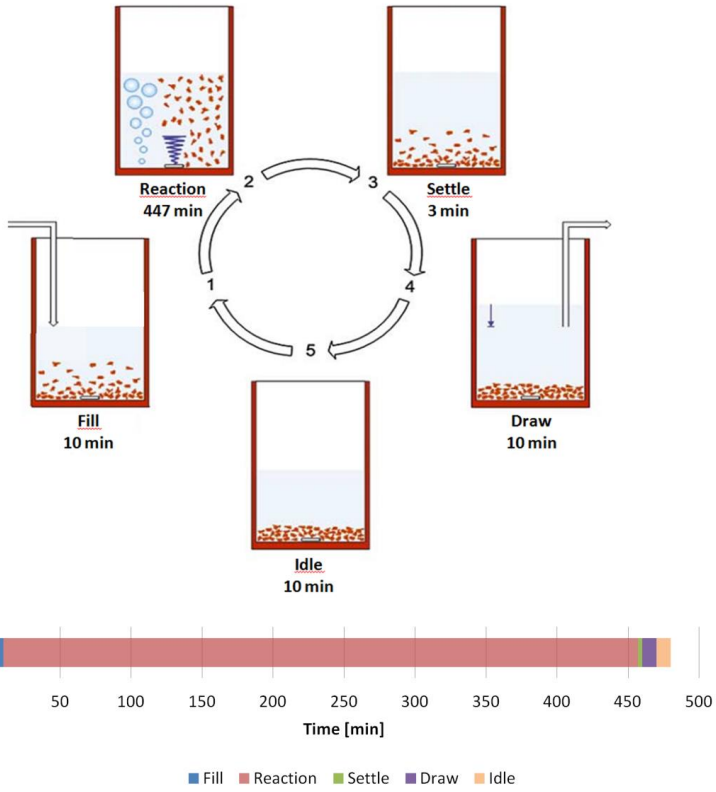

Figure 2.3 Schematic illustration of the phases in the SBR cyclic operation. 1) Fill phase, 2) Reaction phase, 3) Settling phase, 4) Draw phase, 5) Idle phase (adapted from Vlaeminck et al., 2009).

2.1.5 Operation history

The reactors were operated for more than two years. During that period, several changes were imposed to the operation as part of the research plan. Here, the most significant operational changes are briefly outlined:

Cycle length: The reactors were started up with a cycle time of 12 hours and, since the exchange ratio (ER) was 50%, with a concomitant HRT of 24 hours. Later on, when the nitrogen removal rate had reached a sufficient efficiency the cycle time was reduced to 8 hours with a concomitant HRT of 16 hours.

Temperature: The reactors were first controlled at a temperature of 30°C. After an upset in operation due to failure of the temperature controller, the reactors were operated at ambient temperature for a couple of months. However, since a drop in the removal rate was observed as a consequence of this change, the temperature control was subsequently re-established.

N loading: Both reactors were started up with an influent concentration of 200 mg N L^{-1} and a volumetric loading rate of 200 mg N L^{-1} d^{-1}. During operation, this was gradually increased through decreasing cycle length and increasing influent concentrations, such that the final influent concentration was 500 mg N L^{-1} and the volumetric loading rate was 750 mg N L^{-1} d^{-1}.

Aeration: Since aeration was supplied both continuously and as intermittent phases, a range of metrics to characterize the aeration system has been defined below (Table 2.1). During intermittent aeration, the number of sequential aerated and non-aerated phases during one reaction phase was varying leading to different number of transient changes in the redox conditions (f_{redox}).

Table 2.1 Independent and dependent operational parameters related to oxygen supply in SBRs with intermittent aeration.

Parameter	Formula	Definition
	Independent operational parameters	
Q_{air}	-	Air flow rate during aerated phase
t_{on}	-	Length of a single aerated phase
t_{off}	-	Length of a single non-aerated phase
t_{cycle}	-	Length of a total cycle including all phases
	Dependent operational parameters	
f_{redox}	$\frac{t_{cycle}}{t_{on}+t_{off}}$	Number of changes in redox conditions during one SBR cycle
R_{on}	$\frac{t_{on}\cdot f_{redox}}{t_{cycle}}$	Fraction of the cycle time in which the reactor is aerated
L_{O2}	$k_L a\left(S_{O2,sat}-S_{O2,bulk}\right)R_{on}$	Overall volumetric oxygen loading rate per cycle
$k_L a$	$f(Q_{air}$, sludge characteristics$)$	Mass transfer coefficient for oxygen

The aeration is the operational parameter which has been altered the most. It has been changed through manipulation of the air flow rate (Q_{air}), which directly changes the overall oxygen loading to the system, but it has also been changed through alteration of f_{redox} and R_{on}, which are affected by the number of changes from aerated to non-aerated conditions and vice versa, and affected by the duration of the aerated and the non-aerated phases.

Substrate composition: When the reactors were first started up a substrate composition from Kuai and Verstrate (1998) based on tap water was used. At the reinoculation of SBR1 in October 2011 the substrate composition was switched to the composition from van de Graaf et al. (1995) based on demineralized water. The reason for this was to ensure a more stable concentration of the divalent cations (Ca^{2+} and Mg^{2+}) in the influent.

Recirculation: During the first four months of operation, a recirculation line with a peristaltic pump containing the N probe was employed and bulk concentrations of ammonium and nitrate were logged on-line continuously. The reason for this was that the N probe was too big to fit directly in the reactor vessel. However, the pumping had an adverse effect on the biomass structure resulting in completely suspended sludge with no granule formation to observe. The recirculation line was therefore deployed and the N probe was moved to the effluent line (as in Figure 2.2).

Settling time: In the startup phase the settling time was 10 minutes. This was gradually decreased, eventually to remain at 3 minutes corresponding to a critical settling velocity of approximately 2 m h^{-1}.

SRT: From November 2012 sludge was systematically wasted every day to ensure an average sludge age of approximately 100 days. Prior to this, sludge was wasted more irregularly such that a good estimation of SRT could not be made. However, prior to this time point the SRT was longer than 100 days.

2.2 Measurements and analyses

2.2.1 N analyses

The concentrations of NH_4^+-N and NO_3^--N in the effluent were measured by ion selective electrodes (Varion, WTW, Weilheim, Germany). The data were logged on-line and by the end of the operational period also acquired through the online data acquisition system in LabVIEW. The

NH_4^+-N and NO_3^--N concentrations were verified by manual sampling from the effluent line approximately once per week. The samples were filtered using a cellulose acetate 0.45 µm syringe filter (Frisenette, Knebel, Denmark) and analyzed with colorimetric test kits (Merck KGaA, Darmstadt, Germany) (Figure 2.4). NO_2^--N concentration was always measured off-line through sampling and analysis with the colorimetric test kits, where a chemical reaction produces a color intensity dependent on the concentration, which is measured at a given light wavelength.

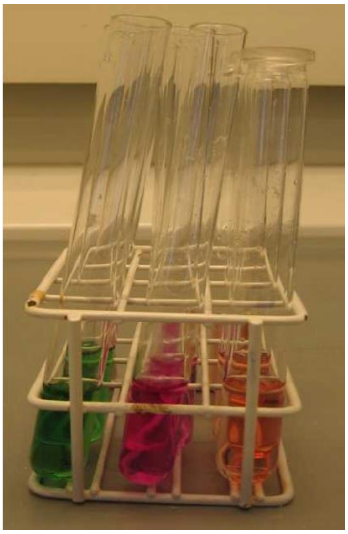

Figure 2.4 Colorimetric test kits - green: ammonium, pink: nitrite, orange/red: nitrate.

2.2.2 Solids concentration

Total and volatile suspended solids (TSS and VSS) were determined according to the Standard Methods (APHA-AWWA-WPCF, 1998). Usually, 5 or 10 mL sample was taken, filtered though pre-weighed glass fiber filters (Pall Corporation, Port Washington, NY, USA), dried at 104°C for 2 hours to remove water present in the sample, weighed again, burned at 550°C for 30 minutes to remove all organics, and finally weighed again.

2.2.3 Particle size distribution

Particle size distribution (PSD) and the volumetric weighted mean particle size were determined by laser diffraction measurements (Mastersizer 2000, Malvern, Worcestershire, UK). Depending

on the solids concentration a sample of 2-15 mL was taken and passed through the laser diffraction chamber and analyzer. All measurements were made in triplicate.

2.2.4 Oxygen transfer coefficient (k_La)

The air was supplied to the bulk liquid through a ring-shaped steel tube with a diameter of approximately 7 cm with holes, through which air was distributed. The compressed air was supplied to the bottom of the reactor and vented through an outlet in the reactor lid. To find out more about the diffuser's oxygen transfer abilities, standard clean water oxygen transfer tests according to the American Society of Civil Engineers (ASCE) were performed.

The reactor was filled with demineralized water and the electrical heating jacket controlled the temperature at 30°C. All oxygen in the system was depleted by sparging with N_2 gas for approximately 15 minutes. Subsequently, the aeration was started at a fixed flow rate and automatic logging of the DO concentration was started. The slope and shape of the increasing DO concentration profile, starting from approximately zero to the saturation concentration was analyzed using a non-linear fitting program (ASCE, 2007), and values for k_La were obtained.

A mass balance was considered:

$$\frac{dC}{dt} = k_L a\left(C^* - C\right) \tag{2.1}$$

Which has the solution:

$$C = C^* - \left(C^* - C_0\right)e^{-kLa \cdot t} \tag{2.2}$$

where C is the DO concentration [mg L^{-1}], C* is the DO saturation concentration [mg L^{-1}], C_0 is the DO concentration at t=0 [mg L^{-1}], and k_La is the volumetric mass transfer coefficient [d^{-1}].

The non-linear regression model was fitted to the DO concentration vs. time data, by estimating C*, C_0, and k_La such that the residual sum of squares was minimized.

2.2.5 Microbiological analysis

Another PhD project focusing on microbial composition and architecture was carried out by PhD fellow A.G. Mutlu in parallel with this study. As a part of her work, biomass samples were taken

during the entire operation and DNA was extracted for microbial analysis such as quantitative polymerase chain reaction (qPCR) and fluorescence in-situ hybridization (FISH). Also, the sludge volume index (SVI) was systematically measured for the last 8 months of operation to assess changes in the settlability of the sludge.

3 Mathematical model

A systematic framework for generating models of biofilm based systems in an efficient and structured way has been developed and used in this work. Subsequently, it has been applied to a case study of single-stage autotrophic nitrogen removal by granular sludge.

In the first part of this section, the general framework, assumptions, model equations, and solutions of these are presented. In the second part, the features specific to the CANR case and parameter values associated to it are presented.

3.1 Conceptual model

In biofilm systems, processes happen at very different spatial and temporal scales, as opposed to in completely mixed reactors where all processes are assumed to happen at the same spatial scale. Modeling of biofilm systems is therefore typically done in two (Wanner et al., 2006) or even three different spatial scales (Xavier et al., 2005). The two scales are here termed the "biofilm scale" and the "reactor scale" (Figure 3.1). At the biofilm scale the microbial metabolism along with transport of soluble and particulate compounds are described. These processes will govern the spatial location of the particulate compounds, i.e. the bacteria, inert material, and other particulates. At the reactor scale the overall mass balances are considered along with the hydrodynamic conditions in the reactor. When a third stage is included, individual cells are modeled separately. In this case, the biofilm scale is only including the transport processes and spatial location, while the individual or cellular scale describes the growth and metabolism of the microorganisms.

At the biofilm scale, either a subset of a microbial functional group (e.g. specific species of AOB), or an entire functional group of microorganisms (e.g. AOB) can be modeled. If individual cells are considered, a certain differentiation in their metabolism might be assumed, whereas if a subset or entire functional group is modeled, their metabolism is assumed identical. The latter is called the lumped approach and can be solved along with the transport equations at the biofilm scale, i.e. it practically results in only two spatial scales.

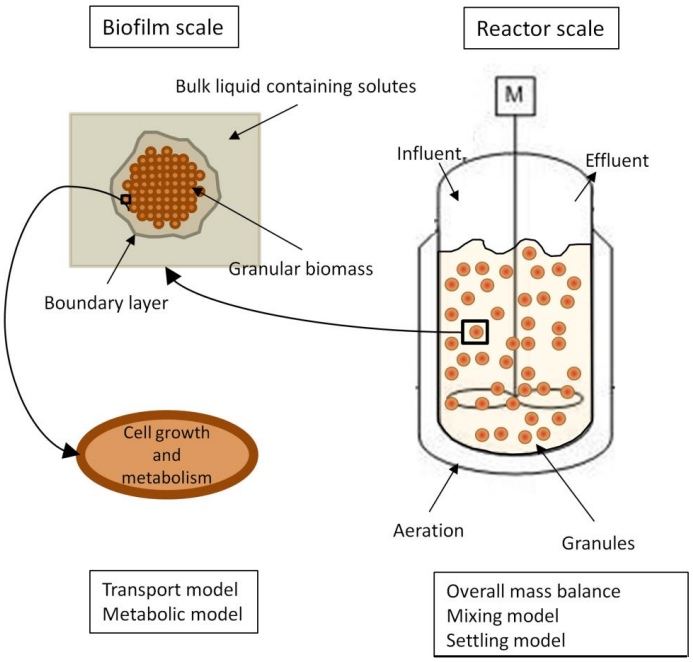

Figure 3.1 Conceptual model of a bioreactor with granular sludge as an example of a multi-scale model. Two spatial scales are illustrated; the biofilm scale and the reactor scale.

3.2 Model development framework

A framework that supports the model construction at the different scales, as well as linking them to each other, has been developed based on the methodology of Heitzig et al. (2010). The framework was developed by studying the workflow typically involved in development of models for multi-scale systems (see Figure 3.2). The first and most important step consists of defining the overall modeling objective. The second step is gathering system information such as, for example, physical and operational conditions of the system. From this information the main assumptions can be established in the third step. Subsequently, the model scenarios of interest should be defined, including which spatial scales and processes are of relevance. From this definition, the individual models to be constructed can be derived. Each of the individual models are either taken from previous studies, if such exist, or they are constructed or modified following the workflow depicted on the right side of Figure 3.2. First, the specific model objective for the individual model and then the corresponding system information and assumptions are defined. The individual model is constructed, and sensitivity analysis of the model parameters is conducted if needed. The model is then calibrated to experimental data by

adjusting the sensitive parameters. Finally, when the individual model has been validated, it is "exported" back into the multi-scale modeling workflow. The individual models are then linked to each other by defining the information needed to be transferred from one spatial scale to another and vice versa. The multi-scale model system can now be solved in steady state by defining appropriate boundary conditions and dynamically by also defining initial conditions.

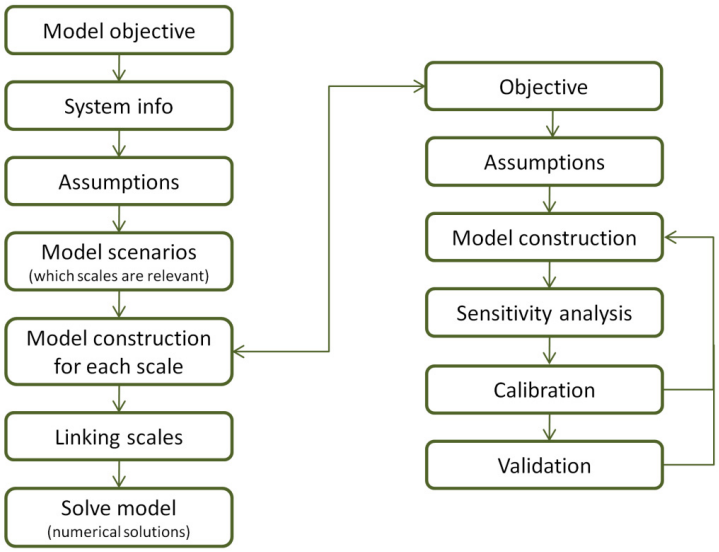

Figure 3.2 Workflow scheme for multi-scale modeling (left) and identification of the individual models (right) (adapted from Heitzig et al., 2010).

3.2.1 Model objective

By following the framework (Figure 3.2), first the modeling goal is defined. The objective here is to construct a general model describing a bioreactor containing granular sludge. The model should be able to determine the reactor performance (i.e. concentrations of suspended compounds) and the microbial composition and distribution.

3.2.2 System info

The system consists of an aqueous phase and a biofilm phase consisting of granular sludge. Processes occurring in the system are microbial catalyzed processes, mass transfer through diffusion and advection plus gas/liquid transfer processes.

3.2.3 Assumptions

There are a number of assumptions that need to be made to support the development of an appropriate level of model complexity. These are:

- All microorganisms belonging to the same microbial group (e.g. AnAOB) are assumed to have the same microbial kinetics. In other words, only two scales (namely biofilm and reactor) will be considered in the model construction.

Reactor scale assumptions:

- The bulk volume of the reactor is considered completely mixed.
- Granules present in the system are perfectly retained. However, free floating cells in the bulk liquid can leave the system in the effluent.
- Formation of new granules and breakup of existing ones are assumed at steady-state. Hence, the number of granules remains constant.

Biofilm scale assumptions:

- Granules are considered identical and spherical, i.e. all granules have the same size and the same spatial distribution of microbial groups.
- Since the bulk liquid is considered completely mixed (without any spatial difference in concentration), the concentration gradients in the granules only take place along the radial coordinate. That means no gradients occur in the polar or azimuth coordinates. Thus, the model will be in one dimension following the radial distance from the center of the granule, perpendicular to the granule surface.

3.2.4 Model equations

Since the objective is to describe bulk liquid concentrations of soluble compounds and the microbial composition inside the granules, the model will be based on mass balances of relevant compounds. A general mass balance can be written as:

$$\text{Accumulation} = \text{Inflow} - \text{Outflow} + \text{Generation} - \text{Consumption} \qquad (3.1)$$

We now move to the right side of the work flow scheme in Figure 3.2. Since the purpose of this chapter is to present the model structure and equations, the sensitivity analysis and calibration and validation procedures will not be presented here, but are described in detail in the following chapters (chapter 4 and 6, respectively).

Biofilm scale

First, the model equations for the biofilm scale are derived.

For a control volume, the mathematical expression of the microscopic mass balance of a compound (i) is as follows:

$$\frac{\partial M_i}{\partial t} = \frac{\partial (C_i V)}{\partial t} = \partial (j_i A) + \partial V r_i \qquad (3.2)$$

Where M_i is the mass of compound i, C_i is the concentration of the soluble or particulate compound i in the biofilm [g m^{-3}], j_i is the flux of the compound [g m^{-2} d^{-1}] in the radial direction, A is the cross sectional area perpendicular to the flux [m^2], V is the volume of the control volume [m^3], and r_i is the production/consumption rate of compound i [g m^{-3} d^{-1}].

Within the biofilm, the inflow and outflow are related to the transport in and out of a given control volume (Figure 3.3). Like in the 1-D model of benchmark problem 3 (BM3), made by the IWA task group on biofilm modeling (Wanner et al., 2006), the transport of soluble compounds is assumed governed solely by diffusion and of particulate compounds solely by advective transport. For both soluble and particulate compounds their generation and/or consumption is a function of their production/removal rate (r_i), which in turn is a function of the microbial metabolism.

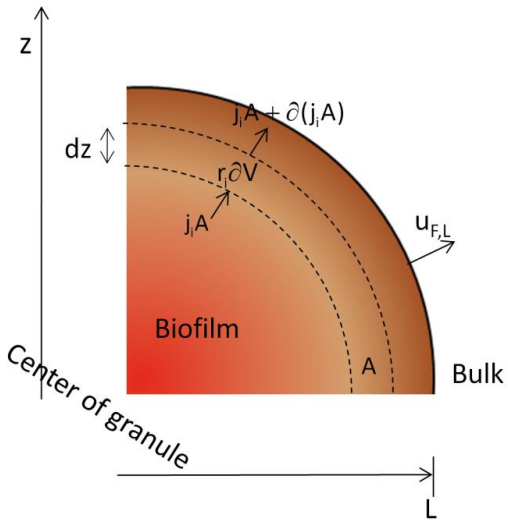

Figure 3.3 Spherical coordinates and the control volume used to describe the mass balance in the biofilm scale.

In a 1-D biofilm system in spatial coordinates, as depicted in Figure 3.3, and assuming that the radial distance between the two points (z and z+dz) bounding the control volume (dV) is approaching zero, the mass balance can be approximated to be:

$$dV\frac{\partial C_i}{\partial t} = \partial\left(j_{Ci}A\right) + dVr_i \tag{3.3}$$

The control volume derived in a spherical geometry is approximated to be:

$$dV \approx 4\pi z^2 dz \tag{3.4}$$

where z is the radial distance from the center of the granule.

The mass balance therefore becomes:

$$4\pi z^2 dz\frac{\partial C_i}{\partial t} = \left(j_{Ci}A\right)\Big|_z - \left(j_{Ci}A\right)\Big|_{z+dz} + r_i 4\pi z^2 dz \tag{3.5}$$

If we derive with respect to z, the entire equation becomes:

$$4\pi z^2\frac{\partial C_i}{\partial t} = \frac{\partial}{\partial z}\left(j_{Ci}A\right) + r_i 4\pi z^2 \tag{3.6}$$

For soluble compounds (concentration denoted by S_i) the flux can be expressed by Fick's first law of diffusion:

$$j_{Si} = -D_{bio,i}\frac{dS_i}{dz} \tag{3.7}$$

where $D_{bio,i}$ is the diffusivity of compound i in the biofilm [$m^2\ d^{-1}$]. Considering the symmetry of the granules, combining equation 3.6 and 3.7 yields the mass balance for soluble compounds in a 1-D biofilm with spherical coordinates (z=radial coordinate):

$$4\pi z^2 \frac{\partial S_i}{\partial t} = -\frac{\partial}{\partial z}\left(-D_{bio,i}\frac{\partial S_i}{\partial z}4\pi z^2\right) + r_i 4\pi z^2$$
$$\Updownarrow$$
$$z^2 \frac{\partial S_i}{\partial t} = D_{bio,i}\frac{\partial}{\partial z}\left(z^2 \frac{\partial S_i}{\partial z}\right) + r_i z^2$$
$$\Updownarrow$$
$$\frac{\partial S_i}{\partial t} = D_{bio,i}\frac{1}{z^2}\frac{\partial}{\partial z}\left(z^2 \frac{\partial S_i}{\partial z}\right) + r_i \qquad (3.8)$$

For particulate compounds (concentration denoted as X_i), the flux is caused by advection and therefore expressed as:

$$j_{Xi} = -X_i u_F \qquad (3.9)$$

where u_F is the velocity [m d^{-1}], which is governed by biofilm growth.

Combining equation 3.6 and 3.9 gives the mass balance for particulate compounds in the granules:

$$4\pi z^2 \frac{\partial X_i}{\partial t} = -\frac{\partial}{\partial z}\left(X_i u_F 4\pi z^2\right) + 4\pi z^2 r_i$$
$$\Updownarrow$$
$$\frac{\partial X_i}{\partial t} = -\frac{\partial}{\partial z}\left(X_i u_F\right) + r_i$$
$$\Updownarrow$$
$$\frac{\partial X_i}{\partial t} = -u_F \frac{\partial X_i}{\partial z} - X_i \frac{\partial u_F}{\partial z} + r_i \qquad (3.10)$$

The growth velocity at a given point k, in the granule, is a function of the net growth (growth minus decay) of all the particulate species located at the inside of that point in the granule. The velocity is therefore mathematically described as:

$$u_{F,k} = \frac{1}{A_k}\int_0^k A_k \left(\sum_{i=1}^{n_{part}} \frac{r_i}{\rho}\right)_k dz \qquad (3.11)$$

where A_k is the area of the sphere at point k and ρ is the density of the biomass. The density is assumed equal among all microbial species and also not changing with space.

The biofilm thickness (L) is also a state variable and varies according to two phenomena: the net growth of the particulate species at the biofilm liquid interface, and their detachment from the granule surface. Its derivative with respect to time is therefore a function of the growth and detachment velocities ($u_{F,L}$ and u_D):

$$\frac{dL}{dt} = u_{F,L} - u_D \tag{3.12}$$

Several mechanisms and therefore also mathematical expressions have been suggested for the detachment. It has been shown to have a significant impact on the modeling result (Morgenroth and Wilderer, 2000). Here, the detachment velocity is modeled according to eq. 3.13 (Lackner et al., 2008):

$$u_D = u_{F,L}\left(\frac{L}{z_{max}}\right)^2 \tag{3.13}$$

where z_{max} is the predefined maximum radius of the granule. At steady state the granules reach the maximum size, because the growth and detachment velocities are equal to each other.

Reactor scale

Now, the model equations for the larger reactor scale are derived.

In the overall mass balance of the reactor, the transport terms are the inflow and outflow from the reactor plus the fluxes in or out of the granules. The generation and consumption are caused by microbial growth and decay of free floating cells in the bulk liquid, and abiotic processes occurring in the bulk, such as gas to liquid transfer processes.

The general mass balance for both soluble and particulate compounds in the completely mixed bulk liquid therefore looks as follows:

$$\frac{dM_{i,bulk}}{dt} = Q_{in}C_{i,in} - Q_{out}C_{i,bulk} - j_{bio,i}A_{biofilm} + r_{i,bulk}V_{reactor} \tag{3.14}$$

where Q_{in} and Q_{out} are the in- and out- flow rates and $A_{biofilm}$ is the total surface area of all the granules. The flux (j_{bio}) in and out of the granules is the link connecting the biofilm and the

reactor scales, and $r_{i,bulk}$ is the production and/or consumption taking place in the bulk. $V_{reactor}$ is the volume of the bulk liquid and has the following derivative expression:

$$\frac{dV_{reactor}}{dt} = Q_{in} - Q_{out} \tag{3.15}$$

Generation and consumptions

The microbial metabolism and hydrolysis processes, in the bulk as well as in the biofilm, along with gas to liquid transfer processes in the bulk are all included in r_i. The net reaction rate for any compound i can be written as the product of the process rate (ρ) and the stoichiometric coefficient (ν), which is summed for all processes (indicated by subscript h) affecting compound i:

$$r_i = \sum_{h=1}^{h=np} \nu_{h,i}\rho_h \tag{3.16}$$

where np is the number of processes.

3.2.5 Linking scales

Once all the model equations have been defined we move back to the workflow in the left side of Figure 3.2, where the next task is to define the link between the different scales.

The link between the reactor scale and the biofilm scale is the flux of the compounds into or out of the granules from the bulk liquid.

Assuming that the film theory holds in the mass transfer boundary layer (Bird et al., 2002), and that there is a continuity of the flux at the biofilm/liquid interface, the flux of the soluble compounds across the interface can be modeled as:

$$j_{bio,Si} = k_i\left(S_{i,bulk} - S_{i,L}\right) = \frac{D_i}{L_B}\left(S_{i,bulk} - S_{i,L}\right) \tag{3.17}$$

where k_i is the mass transfer coefficient [m d^{-1}], D_i is the diffusivity of the soluble compound in water [m^2 d^{-1}], L_B is the thickness of the mass transfer boundary layer [m], $S_{i,bulk}$ is the bulk concentration [g m^{-3}], and $S_{i,L}$ is the concentration at the biofilm/liquid interface [g m^{-3}]. Here, it is assumed that no reactions are taking place in the mass transfer boundary layer.

For particulate compounds the only interaction mechanism between the bulk and the granules is detachment, and the flux of particulates out of the granules, into the bulk can be expressed as:

$$j_{bio,Xi} = u_D X_{i,L} \tag{3.18}$$

where $X_{i,L}$ is the particulate concentration at the biofilm/liquid interface.

3.2.6 Model summary

From the above, it can be concluded that the model is a system of equations consisting of several first and second order partial differential equations (PDEs) along with multiple constitutive algebraic equations (AEs). A summary of the equation system and the number of equations in it can be seen in Table 3.1 below.

Table 3.1 Overview of the model structure through system of equation analysis.

Equation Type	Eq. number	Number
2. order PDE	3.8	N1[a]
1. order PDE	3.10	N2[b]
ODE	3.12, 3.14, 3.15	1 + N1 + N2 + 1
AE	3.11, 3.13, 3.16, 3.17, 3.18	1 +1 + N1 + N2 + N1 + N2
Total		4*N1 + 4*N2 + 4

a) N1 = # soluble compounds, b) N2 = # particulate compounds

3.2.7 Numerical solutions

The PDEs can be solved by the method of lines, i.e. discretization of one of the independent variables (z or t). In this case discretization of the space (z – the radial distance) was chosen, and numerical approximations of the space derivatives, in order to obtain a system of ordinary differential equations (ODEs), were derived. It has been shown that the number of discretized layers or nodes can have a significant impact on the model result (Boltz et al., 2011), and the number should therefore be chosen with care.

The nodes in each of the discretized layers are indicated by subscript k and have an equal distance of Δz in between them (Figure 3.4). The illustration is only containing three control volumes, but a finer grid with more nodes is usually used in order to obtain a higher precision. If

more nodes are employed, the equations describing the inner nodes (all nodes, but the two boundaries) will all be the same as the equations applicable for control volume 2 in Figure 3.4.

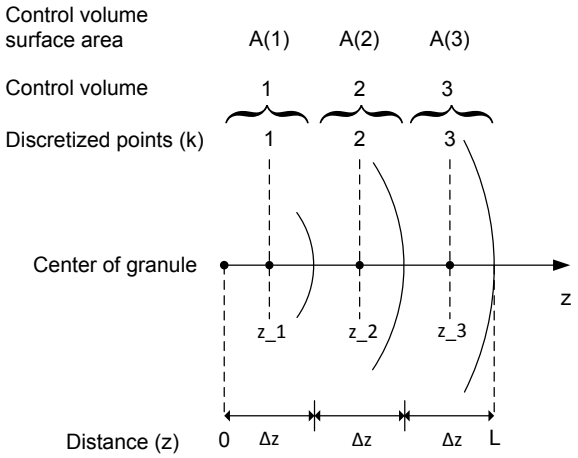

Figure 3.4 Illustration of discretization scheme.

The distance between the nodes is a function of the granule size and the number of nodes (n):

$$\Delta z = \frac{L}{n} \tag{3.19}$$

The second order space derivative of the concentration of soluble compounds can numerically be approximated by the finite central difference method in spherical coordinates:

$$\frac{1}{z_k^{\,2}}\frac{\partial}{\partial z}\left(z^2\frac{\partial S_{i,k}}{\partial z}\right) = \frac{1}{z_k^{\,2}}\frac{\partial}{\partial z}\left(g_k\right) \approx \frac{1}{z_k^{\,2}}\frac{g_{k+1/2}-g_{k-1/2}}{\Delta z} \tag{3.20}$$

where

$$g_{k+1/2} = \left(z^2\frac{\partial S_{i,k+1/2}}{\partial z}\right)_{k+1/2} \approx z_{k+1/2}^2\frac{S_{i,k+1}-S_{i,k}}{\Delta z} \tag{3.21}$$

$$g_{k-1/2} = \left(z^2\frac{\partial S_{i,k-1/2}}{\partial z}\right)_{k-1/2} \approx z_{k-1/2}^2\frac{S_{i,k}-S_{i,k-1}}{\Delta z} \tag{3.22}$$

The approximation of the mass balance for the solute concentrations (eq. 3.8) thus becomes:

$$\frac{dS_{i,k}}{dt} = D_{i,bio} \frac{z_{k+1/2}^2 \left(\frac{S_{i,k+1} - S_{i,k}}{\Delta z} \right) - z_{k-1/2}^2 \left(\frac{S_{i,k} - S_{i,k-1}}{\Delta z} \right)}{z_k^2 \Delta z} + r_{i,k} \tag{3.23}$$

For the particulate compounds, approximations of both the velocity and of the derivative of the velocity are needed. The derivative has been approximated with the following expression:

$$\left(\frac{du_F}{dz} \right)_k \approx \frac{\Delta u_{F,k}}{\Delta z} = \sum_{i=1}^{n_{part}} \frac{r_{i,k}}{\rho} \tag{3.24}$$

The integral in the equation describing the growth velocity (eq. 3.11) is approximated with the trapezoidal rule, so that the approximation of the velocity becomes:

$$u_{F,k} = \frac{1}{A_k} \sum_{1}^{k} \left(\frac{A_k \left(\Delta u_{F,k} / \Delta z \right) + A_{k+1} \left(\Delta u_{F,k+1} / \Delta z \right)}{2} \Delta z \right) \tag{3.25}$$

where A_k is the area of a sphere at the point k with the distance z_k to the center of the granule:

$$A_k = 4\pi z_k^2 \tag{3.26}$$

For the mass balance of the particulate compounds (eq. 3.10), the above expressions are used along with a backward difference approximation of the first order concentration space derivative. The approximated mass balance therefore becomes:

$$\frac{dX_{i,k}}{dt} = -u_{F,k} \frac{X_{i,k} - X_{i,k-1}}{\Delta z} - X_{i,k} \frac{\Delta u_{F,k}}{\Delta z} + r_{i,k} \tag{3.27}$$

For the particulate compounds the mass balance of the first node is approximated with a forward difference instead of a backwards difference as in all other nodes. The mass balance of the first node therefore becomes:

$$\frac{dX_{i,1}}{dt} = -u_{F,1} \frac{X_{i,2} - X_{i,1}}{\Delta z} - X_{i,1} \frac{\Delta u_{F,1}}{\Delta z} + r_{i,1} \tag{3.28}$$

Boundary conditions

In order to solve the equation system containing second order derivatives obtained above, appropriate boundary conditions at the center and at the biofilm/liquid interface need to be specified. At the center of the granule no change in concentration in space can be assumed, due to the symmetry of the granules. The boundary condition therefore becomes:

$$\frac{dS_i}{dz} = 0 \qquad z = 0 \tag{3.29}$$

This gives the following mass balance for the soluble compounds in the first node:

$$\frac{dS_{i,1}}{dt} = D_{i,bio}\frac{z_{1+1/2}^2\left(\frac{S_{i,2}-S_{i,1}}{\Delta z}\right)}{z_1^2\Delta z} + r_{i,1} \tag{3.30}$$

At the biofilm/liquid interface the continuity of flux applies, which means that the flux of mass to or from the internal part of the granules is equal to the flux of mass coming from the bulk. Here it is assumed that no microbial metabolism is taking place in the mass transfer boundary layer.

$$j_{i,L} = -j_{i,bulk} \Leftrightarrow D_{bio,i}\frac{dS_{i,L}}{dz} = k_i\left(S_{i,bulk} - S_{i,L}\right) \tag{3.31}$$

From this assumption, the concentration at the interface can be deduced:

$$\begin{aligned} &D_{i,bio}\frac{S_{i,L}-S_{i,L-1}}{\Delta z} = k_i\left(S_{i,bulk}-S_{i,L}\right) \\ &\Updownarrow \\ &S_{i,L} = \frac{k_i S_{i,bulk} + \left(D_{i,bio}/\Delta z\right)S_{i,L-1}}{D_{i,bio}/\Delta z + k_i} \end{aligned} \tag{3.32}$$

Given these boundary conditions, the reformulation of the PDE system of the process as a system of ODEs is now complete and ready for solution.

3.2.8 Model solving

The model equations derived above were implemented and solved with respect to time in the MATLAB-Simulink® R2009b software (The MathWorks, Natick, MA). The "*ode15s*" solver routine was used, which is a numerical multi-step variable order solver based on numerical differentiation formulas (NDFs).

In order to solve the ODE system dynamically, initial conditions for all dependent state variables were defined.

3.3 Model applied to CANR

Once the general framework for constructing a model describing a granule based bioreactor is in place, it can be applied to more specific cases. In this project investigation of autotrophic nitrogen removal was thoroughly investigated.

In the following, the compounds of interest and the processes affecting them are presented and described in detail. The model presented contains "default" parameters collected from relevant literature and from operation for initial analysis. Subsequent analysis of these parameters is presented elsewhere in the dissertation (see e.g. chapter 6).

3.3.1 Model states and variables

The soluble compounds included in the modeling were the nitrogen species; total ammonium nitrogen ($S_{TAN} = S_{NH4} + S_{NH3}$), total nitrite nitrogen ($S_{TNN} = S_{NO2} + S_{HNO2}$), nitrate ($S_{NO3}$), free nitrogen gas ($S_{N2}$) along with oxygen ($S_{O2}$) and soluble readily biodegradable organic material (S_S) (Table 3.2). The particulate compounds were the autotrophic microbial groups; ammonium oxidizing bacteria (X_{AOB}), nitrite oxidizing bacteria (X_{NOB}), anaerobic ammonium oxidizing bacteria (X_{AnAOB}). Heterotrophic bacteria (X_{HB}) were also included since they can utilize decay products originating from other microbial groups as substrate. So even if organic material is not supplied to the system, there will always be some organic carbon originating from biological activity, which heterotrophic organisms can thrive on. Among the particulate compounds are also inert material (X_I) and particulate organic material (X_S).

Table 3.2 Overview of independent variables and dependent or state variables included in the model.

Independent variables	**Symbol**	**Unit**
Space	z	m
Time	t	d
Dependent variables	**Symbol**	**Unit**
Soluble compounds		
Total ammonium nitrogen	S_{TAN}	g N m^{-3}
Total nitrite nitrogen	S_{TNN}	g N m^{-3}
Nitrate	S_{NO3}	g N m^{-3}
Nitrogen gas	S_{N2}	g N m^{-3}
Oxygen	S_{O2}	g COD m^{-3}
Readily biodegradable organic carbon	S_S	g COD m^{-3}
Particulate compounds		
Aerobic ammonium oxidizing bacteria	X_{AOB}	g COD m^{-3}
Nitrite oxidizing bacteria	X_{NOB}	g COD m^{-3}
Anaerobic ammonium oxidizing bacteria	X_{AnAOB}	g COD m^{-3}
Heterotrophic bacteria	X_{HB}	g COD m^{-3}
Inert material	X_I	g COD m^{-3}
Particulate organic material	X_S	g COD m^{-3}
Granule size	L	m
Volume	V	m^3

3.3.2 Model processes

In this case, the processes considered in the model are biological processes plus hydrolysis and aeration. Aeration is modeled as a mass transfer process from gas to liquid at the reactor scale.

All process rates and stoichiometric coefficients are summarized in Table 3.3 and 3.4.

As biological processes, growth and decay of all the microbial groups were considered. Biomass decay was modeled according to the death-regeneration concept as in the activated sludge model no. 1 (ASM1), which means that the decay rate is a first order expression with respect to the biomass concentration (Table 3.4).

The unionized forms of the compounds were considered to be the true substrates for AOB, NOB (Anthonisen et al., 1976) and AnAOB (van Hulle et al., 2007; Tora et al., 2010). Thus, AOB used ammonia (NH_3) and were product inhibited by free nitrous acid (HNO_2). The AOB growth process rate therefore includes Monod expressions of ammonium and oxygen and an inhibition term for

nitrous acid (Table 3.4). NOB grew on nitrous acid, and Monod expressions of oxygen and nitrous acid are therefore included in the process rate. AnAOB utilized ammonia and nitrous acid and were inhibited by oxygen, which is therefore reflected in the AnAOB growth process rate (Table 3.4). For the HB, three growth terms, using different electron acceptors but always with S_S as electron donor, were considered. All three growth related process rates therefore include Monod expressions of readily degradable organic carbon and TAN, since these compounds are assimilated for new biomass cell production (Table 3.3). The first growth term is based on oxygen as electron acceptor, the second on TNN as electron acceptor, and the third HB growth term is based on nitrate as electron acceptor. The latter two processes assume that the HB perform complete denitrification and N_2 is thus the product of both processes. Both denitrification processes are inhibited by oxygen, which is expressed in the process rate through a Monod inhibition term including the oxygen concentration and through an anoxic correction factor also termed anoxic inactivation constant (η_{HB}) (Henze et al., 1987).

The hydrolysis process converts particulate organic material into soluble organic matter and TAN through a first order rate process (Table 3.4).

Aeration is modeled as a gas to liquid transfer process with the concentration gradient being the driving force, which is multiplied by the volumetric mass transfer coefficient (k_La) (Table 3.4).

For simplicity and as a starting point, the pH is considered constant in space and in time when the model is solved dynamically. In chapter 5, the effect of including pH gradients in the granules is tackled.

The constant pH value considered was 7.5. The acid-base reactions are very fast and the equilibria are therefore considered immediate. The ammonia concentration is thus calculated as:

$$C_{NH_3} = \frac{C_{TAN}}{1+10^{-pH+pK_{NH4}}} \tag{3.33}$$

The nitrous acid concentration was calculated in a similar fashion:

$$C_{HNO_2} = \frac{C_{TNN}}{1+10^{pH-pK_{HNO2}}} \tag{3.34}$$

All kinetic parameters, their default values, and the appropriate references can be seen in Table 3.5. Temperature dependency was considered for maximum growth rates and for decay rates.

Stoichiometric parameters are shown in Table 3.6, while biofilm characteristics and mass transfer parameters are highlighted in Table 3.7.

Table 3.3 Process stoichiometry. Dependent variables in the columns and processes in the rows. The composition of the compounds are given in the last two rows and are helpful in checking the consistency of the model.

Stoichiometric coefficients	S_{TAN}	S_{O2}	S_{TNN}	S_{NO3}	S_{N2}	S_S	X_{AOB}	X_{NOB}	X_{AnAOB}	X_{HB}	X_S	X_I
Compound *i* ▸	1	2	3	4	5	6	7	8	9	10	11	12
Process *h* ▾	g N m^{-3}	g COD m^{-3}	g N m^{-3}	g N m^{-3}	g N m^{-3}	g COD m^{-3}	g COD m^{-3}	g COD m^{-3}	g COD m^{-3}	g COD m^{-3}	g COD m^{-3}	g COD m^{-3}
1. AOB growth	$-\frac{1}{Y_{AOB}}-i_{NXB}$	$-\frac{3.43-Y_{AOB}}{Y_{AOB}}$	$\frac{1}{Y_{AOB}}$				1					
2. NOB growth		$-\frac{1.14-Y_{NOB}}{Y_{NOB}}$	$-\frac{1}{Y_{NOB}}$	$\frac{1}{Y_{NOB}}$				1				
3. AnAOB growth	$-\frac{1}{Y_{AnAOB}}-i_{NXB}$		$-\frac{1}{Y_{AnAOB}}-1.52$	1.52	$\frac{2}{Y_{AnAOB}}$				1			
4. AOB decay							-1				1- f_i	f_i
5. NOB decay								-1			1- f_i	f_i
6. AnAOB decay									-1		1- f_i	f_i
7. HB growth 1	$-i_{NXB}$	$-\frac{1-Y_{HB}}{Y_{HB}}$				$-\frac{1}{Y_{HB}}$				1		
8. HB growth 2	$-i_{NXB}$		$-\frac{1-Y_{HB}}{1.71Y_{HB}}$		$\frac{1-Y_{HB}}{1.71Y_{HB}}$	$-\frac{1}{Y_{HB}}$				1		
9. HB growth 3	$-i_{NXB}$			$-\frac{1-Y_{HB}}{2.86Y_{HB}}$	$\frac{1-Y_{HB}}{2.86Y_{HB}}$	$-\frac{1}{Y_{HB}}$				1		
10. HB decay										-1	1- f_i	f_i
11. Hydrolysis	$\frac{i_{NXB}-f_i i_{NXI}}{1-f_i}$					1					-1	
12. Aeration		1										
N composition (g N/ g default unit)	*1*	*0*	*1*	*1*	*1*	*0*	i_{NXB}	i_{NXB}	i_{NXB}	i_{NXB}	$\frac{i_{NXB}-f_i i_{NXI}}{1-f_i}$	i_{NXI}
COD composition (g COD/ g default unit)	*0*	*-1*	*-3.43*	*-4.57*	*-1.71*	*1*	*1*	*1*	*1*	*1*	*1*	*1*

Table 3.4 Process rate expressions for the 12 processes included in the model.

Process k ▾	*Process Rate* ρ
1. AOB growth	$\mu_{max,AOB}\, X_{AOB}\, \frac{S_{NH3}}{K_{NH3,AOB}+S_{NH3}}\, \frac{S_{O2}}{K_{O2,AOB}+S_{O2}}\, \frac{K_{I,HNO2,AOB}}{K_{I,HNO2,AOB}+S_{HNO2}}$
2. NOB growth	$\mu_{max,NOB}\, X_{NOB}\, \frac{S_{HNO2}}{K_{HNO2,NOB}+S_{HNO2}}\, \frac{S_{O2}}{K_{O2,NOB}+S_{O2}}$
3. AnAOB growth	$\mu_{max,AnAOB}\, X_{AnAOB}\, \frac{S_{NH3}}{K_{NH3,AnAOB}+S_{NH3}}\, \frac{S_{HNO2}}{K_{HNO2,AnAOB}+S_{HNO2}}\, \frac{K_{I,O2,AnAOB}}{K_{I,O2,AnAOB}+S_{O2}}$
4. AOB decay	$b_{AOB}\, X_{AOB}$
5. NOB decay	$b_{NOB}\, X_{NOB}$
6. AnAOB decay	$b_{AnAOB}\, X_{AnAOB}$
7. HB growth 1	$\mu_{max,HB}\, X_{HB}\, \frac{S_{O2}}{K_{O2,HB}+S_{O2}}\, \frac{S_S}{K_{S,HB}+S_S}\, \frac{S_{TAN}}{S_{TAN}+K_{TAN,HB}}$
8. HB growth 2	$\mu_{max,HB}\, X_{HB}\, \lambda_{HB}\, \frac{S_S}{K_{S,HB}+S_S}\, \frac{S_{TNN}}{K_{TNN,HB}+S_{TNN}}\, \frac{K_{I,O2,HB}}{K_{I,O2,HB}+S_{O2}}\, \frac{S_{TAN}}{S_{TAN}+K_{TAN,HB}}$
9. HB growth 3	$\mu_{max,HB}\, X_{HB}\, \lambda_{HB}\, \frac{S_S}{K_{S,HB}+S_S}\, \frac{S_{NO3}}{K_{NO3,HB}+S_{NO3}}\, \frac{K_{I,O2,HB}}{K_{I,O2,HB}+S_{O2}}\, \frac{S_{TAN}}{S_{TAN}+K_{TAN,HB}}$
10. HB decay	$b_{HB}\, X_{HB}$
11. Hydrolysis	$k_H \frac{X_S}{K_X}$
12. Aeration	$k_L a(S_{O2\_sat} - S_{O2\_bulk})$

Parameter values

Table 3.5 Kinetics parameter and their default values.

Parameter	Symbol	Value	Unit	Reference
AOB				
Max growth rate	$\mu_{max,AOB}$	$0.8e^{-0.094(293-T)}$	day^{-1}	(Hao et al., 2002)
Oxygen half saturation constant	$K_{O2,AOB}$	0.3	g O_2 m^{-3}	(Wiesmann, 1994)
Ammonia half saturation constant	$K_{NH3,AOB}$	0.75	g N m^{-3}	(Van Hulle, 2005)
Nitrous acid inhibition constant	$K_{I,HNO2,AOB}$	2.04	g N m^{-3}	(Van Hulle, 2005)
Decay rate	b_{AOB}	$0.05e^{-0.094(293-T)}$	day^{-1}	(Hao et al., 2002)
NOB				
Max growth rate	$\mu_{max,NOB}$	$0.79e^{-0.061(293-T)}$	day^{-1}	(Hao et al., 2002)
Oxygen half saturation constant	$K_{O2,NOB}$	1.1	g O_2 m^{-3}	(Wiesmann, 1994)
Nitrous acid half saturation constant	$K_{HNO2,NOB}$	$3.09*10^{-4}$	g N m^{-3}	(Wiesmann, 1994)
Decay rate	b_{NOB}	$0.033e^{-0.061(293-T)}$	day^{-1}	(Hao et al., 2002)
AnAOB				
Max growth rate	$\mu_{max,AnAOB}$	$0.028e^{-0.096(293-T)}$	day^{-1}	(Hao et al., 2002)
Ammonia half saturation constant	$K_{NH3,AnAOB}$*	$5.33*10^{-3}$	g N m^{-3}	(Van Hulle, 2004)
Nitrous acid half saturation constant	$K_{HNO2,AnAOB}$*	$1.69*10^{-5}$	g N m^{-3}	(Van Hulle, 2005)
Oxygen inhibition constant	$K_{O2,AnAOB}$	0.01	g O_2 m^{-3}	(Strous et al., 1999)
Decay rate	b_{AnAOB}	$0.001e^{-0.096(293-T)}$	day^{-1}	(Hao et al., 2002)
HB				
Max growth rate	$\mu_{max,HB}$	$6e^{-0.069(293-T)}$	day^{-1}	(Henze et al., 2000) (ASM1)
Oxygen half saturation/inhibition constant	$K_{O2,HB}$	0.20	g O_2 m^{-3}	(Henze et al., 2000) (ASM1)
Organic substrate half saturation constant	$K_{S,HB}$	20	g COD m^{-3}	(Henze et al., 2000) (ASM1)
Nitrite half saturation constant	$K_{NO2,HB}$	0.5	g N m^{-3}	(Henze et al., 2000) (ASM1)
Nitrate half saturation constant	$K_{NO3,HB}$	0.5	g N m^{-3}	(Henze et al., 2000) (ASM1)
Ammonium half saturation constant	$K_{TAN,HB}$	0.01	g N m^{-3}	(Henze et al., 2000) (ASM3)
Anoxic correction factor	η_{HB}	0.8	-	(Henze et al., 2000) (ASM1)
Decay rate	b_{HB}	$0.62e^{-0.113(293-T)}$	day^{-1}	(Henze et al., 2000) (ASM1)

* Have been calculated at pH=7.5

Table 3.6 Stoichiometric parameters and their default values.

Parameter	Symbol	Value	Unit	Reference
AOB growth yield	Y_{AOB}	0.21 (0.15)	g COD (g N)$^{-1}$ (g VSS (g N)$^{-1}$)	(Wiesmann, 1994)
NOB growth yield	Y_{NOB}	0.059 (0.042)	g COD (g N)$^{-1}$ (g VSS (g N)$^{-1}$)	(Wiesmann, 1994)
AnAOB growth yield	Y_{AnAOB}	0.159 (0.07)	g COD (g N)$^{-1}$ (mol C (mol N)$^{-1}$)	(Strous et al., 1998)
HB growth yield	Y_{HB}	0.67	g COD (g COD)$^{-1}$	(Henze et al., 2000) (ASM1)
Inert content in biomass	f_i	0.08	g COD (g COD)$^{-1}$	(Henze et al., 2000) (ASM1)
Nitrogen content in inert	i_{NXI}	0.06	g N (g COD)$^{-1}$	(Henze et al., 2000) (ASM1)
Nitrogen content in biomass	i_{NXB}	0.086	g N (g COD)$^{-1}$	(Henze et al., 2000) (ASM1)

Table 3.7 Biofilm and mass transfer parameters and their default values.

Parameter	Symbol	Value	Unit	Reference
Biomass density	ρ	50000	g COD m^{-3}	(Koch et al., 2000)
Biofilm porosity	θ	0.75	-	(Koch et al., 2000)
Max granule radius	z_{max}	0.001	m	(Koch et al., 2000; Vlaeminck et al., 2009)
Boundary layer thickness	L_B	10^{-5}-10^{-4}	m	(Nicolella et al., 1998)
Hydrolysis rate	k_H	$3e^{-0.110(293-T)}$	day^{-1}	(Henze et al., 2000) (ASM1)
Hydrolysis half saturation constant	K_X	$0.3e^{-0.110(293-T)}$	g COD (g COD)$^{-1}$	(Henze et al., 2000) (ASM1)
Diffusivity of Ammonium in water	D_{NH4}	1.7e-4	m^2 day^{-1}	(Perry and Green, 1997)
Diffusivity of Nitrite in water	D_{NO2}	2.6e-4	m^2 day^{-1}	(Perry and Green, 1997)
Diffusivity of Nitrate in water	D_{NO3}	2.6e-4	m^2 day^{-1}	(Perry and Green, 1997)
Diffusivity of Oxygen in water	D_{O2}	2.2e-4	m^2 day^{-1}	(Perry and Green, 1997)
Diffusivity of nitrogen gas in water	D_{N2}	1.6e-4	m^2 day^{-1}	(Perry and Green, 1997)
Diffusivity of Bicarbonate in water	D_{alk}	1.7e-4	m^2 day^{-1}	(Perry and Green, 1997)
Diffusivity of organic matter in water	D_S	1e-4	m^2 day^{-1}	(Hao and van Loosdrecht, 2004)
Ratio biofilm/water diffusivity	f	0.75	-	
Nitric acid dissociation constant	pKa	3.25	-	
Ammonium dissociation constant	pKa	9.25	-	

3.3.3 Reactor operation – CSTR vs. SBR

The abovementioned model can be used to simulate both continuous systems and systems of a more discrete nature such as fed-batch reactors or SBRs.

In a CSTR type system, influent and effluent are continuously fed to and leaving the system, and the bulk liquid is continuously aerated. The bulk liquid volume will thus be constant and its derivative will be equal to zero:

$$\frac{dV_{reactor}}{dt} = 0 \tag{3.35}$$

The mass balance of the compounds in the bulk liquid can therefore be simplified to:

$$\frac{dC_{i,bulk}}{dt} = \frac{Q_{in}C_{i,in} - Q_{out}C_{i,bulk} - j_{bio,i}A}{V_{reactor}} + r_{i,bulk} \tag{3.36}$$

where $V_{reactor}$, Q_{in}, and Q_{out} are constants.

In the SBR system, the model structure is the same, but some parameters change value from one phase to another. An SBR cycle consists of the following phases: Fill, reaction, settling, draw, and idle, as outlined in the description of the experimental setup in the previous chapter 2. Q_{in} has a certain value during the fill phase and is zero during the other phases. The same applies to Q_{out}, which only has a positive value during the draw phase, but is zero during the other phases. Finally the aeration, in the form of the value of the mass transfer coefficient (k_La), is only active during the reaction phase and k_La has a value of zero during the other phases (see Figure 3.5).

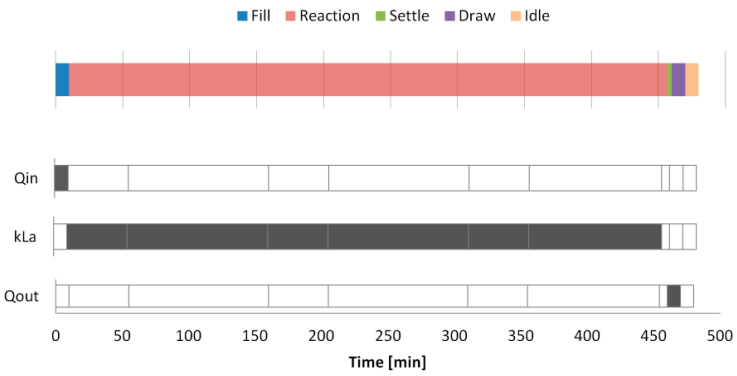

Figure 3.5 Schematic illustration of operational parameters affected by the SBR operation.

Another prominent difference between modeling a continuous and an SBR system is that during the settling phase of the SBR operation, the free cells suspended in the bulk liquid settle to a certain degree. Perfect settling is assumed, and the non-settled fraction is included in the effluent by adding a multiplication factor (φ) to the bulk liquid particulate concentration in the mass balance during the draw phase:

$$\frac{dX_{i,bulk}}{dt} = \frac{Q_{in}X_{i,in} - Q_{out}X_{i,bulk}\varphi - j_{bio,i}A}{V_{reactor}} + r_{i,bulk} \tag{3.37}$$

where $X_{i,in}$ is the influent concentration of the particulate species, which is assumed zero in this case, and a value of φ=1 represents perfect mixing and φ=0 perfect retention.

The value of the non-settled fraction can be found through solving the linear ODE:

$$\frac{dX_{i,bulk}}{dt}\left(V_0 - Q_{out}t\right) = Q_{out}X_{i,bulk}\left(1-\varphi\right) \tag{3.38}$$

This equation can be analytically solved with an integration factor, and φ can be isolated:

$$\varphi = \frac{\log\left(\frac{X_{i,bulk}(t)}{X_0}\right)}{\log\left(\frac{V_0}{V_0 - Q_{out}t}\right)} \tag{3.39}$$

Assuming that 80% of the mass of the free floating cells is retained, a value of φ=0.32 is obtained.

In this project both continuous systems and SBRs were investigated and simulated. A continuous system was used as basis for model investigations presented in chapter 4 and 5, and for idea generation and initial testing of control strategies (chapter 7), while sequential batch mode was used during calibration and validation (chapter 6) and control strategy testing in chapter 8.

3.3.4 Model solution for the CANR system

Since the number of discretization points can significantly affect the results, different numbers of discretization layers were tested, and a number of 100 was found to be sufficient for the solution as no significant change in the results was observed when additional discretization nodes were included.

PART II - Simulation, Scenario, and Sensitivity Analyses

This part presents the results of the simulation studies of the CANR process, which were aimed at gaining a better understanding of the mechanisms and interactions affecting the process. In chapter 4, the relative importance of microbial kinetics and mass transfer was investigated through a global sensitivity analysis study performed under a number of different operation scenarios. In chapter 5, the effect of including pH as a variable in the system (instead of assuming it constant) was investigated by developing a pH model and an effective solution strategy.

4 Sensitivity analysis: Influence of mass transfer versus microbial kinetics

Summary

A comprehensive global sensitivity analysis was conducted under a range of operating conditions. The relative importance of mass transfer resistance versus kinetic parameters was studied and found to depend on the operating regime as follows: When operating under the optimal loading ratio of 1.90 (g O_2 m^{-3} d^{-1})/(g N m^{-3} d^{-1}), the system was influenced by mass transfer (10% impact on nitrogen removal) and performance was limited by AOB activity (75% impact on nitrogen removal), while operating above the optimal loading ratio, AnAOB activity was limiting (68% impact on nitrogen removal). In that case, the negative effect of oxygen mass transfer had an impact of 15% on nitrogen removal. Summarizing such quantitative analyses led to formulation of an optimal operation window, which serves as a valuable tool for diagnosis of performance problems and identification of optimal solutions in nitritation-anammox applications.

4.1 Introduction

A better understanding of which mechanisms and which process steps control and affect the microbial community composition and the process performance is essential for future operation and optimization of the nitrogen removal process.

Previous contributions have attempted to identify the key phenomena involved in the operation and establishment of microbial communities based on local sensitivity analysis studies (Hao et al., 2002a; Terada et al., 2007). In these modeling studies, external mass transfer resistance was neglected and only kinetic and biomass related parameters were considered. The relative importance of the mass transfer and its interaction with microbial kinetics were therefore not examined. It has previously been shown that inclusion of external mass transfer has an impact on the parameter identifiability in nitrifying biofilms (Brockmann et al., 2008), and it is therefore of interest to investigate the sensitivity towards this mass transfer. To overcome the limitations of the local sensitivity analysis and the lack of the external mass transfer resistance of previous studies and to expand the boundary of the process analysis, this study use global sensitivity analysis with a significantly expanded scope. The global sensitivity analysis, e.g. linear regression of Monte Carlo (MC) simulations, has previously been demonstrated as a useful tool to diagnose the state of the system, obtain valuable insights, and identify bottlenecks in a process (Sin et al., 2011).

The aim of the work presented in this chapter was, therefore, to elucidate which mechanisms were the most influential on the process performance of a single-stage complete autotrophic nitrogen removing granular sludge reactor. Specific emphasis was put on diagnosing the key step in the overall process for a given set of operating conditions. Mass transfer parameters and microbial kinetic parameters and their individual impacts on the concentrations of substrates, intermediates, products, and bacterial groups were therefore investigated for several scenarios considering different influent conditions, different operational strategies and different granule sizes. To this end, a model-based methodology that employs global sensitivity analysis techniques along with the 1-D multi-scale multi-species granular biofilm model from chapter 3 was developed and used.

4.2 Methods

Before carrying out the sensitivity analysis, scenarios of interest were first identified, and appropriate models were set up. The key steps in the uncertainty and sensitivity analysis were defined, which included identifying and characterizing parameter uncertainty, sampling of the defined parameter space, and performing Monte Carlo simulations (Sin et al., 2009). The sensitivity of the uncertain parameters was then quantified by constructing linear models of selected model outputs, and finally the sensitivity analysis results were evaluated by putting them into context with the system information of the given scenario.

4.2.1 Step 1: System description

To formulate realistic settings and scenarios for simulations and sensitivity analysis, the physical system in this study was defined considering the lab-scale reactor described in chapter 2 (Table 4.1) as a reference system. The operating temperature was set to 25°C, the pH was 7.5, and the vessel was mixed by a mechanical impeller operated at 80 rpm and by bubble aeration. The mixing in this modeling study was considered sufficient enough to assume the bulk liquid to be a completely mixed compartment.

Table 4.1 Description of scenarios for sensitivity analysis of the autotrophic nitrogen removal system.

Operation variable	Scenario 1 – Mimicking lab-scale reactor - TNN limited	Scenario 2 – Effect of increased aeration rate (double)	Scenario 3 – Effect of smaller granule size	Scenario 4 – Effect of higher loadings
N loading	0.2 g L^{-1} d^{-1}	0.2 g L^{-1} d^{-1}	0.2 g L^{-1} d^{-1}	**0.65 g L^{-1} d^{-1}**
HRT	1 d	1 d	1 d	1 d
k_La	43 d^{-1}	**86 d^{-1}**	43 d^{-1}	140 d^{-1}
Granule size	2 mm	2 mm	**0.5-2 mm**	2 mm
WWT type	Low digester effluent strength	Low digester effluent strength	Low digester effluent strength	**High digester effluent strength**

Scenario formulation for sensitivity analysis

In scenario 1, an experimentally determined oxygen mass transfer coefficient (k_La) was used (43 d^{-1}), and the volumetric nitrogen loading (in the form of total ammonium nitrogen, TAN) was 200

g N m^{-3} d^{-1}. The solids concentration was maintained at 3.14 g VSS L^{-1} in the reactor, which is within the range of lab-scale (Vazquez-Padin et al., 2009; Figueroa et al., 2012) and full-scale observations (Joss et al., 2009). This solids concentration was used as a reference in the simulations and scenarios for the sensitivity analysis. The mass transfer coefficients were determined using a semi-empirical correlation for mixed reactors with aeration (Nicolella et al., 1998). The average thickness of the external mass transfer boundary layer (L_B) was estimated to be 64 μm, which is also within the range reported in attached growth experiments (Masic et al., 2010). Three additional scenarios were evaluated (Table 4.1). In scenario 2, the effect of oxygen supply was investigated by doubling the mass transfer coefficient. In scenario 3, the effect of granule sizes was investigated. Lastly, the effect of high influent loading was investigated in scenario 4. In the latter scenario, the oxygen supply was simultaneously increased by increasing the k_La to 140 d^{-1}.

4.2.2 Step 2: Model description

The model of the CANR process operated as a continuous system, described in chapter 3, was used as basis for the analysis.

The steady state concentrations in the biofilm and the bulk liquid were found by simulating the system for a sufficiently long time (in this case 5000 days) using the default parameter values shown in Table 4.2. These steady state concentrations were used as initial conditions for the mass balance equations for each of the scenarios.

Table 4.2 Parameters included in the uncertainty analysis and the classification of their uncertainties.

No.	Parameter	Default value at 20°C	Unit	Reference	Uncertainty class
1	$\mu_{max,AOB}$	0.80	day^{-1}	Hao et al., 2002b	2
2	$K_{O2,AOB}$	0.30	g O_2 m^{-3}	Wiesmann, 1994	3
3	$K_{NH3,AOB}$	0.04	g N m^{-3}	Wiesmann, 1994	3
4	$K_{HNO2,AOB}$	2.04	g N m^{-3}	Van Hulle et al., 2007	3
5	b_{AOB}	0.05	day^{-1}	Hao et al., 2002b	2
6	$\mu_{max,NOB}$	0.79	day^{-1}	Hao et al., 2002b	2
7	$K_{O2,NOB}$	1.10	g O_2 m^{-3}	Wiesmann, 1994	3
8	$K_{HNO2,NOB}$	3.09e-4	g N m^{-3}	Wiesmann, 1994	3
9	b_{NOB}	0.033	day^{-1}	Hao et al., 2002b	2
10	$\mu_{max,AnAOB}$	0.028	day^{-1}	Hao et al., 2002b	2
11	$K_{O2,AnAOB}$	0.01	g O_2 m^{-3}	Strous et al., 1999	3
12	$K_{NH3,AnAOB}$	1.20e-3	g N m^{-3}	Strous et al., 1998	3
13	$K_{HNO2,AnAOB}$	2.81e-6	g N m^{-3}	Strous et al., 1998	3
14	b_{AnAOB}	0.001	day^{-1}	Hao et al., 2002b	2
15	$\mu_{max,HB}$	6.00	day^{-1}	Henze et al., 2000(ASM1)	2
16	$K_{O2,HB}$	0.20	g O_2 m^{-3}	Henze et al., 2000 (ASM1)	3
17	$K_{S,HB}$	20.0	g COD m^{-3}	Henze et al., 2000 (ASM1)	3
18	$K_{TNN,HB}$	0.50	g N m^{-3}	Henze et al., 2000 (ASM1)	3
19	$K_{NO3,HB}$	0.50	g N m^{-3}	Henze et al., 2000 (ASM1)	3
20	$K_{TAN,HB}$	0.01	g N m^{-3}	Henze et al., 2000 (ASM3)	3
21	η_{HB}	0.80	-	Henze et al., 2000 (ASM1)	2
22	b_{HB}	0.62	day^{-1}	Henze et al., 2000 (ASM1)	1
23	Y_{AOB}	0.21	g COD (g N)$^{-1}$	Wiesmann, 1994	1
24	Y_{NOB}	0.059	g COD (g N)$^{-1}$	Wiesmann, 1994	1
25	Y_{AnAOB}	0.159	g COD (g N)$^{-1}$	Strous et al., 1998	1
26	Y_{HB}	0.67	g COD (g COD)$^{-1}$	Henze et al., 2000 (ASM1)	1
27	f_i	0.08	g COD (g COD)$^{-1}$	Henze et al., 2000 (ASM1)	2
28	i_{NXI}	0.06	g N (g COD)$^{-1}$	Henze et al., 2000 (ASM1)	2
29	i_{NXB}	0.086	g N (g COD)$^{-1}$	Henze et al., 2000 (ASM1)	2
30	k_H	3.00	day^{-1}	Henze et al., 2000 (ASM1)	1
31	K_X	0.30	g COD (g COD)$^{-1}$	Henze et al., 2000 (ASM1)	1
32	D_{NH4}	1.70e-4	m^2 day^{-1}	Perry and Green, 1997	2
33	D_{NO2}	2.60e-4	m^2 day^{-1}	Perry and Green, 1997	2
34	D_{O2}	2.20e-4	m^2 day^{-1}	Perry and Green, 1997	2
35	D_{NO3}	2.60e-4	m^2 day^{-1}	Perry and Green, 1997	2
36	D_{N2}	1.60e-4	m^2 day^{-1}	Perry and Green, 1997	2
37	D_S	1.00e-4	m^2 day^{-1}	Perry and Green, 1997	2
38	L_B	6.40e-5	m	Nicolella et al., 1998	3

4.2.3 Step 3: Uncertainty analysis

Based on the approach of Brun et al. (2002) and Sin et al. (2009), the included parameters were divided into three uncertainty classes based on available expert knowledge. All included parameters were assumed to have a uniform probability distribution, since knowledge about their true distributions was scarce. The parameters in class 1 were considered quite well known and their corresponding uniform distributions were bounded 5% around the default value. The parameters belonging to class 2 had an intermediate level of uncertainty with a uniform distribution bounded 25% around the default value. Finally, the parameters in class 3 were classified to have the highest uncertainty with 50% variability around the default value.

Parameters related to the microbial kinetics and related to mass transfer were selected for sensitivity analysis, while all others, e.g. influent characteristics, were kept constant at the values specified in each scenario. Maximum growth rates, decay rates, half saturation constants, inhibition constants plus composition and yield coefficients of the microbial groups were making up the first group of parameters. The diffusivities and the thickness of the mass transfer boundary layer (MTBL) belonged to the second group of parameters. All together, 38 parameters were included in the uncertainty analysis (Table 4.2).

For the three microbial groups AOB, NOB, and AnAOB, the maximum growth rates and the decay rates were considered intermediately uncertain (class 2), and the half saturation constants and inhibition constants belonged to the most uncertain group of parameters (Hao et al., 2002a). Especially the oxygen half saturation constants of the nitrifying bacterial groups have been a subject of debate in the literature previously (Hao et al., 2002a; Brockmann and Morgenroth 2010). The uncertainties of parameters related to the HB were classified as suggested in Sin et al. (2009). The yield coefficients of all involved microbial groups were considered rather well-known and were placed in the first uncertainty class. The composition of biomass has in many cases been estimated, but the variation within the microbial groups (maybe due to diversity of species) is still considered significant. i_{NXB}, i_{NXI}, and f_i were therefore in class 2. Hydrolysis related parameters have been placed in the first class, because their deviations have been estimated to be low (Insel et al., 2003). The diffusivities were classified as intermediately unknown, because they were experimentally quite well established in aqueous solution. However, the granule matrix composition was an unknown factor affecting the effective diffusivity within the granules, and their values were thus considered intermediately unknown. Finally, the MTBL thickness has been given the highest uncertainty, because it was difficult to estimate and measure its true

value due to its high sensitivity to the hydrodynamic conditions around the granule (Masic et al., 2010; Boltz et al., 2011).

The above defined parameter space was sampled by the Latin Hypercube Sampling (LHS) method (Iman and Conover, 1982). The parameters were considered to be uncorrelated due to unavailability of the information on the correlation matrix. As the sampling number from the joint probability distributions of the uncertain parameter space, 500 samples were taken and used for Monte Carlo simulations of the system for a period of 5000 days, from which the steady state model outputs were obtained. Similar time periods needed to reach steady state in such systems have been reported elsewhere (Volcke et al., 2010).

The model outputs formed the basis of the subsequent sensitivity analysis.

4.2.4 Step 4: Linear regression of Monte Carlo simulations

The sensitivity was found by performing linear regression on each of the model outputs. A first order linear multivariate model was fitted to the model outputs (y_k), which was relating it to the parameter values (θ_i) (Saltelli et al., 2008):

$$y_{reg,k} = a_k + \sum_i b_{k,i}\theta_i \tag{4.1}$$

where a_k and $b_{k,i}$ are linear regression coefficients. The standardized linear regression coefficients (SRCs), $\beta_{k,i}$, were obtained by making eq. 4.1 non-dimensional by mean-centered sigma-scaling, where μ_{yk} and $\mu_{\theta i}$ are the mean values and σ_{yk} and $\sigma_{\theta i}$ are the standard deviations of the model outputs and input parameters, respectively:

$$\frac{y_{reg,k} - \mu_{yk}}{\sigma_{yk}} = \sum_i \left(\beta_{k,i} \frac{\theta_i - \mu_{\theta i}}{\sigma_{\theta i}} \right) \tag{4.2}$$

The linear coefficient ($b_{k,i}$) is related to the standardized coefficient in the following way:

$$\beta_{k,i} = b_{k,i} \frac{\sigma_{\theta i}}{\sigma_{yk}} \tag{4.3}$$

If the model was linearly additive, then $\sum_i \beta_i^2 = 1$ for each model output, and β_i^2 would represent the relative variance contribution of parameter i and thus be giving a measure of the importance of the model output. In this study the model was assumed linear if the squared coefficient of correlation (R^2) between the Monte Carlo simulation output (y_k) and the regressed linear output ($y_{reg,k}$) was above 0.7. A parameter was considered sensitive or significant when $|\beta_i| \geq 0.1$, meaning that the parameter approximately contributed with at least 1% of the model output variance (Sin et al., 2011).

4.3 Results and discussion

Ten selected outputs were evaluated after reaching steady state for every set of parameter values. To obtain more details on how the entire process was affected, the bulk concentrations of TAN, TNN, nitrate, and DO on top of N_2 (which is equal to the nitrogen removal and represents the process performance) were selected for evaluation. The last five model outputs evaluated were the mass fractions of the particulate species within the granules, namely the AOB, AnAOB, NOB, HB, and the inert material, which gave information about the microbial community composition.

4.3.1 Steady state bulk concentrations and microbial composition

The steady state concentrations of soluble compounds and the granule composition, found by simulations using the default parameter values and operation as specified in scenario 1, can be seen in Figure 4.1A. Oxygen and TNN were depleted within the first few hundred μm, while TAN penetrated the entire granule. HB were only present in low concentrations close to the biofilm/bulk liquid interface, and NOB were present in negligible concentrations.

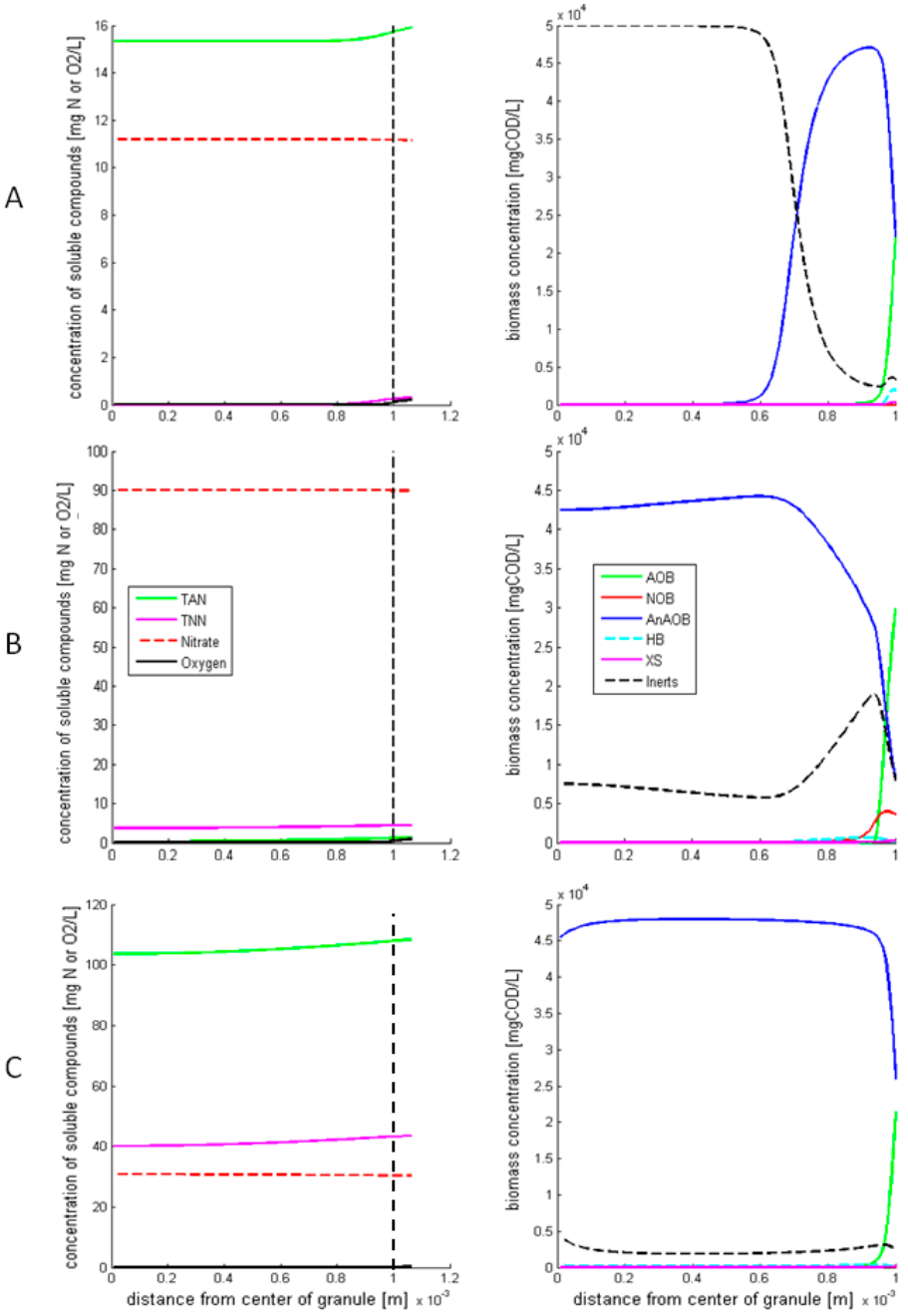

Figure 4.1 Soluble compounds and biomass concentrations inside the granule obtained from simulations using the default parameter values. The dashed vertical line indicates the position of the biofilm/liquid interface. A: scenario 1, B: scenario 2, and C: scenario 4.

Significance of microbial conversion kinetics vs. mass transfer parameters on bulk concentrations and process performance in scenario 1

All model outputs, except for the NOB mass fraction, could be sufficiently linearized to obtain the SRCs. The individual SRCs for each parameter for each scenario can be found in appendix A2. In order to investigate the influence of the microbial kinetics versus mass transfer, all the parameters were consolidated into these two groups. In Table 4.3 the sum of the squared SRCs of these groups are shown.

Overall, microbial kinetics explained most of the variance in the model outputs. However, for N_2, TNN, DO, and for the AOB mass fraction, 10-20% of the variance could be assigned to mass transfer related parameters (Table 4.3). If oxygen and TNN were more available, e.g. by reducing mass transfer resistance by decreasing L_B, it would have a positive impact on the AOB and AnAOB activity, respectively. The TNN availability was limiting the AnAOB activity and thus the overall nitrogen removal process (the N_2 concentration in the bulk). Supporting this model-based finding, the limitation of TNN availability to the AnAOB was also identified as the determining factor in recent experimental studies in the marine environment (Rush et al., 2012) and found to be the limiting factor for the performance in a rotating biological contactor by Koch et al. (2000).

Table 4.3 Grouping and summary of the standardized linear regression coefficients given as sum of the squared SRCs within each group.

Output →	**TAN**	**TNN**	**Nitrate**	**N_2 gas**	**DO**	**AOB**	**AnAOB**	**HB**	**Inerts**
$\sum_{1}^{i=n_{group}} \beta_{k,i}^2$ into the following groups									
Mass transfer	0.08	0.15	0.00	0.12	0.17	0.18	0.02	0.02	0.02
Microbial kinetics	1.07	0.88	1.00	1.02	0.91	0.82	1.31	0.99	1.31
AOB*	0.98	0.29	0.29	0.86	0.91	0.80	0.50	0.40	0.54
AnAOB**	0.04	0.58	0.48	0.15	0.00	0.01	0.80	0.14	0.77
NOB***	0.00	0.00	0.00	0.00	0.00	0.00	0.00	0.00	0.00
HB****	0.02	0.00	0.22	0.01	0.00	0.01	0.00	0.43	0.00
hydrolysis and composition*****	0.02	0.00	0.01	0.00	0.00	0.00	0.01	0.02	0.01

* $\mu_{max,AOB}$, $K_{O2,AOB}$, $K_{NH3,AOB}$, $K_{HNO2,AOB}$, b_{AOB}, Y_{AOB}

** $\mu_{max,AnAOB}$, $K_{O2,AnAOB}$, $K_{NH3,AnAOB}$, $K_{HNO2,AnAOB}$, b_{AnAOB}, Y_{AnAOB}

*** $\mu_{max,NOB}$, $K_{O2,NOB}$, $K_{NO2,NOB}$, b_{NOB}, Y_{NOB}

**** $\mu_{max,HB}$, $K_{O2,HB}$, $K_{TAN,HB}$, $K_{TNN,HB}$, $K_{NO3,HB}$, $K_{S,HB}$, b_{HB}, Y_{HB}, η_{HB}

***** k_H, K_X, i_{NXB}, i_{NXI}, f_i

Significance of microbial conversion kinetics vs. mass transfer parameters on microbial interactions in scenario 1

In order to elucidate the mechanisms affecting the microbial composition and process performance, the kinetic parameters were further divided according to the groups of microorganisms they were related to. From this analysis, the microbial interactions could be inferred. The variance of the AOB mass fraction was predominantly governed by variance of their own kinetic parameters (see Table 4.3), which entails them not being significantly affected by substrate competition with other organisms under these operational conditions. For the AnAOB mass fraction, a significant amount of the variance could be assigned to the AOB parameters (see Table 4.3), because AnAOB were dependent on AOB for production of substrate (TNN) as electron acceptor and removal of the inhibiting oxygen. The variance of HB mainly (43%) originated from their own kinetic parameters, but a large part (40%) could be attributed to the AOB kinetics as well, and a smaller amount (14%) to the AnAOB kinetic parameters. This shows that the HB mainly utilized decay products originating from AOB. The variance in the inert mass fraction was almost solely due to AOB and AnAOB.

Overall, it can be concluded that AOB activity and TNN availability for AnAOB were the main limiting factors for the nitrogen removal in oxygen limited systems. This is furthermore supported by the N_2 mainly being affected by AOB kinetics (see Figure 4.2). The linear model obtained from the linear regression of the Monte Carlo simulations is valid for the given operating point defined in scenario 1 and provides an approximation of the steady state nitrogen removal, in the form of nitrogen gas concentration in the bulk liquid, as a function of parameters, which had an impact of at least 5% (see eq. 4.4). The unit of the number in front of each parameter value has the unit of g N_2-N m^{-3} in the bulk per unit of the given parameter. From this it can be deduced, that as AOB activity increased ($\mu_{max,AOB}$ increased or $K_{O2,AOB}$ decreased) the nitrogen removal simultaneously increased. Also noteworthy is that as the external mass transfer resistance increased (increased L_B), the performance decreased.

$$N_2 = 4.79 \times \mu_{max,AOB} - 13.73 \times K_{O2,AOB} - 132.5 \times Y_{AnAOB} - 27554 \times L_B + 180.5 \quad \left[g\ N/m^3 \right] \qquad (4.4)$$

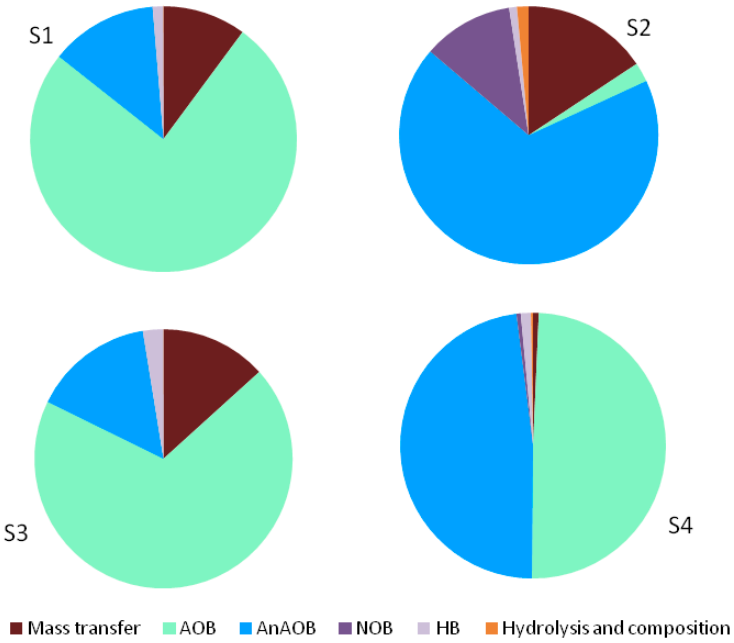

Figure 4.2 Result of sensitivity analyses for the bulk concentration of N_2, which represents the process performance. The slices are given as the sum of the squared SRCs within the given group divided by the sum of all the squared SRCs. The output could be sufficiently linearized for all scenarios except for scenario 4.

4.3.2 Effect of oxygen load on bulk concentrations and microbial composition

In scenario 2, the volumetric mass transfer coefficient for oxygen, k_La, was doubled, which entailed an increased oxygen loading to the system. This resulted in an increase in the bulk DO concentration to 0.5-1.3 g O_2 m^{-3} (in all Monte Carlo simulations), as opposed to 0.1-0.4 g O_2 m^{-3} in scenario 1. Even at double k_La, the oxygen was depleted within the granule. The higher oxygen supply caused the system to no longer be TNN limited (see the left hand side of Figure 4.1B), and NOB could compete for space with the other microbial groups in the granules. Even though AnAOB had a higher affinity for TNN than NOB, competition between the species was possible since NOB could withstand a higher oxygen concentration. As a consequence they could occupy a region close to the source of TNN in the granules (see Figure 4.1B). This is in line with the findings by Hao et al. (2002a), who found that AnAOB win the competition for TNN against NOB, when $K_{O2,NOB}/ K_{O2,AOB} > 0.2$ and $K_{O2,NOB}/ K_{O2,AnAOB} > 3$. This is, however, only valid under sufficiently low oxygen supply conditions, as can be observed from the results obtained here.

The sensitivity analysis results (see Appendix A2) showed that the TAN and TNN bulk concentrations were mainly affected by the microbial kinetics and no longer by mass transfer related parameters. While this result made sense for TNN, it was a bit surprising for TAN. The bulk TNN concentration was no longer affected by the producer's kinetics (AOB), but by its consumers' kinetics (NOB and AnAOB), which underlined, that the TNN production by AOB was no longer a key step for the reactor performance. AOB were slightly dependent on AnAOB kinetics, in contrast with scenario 1. Along with the TAN concentration being affected by AnAOB kinetics, this indicates that the TAN substrate competition between AOB and AnAOB was an important mechanism influencing the overall process.

The performance, represented by the N_2 concentration, was mainly (68%) affected by AnAOB kinetics (see Figure 4.2), especially by $K_{O2,AnAOB}$. This shows that even at very low bulk DO concentrations, AnAOB activity inhibition by oxygen played an important role in the overall nitrogen removal performance. This can also be seen in the linear model, which contains 5 parameters that each impacted the performance at least 5% (eq. 4.5). The linear coefficients indicate that an increase in either the AnAOB maximum growth rate or oxygen inhibition constant increased the nitrogen removal. On the contrary, increased mass transfer, indicated by the coefficients of oxygen diffusivity and the external boundary layer thickness, led to decreased nitrogen removal, hence resulting in a negative effect on the performance as expected from process engineering experiences. The effects of the important parameters are quantified in a simple model:

$$\begin{aligned} N_2 = {} & 376.9 \times \mu_{max,AnAOB} + 1772 \times K_{O2,AnAOB} + 112360 \times L_B \\ & - 54836 \times D_{O2} - 5.59 \times K_{O2,NOB} + 130.5 \quad \left[gN/m^3 \right] \end{aligned} \tag{4.5}$$

4.3.3 Effect of granule size on bulk concentrations and microbial composition

In scenario 3, the effects of four different granule sizes on the microbial composition and bulk concentrations were investigated (0.5, 1, 1.5 and 2 mm diameter). These relatively small granule sizes have been observed in several experimental studies (Vlaeminck et al., 2010; Figueroa et al., 2012), including our own experimental observations, which showed even smaller sizes, with the volumetric average ranging between 0.1 and 0.25 mm in diameter. Slightly larger granule sizes have also been observed, although in a system where higher solids concentrations were

observed as well (Vazquez-Padin et al., 2009). The total solids concentration was kept constant in the different simulation scenarios by increasing the number of granules with decreasing granule size, while assuming a constant granule density for all the granule sizes. This means that external mass transfer resistance will decrease with increasing specific surface area of the granules (i.e. smaller granules, higher mass transfer rate).

In line with this, the AOB mass fraction slightly increased while the bulk DO concentration slightly decreased with decreasing size (Table 4.4 and Figure 4.3). The granule sizes investigated showed quite similar performance results, with the overall process performance slightly increasing with decreasing granule size (Table 4.4). This is in line with the results of Volcke et al. (2010). However, similar to their results, this is expected only to happen when operating under conditions where the performance is limited by AOB activity (as in scenario 1), because the aerobic volume is increased in smaller granules, and not by AnAOB activity, for which larger granules are expected to perform better.

The result of the sensitivity analysis was almost identical to scenario 1 (Figure 4.2), which entails that the mass transfer was still important for AOB, TNN, and N_2 at smaller granule sizes, even though the mass transfer resistance was lowered as the specific surface area increased. The inhibitory effect of oxygen on AnAOB activity is speculated to be the reason, which is also reflected in the changes in the biomass composition; the smaller granules consist of higher amounts of AnAOB (Table 4.4), but with a lower activity due to oxygen inhibition. In line with this finding, Vlaeminck et al. (2010) showed in batch tests conducted with granules belonging to the smallest size fraction that the specific rate of ammonium conversion by AnAOB was lower than in larger granules. However, they also found lower abundance of AnAOB in smaller granules than in bigger ones. This observation could be due to the particular operation history of their OLAND reactor that affected the granule composition and physiology of the biomass (e.g. the performance of the OLAND reactor is a combination of the performance of the different sizes of granules). To resolve this observation, more experimental investigations on different systems are needed. It could thus be deduced that there was no simple relationship between biomass composition and process performance, which was also shown by Lackner et al. (2008) in a modeling study of membrane aerated biofilm reactors.

Since the result of the sensitivity analysis was similar to the observations made in scenario 1, the key step in the overall removal remained the AOB activity and TNN availability for AnAOB.

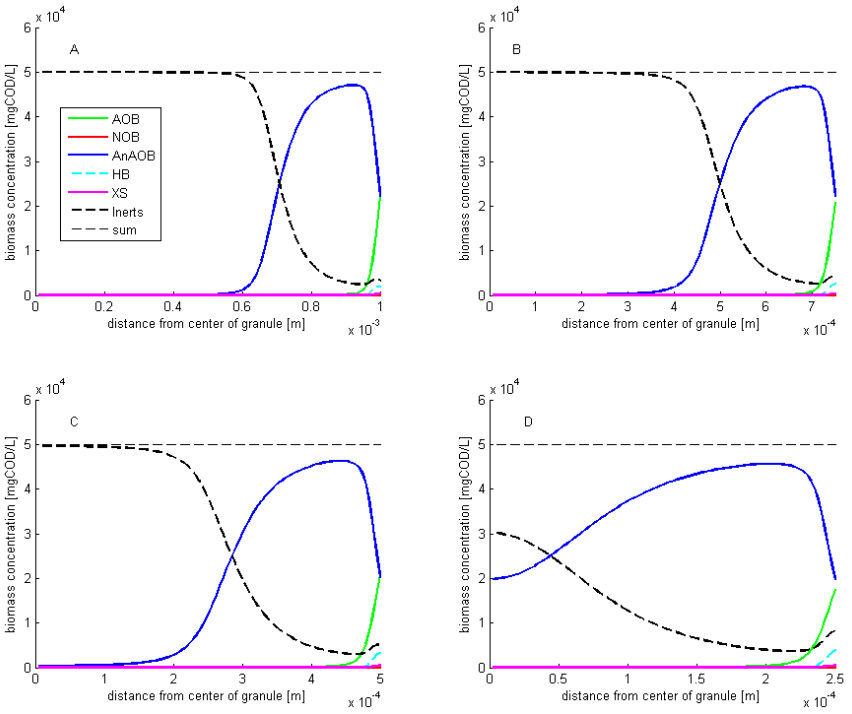

Figure 4.3 Biomass distribution in granules at different granule sizes. (A) r_{gran} = 1 mm, (B) r_{gran} = 0.75 mm, (C) r_{gran} = 0.5 mm, and (D) r_{gran} = 0.25 mm.

It can be argued that systems containing the bigger granules (2 mm in diameter) were containing excess solids and the specific nitrogen removal rate (measured as g $N_{removed}$ g VSS^{-1} d^{-1}) could therefore be increased. The same was found by Ni et al. (2009), who found that anammox performing granules above 1.3 mm in diameter did not perform better, but showed a lower specific nitrogen removal rate.

An interesting observation is that as the N_2 production increased with decreasing size, the bulk nitrate concentration decreased simultaneously (Table 4.4). This may be attributed to HB activity, which indicated that HB, even though low in numbers, had an impact on the performance. As in scenario 1, HB grew on decay products originating from AOB, and when they were present in higher concentration (as is the case with smaller granules with less oxygen limitation), the HB had better conditions to grow. Thus, HB in low concentrations contributed to a slightly better nitrogen removal through a) anoxic heterotrophic activity (denitrification) with N_2 production and nitrate removal and b) TAN assimilation for growth of HB.

Table 4.4 Effect of granule size on bulk concentrations of soluble compounds and microbial composition of the granules.

Granule size		Bulk concentrations						Mass fractions			
Diameter	**Radius**	**TAN**	**TNN**	**DO**	**Nitrate**	**N2**	**AOB**	**AnAOB**	**NOB**	**HB**	**Inert**
mm	mm	gN m^{-3}	gN m^{-3}	gO_2 m^{-3}	gN m^{-3}	gN m^{-3}	%	%	%	%	%
2	1	15.9	0.332	0.222	11.2	170.4	3.16	56.8	0	0.34	39.6
1.5	0.75	15.7	0.208	0.207	11.0	171.0	3.61	61.9	0	0.41	34.0
1	0.5	15.3	0.116	0.179	10.6	172.0	4.28	69.6	0	0.55	25.5
0.5	0.25	14.5	0.050	0.124	9.55	174.2	5.38	81.2	0	0.77	12.6

4.3.4 Effect of high N loading on bulk concentrations and microbial composition

The capability of the simulated system to handle high loads was investigated in scenario 4. In this simulation, the TAN load (i.e. the influent TAN concentration) was increased with a corresponding increase in oxygen supply rate (through increase in k_La), while keeping the granule size and number (and thus the total biomass concentration) the same as in scenario 1 (see Table 4.1). In Figure 4.1C it can be seen that the microbial composition of the granule was dominated by AnAOB in the internal part of the structure, and less than 10% of the mass was made up of inert material.

Only bulk DO concentration and AOB mass fraction, among all of the abovementioned model outputs, could be sufficiently linearized (appendix A2). Nevertheless, the results of the sensitivity analysis on the overall performance (N_2 concentration) were evaluated as well (Figure 4.2), even though conclusions should be drawn with care. The sensitivity analysis indicated that, as in scenario 1, the bulk DO and the AOB mass fraction were affected by the mass transfer parameters (MTBL thickness and oxygen diffusivity), while the N_2 no longer was affected by these (see Figure 4.2). Hence, the system was limited by its biomass inventory (mass of solids), which would have to be increased in order to reach a higher treatment efficiency. This was also evident from unconverted TAN and TNN being present throughout the depth of the granules in relatively high concentrations (see Figure 4.1C). When the system was operated in this regime, the nitrogen removal was therefore limited almost solely by microbial kinetics and negligibly affected by mass transfer.

4.3.5 Summarizing insights: Impact of operational conditions on N removal rates

To sum up the findings from all the abovementioned scenarios, the process performance as a function of the nitrogen and oxygen loading was investigated by simulating 10 TAN loads ranging from 100 to 1000 g N m^{-3} d^{-1} combined with 10 k_La values, ranging from 25 to 250 d^{-1}, resulting in 100 different operational conditions. The system was simulated to steady state with these operational conditions, and the resulting volumetric nitrogen removal rates (g N m^{-3} d^{-1}) and removal efficiencies are shown in Figure 4.4. The graphs presented serve as a two dimensional operation window.

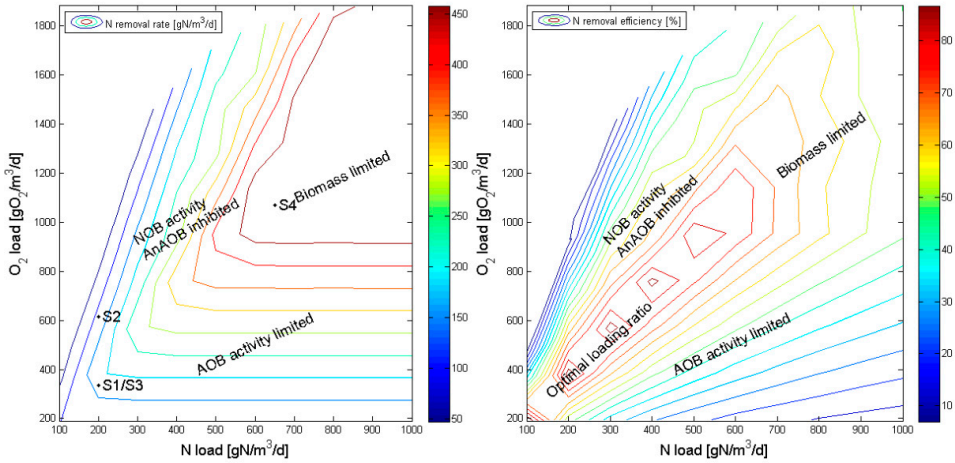

Figure 4.4 Process performance as N removal rate (left) and N removal efficiency (right) as a function of the operational conditions (oxygen and N load). The locations of the four operational scenarios are shown in the left plot.

The observed optimal loading ratio was slightly higher than the theoretical ratio of the stoichiometry of nitrogen and oxygen substrates. The theoretical stoichiometry yields a ratio of 1.83 g O_2 (g N)$^{-1}$, whereas the observed optimal loading ratio was here found to be 1.90 (g O_2 m^{-3} d^{-1})/(g N m^{-3} d^{-1}), as can be seen from Figure 4.5. This is higher than the values reported for conventional flat biofilm and membrane aerated biofilm systems (Terada et al., 2007). In the study of Terada et al. (2007), the optimal surface loading ratio was found to be 1.5-1.6 (g O_2 m^{-2} d^{-1})/(g N m^{-2} d^{-1}), which was below the theoretical value. However, the external mass transfer resistance was neglected in that study, which under certain operational conditions plays an important role. The different results could be caused by the presence of HB, or because the

mass transfer resistance affected the value of the optimal loading ratio significantly, and neglecting either would therefore lead to a suboptimal set point of a potential controller.

The significance of this finding is that optimal performance depends on the optimal ratio of the oxygen to nitrogen loading to the system, and not on a specific DO concentration in the system, which has otherwise often been assumed in previous studies (Hao et al., 2002a+b; Joss et al., 2009; Volcke et al., 2010). A similar conclusion was drawn by Kwak et al. (2012), who optimized the performance of a fixed film, single-stage CANR reactor through tight control of the oxygen loading to the system. Additionally, controlling the bulk DO concentration might be practically challenging, because the concentration often is very low (< 0.1 mg L^{-1}), which is a concentration range where it is difficult to acquire accurate measurements. This finding is an extension of the findings of Bernet et al. (2005), who reported for a partial nitritation biofilm system, that controlling the ratio of the oxygen to ammonium bulk concentration was superior to solely controlling the bulk oxygen concentration.

Moving away from the observed optimal value led to suboptimal performance due to a complex interplay between mass transfer and microbial kinetics as explained below. The results showed that when operating below the optimal oxygen loading/TAN loading for optimal nitrogen removal, the removal would mainly be affected by the AOB activity and also, but to a lesser extent, be influenced by AnAOB kinetics and by mass transfer limitation as observed in scenario 1 and 3 (Figure 4.4). Thus, the AOB activity is limiting the nitrogen removal. At operational conditions giving an oxygen/TAN loading ratio higher than required for optimal nitrogen removal, the AnAOB activity will decrease due to oxygen inhibition, and NOB will be able to compete for the space with the other microbial groups (as in scenario 2). Both the nitrogen removal rate and the removal efficiency decreased with increased oxygen load above this ratio (see Figure 4.4 and 4.5). When reaching a certain nitrogen and corresponding oxygen loading the nitrogen removal rate reached a plateau, because all the biomass in the system was active, and the granules contained a minimum amount of inert material as observed in scenario 4. This means that the nitrogen loading to the system (the food to microorganism (F/M) ratio as g N (g VSS-biomass)$^{-1}$ d^{-1}) exceeded the maximum specific nitrogen removal rate of the biomass inventory in the system. The performance will in this case be influenced almost solely by the microbial kinetics and not at all by mass transfer. It is speculated that the granule size will influence the onset of the plateau and the maximum nitrogen removal rate. The granule size did not have a significant impact on the performance when operating at the oxygen loading limited

regions in Figure 4.4, which was the case in scenario 3. However, if operating at the biomass limited plateau, the size is expected to have an impact on the performance.

The removal efficiency was optimal at a loading ratio of 1.90 (g O_2 m^{-3} d^{-1})/(g N m^{-3} d^{-1}) and at low nitrogen loadings (Figure 4.4). As the nitrogen loading increased, the removal efficiency decreased due to increased AnAOB inhibition by oxygen and limitation of the biomass inventory in the system to convert all nitrogen present in the influent (these operational conditions are indicated in the center of Figure 4.5).

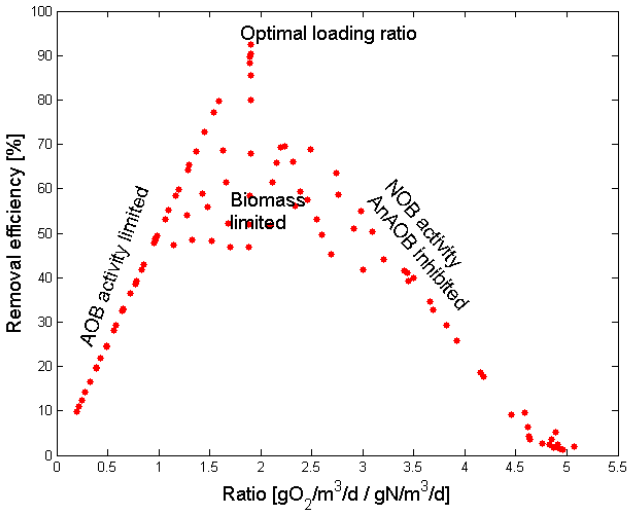

Figure 4.5 Nitrogen removal efficiency as a function of the oxygen to nitrogen loading ratio.

4.4 Conclusions

In this work, phenomena that are the most influential on process performance of nitritation-anammox granular bioreactors were computationally identified and quantified via a global sensitivity analysis. Based on the analysis, an optimal operation window for the system was developed, which among others, revealed that the optimal nitrogen removal performance is critically controlled by the ratio of the oxygen supplied to the nitrogen loading of the system, and not by the DO concentration in the bulk alone.

The relative importance of mass transfer and kinetic parameters were found to depend on the operating regime of the system. Operating under the optimal loading ratio of 1.90 (g O_2 m^{-3} d^{-1})/(g N m^{-3} d^{-1}), the system was influenced by mass transfer (10% impact on N_2) and performance

was limited by AOB activity (75% impact on N_2), while operating above the optimal loading ratio, AnAOB activity was limiting (68% impact on N_2). The negative effect of oxygen mass transfer had an impact of 15% on N_2.

The developed optimal operation window is a valuable tool for diagnosing performance problems, and can contribute significantly to successful scale-up and control development for this important technology.

5 pH variation and influence

Summary

A pH simulator consisting of an efficient numerical solver of a system of nine non-linear equations was constructed and implemented in the modeling software MATLAB®. The pH simulator was integrated in a granular biofilm model and used to simulate the pH profiles within granules performing the nitritation-anammox process for a range of operating points. The simulation results showed that pH profiles were consistently increasing with increasing depth into the granule, since the proton producing aerobic ammonium oxidizers (AOB) were located close to the granule surface. Despite this pH profile, more NH_3 was available for AOB than for anaerobic ammonium oxidizers (AnAOB) located in the center of the granules. However, operating at a higher oxygen loading resulted in steeper changes in pH over the depth of the granule and caused the NH_3 concentration profile to increase from the granule surface towards the center. The initial value of the background charge and influent bicarbonate concentration were found to greatly influence the simulation result and should be accurately measured. Since the change in pH over the depth of the biofilm was relatively small, the activity potential of the microbial groups affected by the pH did not change more than 5% over the depth of the granules.

5.1 Introduction

Among the operating conditions in the reactor, pH has a major impact on the nitrification and on the anammox process, since it has an impact on: 1) the compound speciation, and thus on the substrate concentration; and, 2) the structure and stability of the bacterial cell wall and membrane. In addition, pH varies as a consequence of the activity of these microbial groups, due to their production or consumption of protons during their metabolism (Figure 5.1). The objective of this study was to improve the process understanding by elucidating the close relation between microbial activity and pH in a stratified biofilm structure by means of numerical model simulations. To reach this objective, an efficient pH calculation procedure including a pH model and numerical solution strategy was developed.

5.2 Materials and methods

5.2.1 Model description

The model described in chapter 3 of a continuously run granular sludge reactor consisting of mass balances for soluble and particulate compounds within the granules and in the bulk liquid was used. It was extended to also include HCO_3^- (bicarbonate) as a state variable. The stoichiometric coefficients for bicarbonate and the modified process rates can be seen in Table 5.1 and 5.2. In the model, aeration was included in the bulk liquid mass balance for oxygen. On the contrary, no stripping was considered for any of the other gaseous compounds (CO_2 or N_2) produced or consumed in the system.

The speciation of the true substrates has been, and still is, a point of discussion (Sin et al., 2008c; Jin et al., 2012), with Anthonisen et al. (1976) being among the first to propose that NH_3, rather than NH_4^+ or total ammonium nitrogen (TAN), is the true substrate for AOB. This has since been extended to AnAOB substrates with van Hulle (2005) showing that the unionized species were the true substrates. In this work, the unionized forms of the compounds were assumed to be the true substrates for all autotrophic microbial groups, i.e. AOB, NOB, and AnAOB. Thus AOB use NH_3 and are product inhibited by free nitrous acid (HNO_2), rather than by NO_2^- or total nitrite nitrogen (TNN), NOB grow on HNO_2, and AnAOB utilize NH_3 and HNO_2 (Table 5.2). The pH therefore has a significant impact on the substrate and inhibitor concentrations and availability (Figure 5.1). Additionally, pH affects the structure and permeability of the bacterial cell membrane and the energy required for maintenance of the internal cell proton concentration.

To account for this, a bell-shaped function around the optimal pH value (Henze et al., 1995) was included in the growth rates of AOB, AnAOB, and NOB (Table 5.2) with the parameter values obtained by van Hulle et al. (2007) and used by Ganigue et al. (2010).

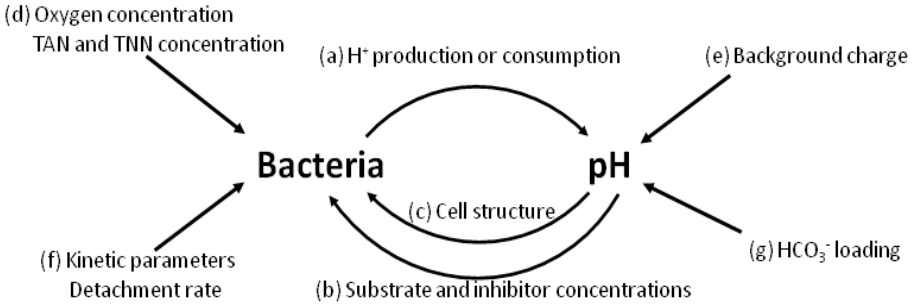

Figure 5.1 Interactions between bacterial activity, pH and reactor environment. a) The pH profile indicates where H^+ production/consumption takes place, d) dictates the location of the bacterial groups. TAN + TNN in combination with pH (b) determines the substrate and inhibitor concentrations which affect bacteria location, c) determines where in the biofilm, growth conditions are the best, e) & g) affect the absolute value and shape of the pH profile, and f) have a high impact on biomass activity and on the inert fraction of the granule.

Table 5.1 Process stoichiometry. The dependent variables in the columns have been extended to include bicarbonate (compound 6).

Stoichiometric coefficients	S_{TAN}	S_{O2}	S_{TNN}	S_{NO3}	S_{N2}	S_{HCO3}	S_S	X_{AOB}	X_{NOB}	X_{AnAOB}	X_{HB}	X_S	X_I
Compound *i* ▸	1	2	3	4	5	6	7	8	9	10	11	12	13
Process *h* ▾	g N m^{-3}	g COD m^{-3}	g N m^{-3}	g N m^{-3}	g N m^{-3}	mole m^{-3}	g COD m^{-3}	g COD m^{-3}	g COD m^{-3}	g COD m^{-3}	g COD m^{-3}	g COD m^{-3}	g COD m^{-3}
13. AOB growth	$-\frac{1}{Y_{AOB}}-i_{NXB}$	$\frac{3.43-Y_{AOB}}{Y_{AOB}}$	$\frac{1}{Y_{AOB}}$			$-\frac{1}{14}\left(\frac{2}{Y_{AOB}}+i_{NXB}\right)$		1					
14. NOB growth		$-\frac{1.14-Y_{NOB}}{Y_{NOB}}$	$-\frac{1}{Y_{NOB}}$	$\frac{1}{Y_{NOB}}$		$-\frac{i_{NXB}}{14}$			1				
15. AnAOB growth	$-\frac{1}{Y_{AnAOB}}-i_{NXB}$		$-\frac{1}{Y_{AnAOB}}-1.52$	1.52	$\frac{2}{Y_{AnAOB}}$	$-\frac{i_{NXB}}{14}$				1			
16. AOB decay								-1				1- f_i	f_i
17. NOB decay									-1			1- f_i	f_i
18. AnAOB decay										-1		1- f_i	f_i
19. HB growth 1	$-i_{NXB}$	$\frac{1-Y_{HB}}{Y_{HB}}$				$-\frac{i_{NXB}}{14}$	$-\frac{1}{Y_{HB}}$				1		
20. HB growth 2	$-i_{NXB}$		$-\frac{1-Y_{HB}}{1.71Y_{HB}}$		$\frac{1-Y_{HB}}{1.71Y_{HB}}$	$-\frac{1}{14}\left(i_{NXB}-\frac{1-Y_{HB}}{1.71Y_{HB}}\right)$	$-\frac{1}{Y_{HB}}$				1		
21. HB growth 3	$-i_{NXB}$			$-\frac{1-Y_{HB}}{2.86Y_{HB}}$	$\frac{1-Y_{HB}}{2.86Y_{HB}}$	$-\frac{1}{14}\left(i_{NXB}-\frac{1-Y_{HB}}{2.86Y_{HB}}\right)$	$-\frac{1}{Y_{HB}}$				1		
22. HB decay											-1	1- f_i	f_i
23. Hydrolysis	$\frac{i_{NXB}-f_i i_{NXI}}{1-f_i}$					$\frac{1}{14}\left(\frac{i_{NXB}-f_i i_{NXI}}{1-f_i}\right)$	1					-1	
24. Aeration		1											

Table 5.2 Modified process rate expressions including pH for the first 3 of the 12 processes included in the model.

Process *k* ▾	*Process Rate ρ*
1. AOB growth	$\mu_{max,AOB}\, X_{AOB}\, \frac{S_{NH3}}{K_{NH3,AOB}+S_{NH3}}\, \frac{S_{O2}}{K_{O2,AOB}+S_{O2}}\, \frac{K_{I,HNO2,AOB}}{K_{I,HNO2,AOB}+S_{HNO2}}\, \frac{S_{HCO3}}{K_{HCO3,AOB}+S_{HCO3}}\, \frac{K_{pH,AOB}}{K_{pH,AOB}-1+10^{\lvert pH_{opt,AOB}-pH\rvert}}$
2. NOB growth	$\mu_{max,NOB}\, X_{NOB}\, \frac{S_{HNO2}}{K_{HNO2,NOB}+S_{HNO2}}\, \frac{S_{O2}}{K_{O2,NOB}+S_{O2}}\, \frac{K_{pH,NOB}}{K_{pH,NOB}-1+10^{\lvert pH_{opt,NOB}-pH\rvert}}$
3. AnAOB growth	$\mu_{max,AnAOB}\, X_{AnAOB}\, \frac{S_{NH3}}{K_{NH3,AnAOB}+S_{NH3}}\, \frac{S_{HNO2}}{K_{HNO2,AnAOB}+S_{HNO2}}\, \frac{K_{I,O2,AnAOB}}{K_{I,O2,AnAOB}+S_{O2}}\, \frac{K_{pH,AnAOB}}{K_{pH,AnAOB}-1+10^{\lvert pH_{opt,AnAOB}-pH\rvert}}$
4. AOB decay	$b_{AOB}\, X_{AOB}$
5. NOB decay	$b_{NOB}\, X_{NOB}$
6. AnAOB decay	$b_{AnAOB}\, X_{AnAOB}$
7. HB growth 1	$\mu_{max,HB}\, X_{HB}\, \frac{S_{O2}}{K_{O2,HB}+S_{O2}}\, \frac{S_S}{K_{S,HB}+S_S}\, \frac{S_{TAN}}{S_{TAN}+K_{TAN,HB}}$
8. HB growth 2	$\mu_{max,HB}\, X_{HB}\, \lambda_{HB}\, \frac{S_S}{K_{S,HB}+S_S}\, \frac{S_{TNN}}{K_{TNN,HB}+S_{TNN}}\, \frac{K_{I,O2,HB}}{K_{I,O2,HB}+S_{O2}}\, \frac{S_{TAN}}{S_{TAN}+K_{TAN,HB}}$
9. HB growth 3	$\mu_{max,HB}\, X_{HB}\, \lambda_{HB}\, \frac{S_S}{K_{S,HB}+S_S}\, \frac{S_{NO3}}{K_{NO3,HB}+S_{NO3}}\, \frac{K_{I,O2,HB}}{K_{I,O2,HB}+S_{O2}}\, \frac{S_{TAN}}{S_{TAN}+K_{TAN,HB}}$
10. HB decay	$b_{HB}\, X_{HB}$
11. Hydrolysis	$k_H \frac{X_S}{K_X}$
12. Aeration	$k_L a(S_{O2\_sat} - S_{O2\_bulk})$

5.2.2 pH calculation and numerical solution

The procedure of the determination of pH was carried out through the solution of a system of equations, consisting of three mass balances of TAN, TNN, and total inorganic carbon (TIC) (eqs. 5.1-5.3), five acid-base equilibrium conditions (eqs. 5.3-5.8), and a global charge balance (eq. 5.9). In the global charge balance, the background charge (Z^+) represents the net charge that participates neither in acid/base equilibria nor in the biological conversions. A value of 10 charge-mol m^{-3} was used in all simulations. As an illustration, addition of NaCl does not contribute to Z^+, since its net charge is zero (the anion Cl^- and the cation Na^+ compensate each other), whereas addition of HCl would decrease the background charge (corresponding to the contribution of the anion Cl^-, which is completely dissociated).

The resulting system of nine nonlinear equations was solved by a multidimensional Newton-Raphson method adapted from Luff et al. (2001).

$$0 = TAN - \left(NH_4^+ + NH_3\right) \quad (5.1)$$

$$0 = TNN - \left(HNO_2 + NO_2^-\right) \quad (5.2)$$

$$0 = TIC - \left(CO_2 + HCO_3^- + CO_3^{2-}\right) \quad (5.3)$$

$$0 = K_W - OH^- \cdot H^+ \quad (5.4)$$

$$0 = K_{e,NH4} \cdot NH_4^+ - NH_3 \cdot H^+ \quad (5.5)$$

$$0 = K_{e,HNO2} \cdot HNO_2 - NO_2^- \cdot H^+ \quad (5.6)$$

$$0 = K_{e,CO2} \cdot CO_2 - HCO_3^- \cdot H^+ \quad (5.7)$$

$$0 = K_{e,HCO3} \cdot HCO_3^- - CO_3^{2-} \cdot H^+ \quad (5.8)$$

$$0 = Z^+ - NO_3^- - HCO_3^- - 2 \cdot CO_3^{2-} - NO_2^- - OH^- + NH_4^+ + H^+ \quad (5.9)$$

The model of the CANR system, consisting of partial differential equations (PDEs) (the compound mass balances), was discretized in space into 100 nodes, each accounting for a given control volume, which resulted in a system of ordinary differential equations (ODEs). The numerical pH solver along with the model was implemented and solved during dynamic simulations in the MATLAB software. The built-in *"ode15s"* solver based on numerical differentiation formulas was used to solve the ODEs. It was assumed that the establishment of the acid-base equilibria was immediate compared to the diffusion and production/consumption of compounds. As a consequence, a new distribution of the chemical species was calculated for every integration time step of the equation system.

However, it was quickly found out that the determination of pH through numerical solution of eqs. 5.1-5.9 was computationally heavy and prone to numerical errors in some implementations, since the Newton-Raphson numerical method was not convergent for every initial guess. To overcome these problems and to obtain an efficient solution strategy, pH was determined off-line (still through the Newton-Raphson method), prior to simulation, for the complete expected range of TAN, TNN, TIC and NO_3^- concentrations. A lookup table was constructed from these results using the Matlab command "*TriScatteredInterp*" and then used to interpolate the value of pH during integration of the ODEs in dynamic simulations. The error of interpolation was

estimated by evaluating the difference between the Newton-Raphson method solution and the interpolation. This was done for 10000 points which were different from the ones used to build the interpolator. The expected root mean squared interpolation error was 0.014 pH units and the variance was $3.87 \cdot 10^{-4}$ (pH unit squared) for the range pH=3 to pH=9. If the range of pH was restricted to the range 6.5-8.5, the expected root mean squared interpolation error became $7.89 \cdot 10^{-5}$ and the variance $6.09 \cdot 10^{-9}$. This error was considered negligible.

For all simulations the initial conditions were the steady state result of a simulation using a constant pH value. To obtain a steady state solution, the dynamic model was solved for a long enough time (in this case 10000 days) and the final values were recorded as steady state results.

5.2.3 Description of scenarios

The four scenarios, comprising four different operating points described in chapter 4, were simulated and evaluated (see Table 4.1).

In scenario 1, an oxygen mass transfer coefficient (k_La) determined through clean water tests was used (43 d^{-1}), the volumetric nitrogen loading was 200 g N m^{-3} d^{-1}, and the bicarbonate loading was 1.22 g HCO_3^- L^{-1} d^{-1}, corresponding to a molar ratio of 1:1.43 TAN-N:HCO_3^-. In scenario 2, the effect of oxygen supply was investigated by doubling the value of the mass transfer coefficient (k_La). In scenario 3, the effect of granule size was investigated by decreasing the granule diameter from 2 mm to 0.5 mm. Finally, the effect of high influent loading for a given amount of biomass was investigated in scenario 4. In the latter scenario, the increased loading of nitrogen implied increasing the supply of bicarbonate to 4.27 g HCO_3^- L^{-1} d^{-1} and the oxygen supply to k_La=140 d^{-1} (see Table 4.1).

5.3 Results and discussion

From the modeling results it was found that the initial value of the background charge had a significant impact on the pH due to its impact on the solution of the system of equations (eqs. 5.1-5.9). Both the value of the pH and the shape of the pH profile were affected by this variable. The higher the background charge, the higher the pH and the flatter the pH profile. The background charge changes with composition and strength of wastewater, and estimation of this prior to pH calculation should therefore preferably be conducted. Unfortunately, the

background charge is very difficult to estimate for a biofilm system for two reasons: the actual detailed composition of the biofilm is not known (or not considered in the model, e.g. ions, along with the extracellular polymeric substances (EPS) making up the biofilm matrix are not considered); and secondly, there is no reason why the background charge should be constant throughout the biofilm thickness.

Since background charge values are rarely reported and vary from system to system, the approach has been to use a value of Z^+ which would give a pH close to 7.2 in the bulk of the reactor, given the concentrations predicted for a constant pH. This resulted in the Z^+ value being 10 charge-mol m^{-3}. The simulations with such a value of charge and with the given bicarbonate concentrations lead to different but relatively close values of pH in the bulk (from approximately 7.2 in scenario 4 to 7.6 in scenarios 1 and 3, as it can be seen below).

The results shown in the Figures 5.2-5.5 were steady state conditions obtained after simulating 10000 days of operation.

5.3.1 Scenario 1. Interpretation of the results

The pH decreased from the center to the surface of the biofilm (Figure 5.2A), where AOB were present at the biofilm/liquid interface (Figure 5.2C). The combination of the TAN concentration profile and the pH profile yielded an NH_3 profile (Figure 5.2B), which despite the shape of the pH profile, showed that less NH_3 was available as substrate for AnAOB, located a bit further inside the granule (Figure 5.2C), than there was for the AOB located at the surface. Both the pH profile and the HNO_2 profile, which also showed a decreasing trend from the surface towards the center of the granule, were opposite compared to observations made by Park et al. (2010). The difference can be found in the consumption of TNN, which in this study is taking place inside the granule at the location of the AnAOB (Figure 5.2C). AOB consumed significantly more alkalinity than the AnAOB, which was evident from the pH profile showing that the greatest change was happening in the vicinity of the biofilm/liquid interface where the AOB were present (illustrating process (a) in Figure 5.1). The microbial composition in this scenario was similar to investigations made without inclusion of the pH effect (Volcke et al., 2010; Vangsgaard et al., 2012), which is reasonable considering the relatively small change in pH value over the depth of the granule. The total nitrogen removal efficiency of the granular reactor was 86.4%.

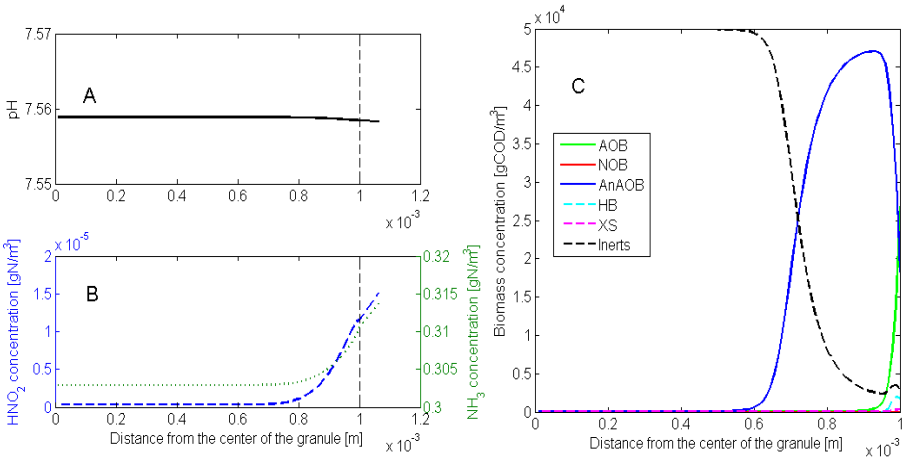

Figure 5.2 A) pH profile with biofilm depth, B) NH_3 and HNO_2 profiles with biofilm depth, and C) biomass composition inside the granular biofilm in scenario 1 simulated with pH effect on microbial growth. The vertical dashed line in A) and B) indicates the biofilm/liquid interface.

5.3.2 Scenarios 2-4. Effect of operating conditions

Simulation of scenario 2 resulted in a similar pH profile as obtained in scenario 1, with a lower pH closer to the biofilm/liquid interface and increasing towards the granule center (Figure 5.3A). However, the shape of the pH profile was very different, with the pH changing over almost the entire depth of the granules, instead of just close to the biofilm/liquid interface, and the slope of the pH profile was much steeper. The effect of the relatively high change in pH resulted in an NH_3 concentration profile showing an increasing trend from the granule surface towards the center of the granule. The AnAOB were located from a couple of hundred µm below the surface of the granules and all the way to the center, where there was a tradeoff between availability of NH_3 and HNO_2 and low oxygen concentrations (Figure 5.3C). It could also be observed that NOB growth appeared close to the biofilm/liquid interface under these conditions. The higher amount of oxygen supplied thus caused nitrification to be the dominating process, and the nitrogen removal efficiency was therefore only 27.2%, while the TAN removal efficiency was 83.5%.

At smaller granule sizes, similar results as in scenario 1 were observed, showing a relatively small change in pH value over the depth of the granules, but with the difference that the pH profile was smoother with on the one hand a reduced slope, and on the other hand a gradient that was penetrating deeper in the granule. The NH_3 concentration did therefore not change much over the depth as a result, and the HNO_2 concentration was mainly a function of the TNN

concentration profile. The HNO_2 penetrated all the way through the granule, albeit in low concentrations in the center of the granule (Figure 5.4B). As a result the granules contained higher amounts of AnAOB, and the inert core took up less space (Figure 5.4C) than in scenario 1. Despite the change in microbial composition, the efficiency of the total nitrogen removal remained similar to scenario 1.

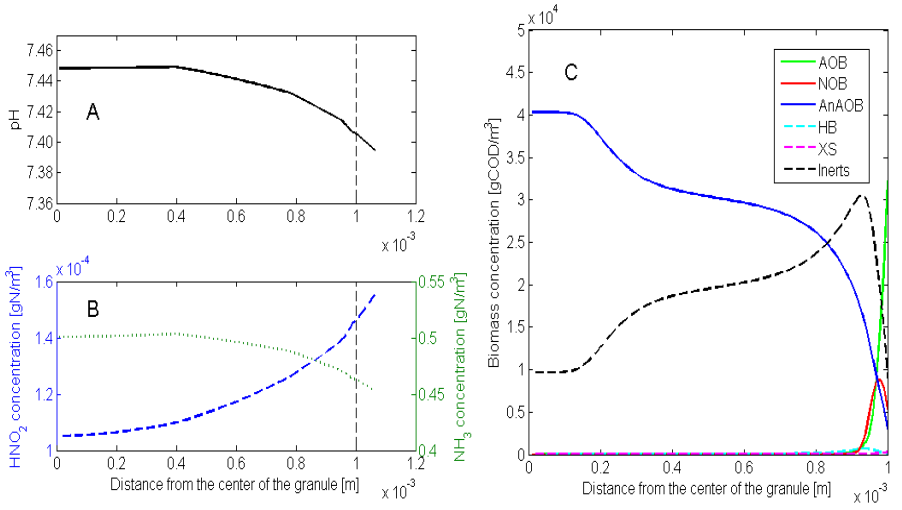

Figure 5.3 A) pH profile with biofilm depth, B) NH_3 and HNO_2 profiles with biofilm depth, and C) biomass composition inside the granular biofilm in scenario 2 simulated with pH effect on microbial growth. The vertical dashed line in A) and B) indicates the biofilm/liquid interface.

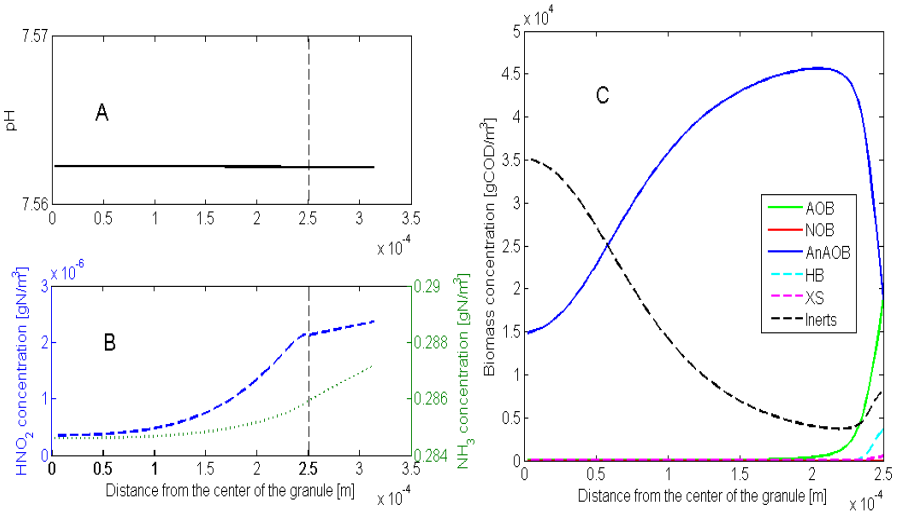

Figure 5.4 A) pH profile with biofilm depth, B) NH_3 and HNO_2 profiles with biofilm depth, and C) biomass composition inside the granular biofilm in scenario 3 simulated with pH effect on microbial growth. The vertical dashed line in A) and B) indicates the biofilm/liquid interface.

In the final scenario, the pH profile obtained showed changes in pH over the entire depth of the granules (Figure 5.5A). Since a higher load was applied, more substrate was available for both the AOB and the AnAOB. This meant that more TAN was converted, and thus more protons produced, causing the slope of the pH profile to last the entire depth of the granules, similar to scenario 2. The higher load also meant that the AnAOB were present in higher concentrations and dominated the interior of the granules (Figure 5.5C). Despite their increase in amount, they were not able to convert all the supplied nitrogen, and the overall nitrogen removal efficiency was therefore just 75.1% of the supplied nitrogen load.

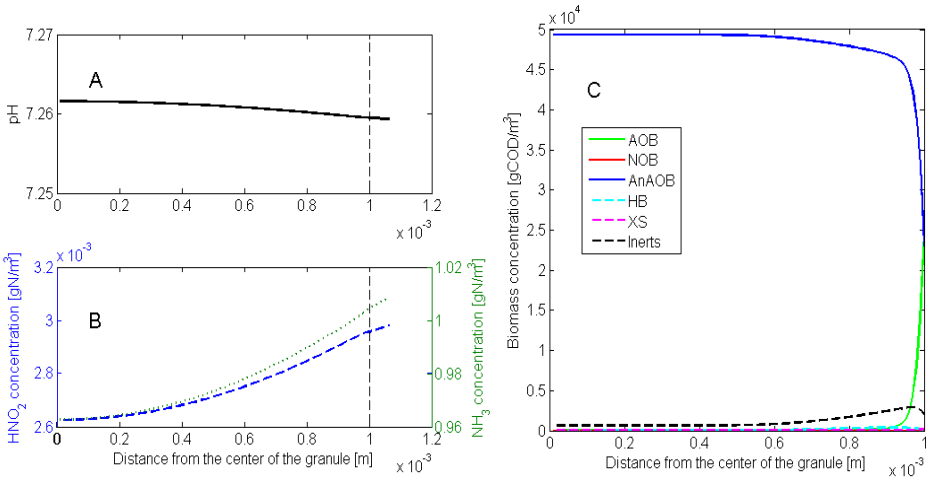

Figure 5.5 A) pH profile with biofilm depth, B) NH_3 and HNO_2 profiles with biofilm depth, and C) biomass composition inside the granular biofilm in scenario 4 simulated with pH effect on microbial growth. The vertical dashed line in A) and B) indicates the biofilm/liquid interface.

5.4 Conclusions and outlook

A pH simulator was constructed through a numerical solver of a system of nine nonlinear equations and was implemented in the MATLAB® software. The pH simulator was coupled to the dynamic granule model by using a lookup table to facilitate the computational efficiency. In this way, the pH profiles within granular sludge performing the nitritation-anammox process, at a range of different operating points, were simulated. The results showed the following: granules containing proton producing AOB in the outer layers of the granules, next to the biofilm/liquid interface, always resulted in an increasing pH with increasing depth into the granules.

A number of approximations were needed to complete the solution of the whole model, e.g. the value of the background charge and bicarbonate concentrations. This was found to have a great impact on the value and shape of the pH profile, and estimating or measuring an appropriate and correct value of these variables is therefore of great importance. As a conclusion, these results represent a first step in the evaluation of the impact of pH in granular systems. However, more information about the effect on the cell structure and the background charge estimation, supported by experimental essays, will be needed to verify the conclusions and consolidate the pH effect on microbial activities.

Despite the difficulty related to determining the appropriate value of the background charge, it is believed that the approach developed and described in this work provides valuable information about how the pH impacts the processes and the relation between microorganisms within the granule. Even though a pH profile could be simulated and constructed over the depth of the granules, it was evident that the change in pH over the depth was relatively small (highest in scenario 2 and lowest in scenario 3), due to the buffering capacity of bicarbonate. Thus, the stratification was present for pH, but the difference in impact on the activity potential of the different microbial groups, caused by predicted pH change over the depth of the granules, was relatively small (about 5% at most). Compared to the impact on the activity potential caused by e.g. the stratified oxygen concentration, the impact caused by pH changes on the microbial activity potential was relatively small.

As a future perspective, ultimately, experimental work (e.g. with micro-sensors) should be carried out to give more insight about the actual conditions of pH and background charge inside the granule as these two are important to validate any pH modeling efforts.

Further, the above presented simulation scenarios for pH assumes negligible impact of aeration through CO_2 stripping – an assumption valid for relatively small aeration regimes which is the case for the investigated granular CANR system in this work. However, for the sake of generalization and scale-up efforts of this technology, it is important to also study the effect of CO_2 stripping on pH under a different range of aeration rates and especially in systems exposed to high aeration rates. CO_2 stripping has previously been included in activated sludge models (e.g. Sin and Vanrolleghem, 2007), and should be relatively easily incorporated in the presented model. Related to this, it will also be relevant to consider scenarios with different bicarbonate and alkalinity concentrations.

PART III – Control and Optimization

In this part, the possibilities of optimizing and controlling the CANR process are explored. In order to test and evaluate control strategies, a model able to predict process performance was needed. This was obtained through calibration and validation of the model presented in chapter 3 to experimental data collected in the lab-scale reactors. The procedure of the calibration and validation is presented in chapter 6. Subsequently, using a process oriented approach, several novel control strategies were developed, designed, and evaluated based on extensive model simulations of continuous operation with the validated model (chapter 7). Finally, the most promising technology from the simulation investigations was tested experimentally in one of the lab-scale reactors presented in chapter 2. The experimental validation of the control strategy is presented in chapter 8.

6 Calibration and validation of a model of a granular SBR system

Summary

A validated model describing the nitritation-anammox process in a granular SBR system is an important tool for: a) design of future experiments and b) prediction of process performance during optimization, while applying process control, or during system scale-up. To this end, a model was calibrated using a step-wise procedure customized to the specific needs of the system. The important steps in the procedure were initialization, steady-state and dynamic calibration, and validation. A fast and effective initialization approach was developed to approximate pseudo steady-state in the biofilm system. For oxygen mass transfer coefficient (k_La) estimation, long-term data, removal efficiencies, and the stoichiometry of the reactions were used. For the dynamic calibration a pragmatic model fitting approach was used - in this case an iterative Monte Carlo based screening of the parameter space proposed by Sin et al. (2008b) - to find the best fit of the model to dynamic data. Finally, the calibrated model was validated with an independent data set.

The presented calibration procedure is the first customized procedure for this type of system and is expected to contribute to achieve a fast and effective model calibration, an important enabling tool for various biochemical engineering design, control, and operation problems.

6.1 Introduction

Good modeling practice requires, among other things, following a systematic model calibration guideline for quality check and consistency purposes (Sin et al., 2008b). For this purpose, a number of calibration protocols have previously been presented targeting SBR systems (Insel et al., 2006; Ganigue et al., 2010). However, a general guideline for calibration of biofilm reactor models is still under way (Boltz et al., 2012).

The issue of model calibration in wastewater treatment has been extensively studied and debated by both academia and practicing modelers/consultants (e.g. WERF protocol, HSG guidelines). Broadly speaking there are two schools of thought: (1) a systems analysis approach that aims to ground the model calibration on a more scientific basis by using parameter estimation theory and comprehensive sensitivity/identifiability analyses that come along with it; and, (2) an expert approach which relies on experiences for model fitting including parameter subset selection and manual fine-tuning of the selected parameter values.

In the systems analysis approach, the identifiability of the selected parameters must be ensured when estimating parameter values. Previous studies have investigated the parameter identifiability issue caused by model structure, where the model is typically overparameterized. Ruano et al. (2007) compared different approaches for subset selection of activated sludge models and found that up to 13 parameters could be identified, if sufficient data was available. Brun et al. (2002) found a maximum of 9 identifiable parameters consisting of a smaller subset of parameters belonging to different parameter/microbial groups in the ASM2d. Brockmann et al. (2008) found a maximum of 4 identifiable parameters in a nitrifying biofilm model. Findings like these led Gujer to conclude that “the unique identification of model parameters of ASM2d becomes impossible” (Gujer, 2006). In other words, model complexity is believed to make it impossible to allow unique parameter values resulting from a parameter estimation procedure. In addition to this, there are many other issues with systems analysis as discussed in Sin et al. (2008b): (1) search algorithms can get stuck without finding a global minimum; (2) identifiability analysis returns a limited number of parameters as identifiable while the remaining parameters (which cannot be identified) need to be assigned arbitrary default values. This makes parameter estimation conditional to other fixed values of parameters; (3) many parameter subsets exist as identifiable candidates without an obvious one to choose; (4) both sensitivity and identifiability analysis and parameter estimation are computationally very demanding. Given these practical challenges and constraints associated with using a systems analysis approach in model calibration studies, Sin et al. (2008b) proposed a pragmatic Monte Carlo based approach for

model fitting purposes. In fact, the recently published IWA GMP guidelines (Rieger et al., 2013) also suggest a combination of heuristics, expert knowledge, and sensitivity analysis as an option for parameter subset selection for the task of model calibration.

Calibration is strongly dependent on the purpose of the model usage. In this work, it was decided to use the pragmatic approach, since the overall objective of this current study was to obtain a model, which could capture the performance of the SBR by adequately predicting the concentrations of the soluble nitrogen species in the bulk liquid.

The aim of this work was therefore to calibrate a model of nitrogen conversion in granular sludge dominated by autotrophic microorganisms. To this end, first a customized calibration protocol, addressing the specific needs and features of the autotrophic nitrogen removal systems was developed. Second long-term data approximating steady-state performance and short-term dynamic data sets were collected from the lab-scale SBR reactor and used for model calibration and validation.

6.2 Modeling and methods

6.2.1 Granular sequencing batch reactor

One of the lab-scale SBRs described in chapter 2 was operated and data for calibration and validation were collected from it. The reactor was operated as described in the default operation with the following exceptions. The 8 hour cycle was distributed in a 10 minute fill phase, a 444 minute reaction phase, which was divided into three aerated and three non-aerated phases (see Figure 6.1), a 6 minute settling phase, a 10 minute draw phase, and a 10 minute idle phase. During the aerated phases the air flow was controlled at 1.2 L min^{-1}.

The DO signal was logged on-line, but the measured concentration was typically below the detection limit.

The concentrations of NH_4^+-N, NO_2^--N, and NO_3^--N were measured with the colorimetric test kits during the dynamic calibration measurement campaign. During long-term operation, NH_4^+-N and NO_3^--N in the effluent were logged on-line with the ion selective electrodes (ISE), while NO_2^--N was manually measured with the test kits. Total and volatile suspended solids were determined and the particle size distribution and the volumetric weighted mean particle size were measured as described in chapter 2.

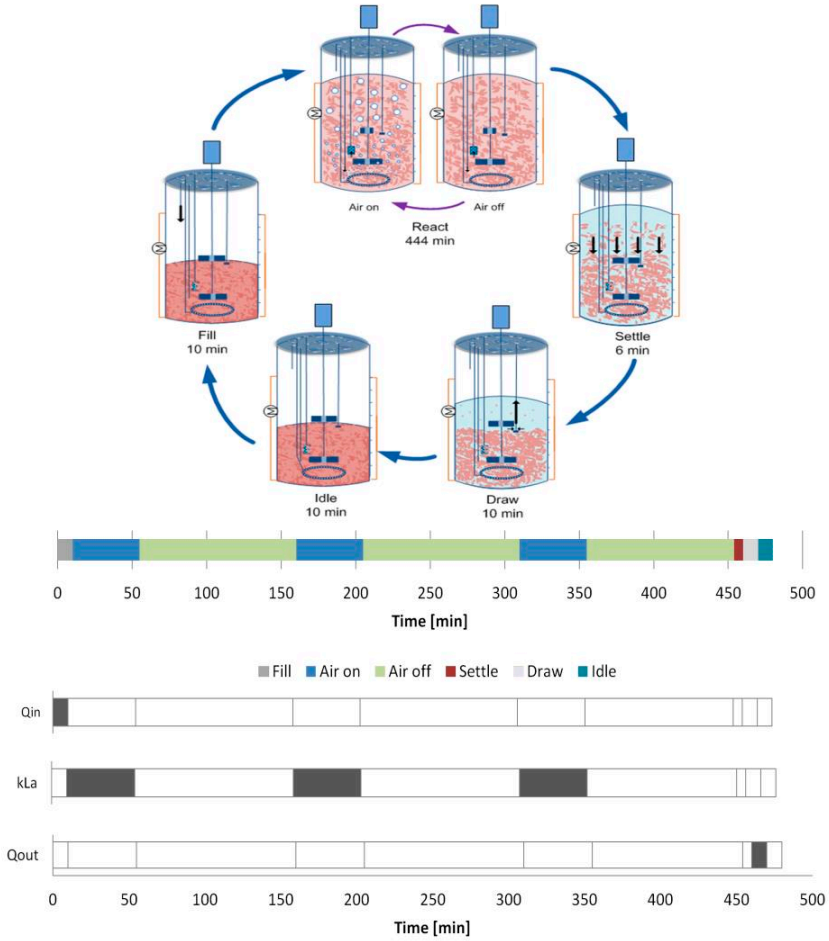

Figure 6.1 Scheme of the sequencing batch reactor operation with illustration of the phases.

6.2.2 Model description

The model described in chapter 3, consisting of mass balances for all of the compounds throughout the depth of the granules as well as in the bulk liquid, was employed.

The SBR operation was introduced to the model by letting the inflow, outflow, and oxygen supply, in the form of k_La, only being active during certain phases of the SBR cycle (see Figure 6.1, bottom). Ideal settling was assumed, such that 80% of the suspended cells in the bulk was retained during the draw phase as explained in chapter 3.

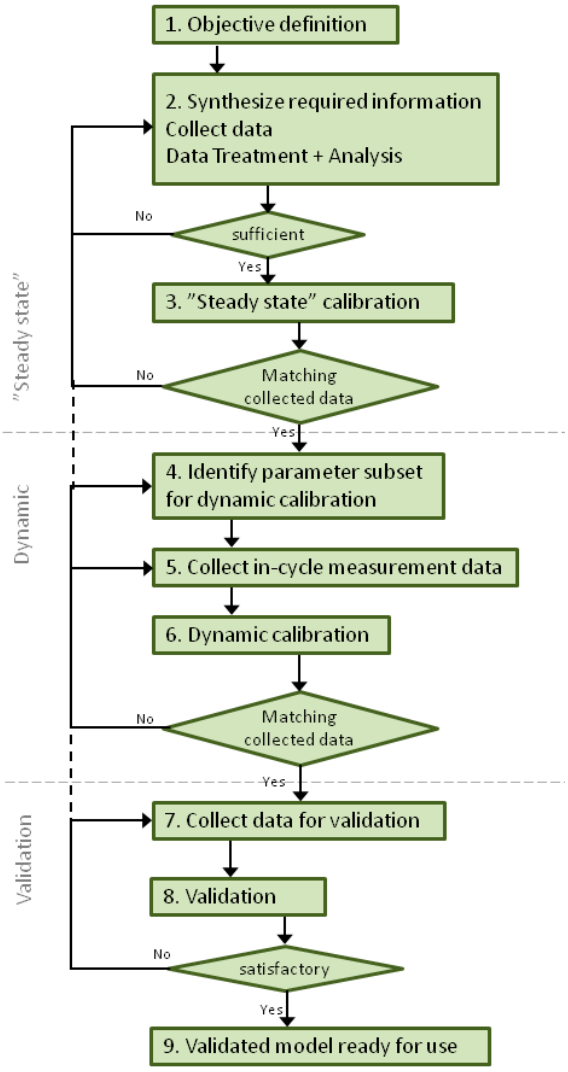

Figure 6.2 Flow diagram of the step-wise model calibration procedure.

6.2.3 Calibration methodology

In the calibration procedure a distinction between "steady-state" (pseudo steady-state, meaning that the performance of one cycle was similar to the previous one) and dynamic calibration was made (see Figure 6.2). In the steady-state calibration, the model was fitted to the overall reactor performance data, by calibrating operational parameters, which could not be determined

accurately by experimentation (e.g. oxygen transfer coefficient, granule size, or solids concentration), while in the dynamic calibration the specific removal and production rates due to the inherent dynamics of cyclic batch operation were evaluated (by calibration of a subset of parameters). Finally, after both steady-state and dynamic calibration the model was subjected to a validation procedure. Following this methodology, a workflow was developed as can be viewed in Figure 6.2. Below, the steps in the methodology are explained in detail.

6.2.4 Steady-state calibration

Step 1. Objective definition

As stated earlier, the objective of the calibration was to obtain a model which could capture the performance of the SBR by adequately predicting the concentrations of the soluble nitrogen species in the bulk liquid.

Step 2. Synthesis of required information, data collection, and data treatment

In the next step the required information was synthesized by defining the evaluation criteria to be used in the steady-state calibration. In order to represent the overall microbial activity and performance, five evaluation criteria were defined; three ratios of the production or consumption of the soluble nitrogen species from the start to the end of one cycle (Mutlu et al., 2013), and two removal efficiencies (see eqs. 6.1-6.5). The first ratio was nitrite produced over ammonium consumed, R_{NitAmm}, which was a measure of AOB activity (nitrite producer) vs. AnAOB+NOB activity (nitrite consumers) and expected to be approximately zero, since nitrite was an intermediate compound in the overall removal process. The second ratio was the ammonium removed over the total nitrogen removal, R_{AmmTot}, which gave information on AOB vs. AnAOB activity and was, based on reaction stoichiometry, expected to be around 1.09 for a balanced nitritation-anammox process. Finally, the third ratio was nitrate produced over total nitrogen removal, R_{NatTot}, indicating NOB vs. AnAOB activity (both nitrate producers), and was expected to have a value of approximately 0.07, when AnAOB were the only nitrate and nitrogen gas producers. All ratios were also affected by the possible activity of heterotrophic bacteria (HB), which can be present in these types of systems even though no external organic carbon source is supplied (Dapena-Mora et al., 2004).

The ratios thus gave information on the relative activity of the microbial groups, whereas the removal efficiencies supplied information on their absolute activity.

$$R_{NitAmm} = \frac{\left|NO_{2,start}^{-} - NO_{2,end}^{-}\right|}{\left|NH_{4,start}^{+} - NH_{4,end}^{+}\right|} = \frac{\Delta NO_{2}^{-}}{\Delta NH_{4}^{+}} \quad (6.1)$$

$$R_{AmmTot} = \frac{\left|NH_{4,start}^{+} - NH_{4,end}^{+}\right|}{\left|NH_{4,start}^{+} + NO_{2,start}^{-} + NO_{3,start}^{-} - NH_{4,end}^{+} - NO_{2,end}^{-} - NO_{3,end}^{-}\right|} = \frac{\Delta NH_{4}^{+}}{\Delta TN} \quad (6.2)$$

$$R_{NatTot} = \frac{\left|NO_{3,start}^{-} - NO_{3,end}^{-}\right|}{\left|NH_{4,start}^{+} + NO_{2,start}^{-} + NO_{3,start}^{-} - NH_{4,end}^{+} - NO_{2,end}^{-} - NO_{3,end}^{-}\right|} = \frac{\Delta NO_{3}^{-}}{\Delta TN} \quad (6.3)$$

$$E_{Amm} = \frac{NH_{4,in}^{+} - NH_{4,end}^{+}}{NH_{4,in}^{+}} \cdot 100\% \quad (6.4)$$

$$E_{Tot} = \frac{NH_{4,in}^{+} + NO_{2,in}^{-} + NO_{3,in}^{-} - NH_{4,end}^{+} - NO_{2,end}^{-} - NO_{3,end}^{-}}{NH_{4,in}^{+} + NO_{2,in}^{-} + NO_{3,in}^{-}} \cdot 100\% \quad (6.5)$$

where the subscript “start” denotes the concentration in the beginning of a cycle, the subscript “end” denotes the concentration at the end of a cycle, and the subscript “in” denotes the concentration in the influent.

The data collection for the steady-state calibration was considered sufficient when, during one week of operation, the evaluation criteria varied less than 5% (the evaluation criteria were calculated once per day).

Step 3. “Steady-state” calibration

A one week period of “pseudo steady-state” operation was used as the calibration period (see Figure 6.3), and average values of the evaluation criteria were used to compare with the simulation results.

A challenging task in biofilm modeling is initialization, i.e. simulating sufficient time to reach steady-state. Since the retention time of the solids increases over the depth of the biofilm, the normal rule of thumb of simulating operation for three times the SRT cannot be applied. Previously, 1000 days (Sin et al., 2008a) and 10000 days (Volcke et al., 2010) of operation have been simulated to reach steady-state in continuously operated biofilm systems. In addition, the discrete nature of SBR operation causes fast dynamics and steep concentration gradients in the system. The combination of these very slow biofilm dynamics with the relatively fast SBR operation dynamics makes it computationally very heavy to solve the model. In this work, this

problem was tackled by initializing the model by simulating 1000 days (assumed steady-state) of continuous operation, with continuous influent, effluent, and aeration, followed by 10 days of SBR operation. Finally, the values of the evaluation criteria were calculated on the basis of the last cycle of the 10 days of SBR operation.

6.2.5 Dynamic calibration

Following the pragmatic approach of Sin et al. (2008b), first a parameter subset was selected by using process knowledge, previous experiences, and sensitivity analysis. Then the Latin Hypercube Sampling (LHS) technique was used to efficiently sample the parameter subspace (defined by an upper and lower range assigned for each parameter in the subset). The Monte Carlo simulations were performed with these samples, and the resulting model fits to the data were assessed and ranked. The best fit was selected and thereby concluded the model fitting task. In this approach, the parameter values obtained are interpreted as an arbitrary combination of values from a parameter subspace (among many other possible ones) that provided a good fit to data. The values are not considered unique estimates of the parameter values, as one would get from parameter estimation theories, and hence no physical meaning is attached to them.

Step 4. Parameter subset identification

In the dynamic calibration, the first step was to define a parameter subset to be used for calibration (see Figure 6.2). Previously, different approaches have been used to select the parameter subset, ranging from the simplest approach based on expert knowledge to the more computationally demanding identifiability analysis (Ruano et al., 2007; Brockmann et al., 2008). In this work we used a combination of expert knowledge, process knowledge, and sensitivity analysis as commonly used for selecting parameters for fitting models to data, see e.g. the STOWA protocol (Hulsbeek et al., 2002) and the IWA GMP guidelines (Rieger et al., 2013) among others.

Step 5. In-cycle data collection

In the following step of the calibration procedure, data of the bulk concentrations of the soluble nitrogen species were collected by manually sampling from the reactor vessel every 15 minutes, which in total gave 30 data points for each measured compound during one cycle.

Step 6. Dynamic calibration

100 samples were taken from the defined parameter space by LHS (Iman and Conover, 1982) and the resulting 100 Monte Carlo simulations were run. Similar to the steady-state calibration, each of the 100 simulations of the model was initialized by simulating 1000 days of continuous operation followed by four cycles of SBR operation. Simulation of four cycles was found to be sufficient to reach "pseudo steady-state", where the nitrogen concentration profiles did not change more than 1% from one cycle to the next. The last of these four cycles was therefore used for comparison with the experimental data.

Different objective functions was used to assess the quality of the model fit, such as root mean squared error (RMSE) and weighted sum of squared errors (WSSE) (see eqs. 6.6 and 6.7):

$$RMSE = \sqrt{\frac{1}{n}\sum_{i=1}^{n}\left(y_{meas,i} - y\left(t_i,\theta\right)\right)^2} \tag{6.6}$$

$$WSSE = \sum_{k=1}^{m}\sum_{i=1}^{n}\left(\frac{y_{meas,k}(t_i) - y_{model,k}(t_i,\theta)}{\sigma_k}\right)^2 \tag{6.7}$$

where *m* is the number of variables measured (three; ammonium, nitrite, and nitrate), *n* is the number of experimental observations (the number of sample times), $y_{meas,k}$ is the observed value, $y_{model,k}$ is the simulated output value, θ represents the values of the parameters in a given subset, and σ_k represents the measurement error of variable k, which was found as the standard deviation resulting from triplicate measurements of a standard concentration of each of the three variables (ammonium, nitrite, and nitrate). The Monte Carlo simulations were ranked, and the parameter set in the sample resulting in the lowest error was selected.

In order to ensure that the dynamically calibrated parameters also captured the overall performance, a long-term simulation, consisting of 1000 days of continuous operation followed

by 10 days of SBR operation as in the steady-state calibration, was conducted and the five evaluation criteria were calculated and compared to the experimental values.

6.2.6 Validation

Step 7. Data collection for validation

It is desirable to collect data at a different operating point, than the one where the calibration was conducted, to ensure that the validity range of the model is as wide as possible. Samples were taken every 15 minutes as in the data collection for calibration.

Step 8. Validation

A simulation, with the different conditions and the new values of the parameters in the calibrated subset, was conducted in a similar fashion as for the calibration, by first simulating 1000 days of continuous operation followed by four SBR cycles. In order to ensure the model's validity before application, the calibrated parameters were checked by comparing the RMSEs from the calibration to the RMSEs from the validation and through calculation of the Janus coefficient (J) (Power, 1993):

$$J^2 = \frac{\frac{1}{n_{val}}\sum_{i=1}^{n_{val}}\left(y_{meas,i} - y_{model}\left(t_i,\theta\right)\right)^2}{\frac{1}{n_{cal}}\sum_{i=1}^{n_{cal}}\left(y_{meas,i} - y_{model}\left(t_i,\theta\right)\right)^2} \quad (6.8)$$

where n_{val} is the number of experimental observations for validation and n_{cal} is the number of experimental observations for calibration.

6.3 Results and discussion

6.3.1 Steady-state calibration

The solids concentration was 4.2 g VSS L^{-1}, and a particle size distribution was determined by laser diffraction with the average granule/floc diameter being 100 µm. The k_La value was first estimated by conducting clean water tests in the lab-scale SBR, since it could not be determined in-situ with the sludge present in the reactor, as this would lead to inhibition of the anoxic microbial groups (i.e. AnAOB). However, simulation results quickly showed that the actual k_La

value in the SBR during microbial reaction was strongly underestimated, which can be seen on the predicted removal efficiencies of simulation 1 in Table 6.1. This discrepancy is speculated to be caused by differences in the ionic strength, viscosity, etc. between the clean water and the synthetic influent/sludge mixture. The k_La value was therefore chosen as a calibration parameter in the steady-state calibration, while all other operational parameters were assumed accurately measured. Based on theoretical reaction stoichiometry, a set of k_La values was selected as first guesses for the correct k_La value (simulation 2 to 5 in Table 6.1).

Table 6.1 Simulations for k_La determination. Simulation no. 1 corresponds to the k_La obtained from clean water test estimation, while simulations no. 2 to 5 were simulated to obtain the best fit to the steady-state experimental values.

	k_La	R1	R2	R3	NH_4^+ removal	TN removal
No. Simulation	d^{-1}	$\Delta NO_2^-/\Delta NH_4^+$	$\Delta NH_4^+/\Delta TN$	$\Delta NO_3^-/\Delta TN$	%	%
1	369	0.000	1.047	0.045	47.9	44.7
2	444	0.000	1.051	0.048	67.7	64.6
3	516	0.000	1.052	0.049	82.1	78.2
4	533	0.000	1.051	0.049	84.3	80.3
5	565	0.000	1.051	0.049	90.2	85.9
Experimental		0.001	1.072	0.071	86.9	81.0
Expected*		0.00	1.09	0.07		

***** From stoichiometric reactions of complete autotrophic nitrogen removal, i.e. AOB and AnAOB activity without any activity of NOB and HB.

The simulations were assessed by calculating the sum of the relative errors of the five evaluation criteria. The values of evaluation criteria were obtained as an average of one week of SBR operation data, where measurements were made once per day. From the simulation results, evaluation criteria were calculated for one cycle after 10 days of simulated SBR operation. In simulation, the cycles were already repeatable after four cycles, with the nitrogen concentrations changing less than 1%, but in order to visually compare data and modeling results (Figure 6.3), 10 days of operation were simulated. As a result, the k_La during the aerated phases of the SBR cycle was determined to be the average of the k_La values used for simulations 3 and 4, i.e. k_La=524 d^{-1} (see Table 6.1). Results of the simulation with k_La=524 d^{-1} along with the experimental data from the calibration period can be seen in Figure 6.3. This calibrated value is relatively far from the measured value in clean water, and it is therefore important to stress that the calibrated value does not carry any physical meaning, but captures the performance and state of the system.

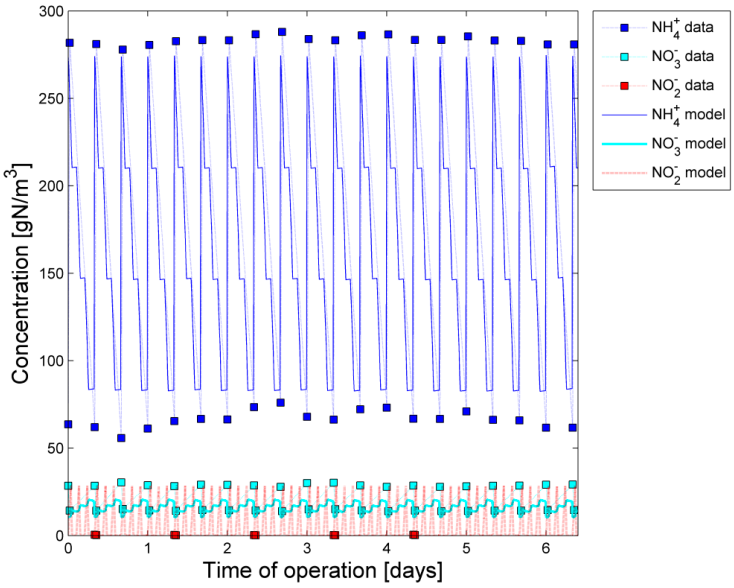

Figure 6.3 "Long-term" (1 week) concentration data at the beginning and at the end of the SBR cycles along with model results.

6.3.2 Dynamic calibration

From a global sensitivity analysis (Vangsgaard et al., 2012), the squared standardized regression coefficients (SRCs) of the bulk concentrations of ammonium, nitrite, and nitrate for each parameter were calculated, and a cut off value of 0.05 (corresponding to 5% impact) was used to distinguish the significant parameters from the non-significant ones. Conducting this analysis, a parameter subset containing one stoichiometric and five kinetic parameters was selected (see Table 6.2). Uniform probability distributions of the parameter values were assumed, since no *a priori* information about the true statistical distributions was available. The variability of the parameters in the subset was assigned based on expert knowledge and previous experiences (Sin et al., 2009). For $\mu_{max,AOB}$, b_{AOB}, and $\mu_{max,AnAOB}$ the uniform distribution was bounded 25% around the default value, for $K_{O2,AOB}$ and $K_{O2,AnAOB}$ the distribution was bounded 50% around the default value and for Y_{AnAOB}, which was considered relatively well-known, the distribution was bounded 5% around the default value. All Monte Carlo simulations are shown along with the experimental data in Figure 6.4.

The calibrated values obtained from the parameter subset giving the smallest value of WSSE can be seen in Table 6.2.

Table 6.2 Default values, upper and lower boundaries of the uniform distribution and calibrated values of the selected parameter subset.

Parameter	Name	Unit	Default value	Lower bound	Upper bound	Calibrated value
Max growth rate of AOB	$\mu_{max,AOB}$	d^{-1}	2.050	1.538	2.563	2.450
Oxygen affinity constant for AOB	$K_{O2,AOB}$	g O_2 m^{-3}	0.300	0.150	0.450	0.165
AOB decay rate	b_{AOB}	d^{-1}	0.130	0.098	0.163	0.136
Max growth rate of AnAOB	$\mu_{max,AnAOB}$	d^{-1}	0.073	0.055	0.091	0.068
Oxygen inhibition constant for AnAOB	$K_{O2,AnAOB}$	g O_2 m^{-3}	0.010	0.005	0.015	0.011
AnAOB growth yield	Y_{AnAOB}	g COD (g N)$^{-1}$	0.160	0.152	0.168	0.166

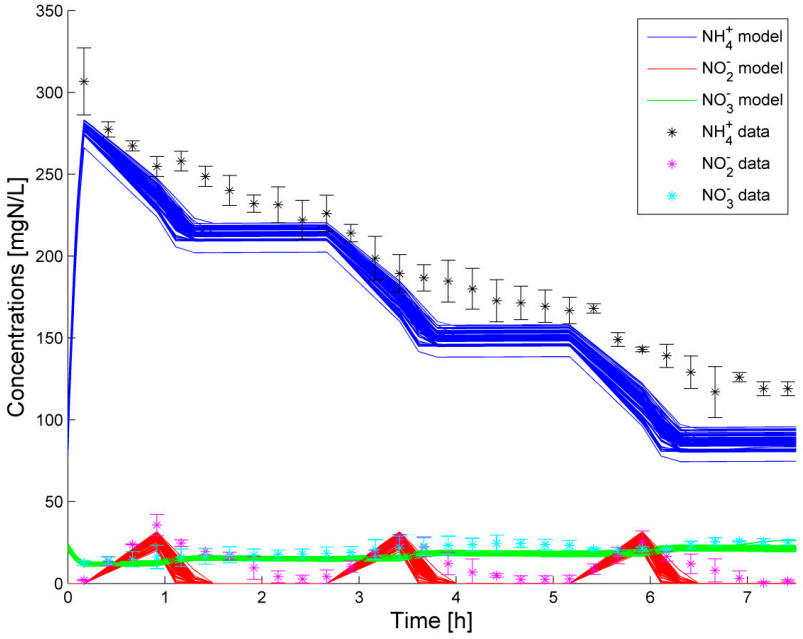

Figure 6.4 Experimental data from three cycle analyses shown as averages with standard deviations, compared to the results of the last cycle from the Monte Carlo simulations.

As can be seen in Figure 6.4, all of the MC simulations have an offset compared to the data collected, especially for ammonium. Two measures were therefore taken in order to tackle this problem.

First, the dynamic calibration step was iterated once again by revising the parameter subset (this option is indicated in the workflow in Figure 6.2). The parameter subset was therefore extended to also include $\mu_{max,NOB}$, $K_{O2,NOB}$, b_{NOB}, $K_{HNO2,AnAOB}$, Y_{AOB}, D_{NO2}, L_B and the parameter space was expanded to be ±50% around the default value in a uniform distribution for all of the parameters in the subset. The new parameter subset selection was based on a combination of the most sensitive parameters based on model analysis (like in the previous iteration) and parameters expected to have an impact based on practical experiences. Thus a combination of expert knowledge and sensitivity analysis was applied in this iteration. Among these last parameters were kinetic parameters of NOB, which according to the sensitivity analysis should not have a large impact, but which by experience can strongly influence the reactor system. The new subset and its upper, lower, and default values can be seen in Table 6.3.

Secondly, both the data and the model result were scaled based on the initial concentrations, such that any inaccuracy caused by equipment, but not included in the model (e.g. deviations in pump flow rates which were assumed constant in the model), did not influence the calibration. The ammonium and nitrate concentrations were scaled by dividing all of the concentrations in the measured points by the first measurement point (the start of the reaction phase). The nitrite concentrations were scaled by dividing all the measurements by the concentration corresponding to the fourth measurement (55 minutes into the cycle) in order to avoid dividing by zero, which was the value of the concentration at the beginning of the cycle. The new MC simulations and the scaled concentrations can be seen in Figure 6.5.

Table 6.3 Default values, upper and lower boundaries of the uniform distribution and calibrated values of the selected parameter subset after iteration.

Parameter		Unit	Default value	Lower bound	Upper bound	Calibrated value
Max growth rate of AOB	$\mu_{max,AOB}$	d^{-1}	2.050	1.025	3.075	2.064
Oxygen affinity constant for AOB	$K_{O2,AOB}$	$g\ O_2\ m^{-3}$	0.300	0.150	0.450	0.332
AOB decay rate	b_{AOB}	d^{-1}	0.130	0.065	0.195	0.150
Max growth rate of NOB	$\mu_{max,NOB}$	d^{-1}	1.454	0.727	2.181	0.974
Oxygen affinity constant for NOB	$K_{O2,NOB}$	$g\ O_2\ m^{-3}$	1.100	0.550	1.650	0.752
NOB decay rate	b_{NOB}	d^{-1}	0.061	0.030	0.091	0.069
Max growth rate of AnAOB	$\mu_{max,AnAOB}$	d^{-1}	0.073	0.037	0.110	0.088
Oxygen inhibition constant for AnAOB	$K_{O2,AnAOB}$	$g\ O_2\ m^{-3}$	0.010	0.005	0.015	0.013
HNO_2 affinity constant for NOB	$K_{HNO2,AnAOB}$	$g\ N\ m^{-3}$	2.81e-6	1.41e-6	4.22e-6	2.92e-6
AOB growth yield	Y_{AOB}	$g\ COD\ gN^{-1}$	0.210	0.105	0.315	0.292
AnAOB growth yield	Y_{AnAOB}	$g\ COD\ gN^{-1}$	0.160	0.080	0.240	0.124
Diffusivity of nitrite	D_{NO2}	$m^2\ d^{-1}$	2.60e-4	1.30e-4	3.90e-4	1.70e-4
Mass transfer boundary layer	L_B	m	1.76e-5	8.80e-6	2.64e-5	2.26e-5

The calibrated values in Table 6.3 were obtained from the parameter subset sample, which resulted in the lowest RMSE value. RMSE (see the values in Table 6.4) was used instead of WSSE, since the data points were already scaled by the initial concentration in this approach. This simulation with the parameter subset sample resulting in the smallest RMSE is plotted along with the data in Figure 6.6, which shows a much better model fit than in the previous iteration (Figure 6.4).

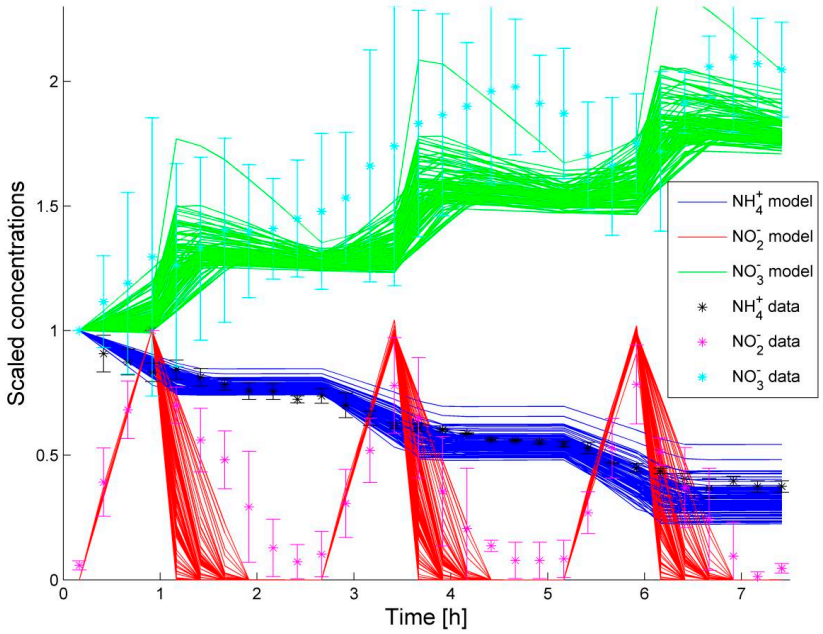

Figure 6.5 Scaled model result of the last cycle of all Monte Carlo simulations along with scaled experimental data from three cycles.

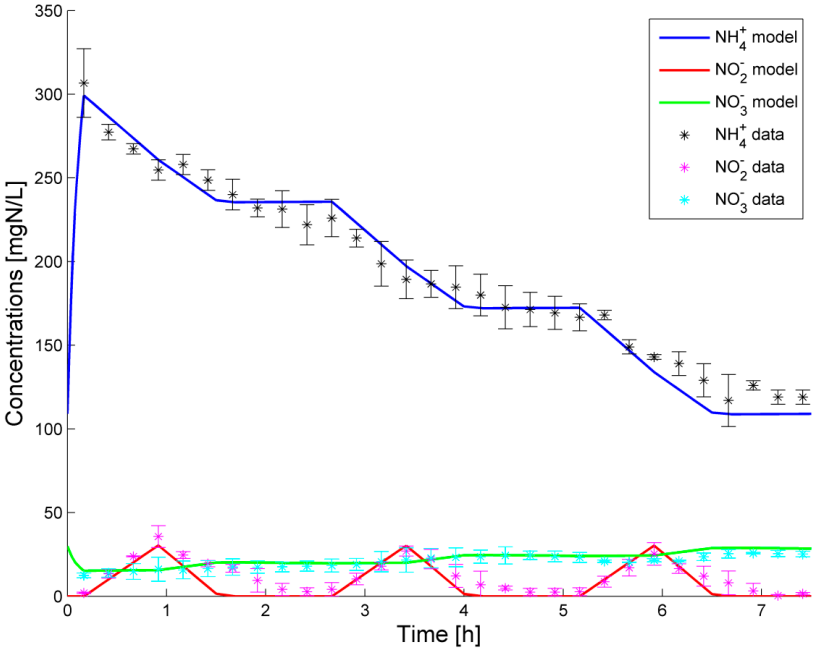

Figure 6.6 Experimental data with simulation result with best fitting parameter subset.

6.3.3 Validation

The data for validation were collected approximately three months after collection of the data for calibration. From the collection of the data for calibration to the collection of data for validation, the solids concentration had increased to 4.4 g VSS L^{-1} and the volumetric weighted mean of the granule/floc diameter had decreased from 100 µm to 70 µm. Since the model was describing a biofilm, the mass transfer phenomena were accounted for explicitly. This means that the microbial kinetic parameter values (e.g. K_S values) in this model are solely describing the microbial metabolism, and not accounting for the effects of mass transfer limitation, which they otherwise do in suspended growth systems, as described by activated sludge models. It was therefore not expected that the kinetic parameter values would change when the mass transfer conditions were altered, which was the case from calibration (100 µm) to validation (70 µm).

Table 6.4 Statistical tests for calibration and validation.

Model output	RMSE		Janus coefficient (J)
	Calibration	Validation	
Ammonium	0.039	0.057	1.478
Nitrite	0.366	0.173	0.473
Nitrate	0.171	0.093	0.544

The statistical tests in Table 6.4 show that the model fitted the data better for nitrite and nitrate during the validation. For ammonium the validation was slightly worse compared to the calibration, which was also found in the SBR calibration reported by Ganigue et al. (2010). These trends can also be observed in the graphs in Figure 6.7. It could be caused by the smaller amount of data being used in validation compared to the calibration. However, the results of RMSE calculations were within the same order of magnitude in calibration and validation, and the Janus coefficients were relatively close to 1 for all the three outputs, which implied a good model fit. No change in the model structure from the calibration to the validation could therefore be assumed.

Since both the data for calibration and validation were collected in the same reactor the extent of the validity of the model remains within this reactor. If the model should be applied to other reactor systems a new validation should be performed.

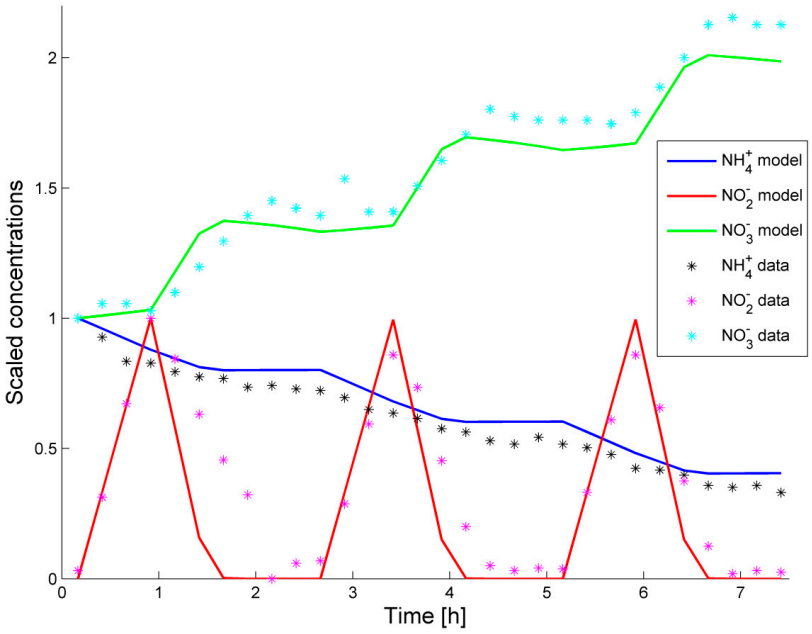

Figure 6.7 Scaled validation simulation result along with the scaled experimental data.

This approach proves suitable for obtaining a model, which can successfully capture the performance of the system. However, interpreting the meaning of the new values of the calibrated parameters might not be possible, since a pragmatic brute force method was used. The objective of the calibration is thus of great importance. This calibration procedure can therefore be applied to other autotrophic nitrogen removing systems as a systematic approach to guide the calibration efforts, however, the calibrated parameter values themselves should be transferred with care.

6.4 Conclusions

The presented calibration procedure is the first customized procedure for this type of system and contributes to achieve a fast and effective model calibration. An efficient initialization approach was developed to approximate pseudo steady-state in the biofilm system by simulating 1000 days of continuous operation followed by the much more dynamic SBR operation. For the k_La estimation, long-term performance data of removal efficiencies and the

stoichiometry of autotrophic nitrogen removal reactions were used as novel evaluation criteria. This resulted in a calibrated k_La value of 524 d^{-1}. Second, a subset of microbial kinetic parameters was calibrated to dynamic data collected during SBR cycles by a pragmatic Monte Carlo based model fitting method, which needed iteration until satisfactory results were obtained. Finally, the model was successfully validated and will serve a useful tool for: a) design of future lab-scale experiments, and b) prediction of process performance, which is important in future process optimization, control applications, and up-scaling.

7 Development of novel control strategies: A process oriented approach

Summary

In this contribution, a new process oriented approach was used to develop, evaluate and benchmark control strategies to ensure stable operation and rejection of disturbances. Three control strategies were developed: a feedforward control (control strategy 1 – CS#1), a rule-based feedback control (CS#2), and a feedforward-feedback controller, in which the feedback loop updates the set point of the feedforward loop (CS#3). The CS#1, based on influent measurements, was giving the best performance against disturbances in the ammonium concentration, whereas the CS#2 was providing the best performance against disturbances in the readily degradable organic carbon concentration. The CS#3 rejected both disturbances satisfactorily. Thus, this controller provided versatility towards disturbance rejection, at the expense of a slightly larger offset in the controlled variable, which was the removal efficiency, and a slightly more complex control structure.

7.1 Introduction

The automatic control of bioreactors utilizing mixed cultures, such as single-stage CANR, is challenging given their highly nonlinear behavior, interactive dynamics, and variations in the influent (flow rate, composition, temperature, etc.). Furthermore, only a few actuators are usually available to reject disturbances and maintain a stable operation, which is complicated due to competing microbial groups. In this context, advanced control can improve the process performance: i.e. nonlinear controllers, such as gain scheduling, are suitable to address the nonlinear behavior of the bioreactor, or model predictive control (MPC) can tackle the relationships between the multiple microbial groups. However, the development of such advanced control strategies in bioreactors is usually hindered by the low accuracy of models describing the microbial metabolism, the long simulation times required to solve such models, and by the complexity of such controllers (Olsson, 2011). In this respect, the simplicity of a controller is an important characteristic in a bioreactor, since it is likely that frequent maintenance will be needed as a result of variations in the feed, seasonal variations, and even because of microbial evolution. Hence, a tradeoff must be achieved between efficient control and monitoring tools on the one hand and simplicity on the other hand, in order to ensure the success of the control strategy.

Previously, several control strategies for the two-stage CANR process have been developed and tested (i.e. Volcke et al., 2007). However, results cannot be directly transferred to the intensified single-stage system, since fewer actuators are available and the process dynamics are more complex. This is a common issue faced in intensified systems (Nikacevic et al., 2012). For single-stage treatment, pH (Wett, 2007) and ammonium and nitrate measurements (Christensson et al., 2013) have been used as measured variables providing the necessary on-line data to control the DO concentration. Yet, these strategies only tackle the regulation of the process, not the performance. As a result, no strategies have so far aimed at directly controlling the nitrogen removal efficiency.

In the previous modeling study in chapter 4, the oxygen to ammonium loading ratio (RO), as opposed to the concentration ratio or solely the DO concentration, was identified as a key factor for securing a high removal efficiency and conversion rate, while avoiding growth of undesired microbial groups. A similar finding was made by Kwak et al. (2012). Additionally, ranges of ratios of nitrogen species, consumed or produced in the process that indicate a suitable operation, have been formulated based on reaction stoichiometry and process knowledge (Mutlu et al., 2013). Among these, a ratio between the ammonium removal and the total nitrogen removal

(R_{AmmTot}) has been formulated as a measure of the relative activity of microbial groups present in the system (eq. 6.2).

The aim of this work was to design a control system through a systematic process oriented approach, for a single-stage treatment system, by utilizing process insights obtained from previous model and experimental studies. This has been illustrated through numerical simulations of a continuously operated reactor system, utilizing the experimentally calibrated and validated model from the previous chapter 6. The objective of the controller was to keep the intensified process at a stable and efficient performance during disturbances in influent composition and set point changes.

7.2 A process oriented approach to controller design

The controllers were developed by following a step-wise procedure consisting of the following steps (Figure 7.1): The first step was the definition of the control objective, in which the specific aim of the controller was specified. This was then followed by a variable analysis and degrees of freedom analysis, where the measurements and actuators available were specified. Subsequently, the controlled and manipulated variables were identified from the analysis result generated in the previous step. Once these were identified the control structures were formulated, followed by a definition of the control laws, which concluded the controller design. Finally, the simulation scenarios and evaluation criteria were defined. The entire workflow can be viewed in Figure 7.1. Each step of this procedure applied to the CANR process is explained in more detail below.

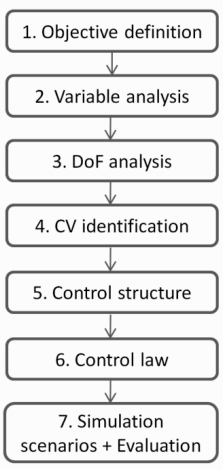

Figure 7.1 Workflow used for controller development.

Step 1 - Objective

In line with the aim of the work, the objective of each controller was to obtain a high and stable nitrogen removal efficiency.

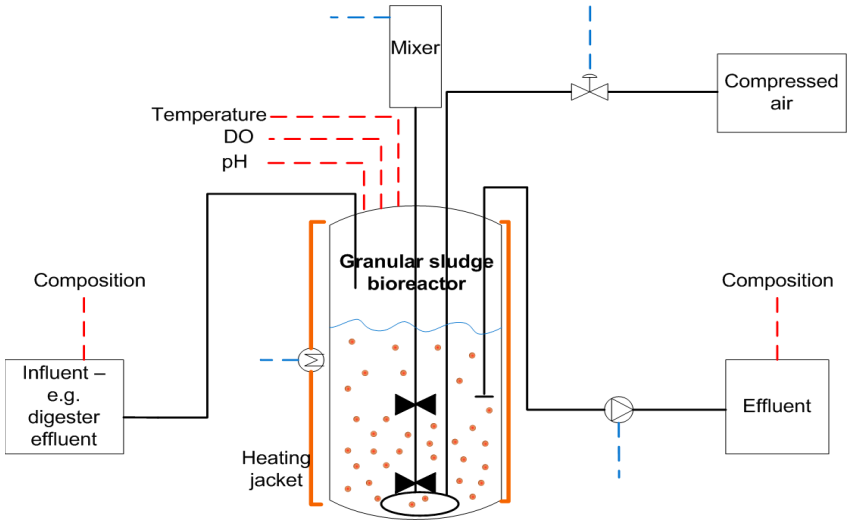

Figure 7.2 Reactor system scheme indicating potential MVs (dashed blue lines) and measured variables (dashed red lines).

Table 7.1 Variable analysis. MV = Manipulated variable, CV = Controlled variable.

Variable	Unit	Candidate for:	Description
Q_{out}	L d^{-1}	MV	Reactor outflow
Heating	W	MV	Electrical heating jacket
Mixer	rpm	MV	Electrical motor for rotor
k_La	d^{-1}	MV	Oxygen mass transfer coefficient
$NH_{4\ out}^{+}$	mg N L^{-1}	CV	Effluent ammonium concentration
$NO_{2\ out}^{-}$	mg N L^{-1}	CV	Effluent nitrite concentration
$NO_{3\ out}^{-}$	mg N L^{-1}	CV	Effluent nitrate concentration
DO_{bulk}	mg COD L^{-1}	CV	Dissolved oxygen concentration in bulk
pH	-	CV	pH in the bulk liquid
T	^{o}C	CV	Temperature in the bulk liquid
RT	-	CV	Total nitrogen removal efficiency
R_{AmmTot}	-	CV	Ammonium to total nitrogen removal – metric of relative activity of microbial groups
$NH_{4\ in}^{+}$	mg N L^{-1}	Disturbance	Influent ammonium concentration
S_S	mg COD L^{-1}	Disturbance	Influent organic carbon concentration

Step 2 - Variable analysis

The potential controlled variables (CVs) and potential manipulated variables (MVs) can be seen in Figure 7.2, where sensors and actuators are indicated in red and blue, respectively. Descriptions of these, along with a description of the disturbances in the system, are provided in Table 7.1.

The removal efficiency (RT) in Table 7.1 is defined similarly as the evaluation criteria in the previous chapter in eq. 6.5, however here it is given as a fraction instead of in percent. It is calculated as the total nitrogen removed (ΔTN) over the total nitrogen in the influent (TN_{in}), and is thus a combination of measurements of influent and effluent composition concentrations:

$$RT = \frac{\Delta TN}{TN_{in}} = \frac{NH_{4,in}^{+} + NO_{2,in}^{-} + NO_{3,in}^{-} - NH_{4,out}^{+} - NO_{2,out}^{-} - NO_{3,out}^{-}}{NH_{4,in}^{+} + NO_{2,in}^{-} + NO_{3,in}^{-}} \quad (7.1)$$

And R_{AmmTot} is the ammonium removal over the total nitrogen removal, as defined previously in chapter 6. However, since in this chapter a continuous operation was considered, it was calculated as a combination of influent and effluent measurements of nitrogen species concentrations:

$$R_{AmmTot} = \frac{\Delta NH_4^{+}}{\Delta TN} = \frac{NH_{4,in}^{+} - NH_{4,out}^{+}}{NH_{4,in}^{+} + NO_{2,in}^{-} + NO_{3,in}^{-} - NH_{4,out}^{+} - NO_{2,out}^{-} - NO_{3,out}^{-}} \quad (7.2)$$

The concentrations of ammonium and organic carbon were identified as the two main disturbances. From practical experiences, these are the disturbances that show most variation and which are most frequently observed in side-streams originating from dewatering of anaerobic digestion sludge, along with changes in flow rate and temperature of the stream.

Step 3 - Control degree of freedom analysis

Four potential actuators (MVs) were identified in the system; namely the effluent pump, the mixer, the electrical heating jacket, and the air supply (Figure 7.2 and Table 7.1). The influent stream was assumed to originate from a sludge digester upstream and was therefore a disturbance to the system through variations in the influent concentrations. The effluent pump was assumed to perfectly control the level, and thus the HRT in the reactor at a given set point (a good assumption considering that flow variations are several orders of magnitude faster than the reactions catalyzed by the microbial groups active in the CANR process). The heating jacket was assumed to perfectly control the temperature. The impact of mixing on the mass transfer conditions was previously established through a semi-empirical relation (Nicolella et al., 1998; Vangsgaard et al., 2012). However, a certain amount of shear should be supplied in order to trigger granule formation, but at the same time should not be so high that the granules disintegrate (Tay et al., 2006). How much shear force is needed, and how this is related to the mixing conditions, is not yet fully established (Vlaeminck et al., 2012), hence the mixer was not considered a suitable actuator. Consequently, it was concluded that the only available actuator for control was the air supply. For simplicity, this manipulated variable was represented by the oxygen mass transfer coefficient, k_La, in the model simulations.

Step 4 - Identification of controlled variable

Since only one MV was available, pairing it with an appropriate CV was of essential importance. The measured variables are indicated on Figure 7.2 and in Table 7.1, and at a first glance the obvious CV candidate is DO or failing that, the effluent concentrations of the nitrogen species ammonium, nitrite or nitrate. However, DO, which is often used as a CV in biological nitrogen removal in wastewater treatment (Olsson, 2012; Åmand et al., 2013; Christensson et al., 2013), was not a suitable CV in this case, since its concentration was very low in the reactor, i.e. often below the detection limit. Besides, none of the aforementioned variables could be directly related to nitrogen removal efficiency due to the complexity of the intensified process. Hence, RT, which is a function of both influent concentration and effluent concentration measurements, was proposed directly as the CV.

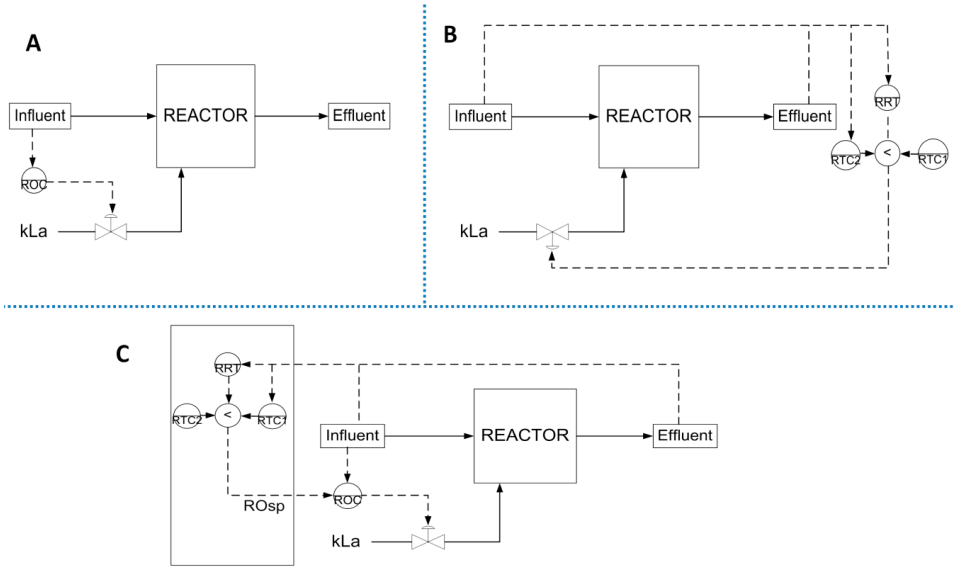

Figure 7.3 Layout of the three control strategies. A) Case 1: Feedforward control, B) Case 2: Rule based feedback control, and C) Case 3: Feedforward-feedback control.

Step 5 - Control structures

As a consequence of the variable analysis, three control strategies were developed with RT as the CV and k_La as the MV. They are presented in detail below.

Control strategy 1 (CS#1): The first strategy identified was a feedforward control (Figure 7.3A) based on the optimal oxygen to ammonium volumetric loading ratio (RO). This strategy was inspired by the findings from previous simulation studies from chapter 4. The optimal RO can be seen in Figure 7.4, where the efficiency is plotted as a function of RO. Operating below the optimal ratio leads to ammonium accumulation and the overall removal being limited by AOB activity. Above the optimal ratio nitrite and/or nitrate accumulates and the removal efficiency is compromised by NOB growth and/or AnAOB inhibition.

Assuming that the bulk oxygen concentration was always zero (or below the detection limit), the oxygen to ammonium volumetric loading ratio can be expressed by the following equation:

$$RO = \frac{L_{O_2}}{L_{NH4}} = \frac{k_L a\left(S_{O2,sat}\right)}{NH^{+}_{4,in} / HRT} \tag{7.3}$$

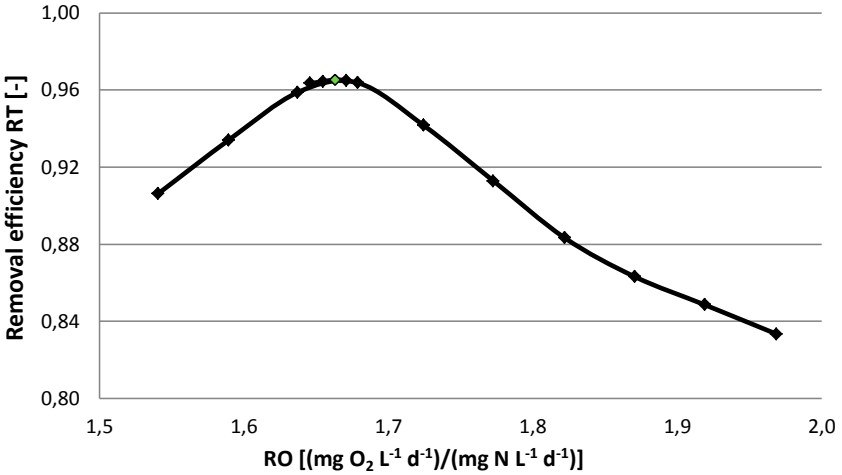

Figure 7.4 Nitrogen removal efficiency (RT) represented as a function of the volumetric oxygen to nitrogen loading ratio (RO). Simulation results based on the calibrated and validated model from chapter 6. The green point indicates the optimal RO value.

Control strategy 2 (CS#2): The second control strategy (Figure 7.3B) consisted of a feedback loop, where the control action was determined by the offset in removal efficiency ($e(t) = RT_{sp}-RT(t)$) and the value of R_{AmmTot} was used to diagnose the system. The rationale behind the introduction of R_{AmmTot} was the following: The offset from the optimal removal could be caused either by an excess oxygen supply or a lack of oxygen supply (Figure 7.4). Therefore, a criterion was needed to establish the cause of the removal efficiency offset. A value above the set point of R_{AmmTot} indicated nitrite or nitrate accumulation leading to a lower total removal efficiency (Figure 7.4 and 7.5). The oxygen supply should therefore be decreased in order to return to a balanced activity state. If the R_{AmmTot} value was below the set point value, the activities were balanced, but there was an excess of ammonium. Hence, aeration should be increased, such that more ammonium could be removed and thereby increase the efficiency. The relation between R_{AmmTot} and the oxygen to nitrogen loading ratio can be seen in Figure 7.5, where the set point value is also indicated.

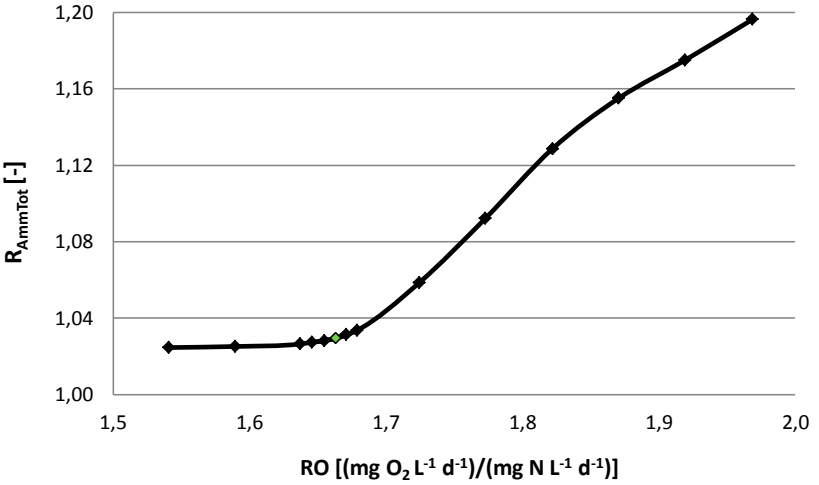

Figure 7.5 R_{AmmTot} as a function of the volumetric oxygen to nitrogen ratio (RO). Simulation results based on the calibrated and validated model from chapter 6. The green point indicates the set point value of R_{AmmTot}.

Control strategy 3 (CS#3): The third control strategy (Figure 7.3C) was a feedforward-feedback control system, where the feedback loop updated the set point of the feedforward loop, merging the two strategies presented earlier. The RO feedforward control acted as the "slave", and its set point was controlled by the "master" loop, where the offset in RT was the error and R_{AmmTot} was deciding the direction of the action of the controller, analogously to the previous strategy (CS#2).

Step 6 - Control laws

The control law for CS#1 was derived from the steady-state model by isolating the k_La from the expression, and resulted in the following equation:

$$RO_{sp} = \frac{k_La\left(S_{O2,sat}\right)}{NH_{4,in}^{+} / HRT} \Leftrightarrow k_La = \frac{RO_{sp}NH_{4,in}^{+}}{HRT\left(S_{O2,sat}\right)} \quad (7.4)$$

For the CS#2, a proportional-integral (PI) controller was implemented. With the R_{AmmTot} deciding the direction of the control action, the expression became:

$$k_La(t)=\begin{cases} k_La_{\infty}-K*e(t)-\dfrac{K}{\tau_I}\displaystyle\int_0^{\tau}e(t)dt, & R_{AmmTot}(t)>R_{AmmTot,sp} \\ k_La_{\infty}+K*e(t)+\dfrac{K}{\tau_I}\displaystyle\int_0^{\tau}e(t)dt, & R_{AmmTot}(t)\le R_{AmmTot,sp} \end{cases} \quad (7.5)$$

Controller tuning: The internal model control (IMC) rules were used to properly tune the controller parameters. To this end, the transfer function that relates the output (the removal efficiency) to the input (k_La) was first identified as follows:

$$G_{RT}(s)=\frac{0.0061(-0.101s+1)(0.608s+1)}{(0.062s+1)(0.541s+1)(0.636s+1)} \quad (7.6)$$

The transfer function was approximated to a first-order-plus-delay model using the half rule defined by Skogestad (2003), resulting in the following transfer function:

$$G_{RT}(s)=\frac{0.0058e^{-0.132s}}{0.572s+1} \quad (7.7)$$

Finally, using the IMC guidelines and selecting a moderate closed loop time constant (τ_C) (Skogestad, 2003) of 0.132 d, a value of the proportional gain of K = 371.3 d^{-1} was obtained and an integral time of τ_I = 0.572 d was found. In order to avoid chattering, a deadband above 95% removal was used in this case.

The CS#3 consisted of the controller designed for CS#1 (eq. 7.4) as the slave controller, whose set point was obtained by the following proportional (P) controller:

$$RO_{sp}(t)=\begin{cases} RO_{sp,\infty}-K_C*e(t), & R_{AmmTot}(t)>R_{AmmTot,sp} \\ RO_{sp,\infty}+K_C*e(t), & R_{AmmTot}(t)\le R_{AmmTot,sp} \end{cases} \quad (7.8)$$

Controller tuning: The proportional gain, K_C, was found as the inverse of the process gain to be norm|ΔRO/ΔRT|, from simulations of both a positive and a negative step change in the k_La value

in the open-loop system with no controller implemented. The gain value obtained from these simulations was 2 (mg O_2 L^{-1} d^{-1})/(mg N L^{-1} d^{-1}).

A P controller was used in order to keep the controller as simple as possible. A deadband above 95% was also implemented on the feedback controller in this case.

Optimal set point values: The optimal set point values were obtained by deriving the optimal oxygen to nitrogen loading ratio by simulating a range of RO conditions with the validated model (see Figure 7.4 and 7.5). These resulted in the following set point values: $RO_{sp,\infty}$ = 1.66, RT_{sp} = 0.965, and $R_{AmmTot,sp}$ = 1.03.

Step 7 – Simulation scenarios and control performance evaluation

The validated model and the three control strategies were implemented and simulated in Matlab-Simulink.

To test the flexibility of the control strategies and the capability of the controllers to recover the system performance, set point change simulations were conducted (sim#1 in Table 7.2). Here, the set points were changed as specified below and simulated until steady state was obtained, after which the original set point was re-established, and the response of the system returning to the original state was tracked. For the CS#1 a 5% increase and decrease of RO_{sp} were simulated. For the CS#2, RT_{sp}=0.9 was simulated, and for the CS#3 a 5% increase and decrease of $RO_{sp,\infty}$, both combined with RT_{sp}=0.9 were simulated.

Table 7.2 Simulation scenarios for controller evaluations.

Sim #	Simulation scenario	Disturbances or changes
1	Set point changes	5-10% changes in RT_{sp} and/or RO_{sp} depending on control structure
2	Step changes	±10% influent ammonium concentration +100/200 mg COD L^{-1}
3	Dynamic influent	Constant fluctuations in ammonium and readily degradable organic carbon influent concentrations

For the controller performance evaluation, disturbance analyses were performed. In order to achieve this, step changes of the concentration of two compounds in the influent were

simulated, with two different levels of each (sim#2 in Table 7.2). For ammonium, a positive and negative perturbation were simulated in the form of a ±10% change in the default concentration of 500 mg N L^{-1}, while concentrations of 100 and 200 mg COD L^{-1} were used for soluble readily degradable organic carbon (S_s) in the influent, where a default concentration of zero was otherwise used. These two compounds were the ones of major concern, since i) the main objective of the process was to remove nitrogen from the wastewater stream, and ii) the organic carbon concentration often shows large variations, leading to the growth of microbial groups which can comprise the granule structure, since they compete for substrates with the desirable microbial groups performing nitrogen removal.

A more realistic test was carried out using an influent originating as the effluent from an anaerobic digester. The dynamic profile of the influent was obtained from the benchmark simulation model no. 2 (BSM2) (Jeppsson et al., 2007) (sim#3 in Table 7.2) and featured continuous variations of both ammonium and readily degradable organic carbon concentrations. The average ammonium concentration was normalized to 500 mg N L^{-1} and organic carbon to 200 mg COD L^{-1} to be in ranges comparable to the step changes that were simulated earlier.

The ability of the controllers to reject the disturbances and to cope with the set point changes were evaluated by the integral of the absolute error (IAE) criterion defined as follows:

$$IAE = \int_0^{t_{end}} |e(t)| dt \tag{7.9}$$

In all the three cases the error was the distance of RT from its set point, and the IAE was calculated during an operating time of 10 days.

The cost of the change of the actuator was evaluated by the total variation (TV), which was calculated as follows:

$$TV = \sum_{i=1}^{n} |u_{i+1} - u_i| \tag{7.10}$$

where u_i is the value of the MV and subscripts i and i+1 indicate consecutive sampling times. A measurement interval of 0.1 d was used. Scaled values of both IAE and TV will be presented.

7.3 Results and Discussion

7.3.1 Set point change responses

In Table 7.3 and Figure 7.6, it can be seen that the CS#1 was better at returning the system to its original performance than both the CS#2 and CS#3. Since the CS#1 is a feedforward controller, it is logical that it responds faster to an influent disturbance than the other controllers. However, for all simulated set point change scenarios, the control systems were generally able to bring the system back to its original performance within a few days of operation (Figure 7.6).

Table 7.3 Response of the controllers to set point changes.

Control strategy	Initial condition	IAE	TV
CS#1	-5% RO_{sp}	0.099	0.005
	+5% RO_{sp}	0.081	0.007
CS#2	RT_{sp}=0.9	0.156	0.103
CS#3	-5% RO_{sp} and RT_{sp}=0.9	0.126	0.018
	+5% RO_{sp} and RT_{sp}=0.9	0.019	0.003

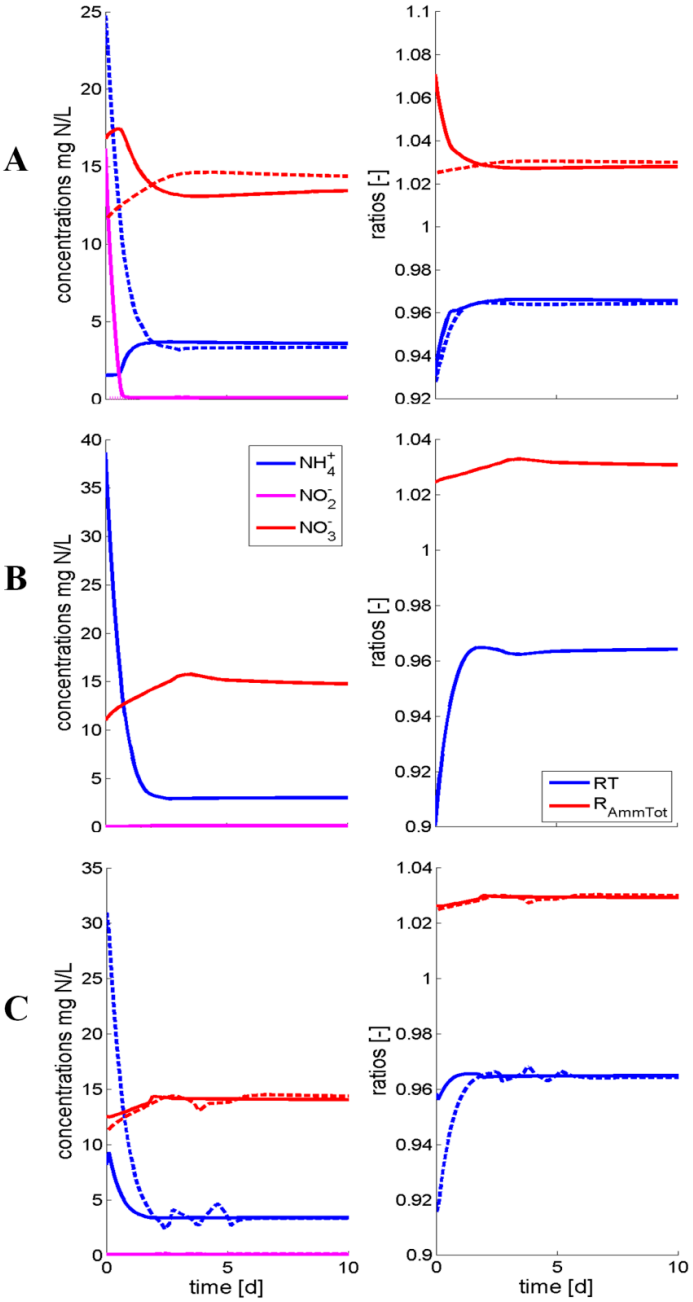

Figure 7.6 Responses of effluent concentrations and controlled variables to set point changes. A) CS#1 response – full line corresponds to initial conditions being +5% RO_{sp} and dashed line corresponds to -5% RO_{sp}, B) CS#2 response, and C) CS#3 response – full line corresponds to initial conditions being +5% RO_{sp} and RT_{sp}=0.9, and dashed line corresponds to -5% RO_{sp} and RT_{sp}=0.9.

7.3.2 Input disturbances: step change analyses

In Table 7.4 and Figure 7.7A, it can be seen that the feedforward control strategies from CS#1 and CS#3 were handling the ammonium step change best, with the lowest IAE and TV values. This was due to the almost immediate response of these control strategies to the incoming disturbance through the feedforward loop. This is not so surprising, since the feedforward loop was designed to handle exactly this disturbance.

However, the CS#2 control strategy also showed a better performance than the open-loop system with no control action. The deadband implementation can be seen in this case with the effluent ammonium concentration leveling off at a higher value than the initial concentration. Regardless, the concentration profile, within the first two days after the step changes, shows that the dynamic response of this control strategy was much slower and with a larger offset than for CS#1 and CS#3.

The same trends can be observed when decreasing the ammonium influent concentration with 10% (Table 7.4).

Even though CS#1 comes out as the best strategy at handling ammonium concentration disturbances, it is important to note that in case of failure in the microbial conversion or in case of a model mismatch no action will be taken if this strategy is implemented. However, the two other strategies have a feedback loop to catch offsets in the performance, which will result in some sort of action in order to try to correct an offset, independent of the source of this offset.

Table 7.4 Responses of the open loop and the three control strategies to ±10% step changes in the ammonium concentration and readily degradable organic carbon concentrations of 100 and 200 mg COD L^{-1} in the influent. The reported value of RT was obtained after 10 days of operation.

Control strategy	Disturbance	IAE	TV	RT	Disturbance	IAE	TV	RT
No control	+10% $NH_4^+{}_{in}$	2.708	-	0.890	100 mg COD L^{-1}	0.344	-	0.954
	-10% $NH_4^+{}_{in}$	2.975	-	0.881	200 mg COD L^{-1}	2.532	-	0.877
CS#1	+10% $NH_4^+{}_{in}$	0.068	0.002	0.964	100 mg COD L^{-1}	0.406	0.003	0.951
	-10% $NH_4^+{}_{in}$	0.085	0.002	0.967	200 mg COD L^{-1}	2.463	3.6e-9	0.885
CS#2	+10% $NH_4^+{}_{in}$	0.628	0.087	0.950	100 mg COD L^{-1}	0.298	0.000	0.957
	-10% $NH_4^+{}_{in}$	0.629	0.083	0.950	200 mg COD L^{-1}	0.613	0.077	0.950
CS#3	+10% $NH_4^+{}_{in}$	0.072	0.003	0.964	100 mg COD L^{-1}	0.411	0.002	0.951
	-10% $NH_4^+{}_{in}$	0.090	0.002	0.967	200 mg COD L^{-1}	1.394	0.048	0.920

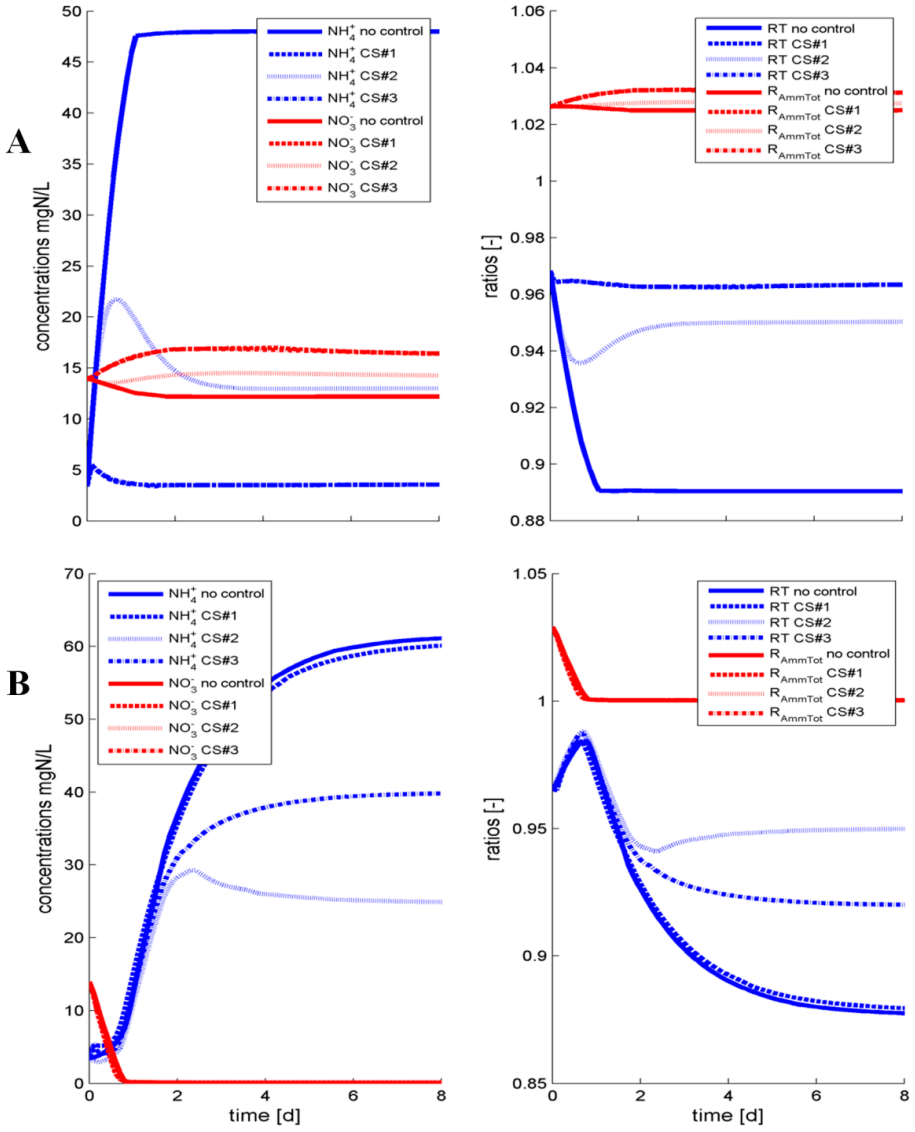

Figure 7.7 Responses of effluent concentrations and controlled variables to step changes. A) +10% in ammonium influent concentration, and B) +200 mg COD L^{-1} in the influent concentration.

When simulating a disturbance scenario with an influent concentration of organic carbon of 100 mg COD L^{-1}, the increase in ammonium concentration in the effluent was lower than the removal of nitrate through the denitrification process catalyzed by heterotrophic bacteria. This meant that the removal efficiency was not negatively impacted (right side of Table 7.4), and the implementation of the control strategies did therefore not have a significant effect on the performance.

However, for an organic carbon concentration of 200 mg COD L^{-1}, the competition for oxygen as electron acceptor between heterotrophs and nitrifiers became important when all nitrate was depleted by the heterotrophs after about 1 day (Figure 7.7B). The CS#1 controller failed to reject the disturbance, whereas CS#2 did a very good job of keeping a high removal efficiency by increasing the oxygen supply, thus providing sufficient oxygen to oxidize both the ammonium and the organic carbon (Figure 7.7B). Since the removal efficiency decreased, but the balance between the desired microbial groups was intact (R_{AmmTot} was below its set point value), the oxygen supply increased in CS#2 and CS#3. As expected, CS#1 failed in handling this disturbance, since it was designed to only handle the disturbances in the ammonium concentration and not to act on any other disturbance. For CS#2, a new steady state was reached after about 5 days with an ammonium effluent concentration of 25 mg N L^{-1}. This corresponds to the allowable concentration according to the deadband above 95%, when no other soluble nitrogen species were present in the effluent. The CS#3 controller showed a performance somewhere in between the CS#1 and CS#2, and thus rejected the disturbance to some extent, but not quite as well as the CS#2, as noted by the integral absolute errors shown in Table 7.4 and the longer time to reach a new steady-state (about 6-7 days) (Figure 7.7B).

7.3.3 Controller response to dynamic influent profile

The response of the system to the dynamic influent profile without any controller and with the three control strategies is reported in Table 7.5. The CS#1 controller showed a slight improvement in performance compared to operation without any controller, whereas CS#2 showed a much better performance. CS#3 was, maybe not surprisingly considering the results of the step change analyses, the best strategy at rejecting simultaneous disturbances in ammonium and organic carbon influent concentrations with a slightly lower IAE value than CS#2.

Table 7.5 Integral absolute error and total variance responses to 10 days of dynamic influent conditions.

Control strategy	Disturbance	IAE	TV
No control	Dynamic influent profile	2.680	-
CS#1	Dynamic influent profile	2.637	0.137
CS#2	Dynamic influent profile	0.556	0.569
CS#3	Dynamic influent profile	0.546	0.187

As all of the strategies are considering the same actuator and controlled variable, the measurement equipment needed to practically implement them is the same. However, as the CS#1 does not require a measurement of the removal efficiency, this can be determined off-line which might reduce the operating costs.

The control strategies presented here are novel for this process, since they are designed for an intensified system with limited actuator availability. Thanks to previous contributions, which assessed the operation of the reactor, it was possible to design control structures that addressed the regulation of the system while fulfilling the control objectives, by directly including the performance objective in the controller designs. The most promising strategy has been implemented at lab-scale and experimentally tested for validation (see chapter 8).

7.4 Conclusions and outlook

Three novel control strategies for a granular sludge bioreactor removing ammonium from high strength streams were developed using a systematic process oriented approach. The CS#1, a simple feedforward controller, was best at handling disturbances in the ammonium concentration as expected. The CS#2, a feedback controller, was best at rejecting disturbances in the organic carbon concentration in the influent. A combination of the two strategies, presented in CS#3, was able to reject both disturbances satisfactorily, albeit not as well as CS#1 and CS#2 for ammonium and organic carbon, separately. Versatility toward disturbances could be obtained with the CS#3, at the expense of slower dynamic responses and a more complex controller structure. The performance of the CS#3 was also verified by using a dynamic influent profile from a realistic effluent from an anaerobic digester containing both ammonium and organic carbon disturbances, which resulted in a better performance of CS#3 compared to CS#2 and CS#1. Hence the appropriate design will depend on the particular requirements of the process, and in particular on the disturbances originating in the upstream units, which should therefore be thoroughly investigated. In any case, implementing the CS#3 will ensure the safest operation.

8 Experimental validation of a novel control strategy

Summary

The feedforward-feedback control strategy developed in chapter 7 was adapted from continuous operation to SBR operation. The adaptation required model identification for the SBR process and retuning of the controller algorithm resulting in a new gain and new set points for the controller. The resulting strategy is called a batch-to-batch control strategy, since the feedback was provided after the conclusion of a batch cycle. The strategy was experimentally tested in a lab-scale SBR through set point changes and disturbance rejection experiments. Compared to the manual operation mode, with a constant air supply, the performance was significantly improved for disturbances in the influent ammonium concentration. Comparing the previous numeric simulations with the experimental setup, the results obtained were qualitatively similar. Therefore, with the insight obtained from the prior simulation studies, it was possible to implement and start up the controller fast and efficiently compared to the traditional experience-based trial and error approach for controller operation and tuning. During the testing, a slight retuning of the controller was needed in order to avoid oscillatory behavior under high ammonium loading rate conditions. The successful validation of the controller in the lab-scale reactor is a promising result which brings this control strategy one step closer to full-scale implementation. The results also add credit to the systematic model-based approach at large, which has been used to develop and optimize the controller for the system.

8.1 Introduction

Operating a single-stage CANR system in a stable and efficient manner requires an appropriate control strategy. This has typically been developed and operated through an experience-based approach (Vlaeminck et al., 2012). In this study, an alternative approach is presented in which a control strategy is developed following a systematic and methodological approach that employs modeling and simulation studies together with control theory and experimentation in a synergistic manner.

In the previous chapter 7, a feedforward-feedback control strategy was found to be the most versatile among the three designed controllers, and hence the best strategy at handling disturbances coming to the system. It was therefore decided to test this control strategy in a lab-scale SBR. The control strategy developed for a continuously operated system was modified to fit the sequential batch operation, as described in the materials and methods section of this chapter.

The goal of the experimental testing of the controller is to validate that the control strategy can reject disturbances in the influent while maintaining a stable (and efficient) performance of the nitrogen removal. This is done by subjecting the lab-scale reactor to designed perturbations in the operation while monitoring the resulting effect on the performance of the system. The controller is evaluated by comparing the results of the controlled system to the reference operation mode of the reactor that uses a manual controller, in which the oxygen supply rate is kept constant.

8.2 Material and methods

8.2.1 Reactor features and operation

One of the two lab-scale reactors described in chapter 2 was used for the experimental work. It had a volume of 4 L, was fed with synthetic wastewater, and was operated in a sequential batch manner in cycles of 8 hours. They consisted of a 10 minute fill phase, a 447 minute reaction phase, a 3 minute settling phase, a 10 minute draw phase, and a 10 minute idle phase.

8.2.2 Measurements and actuator

Effluent measurements of ammonium and nitrate were available on-line through the ion selective electrodes, while influent concentrations and nitrite effluent concentration were measured by manual sampling and subsequent use of colorimetric test kit analyses. The measured DO concentration was available on-line during the reaction phase of the SBR cycle.

The actuator, considered in the modeling investigation in the previous chapter, was the k_La of oxygen. In the physical setup, the air was supplied through a mass flow controller (MFC) and the setting of this MFC was therefore considered the actuator in the experimental laboratory implementation.

8.2.3 Structure of the controller

With the composition measurements of the influent and the effluent concentration only being available once per cycle and the nature of the operation being different when comparing a continuous system – used in chapter 7 – to an SBR, a batch-to-batch type controller was constructed, in which the feedback was provided after the conclusion of a batch cycle, and the feedforward was active once per cycle during the fill phase, when the influent was pumped to the reactor (Figure 8.1). This resulted in the aeration (i.e. the k_La value), manipulated by the controller, changed once per cycle.

The calculations used in the controller were modified slightly compared to the strategy developed for continuous operation presented in the previous chapter. All modified expressions are presented below.

The volumetric oxygen loading to the system during one cycle was calculated as:

$$L_{O2,g} = k_L a_g \cdot S_{O2,sat} \frac{t_{aer,g}}{t_{cycle,g}} \tag{8.1}$$

where the subscript g denotes the number of the cycle, $t_{aer,g}$ is the length of time that aeration is turned on during cycle g, and $t_{cycle,g}$ is the length of the entire cycle.

Likewise, the volumetric ammonium loading rate was defined as:

$$L_{NH4,g} = \frac{NH^+_{4,in,g} ER + NH^+_{4,out,g-1} \left(1 - ER\right)}{t_{cycle,g}} \tag{8.2}$$

where $NH_{4,in,g}^{+}$ is the concentration of the influent being pumped in during the fill phase of cycle g, ER is the volumetric exchange ratio, defined as the volume leaving the reactor at the end of the cycle divided by the entire volume of the reactor when full, and $NH_{4,out,g-1}^{+}$ is the effluent concentration of the cycle before cycle g, i.e. g-1.

The oxygen to ammonium loading rate ratio thus looked as follows:

$$RO_g = \frac{k_L a_g S_{sat,O2} t_{on,g}}{\left(NH_{4,in,g}^{+} ER + NH_{4,out,g-1}^{+}\left(1-ER\right)\right)} \tag{8.3}$$

The feedforward control law therefore became:

$$k_L a_g = \frac{RO_{sp,g}\left(NH_{4,in,g}^{+} ER + NH_{4,out,g-1}^{+}\left(1-ER\right)\right)}{S_{sat,O2} t_{aer,g}} \tag{8.4}$$

The removal efficiency was calculated as presented earlier in chapter 6. Its value was updated once per cycle, resulting in the following expression:

$$RT_g = \frac{\Delta TN_g}{TN_{in,g}} = \frac{NH_{4,in,g}^{+} + NO_{2,in,g}^{-} + NO_{3,in,g}^{-} - NH_{4,out,g}^{+} - NO_{2,out,g}^{-} - NO_{3,out,g}^{-}}{NH_{4,in,g}^{+} + NO_{2,in,g}^{-} + NO_{3,in,g}^{-}} \tag{8.5}$$

R_{AmmTot}, the metric capturing the relative activity of the microbial groups, was defined as:

$$R_{AmmTot,g} = \frac{NH_{4,start,g}^{+} - NH_{4,out,g}^{+}}{TN_{start,g} - TN_{out,g}} = \frac{\left(NH_{4,in,g}^{+} ER + NH_{4,out,g-1}^{+}(1-ER)\right) - NH_{4,out,g}^{+}}{\left(\left(NH_{4,in,g}^{+} + NO_{2,in,g}^{-} + NO_{3,in,g}^{-}\right) ER + \left(NH_{4,out,g-1}^{+} + NO_{2,out,g-1}^{-} + NO_{3,out,g-1}^{-}\right)\left(1-ER\right)\right) - NH_{4,out,g}^{+} - NO_{2,out,g}^{-} - NO_{3,out,g}^{-}} \tag{8.6}$$

The feedback control law, correcting the oxygen to ammonium loading rate ratio, takes the removal efficiency and the R_{AmmTot} value from the previous cycle into account:

$$RO_{sp,g+1} = \begin{cases} RO_{sp,\infty} - K_C * \left(RT_{sp} - RT_g\right), & R_{AmmTot,g} > R_{AmmTot,sp} \\ RO_{sp,\infty} + K_C * \left(RT_{sp} - RT_g\right), & R_{AmmTot,g} \leq R_{AmmTot,sp} \end{cases} \quad (8.7)$$

where K_C is the proportional gain, whose value was selected as the inverse of the steady-state gain between the manipulated RO and the controlled variable RT. It was therefore found as $|\Delta RO/\Delta RT|$ in simulations of a step change in the k_La value. The value obtained from this exercise was 2 (mg O_2 L^{-1} d^{-1})/(mg N L^{-1} d^{-1}).

The control structure, and the relation between the cycle number, data acquisition and controller action can be seen in Figure 8.1.

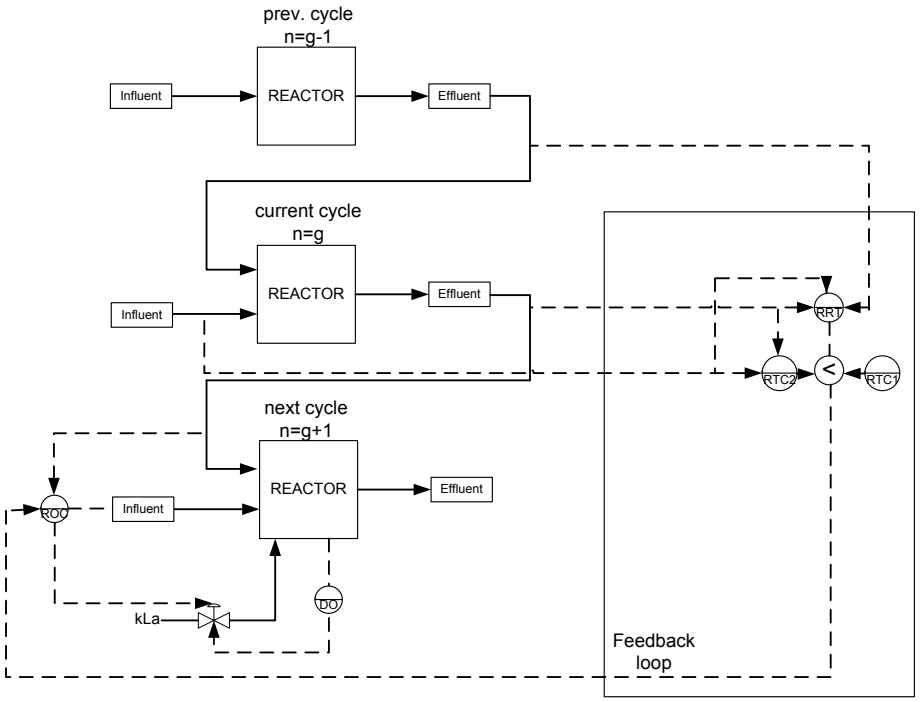

Figure 8.1 Structure of the controller. n is the cycle number, RRT is the R_{AmmTot} transmitter, RTC1 and RTC2 are the removal efficiency controllers (1 indicating a positive control action and 2 indicating a negative control action), and ROC is the oxygen to ammonium loading ratio controller.

A new feature which can also be seen in Figure 8.1, is the usage of the DO signal. It was implemented as an override loop in the following proportional manner:

$$k_La = \begin{cases} k_La & DO < 0.2 mg O_2 L^{-1} \\ k_La - K_{C,DO}\left(DO - 0.2\right) & DO \geq 0.2 mg O_2 L^{-1} \end{cases} \quad (8.8)$$

This extra loop ensured that the aeration intensity was decreased in case the DO rose above 0.2 mg O_2 L^{-1} in the bulk liquid. The value of $K_{C,DO}$ was set to 130 d^{-1} (mg O_2 L^{-1})$^{-1}$. Negative k_La values, obtained from this calculation, were set equal to zero, meaning a complete stop of the aeration, which happened around a DO concentration of approximately 2 mg O_2 L^{-1} depending on the original value of k_La during the given cycle.

From the control laws presented above, a k_La value was obtained. This had to be translated to a valve setting, in percent, for the mass flow controller. As nicely illustrated by Åmand et al. (2013), the relationship between k_La and air flow rate (Q_{air}) is not always linear, neither between air flow rate and valve setting. The following exercise was therefore done to find an appropriate relationship between the k_La and the valve setting.

First, an empirical correlation was used to check the relation between the air flow rate and the oxygen mass transfer coefficient (Van't Riet, 1979).

$$k_La = 0.026\left(\frac{P}{V}\right)^{0.4} \upsilon_s^{0.5} \quad (8.9)$$

where (P/V) is the power to volume number and υ_s is the superficial gas velocity. Both P and υ_s are proportional to Q_{air}, which results in k_La being proportional to $Q_{air}^{0.9}$.

Using this correlation, it was found that within the air flow range used in the reactor operation, the relation was very close to linear (R^2=0.98).

A linear relationship between Q_{air} and k_La, based on the value obtained in the steady state calibration in chapter 6 and an interception at (0,0), was therefore assumed (Figure 8.2).

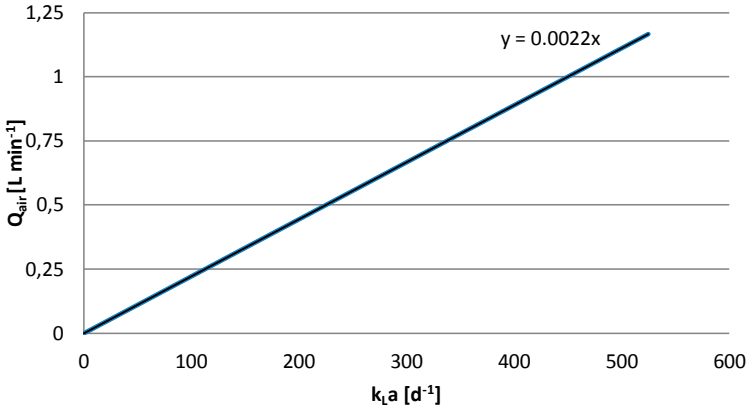

Figure 8.2 Linear relationship between air flow rate (Q_{air}) and oxygen mass transfer coefficient (k_La).

The next step was to relate the air flow rate to the setting of the mass flow controller. This was done through an experimental calibration, where two ranges were identified, an upper range and a lower range. A piece-wise linear relation consisting of two linear ranges was therefore established (Figure 8.3).

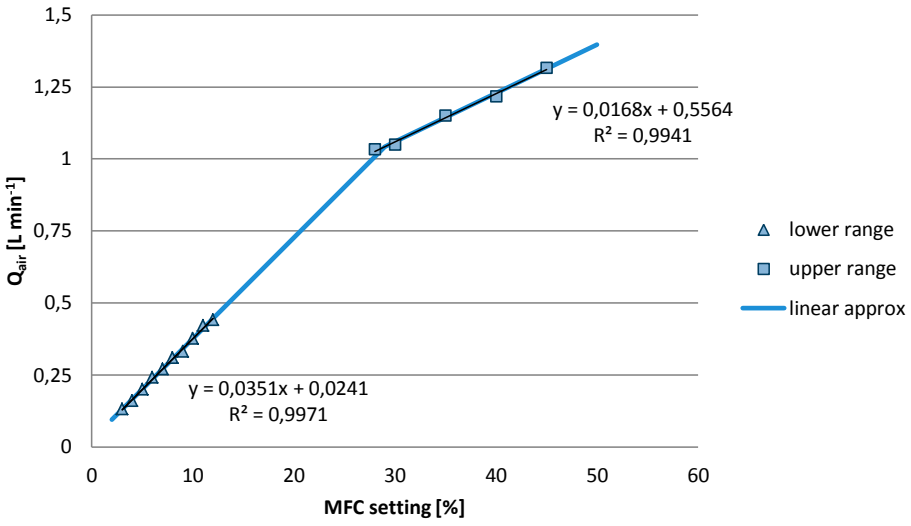

Figure 8.3 Piece-wise linear relationship between air flow rate (Q_{air}) and mass flow controller setting.

By combining the relations shown in Figure 8.2 and 8.3 a relationship between k_La and the MFC setting was obtained.

For the data acquisition and control purposes LabVIEW (National Instruments, Austin, TX, USA) was used, and the control algorithm was therefore also coded in a LabVIEW routine, which controlled the reactor operation.

Since the influent ammonium and effluent nitrite concentrations were measured manually, their values were updated for two out of the three 8 hour cycles per day. For the third cycle, during the night, the values obtained from the second cycle of the day were used. The effluent ammonium and nitrate concentrations were updated every cycle, because they were continuously logged on-line.

8.2.4 Design of control performance experiments

Set point change

In order to first check that the controller could perform set point tracking, a set point change in which RT_{sp} was set to 0.7 for a period of 8 days followed by a set point increase to RT_{sp}=0.925 was employed to bring the performance back to the starting point. During the set point change experiment t_{aer} was 390 minutes, which was distributed on three aerated phases of 130 minutes each.

Disturbance in feed

Feed concentration disturbances were performed with the shape of a square signal, i.e. an increase followed by a decrease back to the original level in ammonium concentrations. One experiment was conducted with the reference reactor operation (actuator value fixed) and one experiment was conducted with the controller active. The ammonium concentration was increased approximately 20% from around 500 mg N L^{-1} to around 600 mg N L^{-1} for one day, i.e. during three SBR cycles. The reactor was continuously aerated during the reaction phase, which resulted in t_{aer}= 447 minutes.

Dynamic influent profile

A dynamic influent profile was imposed to the system during five days, in which the influent concentration ranged between approximately 400 mg N L^{-1} and 700 mg N L^{-1} and changed once per day (Figure 8.4). After these disturbances in the feed, the influent ammonium concentration was restored to a level around 500 mg N L^{-1}, and the reactor was operated with this influent for 10 days in order to allow a more long-term monitoring of the system performance. As in the disturbance in the feed experiment, the reaction phase was continuously aerated during the dynamic influent experiment, such that t_{aer}= 447 minutes.

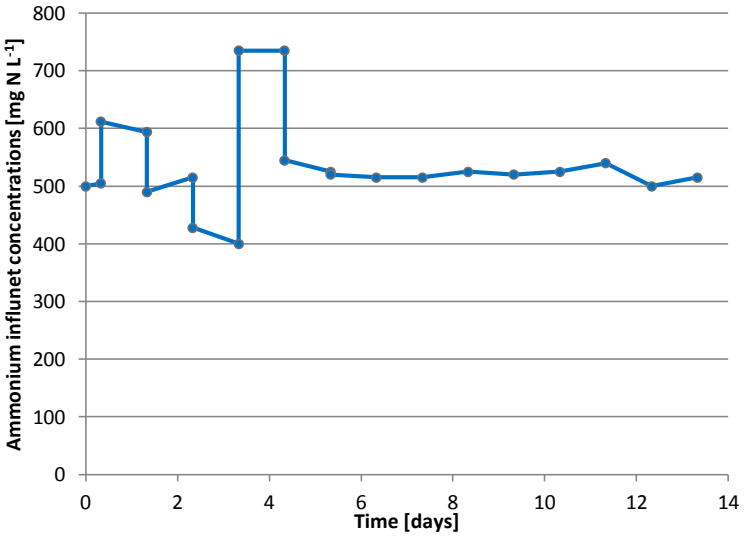

Figure 8.4 Dynamic influent concentration profile during the long-term experiment.

Controller settings

During all experiments, $R_{AmmTot,sp}$ = 1.15 was used. This value was obtained from long-term observation of the lab-scale reactor prior to the start of the controller validation experiments (Figure 8.5). The steady state set point value of the oxygen to ammonium loading ratio was found through simulation studies to be $RO_{sp,\infty}$ = 1.67 (mg O_2 L^{-1} d^{-1})/(mg N L^{-1} d^{-1}). During the disturbance introduction experiments RT_{sp} = 0.925 was used, however this value was readjusted to 0.90 during the dynamic influent profile experiment on the basis of experimental observations showing that the maximum removal efficiency produced by the system never reached higher than 0.90.

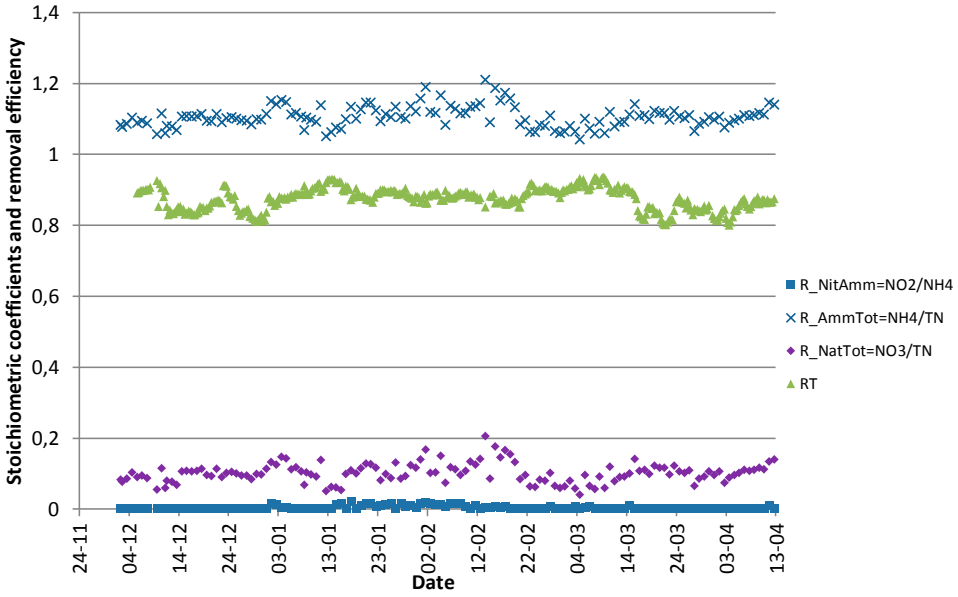

Figure 8.5. Reactor operational data from before the controller experiments were conducted. From this the set point values of R_{AmmTot} and RT were obtained.

8.3 Results

8.3.1 Set point change response

The performance of the reactor was relatively stable before the implementation and testing of the controller (Figure 8.5 and 8.6). At day 2 of the experiment the controller was implemented, and the performance dropped to a lower level where it stabilized within 1-2 days (Figure 8.6). The set point was increased on day 10 of the experiment, and, apart from a point accounted for by an operational upset due to a pump failure on day 11, the performance went back up to the initial level of around 89% within one day.

However, when the low set point of RT_{sp} = 0.7 was used, the offset was rather significant. A slight retuning of the controller was therefore introduced by increasing the proportional gain of the controller, first from 2 to 3 (mg O_2 L^{-1} d^{-1})/(mg N L^{-1} d^{-1}) and later from 3 to 4 (mg O_2 L^{-1} d^{-1})/(mg N L^{-1} d^{-1}). Subsequently, the performance leveled off at a TN removal of 82%, which showed an offset from the set point of 70%, but still showed a significant change in the performance from the reference operation achieved before the controller implementation (Figure 8.6). The significant offset was caused by the proportional-only control law, which results in a significant steady state error, regardless of the controller gain.

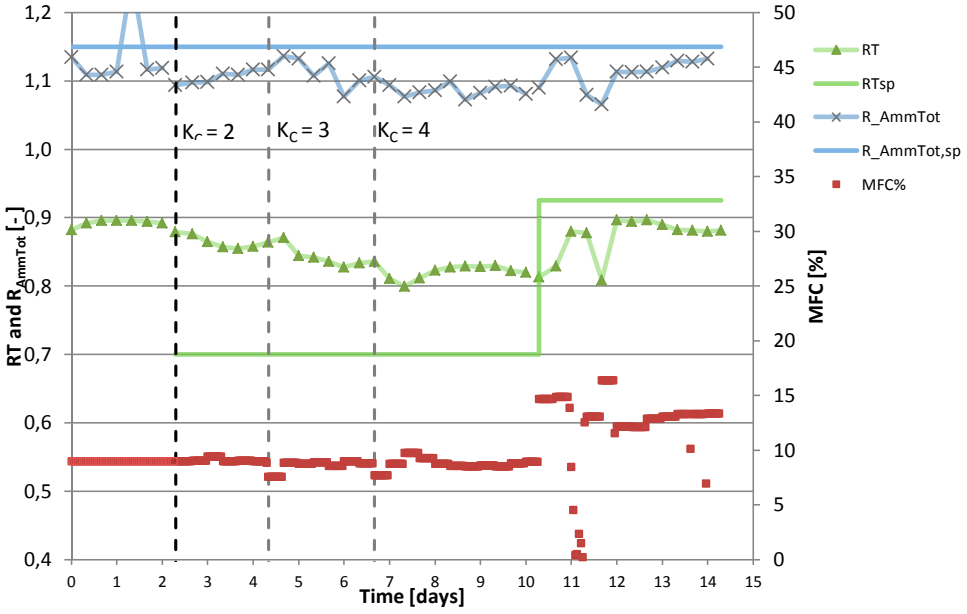

Figure 8.6 Set point change experiment. Evolution of controlled and manipulated variables as a function of time. The vertical dashed black line indicates the transition from reference operation to operation with an active controller. The vertical grey dashed lines indicate the fine tuning of the controller gain.

8.3.2 Responses to influent ammonium disturbances

During the manual operation (the MFC set point being a constant value (Figure 8.7, bottom)), it was observed that the increase in ammonium concentration in the influent propagated to the effluent (Figure 8.7, top). Concurrently, the nitrate concentration dropped slightly. In the controlled case the ammonium concentration remained low throughout the experiment, but the nitrite concentration increased a bit and varied between 0 and 10 mg N L^{-1} (Figure 8.7, top). The fluctuations in effluent concentrations were reflected in the larger offset in the removal efficiency in the reference operation case than in the controlled case (Figure 8.7, bottom). In the controlled case, it was observed that the actuator set point was lowered when the value of R_{AmmTot} exceeded its set point value, e.g. in cycle two and eight, counting from the start of the experiment. Finally, the effect of the DO override loop could also be observed in the second cycle, in the end of which the MFC value decreased (Figure 8.7, bottom), because the DO concentration went above 0.2 mg O_2 L^{-1}. This coincided with a very low (practically zero) effluent ammonium concentration, which confirmed that the DO increased due to oxidation of all present ammonium before the end of the reaction phase.

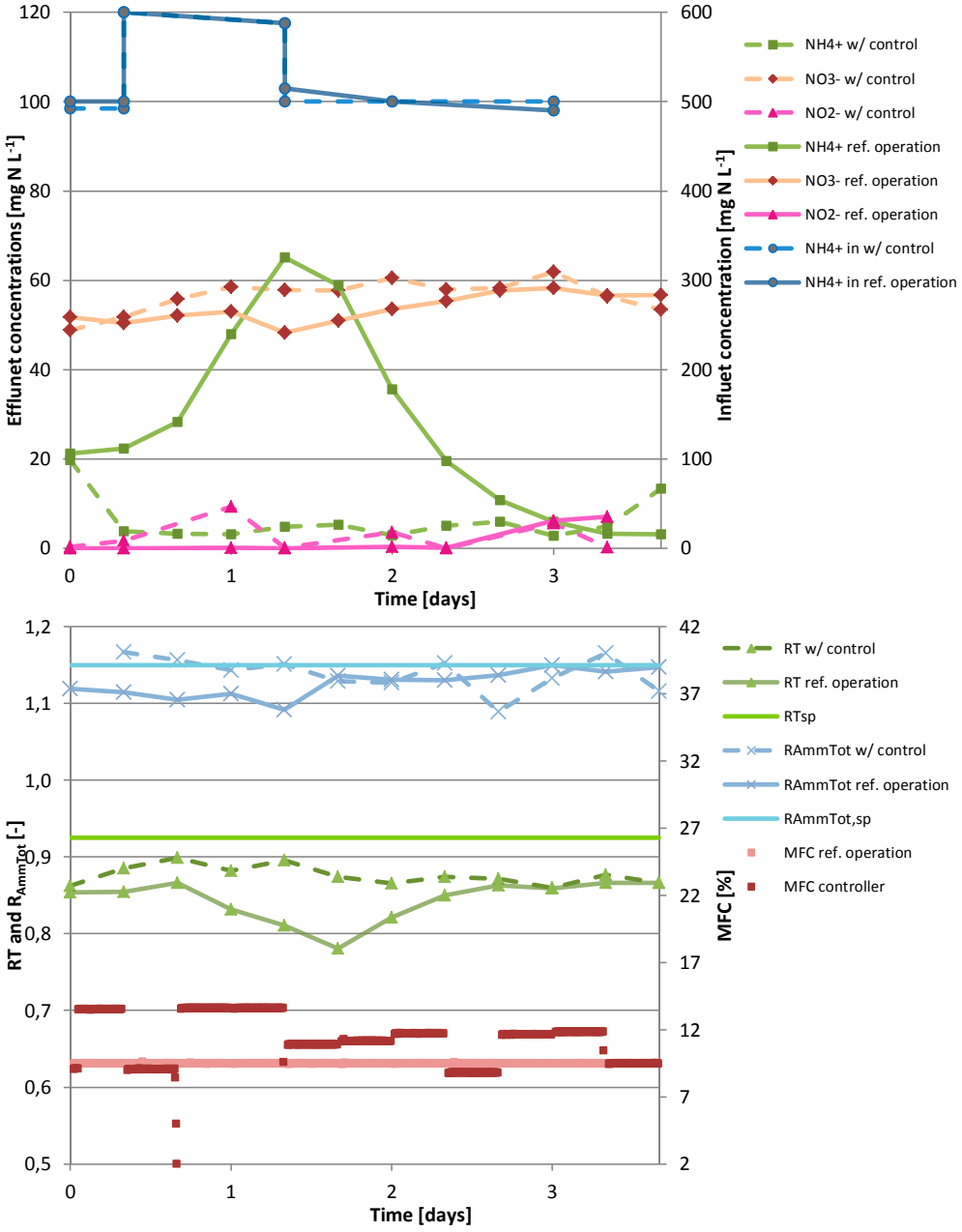

Figure 8.7 Top: Influent and effluent concentrations during the disturbance introduction experiment. Bottom: Evolution of the controlled and manipulated variables as a function of time. Full lines: Experiments conducted with constant MFC setting. Dashed line: Experiment with controller implemented.

8.3.3 Dynamic influent response

In order to test the stability and long-term effects and impacts of the control strategy, a dynamic influent profile was imposed to the reactor with implemented controller, and it was observed for 15 days.

The results showed that the removal efficiency was not optimal in the beginning of the experiment, with a bit of ammonium remaining in the effluent (Figure 8.8, top). This effluent ammonium concentration was quickly reduced despite the fluctuations in the influent concentration, thus demonstrating that the controller could quickly produce a good and stable effluent quality under varying load conditions. At day 4 of the experiment, the influent concentration increased to 735 mg N L^{-1}, which resulted in an increase in the ammonium effluent concentration. Subsequently, the nitrite concentration increased and fluctuated between 5 and 45 mg N L^{-1} for the following 3 to 4 days. During this time the nitrate concentration reached a lower level than in the beginning of the experiment and after this period it increased slightly again.

As a consequence of, mainly, the effluent concentration variations, the total nitrogen removal efficiency dropped at day 4 of the experiment (Figure 8.8, bottom). Since both ammonium and nitrite were present in the effluent, it could be deduced that AnAOB activity was not sufficient to keep a high removal efficiency. There could be two reasons for this: 1) The maximum capacity of the sludge present in the reactor was reached, and the biomass did not have enough time to grow to produce sufficient biomass to convert all ammonium and nitrite present, or 2) due to the higher oxygen supply (Figure 8.9), the AnAOB were oxygen inhibited to some extent, despite the fact that the DO bulk level never reached detectable concentrations during this part of the experiment. Studies have shown AnAOB inhibition at concentrations as low as 0.2 mg O_2 L^{-1} (Jung et al., 2007). From these results, it cannot be deduced whether it was insufficient AnAOB capacity, AnAOB inhibition, or a combination of the two, which was responsible for the observed efficiency decrease. Despite the drop in removal efficiency on day 4 of the experiment, the total nitrogen removal rate was higher, than in the beginning of the experiment, during this day of operation, due to the higher loading rate (Figure 8.9).

The oscillations in nitrite concentrations from day 4 to 8 of the experiment initiated oscillations in R_{AmmTot} around the set point value (Figure 8.8, bottom). This in turn caused oscillations in the set point of the actuator (the MFC set point which varied from cycle to cycle). These oscillations were reflected in the oxygen to ammonium loading ratio and in the oxygen loading rate (Figure 8.9).

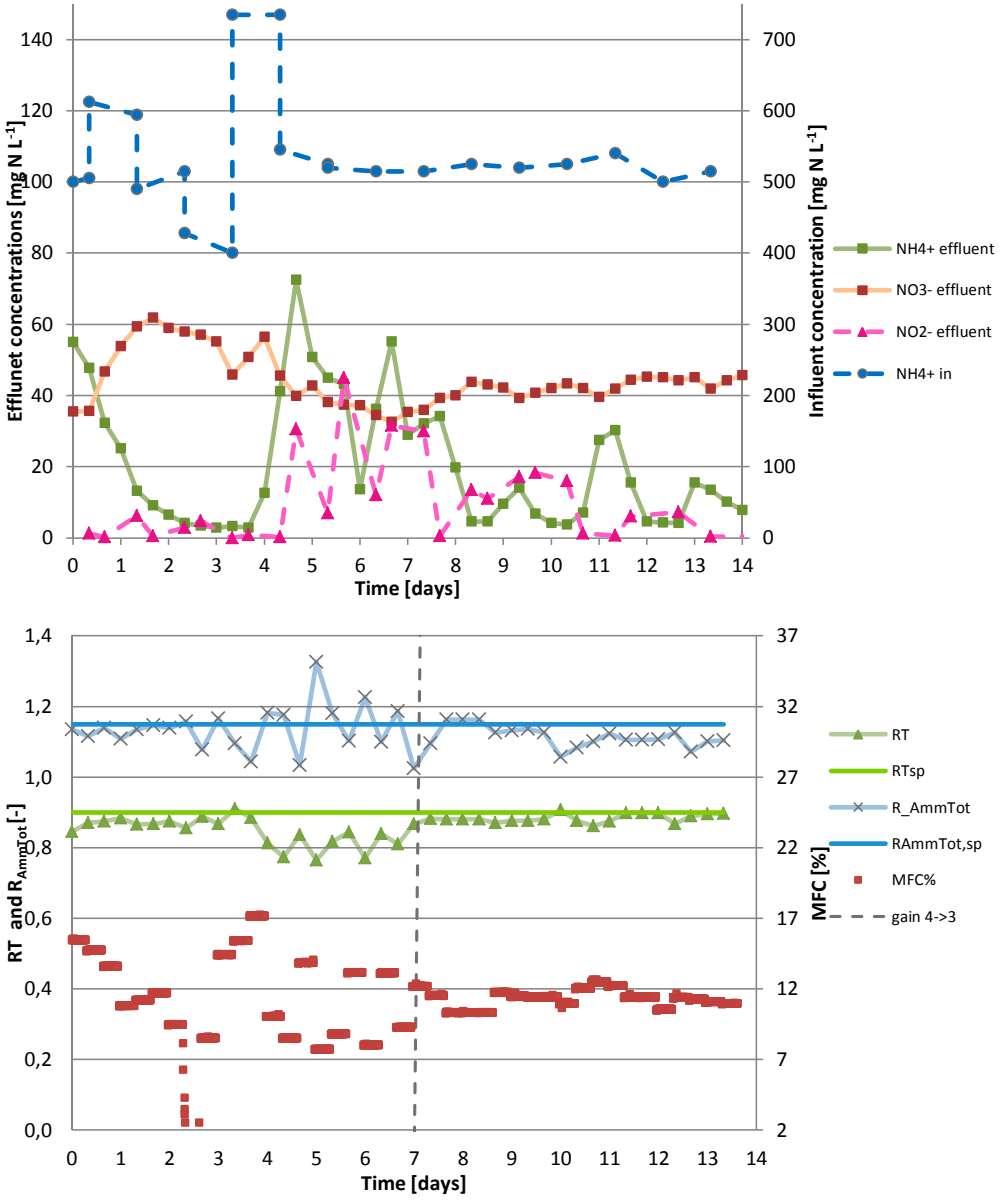

Figure 8.8 Top: Influent and effluent concentrations during the dynamic influent experiment. Bottom: Evolution of controlled and manipulated variables as a function of time.

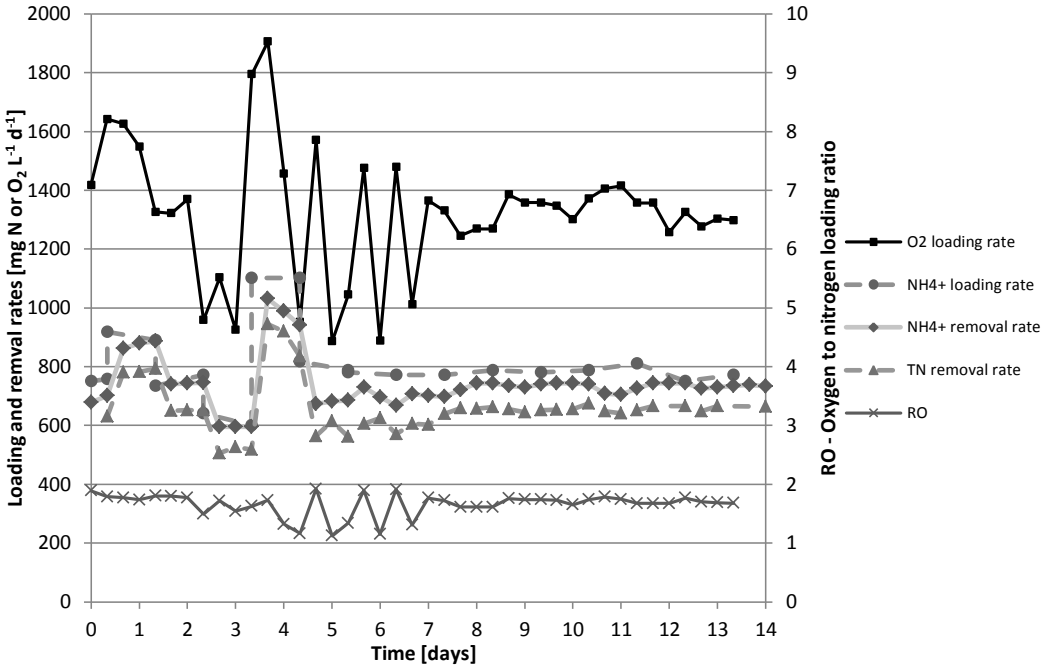

Figure 8.9 Ammonium and oxygen volumetric loading rates, the ratio between the two loading rates (RO), and ammonium and total nitrogen removal rates as a function of time.

As a consequence of this oscillatory behavior and the relatively low removal efficiency, the controller was retuned at day 7 of the experiment, by decreasing the proportional gain from 4 back down to 3 (mg O_2 L^{-1} d^{-1})/(mg N L^{-1} d^{-1}), which was also closer to the gain of 2 (mg O_2 L^{-1} d^{-1})/(mg N L^{-1} d^{-1}) found in the tuning conducted in the simulation study. After this point, the oscillations dampened and the performance again reached a high and stable level (Figure 8.8, bottom and 8.9).

8.4 Discussion

The feedforward-feedback control strategy was extensively tested experimentally both for set point tracking and rejection of disturbances in influent ammonium concentration. The experimental testing showed that the controller was able to reject disturbances in the influent (to a high extent, however depending on the inherent capacity of the present nitritation and

especially anammox bacteria), where the reference reactor operation with fixed MFC value would fail. The controller was also able to perform set point tracking albeit with a significant offset.

The controller performance: Comparison with simulation results

Qualitatively, similar trends can be observed between the experimental results from the influent ammonium concentration perturbations both with the controller and with the reference operation (Figure 8.7) and the simulation results (Figure 8.10) of the same influent profile. Seeing how the trends agree between experiments and simulation emphasizes the usefulness of the simulation based development methodology used throughout this thesis.

However, of notable deviations between experiments and simulation results, it can be observed that the response in the ammonium effluent concentration, and hence also the response in removal efficiency, with reference operation, was faster in simulation (Figure 8.10) than in the experimental observations (Figure 8.7). This leads us to speculate that there might be a practical time delay, which is not included in the model, e.g. caused by probe response time or due to a lag in bacterial activity, when exposed to changing operating conditions, like in the SBR operation or during intermittent aeration, which has previously been observed (Katsogiannis et al., 2003; Zhang et al., 2011; Wett et al., 2013). Including such phenomena in the model is therefore expected to result in a better agreement between model and simulations (as in Vanrolleghem et al., 2004), and will thus further refine the quality of the model. A better and more correct estimation of the time constants and delays in the system is therefore expected to result in a better controller tuning and thus a better performance.

Secondly, a difference in the level of nitrate concentration could be observed, with the concentration in the experimental observations being higher than the simulation results. This is likely due to the estimated heterotrophic denitrification rate being higher in simulation than in the reactor during the experiments. The lower amount of HB activity also affects the values of RT_{sp} and $R_{AmmTot,sp}$, which were, precisely for this reason, based on experimental observations from about a month before the start of the experiments (see Figure 8.5 in the Materials and methods section), instead of directly based on the values obtained from simulation.

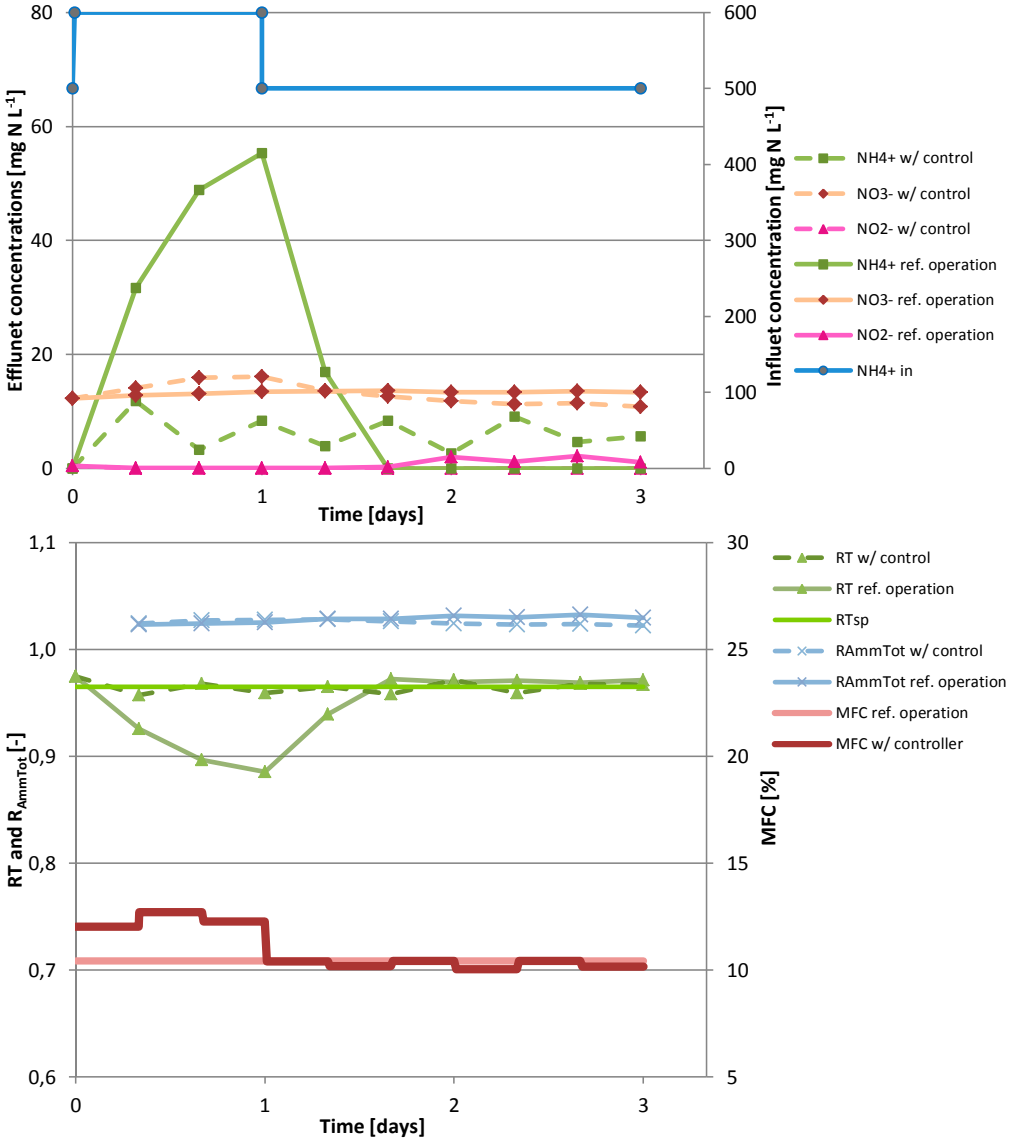

Figure 8.10 Top: Simulation results showing influent and effluent concentrations during an influent disturbance introduction. Bottom: Simulation results of the controlled and manipulated variables matching the influent disturbance introduction.

Steady state offset

A model mismatch is corrected by the feedback loop in cases with offset-free operation (Seborg et al., 2004). However, that was obviously not the case here during the lowering of the set point as can be seen from the experimental results (Figure 8.6). When operating with steady state

offsets, as in this proportional controller case, a model mismatch can result in either a higher or lower steady state offset than expected from previous model simulations. The steady state offset observed here was slightly higher than expected from model simulations, which indicates a slight model mismatch. One way to handle this difference and to overcome an undesired large offset could be to implement an integral term in the feedback loop, instead of having a purely proportional feedback action. However, the practical implementation of this in the batch-to-batch control operation is not straightforward without a sound anti-reset windup strategy, since the meaning of the error integration between batch cycles is not completely clear. It was therefore not tested here but is an obvious point of future investigations. For now the proportional controller was deemed sufficient, because offsets from the removal efficiency set point could be tolerated, as the effluent from reactors using this technology is most often recycled back to the main stream treatment, and not directly discharged, and does therefore not have to live up to any strict discharge limits.

Sensor equipment

A practical issue faced in this study was related to the fact that influent ammonium and especially effluent nitrite concentration values were only updated for two out of three cycles. In cases where the nitrite concentration varied from cycle to cycle, only updating the controller two out of three times did not help to decrease the oscillatory behavior (Figure 8.8), and very likely it even worsened them. On-line measurements of nitrite, e.g. from on-line UV light absorption measurements (Rieger et al., 2004) or by ion selective electrodes (Kaelin et al., 2008), is expected to improve the controller performance. It is however, not quite common practice to use nitrite sensors in large scale facilities yet, as they require a high amount of maintenance (Kaelin et al., 2008), but this type of equipment is expected to become more widely used within the coming years.

Feedback vs. feedforward loop

Since only disturbances in ammonium influent concentration were tested in this experimental study, one can argue that only the feedforward part of the controller was tested. However, disturbances originating from within the process were handled by the feedback loop, as happened in the dynamic influent profile experiment following the instability issue. Also, the feedback loop ensured correction of the set point of the actuator in case there were offsets

originating from the tuning of the feedforward loop or the translation of a k_La value to the proper MFC setting.

Actuator dynamics

As can be seen in Figure 8.2 and 8.3, the established relationship between the k_La and the value of the MFC setting (the actuator of the physical equipment) has a considerable impact on the MFC setting value obtained from the controller. In case this curve is not correct the feedback loop will try to compensate for it, however, some steady state offset will occur. Calibrating this curve should therefore be done on a frequent basis, and a solid knowledge of this relationship every time a new system is started up is definitely a necessity. The option of directly including the MFC setting in the control law was considered, but since a piece-wise linear relationship was found between the k_La and the MFC setting, this would have resulted in a gain scheduling depending on where, within the MFC range, the system was operating. In order to keep the translation transparent and easily available for future changes and edits, the translation was kept as a separate step of the controller.

Tuning of the controller gain

As observed during the set point change experiment, a higher gain resulted in a smaller offset from the set point without resulting in instability and oscillatory behavior. However, as seen in cases of system capacity limitation (high concentrations during the dynamic influent experiment), the system was very sensitive towards the gain value of the proportional feedback control loop. It is therefore speculated that gain scheduling could be an advantageous attribute from which this controller could benefit considerably (Seborg et al., 2004). This could be done by defining a metric (error signal), which gives information on the distance between the current state of the system and its capacity limit, and based on this information the gain value would change accordingly. I.e. the gain would be higher, the further the current operation is from the capacity limit. Such a metric could e.g. be a batch assay measuring the specific removal rate of the sludge present in the reactor, and by comparing this to the load coming to the system, a measure of how far from the maximum capacity the system was operating could be obtained. Conducting a measurement like this might be a costly and time consuming thing to do, but if conducted with an appropriate frequency (e.g. once per week), it could definitely improve performance of the system.

Startup of reactor operation

From the experience obtained in this work, it is believed that the control strategy can also be implemented during a startup of nitritation-anammox reactors. What is often also controlled during startups is the ammonium loading to the system (e.g. Christensson et al., 2013), which is slowly ramped up as the concentrations of the microbial groups slowly increase to the desired levels (van der Star et al., 2007). As the ammonium loading is an input to the controller presented here, this information can simply be fed to the controller, which will ensure to supply the appropriate amount of oxygen to the system in order to cope with the current load received by the system.

Possibility of multi-loop extensions

Finally, it should also be mentioned, that the control strategy validated in this study was a mere single-loop controller considering one actuator. Possibilities of extending it to a multi-loop strategy include utilizing the pH signal to control the exchange ratio or to control the length of the SBR cycle, similarly to the study by Lemaire et al. (2008), by which the volumetric removal rate might be improved due to higher loading rates. The pH signal has previously been used to control the nitritation processes (Volcke et al., 2006a) and a single-stage nitritation-anammox process (Wett, 2007). From experimental experiences (results not shown), it was found that the pH signal often responded faster, by changing from a decreasing to an increasing trend, compared to the DO signal in cases of ammonium depletion before the end of the reaction phase. It is therefore believed that utilizing this measurement as well could further optimize the reactor performance.

8.5 Conclusions

A batch-to-batch control strategy for a single-stage CANR process was developed, tested, and validated in a lab-scale SBR. Through extensive experimental testing of a feedforward-feedback control strategy promising results have been obtained. The main conclusions are:

- The controller successfully rejected the disturbances in the influent ammonium concentration and maintained a high removal efficiency, while the reference operation strategy simply failed at rejecting the disturbance.

- Due to insight obtained from the previous simulation studies the controller was implemented and started up in a rapid manner compared to experience-based trial and error operation and tuning of a controller.
- Qualitatively similar results were obtained in disturbance handling when comparing simulations and experimental work. The observation, that these trends agree, confirms the importance of the simulation based methodology used throughout this thesis.
- Retuning of the controller was needed in order to avoid oscillatory behavior during high ammonium loading rates due to limitation of the nitritation-anammox capacity of the microbial community present in the reactor.
- Careful calibration of actuator equipment and tuning of the controller is therefore necessary to ensure good controller performance and disturbance rejection.
- Future perspectives include, further consolidating the control strategy by including inherent time constants and delays observed experimentally in the model and propose a better tuning of the control parameters, inclusion of more on-line sensors to facilitate a better automation, and utilization of measurements for development of multi-loop strategies, e.g. by considering pH and timing of the SBR cycle.

PART IV – Conclusions and Future Perspectives

This last part of the thesis consists of one chapter, in which the findings obtained as a direct consequence of the work conducted during this PhD project are presented first, followed by a general discussion of the implications that these findings might have. Finally, ideas on how this field is evolving in the future and possibilities for further improvements of the methodologies used in this thesis are presented in the future perspectives section.

9 Conclusions

9.1 Findings

Through an integrated approach including modeling, experimentation, and control the following was obtained:

- A comprehensive mechanistic model of a granular CANR reactor was successfully constructed by applying a multi-scale modeling framework. In order to be able to solve the resulting non-linear system of PDEs and AEs that the model consisted of, a solution strategy considering appropriate numerical approximation schemes was formulated and applied.
- The developed model was used for simulation studies and analyzed through sensitivity analysis techniques, aiming at obtaining a deeper process understanding. In particular, this analysis revealed that AOB related parameters along with mass transfer related parameters are the most important model parameters during aeration limited operation. During excess aeration the AnAOB related parameters were the most important along with the mass transfer related parameters. However, here the impact of improved mass transfer had a negative impact on the overall nitrogen removal due to AnAOB inhibition.
- The best removal efficiency was found to be almost linearly dependent on the volumetric oxygen to nitrogen loading ratio and not solely on the bulk oxygen concentration.
- An efficient numerical solution scheme to calculate the pH profile inside the granules was developed and used to simulate and investigate the two-way interactions between medium pH and microbial activities in the granules. The solution scheme showed the ability to cope with the additional numerical complexity related to the solution of the pH equations along with the PDEs of the existing model.
- The mechanistic process model was calibrated to process performance data. Following good modeling practice principles, a customized calibration and validation protocol for granular SBR systems was developed and used to ensure consistency and quality of the model calibration efforts. The protocol included two new features: a) a fast model initialization and b) novel evaluation criteria based on stoichiometric ratios of nitrogen species, which were measures of the relative microbial activities.

- Three novel single-loop control strategies were developed based on process understanding gained from model simulations and experimental work. All of the control strategies used oxygen supply as the actuator and removal efficiency as the controlled variable. These control strategies are:
    - A feedforward controller: This was based on the finding of the optimal removal efficiency being proportional to the volumetric oxygen to nitrogen loading rate. Thus the oxygen supply was regulated based on the incoming ammonium load.
    - A feedback controller: This was based on experiences from experimental start-up of lab-scale reactors. The feedback action is based on an offset in the removal efficiency from the optimal set point and a metric of the relative activity of the microbial groups, taking into account the removed and produced nitrogen species in the system and the reaction stoichiometry, deciding the direction of action of the controller.
    - A feedforward-feedback controller: In this controller, the offset in removal efficiency, through a feedback loop, corrects the set point of oxygen to nitrogen loading ratio in the feedforward loop.
- The three strategies were tested through simulations of step change disturbances in the influent load, set point changes of the controlled variable, and dynamic changes in the influent load mimicking the composition of effluent of an anaerobic digester. The results highlighted that the feedforward controller was best at handling disturbances in ammonium loading, while the feedback controller was best at handling different organic carbon loadings. Overall the feedforward-feedback controller was found to be the most versatile towards the disturbances at the expense of slightly slower dynamic responses and a slightly more complex control structure.
- Since the feedforward-feedback controller was deemed the most successful from simulation analyses its functionality was tested experimentally, where it was shown to reject disturbances in the influent ammonium concentrations. However, during very high ammonium loadings, when the capacity of the present sludge was reached, an oscillatory response was observed. A proper retuning of the controller was therefore needed to solve the problem and was identified as a task of essential importance.

Based on the abovementioned findings and results, it can be concluded that a systematic and integrated modeling and experimentation approach was successful as a research methodology in providing an improved understanding of the process. It has helped developing novel control alternative concepts and strategies, aiming directly at keeping a high and stable removal

efficiency of the process. The developed promising operation and control strategies will contribute to realization of the full potential of this nitrogen removal technology in full-scale plant applications.

9.2 General discussion

As anticipated in the introduction, the integration of the CANR process in a single reactor with granular sludge containing a mixture of microbial groups resulted in many simultaneous processes and phenomena occurring, complicating the observation and understanding of the overall process. In order to overcome this issue, a mechanistic structured model of the system was developed and model-based tools, such as sensitivity analysis, were used to try to unravel which processes and interactions were influential during different operational conditions. Through this exercise, an improved understanding of the CANR technology was obtained, which help direct the efforts trying to improve the operation. It was established that both microbial metabolism along with mass transfer resistance had an impact on the overall performance, and improvement of the performance was therefore not a straightforward task. The oxygen supplied in relation to the ammonium present in the stream to be treated was identified as a key factor, which resulted in efforts in developing control strategies utilizing this knowledge. These strategies can be used in operation of granular SBR type systems, where things to be considered as well are granule sizes, their distribution and the timing and configuration of the sequential operation. The SBR technology is a great option for implementation of CANR, since it utilizes a cheap strategy for biomass retention, i.e. gravity in the settling phase as opposed to expensive alternatives, such as hydrocyclones or membrane separation, while it still allows manipulation of the microbial composition through discrimination of different size fractions of the biomass. Also, the load handling of the SBR is easily changeable through the sequential operational scheme, which is a big advantage when treating streams that are not stable in flow and composition.

Even though the findings in this work were specified for granular sludge performing CANR and at some points specified for SBR operation, similar ideas can be extrapolated to other types of sludge systems and operations. For example, utilizing the control strategies in continuous or SBR type MBBRs or other attached growth systems is easily applicable. The controller structure will remain the same, but what is different in other systems is quite likely the role of mass transfer limitation. The implementation of the control law will therefore require a new identification of

the optimal oxygen to nitrogen loading ratio along with identification of the process transfer function, in order to obtain a proper tuning following the IMC rules.

In the controller development and analysis, different control alternatives were identified with different alternatives being best at handling different types of disturbances. This brings the attention to the importance of investigating and obtaining a detailed knowledge of the events in the upstream units from the CANR process as an important prerequisite for the design and control of such systems. In line with this, the CANR control scheme should be considered a "module" as a part of a bigger plant-wide control scheme, in which measurements and data from other units are utilized to anticipate the disturbances and the settings of the controller. This is expected to benefit the plant-wide operation, more than if the controller is considered a standalone application.

Since the number of implementations of the CANR process in full-scale is steadily increasing, the importance of proper control and operation is increasingly important to realize the full potential of this technology in practice. It is believed that the control strategy developed here is an important contribution to the field. Also, modeling should be used first, before the implementation and not after the implementation to check and understand the results. As demonstrated in this thesis, the use of simulation and experimentation tools is complimentary and synergistic. By utilizing this approach, the application will move towards a more systematic, knowledge based, standard implementation, as opposed to the case-by-case and experience based approach followed to implement this technology in practice.

9.3 Future works

Here, suggestions and ideas about where future efforts should be put within modeling, control, and experimentation are presented. First, model extensions and integration with other important areas of research is introduced, followed by a comment on calibration methodology improvement. Secondly, a discussion on improvements and extensions of the control of the CANR process is provided, through an introduction of ideas for multi-loop control strategies, improvements to the control laws, and alternative control methods. In particular, the use of fuzzy logic has been explored, and is therefore introduced a bit more in detail. Finally, future experimental work is presented.

9.3.1 Modeling

With respect to the modeling efforts involving the CANR process, there are a number of obvious points of extensions and/or improvements which are discussed below.

Green house gas emissions

Currently, a lot of efforts are being put into investigations of green house gas (GHG) formation and emissions, since there are indications that a substantial amount of nitrous oxide (N_2O) is produced in biological treatment systems using low aeration intensity configurations (Kampschreur et al., 2009) and since nitrous oxide is a very potent GHG having a global warming potential approximately 300 times higher than CO_2 (IPCC, 2000). Inclusion of this compound in the modeling studies of CANR could improve the understanding of the emissions and, maybe even more importantly, help the development of operational and control strategies that also minimize the emissions, instead of only focusing on optimizing the removal efficiency. Seeing how many studies have investigated emissions from conventional biological treatment system through simulation (Flores-Alsina et al., 2011; Corominas et al., 2012; Ni et al., 2013), this is definitely a direction that the CANR modeling will be moving in as well.

Model integration – plant-wide modeling

Another effort is moving towards a more holistic understanding of the biological treatment processes. This can be obtained through integrating the anammox process model with models of other important microbial groups, e.g. phosphorus accumulating organisms (PAO) or special heterotrophic bacteria. By keeping on expanding the model like this, a model of the entire microbial ecosystem can be obtained. Efforts based on microbial and molecular tools and investigations (Nielsen et al., 2010) have been made to construct conceptual models like this, taking into account the core microbial species in a treatment plant. This is an important effort towards establishing interactions between the most important microbial groups in a modern up-to-date biological WWTP. For CANR, this especially becomes of interest when the technology is considered for treatment of the mainstream in the WWTP (Wett et al. 2013; Hu et al., 2013b) where other microbial processes are occurring at the same time as CANR.

The model developed in this work (both the biofilm feature and the single-stage CANR containing part) could be part of an extension for the BSM platform, as these are features that

are present more and more often in modern day WWTPs. Biofilm models are considered to be included in the future (Jeppsson et al., 2013) and GHG emissions has already been incorporated (Flores-Alsina et al., 2011). The two-stage SHARON-Anammox process has been evaluated in the BSM2 platform (Volcke et al., 2006b), yet single-stage CANR still needs to be investigated.

Mixing conditions

Concentration gradients in the reactor caused by imperfect mixing may take place, especially when scaling up the process to larger tanks and possibly higher biomass concentrations. These mixing conditions can be simulated by computational fluid dynamics (CFD), which can serve as a useful tool to investigate and suggest improvements to the mixing conditions. Nevertheless, the CFD simulation of a three-phase bioreactor is a complex task, resulting in a manifold multiplication of the number of model equations to be solved, and the lack of certainty about essential model parameters (e.g. biomass effect on fluid properties such as viscosity) cannot guarantee achieving accurate results. It is therefore not clear whether the information obtained from such a CFD simulation is sufficient to optimize conditions. Hence, before moving to this level, other shortcut analyses can be used to check the mixing conditions, such as micromixing analysis (Baldyga and Bourne, 1990) or time-regime analysis (Van't Riet and Tramper, 1991), and depending on these results decide whether CFD or simpler compartmental models are needed.

Influence of granule/particle size on process performance

Investigations of the interaction between biofilm/granules and suspended cell growth are of great interest, since observations of a bi-modal distribution in the PSD (Mutlu et al. in prep.) indicate that the microbial groups have different preferences with respect to how they spatially organize themselves. Investigations show that different size fractions of the granular biomass have a different microbial composition with the small sizes consisting of mainly AOB and the bigger granules containing almost only AnAOB (Mutlu et al. in prep.; Wett et al., 2013; Vlaeminck et al., 2010). Masic and Eberl (2012) did model investigations of the interaction between wall-attached and suspended growth in a single-species system, and found that although most biomass was found in the biofilm, the suspended biomass in the bulk contributed significantly to the substrate conversion. Since, the observed bi-modal distribution can be conceived as suspended biomass (peak in small particle sizes) and actual granules (peak in bigger particle sizes), it would be interesting to do the same sort of modeling exercise here, to see how

the interactions between the microbial groups might influence the performance. The final objective of an exercise like this would be to investigate whether an extra handle/actuator would be available for control or manipulation of the microbial composition in case size segregation is possible, in order to optimize the performance and operation.

Another approach to address the same issue is to model a particle size distribution (PSD) and not just a single size granule as done in this work. The consequence of this would be adding one more dimension, thus one more level of discretization. Modeling a PSD would result in a population balance type model (PBM), which is often computational very heavy to solve. An approach in between a PBM and a single granule size model has been presented by Volcke et al. (2012), investigating the consequence of considering more classes of granule sizes. It would be useful to investigate this approach for the presented model to see whether the findings related to mass transfer importance and optimal operational conditions would be different from the findings obtained with the single size assumption.

While different modifications of the model can be made in order to obtain higher resolution of the results or obtain more detailed information, as stated above, it is very important to keep the objective in mind, since these modifications most likely come at very high computational time costs. One should therefore ensure that it is worthwhile to do such an extra effort.

Calibration

Finally, with respect to the methodology used for the calibration, an issue which could be addressed is to include measurements of abundance of microbial groups in the model calibration methodology. This requires highly reliable and accurate measurement techniques, which for now are at a state where qualitative comparisons can be made, yet for quantitative comparison they are not quite accurate enough.

9.3.2 Control

In this work, alternatives to existing control schemes were developed based on traditional control theory. Below, ideas of how these can be extended, improved, and combined with existing ones are discussed.

Multi-loop strategy

The use pH or ORP measurements to control the cycle or aeration length in SBR operation has previously been investigated (e.g. Lemaire et al., 2008; Lackner et al., 2012) and was shown to improve the performance of nitritation systems. Since timing was not considered an actuator in the work presented here, it is speculated that improvements to the system can be obtained by starting to utilize this. An example of such an application is the observation of the pH signal. The value of the pH measurement usually decreases during an SBR cycle due to proton production by the AOB. Once all of the ammonium present in the reactor has been oxidized the pH value starts increasing due to stripping of CO_2 by aeration, an effect which then starts dominating over the proton production, which has now stopped (a similar observation has been made in many nitrification-denitrification studies, e.g. Andreottola et al. (2001)). Ending the cycle at this point in time, instead of waiting until a fixed time has elapsed, allows for a lowering of the HRT, which means that the system would be able to handle higher volumetric loads. It is therefore believed that the treatment capacity of the system can be increased in this manner.

Control law

Related to the specific control strategies presented in this thesis, a PI controller for the feedback loop in the feedforward-feedback controller instead of a P-only controller is expected to reduce the offset from the set point significantly, an issue which was observed both in modeling and experimental studies during set point changes.

Finally, a future investigation could also be the design of a non-linear DO controller, which takes into account the non-linear oxygen transfer function, instead of assuming a linear or piece-wise linear relation around the point of normal operation. This was previously shown to reduce the aeration consumption in biological treatment removing ammonium (Lindberg and Carlsson, 1996) and is speculated to be able to contribute to improve performance of controllers developed in this thesis as well.

Control method

MPC

In future control applications, more advanced control methods, such as model predictive control (MPC), are expected to play an increasing role. This is possible if a reduced order model that only links input to output can be obtained. However, a reduced order model only makes sense within a narrow range of operation, and its applicability is therefore limited. Numerous investigations of MPC applications already exists in aeration controllers in conventional biological treatment systems, however, all utilizing simpler models. For an extensive review the reader is referred to Åmand et al. (2013).

Fuzzy logic control

Fuzzy decision methods have been used for diagnosis of performance since it is a means to formalize the knowledge accumulated by the process operators (Honda and Kobayashi, 2000), and it is adapted to the use of expert knowledge and quantitative models. For instance, Comas et al. (2008) developed a fuzzy diagnosis method to establish the risk for occurrence of microbiology related settling problems in activated sludge systems. Likewise, fuzzy decision can also be used in control of bioprocesses, allowing synthesis of the available information from the process and applying it for the automatic control of the process (Ruano et al., 2010).

Since controllers depending on set point values for DO, nitrogen species, and pH alone may not be enough to deduce whether the microbial community activities are balanced and performance is stable (Vangsgaard et al., 2012), a fuzzy logic based application is a good alternative for diagnosis and control in CANR applications. Fuzzy diagnosis and control have previously been combined in anaerobic digesters (Punal et al., 2001; Lardon et al., 2005) and configured similarly to a state controller with a filter for state estimation.

The use of fuzzy logic for diagnosis of the CANR process taking into account the stoichiometric ratios of formed or produced nitrogen species as previously used by Mutlu et al. (2013) has therefore been conducted here, with the intention of extending it to a control application. Below, the diagnosis procedure is briefly outlined for the reader to get an idea about how and why this might be a smart way to diagnose and control this system.

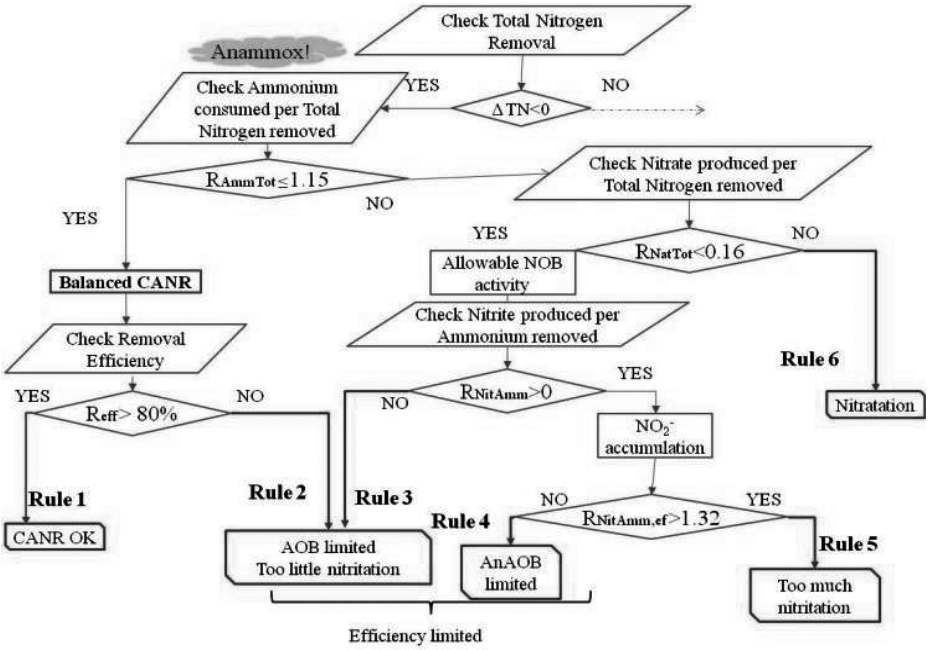

Figure 9.1 Decision tree developed for diagnosis of SBRs performing single-stage CANR (adapted from Mutlu et al., 2013)

In the fuzzy diagnosis the measurement inputs (ΔTN, R_{AmmTot}, R_{NatTot}, R_{NitAmm}, R_{eff}, $R_{NitAmm,ef}$) were linked to the outputs through a rule-base and defined membership functions (MFs).

The decision tree formulated in Figure 9.1 is based on a number of rules formulated based on process stoichiometry and experiences:

Rule 1. The optimal performance is the case where balanced nitritation-anammox is achieved and more than 80% ammonium removal is observed.

Rule 2. If the removal efficiency is not sufficient, yet R_{AmmTot} (as defined in previous chapters) is within the target range, the system is limited by nitrite production.

Rule 3. If the system moves away from balanced CANR, nitrite or nitrate accumulates. If such an accumulation is still relatively small, within the allowable ranges, the AOB activity is still limiting.

Rule 4. When NOB activity is within allowable limits, the system is experiencing nitrite accumulation due to low AnAOB activity.

Rule 5. When NOB activity is within allowable limits, the system is experiencing nitrite accumulation due to too high nitritation.

Rule 6. If nitrate accumulates to more than the allowed levels, then nitratation is prevailing in the system.

It must be highlighted that the core of a fuzzy inference system is the set of production rules (Kovacic and Bogdan, 2005). It is therefore essential that the rules gather all the information available about the system and are self-consistent.

Evaluation of diagnosis tool

The diagnosis tool was tested assessing real data from one of the lab-scale reactors during 100 days. This assessment was done *a posteriori* and did not influence the policy followed by the operator, hence an open-loop analysis.

The diagnosis results for four defined outputs (Figure 9.2) show the following evolution of the reactor: at the beginning the autotrophic nitrogen removal (ANR) was limited by the AnAOB metabolism and in a few occasions by too much nitratation. As nitritation became lower due to a decrease in the oxygen supply, the process was no longer limited by AnAOB and nitratation became less significant. However, since nitritation became too low (after day 50) the ANR still did not quite reach a satisfactory level. These status diagnoses are very much in line with what was observed during the operation.

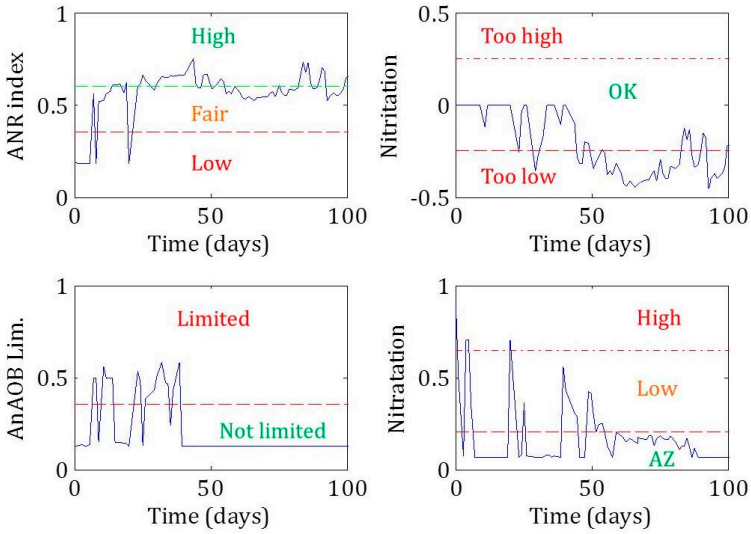

Figure 9.2 Results of the diagnosis tool for 100 days of experimental operation data of the SBR.

In the future, this work will be extended such that the on-line measurement of the nitrogen species in the reactor is used for diagnosis of the system, which is carried out first, and this information is then passed on to a fuzzy controller that decides on the appropriate action to be taken. The separation of diagnosis and control is expected to be an efficient way to implement this tool resulting in an alternative simple control structure.

9.3.3 Experimentation

All possible model extensions, mentioned in the previous section, need to be supported by experimental observations. Thus, depending on which direction is decided to be further elucidated, experimental efforts should be simultaneously extended in this direction.

From the findings in this work, a place to start investigating control of other types of systems both with respect to the sludge type (suspended vs. granular vs. attached) and with respect to the operation type (SBR vs. continuous, within SBR long vs. short feeding phase, intermittent vs. continuous aeration) would be through further experimental validation in these systems.

References

1. Alpkvist E., Picioreanu C., van Loosdrecht M.C.M., Heyden A. (2006) Three-Dimensional biofilm model with individual cells and continuum EPS matrix. Biotechnol. Bioeng. **94**(5), 961-979.

2. Andreottola G., Foladori P., Ragazzi M. (2001) On-line control of a SBR system for nitrogen removal from industrial wastewater. Water Sci. Technol. **43**(3), 93-100.

3. Anthonisen A.C., Loehr R.C., Prakasam T.B.S., Srinath E.G. (1976) Inhibition of nitrification by ammonium and nitrous-acid. Journal Water Pollution Control Federation **48**, 835-852.

4. APHA-AWWA-WPCF (1998) Standard Methods for Examination of Water and Wastewater, 20th edition. American Public Health Association, Washington, USA.

5. ASCE (2007) Measurement of oxygen transfer in clean water: ASCE Standard, ASCE/SEI 2-06/ American Society of Civil Engineers, American Society of Civil Engineers, Reston, Virginia, USA.

6. Baldyga J., Bourne J.R. (1990) Comparison of the engulfment and the interaction-by-exchange-with-the-mean micromixing models. Chem. Eng. J. **45**(1), 25-31.

7. Bernet N., Sanchez O., Cesbron D., Steyer J. P., Delgenes J. P. (2005) Modeling and control of nitrite accumulation in a nitrifying biofilm reactor. Biochem. Eng. J. **24**(2), 173-183.

8. Bernet N., Peng D., Delgens J.P., Moletta R. (2001) Nitrification at low oxygen concentration in biofilm reactor. J. Environ. Eng. **127**(3), 266-271.

9. Boltz J.P., Morgenroth E., Brockmann D., Daigger G.T., Henze M., Rittmann B., Sørensen K.H., Takacs I., Vanrolleghem P.A., van Loosdrecht M.C.M. (2012) Framework for biofilm reactor model calibration. Proceedings from 3rd IWA/WEF Wastewater Treatment Modelling Seminar, Mont-Sainte-Anne, Quebec, 143-146.

10. Boltz J.P., Morgenroth E., Brockmann D., Bott C., Gellner W.J., Vanrolleghem P.A. (2011) Systematic evaluation of biofilm models for engineering practice: components and critical assumptions. Water Sci. Technol. **64**(4), 930-944.

11. Brockmann D., Morgenroth E. (2010) Evaluating operating conditions for outcompeting nitrite oxidizers and maintaining partial nitrification in biofilm systems using biofilm modeling and Monte Carlo filtering. Water Res. **44**(6), 1995-2009.

12. Brockmann D., Rosenwinkel K. H., Morgenroth E. (2008) Practical identifiability of biokinetic parameters of a model describing two-step nitrification in biofilms. Biotechnol. Bioeng. **101**(3), 497-514.

13. Broda E. (1977) 2 kinds of lithotrophs missing in natrue. Zeitschrift Fur Allgemeine Mikrobiologie **17,** 491-493.

14. Brun R., Kuhni M., Siegrist H., Gujer W., Reichert P. (2002) Practical identifiability of ASM2d parameters - systematic selection and tuning of parameter subsets. Water Res. **36**(16), 4113-4127.

15. Bundgaard E., Andersen K.L., Petersen G. (1989) BIO-DENITRO and BIO-DENIPHO Systems – Experiences and Advanced Model Development: The Danish Systems for Biological N and P Removal. Water Sci. Technol. **21**(12), 1727-1730.

16. Chen A.C., Chang J.S., Yang L., Yang Y.H. (2001) Nitrogen removal from sewage by continuous flow SBR system with intermittent aeration. Environ. Technol. **22**, 553-559.

17. Christensson M., Ekström S., Andersson Chan A., Le Vaillant E., Lemaire R. (2013) Experience from start-up of the first ANITA Mox Plants. Water Sci. Technol. **67**(12), 2677-2684.

18. Christensson M., Ekström S., Lemaire R., Le Vaillant E., Bundgaard E., Chauzy J., Stålhandske L., Hong Z., Ekenberg M. (2011) ANITA Mox – A BioFarm solution for fast start-up of deammonifying MBBRs. Conference proceedings WEFTEC 2011, Los Angeles.

19. Claros J., Serralta J., Seco A., Ferrer J., Aguado D. (2012) Real-time control strategy for nitrogen removal via nitrite in a SHARON reactor using pH and ORP sensors. Process Biochem. **47**(10), 1510-1515.

20. Comas J., Rodríguez-Roda I., Gernaey K.V., Rosen C., Jeppsson U., Poch M. (2008) Risk assessment modelling of microbiology-related solids separation. Environmental Modelling & Software **23**, 1250–1261.

21. Corominas L., Flores-Alsina X., Snip L., Vanrolleghem P.A. (2012) Comparison of different modeling approaches to better evaluate greenhouse gas emissions from whole wastewater treatment plants. Biotechnol. Bioeng. **109**(11), 2854-2863.

22. Dalsgaard T., Cranfield D.E., Petersen J., Thamdrup B., Acuna-Gonzalez J. (2003) N_2 production by the anammox reaction in the anoxic water column of Golfo Dulce, Costa Rica. Nature **422**, 606-608.

23. Dapena-Mora A., van Hulle S.W.H., Campos J.L., Mendez R., Vanrolleghem P.A., Jetten M. (2004) Enrichment of Anammox biomass from municipal activated sludge: experimental and modelling results. J. Chem. Technol. Biotechnol. **79**, 1421-1428.

24. Dold P.L., Ekama G.A., Marais (1980) The activated sludge process 1. A general model for the activated sludge process. Progress Water Technol. **12**(6), 47-77.

25. Downing L.S., Nerenberg R. (2008) Effect of Oxygen Gradients on the Activity and Microbial Community Structure of a Nitrifying, Membrane-Aerated Biofilm. Biotechnol. Bioeng. **101**(6)**,** 1193-1204.

26. Egli K., Fanger U., Alvarez P.J.J., Siegrist H., van der Meer J.R., Zehnder A.J.B. (2001) Enrichment and characterization of an anammox bacterium from a rotating biological contactor treating ammonium-reach leachate. Arch Microbiol. **175**, 198-207.

27. Figueroa M., Vazquez-Padin J.R., Mosquera-Corral A., Campos J.L., Mendez R. (2012) Is the CANON reactor an alternative for nitrogen removal from pre-treated swine slurry? Biochem. Eng. J. **65**, 23-29.

28. Flores-Alsina X., Corominas L., Snip L., Vanrolleghem P.A. (2011) Including greenhouse gases emissions during benchmarking of wastewater treatment plant control strategies. Water Res. **45**(16), 4700–4710.

29. Furukawa K., Lieu P.K., Tokitoh H., Fujii T. (2006) Development of single-stage nitrogen removal using anammox and partial nitritation (SNAP) and its treatment performances. Water Sci. Technol. **53**(6), 83-90.

30. Fux C., Huang D., Monti A., Siegrist H. (2004) Difficulties in maintaining long-term partial nitrification of ammonium-rich sludge digester liquids in a moving-bed biofilm reactor (MBBR). Water Sci. Technol. **49**(11-12), 53-60.

31. Ganigue R., Volcke E.I.P., Puig S., Balaguer M.D., Colprim J., Sin G. (2010) Systematic model development for partial nitrification of landfill leachate in a SBR. Water Sci. Technol. **61**(9)**,** 2199-2210.

32. Grady C.P.L.Jr., Gujer W., Henze M., Marais G.v.R., Matsuo T. (1986) A model for single-sludge wastewater treatment systems. Water Sci. Technol. **18**(6), 47-61.

33. Gujer W. (2010) Nitrification and me – A subjective review. Water Res. **44**(1), 1-19.

34. Gujer W. (2006) Activated sludge modelling: past, present and future. Water Sci. Technol. **53**(3), 413-420.

35. Gujer W., Henze M., Mino T., van Loosdrecht M.C.M. (1999) Activated sludge model no. 3. Water Sci. Technol. **39**(1), 183-193.

36. Hao X.D., van Loosdrecht M.C.M. (2004) Model-based evaluation of COD influence on a partial nitrification-Anammox biofilm (CANON) process. Water Sci. Technol. **49**(11-12), 83-90.

37. Hao X.D., Heijnen J.J., van Loosdrecht M.C.M. (2002a) Sensitivity analysis of a biofilm model describing a one-stage completely autotrophic nitrogen removal (CANON) process. Biotechnol. Bioeng. **77**(3), 266-277.

38. Hao X.D., Heijnen J.J., van Loosdrecht M.C.M. (2002b) Model-based evaluation of temperature and inflow variations on a partial nitrification-ANAMMOX biofilm process. Water Res. **36**(19), 4839-4849.

39. Heitzig M., Sin G., Glarborg P., Gani R. (2010) A computer-aided framework for regression and multi-scale modelling needs in innovative product-process engineering. Computer Aided Chem. Eng. **28**, 379-384.

40. Hellinga C., van Loosdrecht M.C.M., Heijnen J.J. (1999) Model based design of a novel process for nitrogen removal from concentrated flows. Math. Comput. Model. **5**(4), 351-371.

41. Hellinga C., Schellen A., Mulder J.W., van Loosdrecht M.C.M., Heijnen J.J. (1998) The SHARON process: An innovative method for nitrogen removal from ammonium-rich waste water. Water Sci. Technol. **37**(9), 135-142.

42. Helmer C., Tromm C., Hippen A., Rosenwinkel K.H., Seyfried C.F., Kunst S. (2001) Single stage biological nitrogen removal by nitritation and anaerobic ammonium oxidation in biofilm systems. Water Sci. Technol. **43**(1), 311-320.

43. Henze M., Harremoes P., Jansen J.L.C., Arvin E. (2002) Wastewater Treatment: Biological and Chemical Processes. Third edition, Springer-Verlag, New York.

44. Henze M., Gujer W., Mino T., van Loosdrecht M.C.M. (2000) Activated Sludge Models ASM1, ASM2, ASM2D and ASM3, Scientific Technical Report No. 9, IWA Publishing, London.

45. Henze M., Gujer W., Mino T., Matsuo T., Wentzel M.C., Marais G.v.R., van Loosdrecht M.C.M. (1999) Activated sludge model no. 2d. Water Sci. Technol. **39**(1), 165-182.

46. Henze M., Grady C.P.L.Jr., Gujer W., Marais G.v.R., Matsuo T. (1987) A general model for single-sludge wastewater systems. Water Res. **21**(5), 505-515.

47. Henze Christensen M. (1975) Denitrification of sewage by alternating process operation. Progress in Water Technol. **7**(2), 339-347.

48. Honda H., Kobayashi T. (2000) Fuzzy Control of Bioprocess. J. Biosci. Bioeng. **89**(5), 401-408.

49. Hu Z., Lotti T., van Loosdrecht M.C.M., Kartal B. (2013a) Nitrogen removal with the anaerobic ammonium oxidation process. Biotechnol. Lett. **35**(8), 1145-1154.

50. Hu Z., Lotti T., de Kreuk M., Kleerebezem R., van Loosdrecht M.C.M., Kruit J., Jetten M.S.M., Kartal B. (2013b) Nitrogen Removal by a Nitritation-Anammox Bioreactor at Low Temperature. Appl. Environ. Microbiol. **79**(8), 2807-2812.

51. Hulsbeek J.J.W., Kruit J., Roeleveld J.P., van Loosdrecht M.C.M. (2002) A practical protocol for dynamic modelling of activated sludge systems. Water Sci. Technol. **45**(6), 127–136.

52. Iman R.L., Conover W.J. (1982) A Distribution-Free Approach to Inducing Rank Correlation among Input Variables. Commun. Stat. B-Simul. **11,** 311-334.

53. Ingildsen P., Jeppsson U., Olsson G. (2002) Dissolved oxygen controller based on on-line measurements of ammonium combining feed-forward and feedback. Water Sci. Technol. **45**(4-5), 453-460.

54. Insel G., Sin G., Lee D., Nopens I., Vanrolleghem P.A. (2006) A calibration methodology and model-based systems analysis for SBRs removing nutrients under limited aeration conditions. J. Chem. Technol. Biotechnol. **81,** 679-687.

55. Insel G., Orhon D., Vanrolleghem, P.A. (2003) Identification and modelling of aerobic hydrolysis - application of optimal experimental design. J. Chem. Technol. Biotechnol. **78**(4), 437-445.

56. IPCC (2000) Intergovernmental Panel on Climate Change (IPCC). Special Report on Emissions Scenarios. Cambridge University Press, Cambridge, UK.

57. Jardin N., Hennerkes J. (2012) Full-scale experience with the deammonification process to treat high strength sludge water – a case study. Water Sci. Technol. **65**(3), 447-455.

58. Jeppsson U., Alex J., Batstone D.J., Benedetti L., Comas J., Copp J.B., Corominas L., Flores-Alsina X., Gernaey K.V., Nopens I., Pons M.N., Rodríguez-Roda I., Rosen C., Steyer J.P., Vanrolleghem P.A., Volcke E.I.P., Vrecko D. (2013) Benchmark simulation models, *quo vadis?* Water Sci. Technol. **68**(1), 1-15.

59. Jeppsson U., Pons M.N., Nopens I., Copp J.B., Gernaey K.V., Rosen C., Steyer J.P., Vanrolleghem P.A. (2007) Benchmark simulation model no 2: general protocol and exploratory case studies. Water Sci. Technol. **56**(8), 67-78.

60. Jetten M.S.M., Wagner M., Fuerst J., van Loosdrecht M.C.M., Kuenen G., Strous M. (2001) Microbiology and application of the anaerobic ammonium oxidation ('anammox') process. Current Opinion in Biotechnol. **12**, 283-288.

61. Jetten M.S.M, Strous M., van de Pas-Schoonen K.T., Schalk J., van Dongen U.G.J.M., van de Graaf A.A., Logemann S., Muyzer G., van Loosdrecht M.C.M., Kuenen J.G. (1999) The anaerobic ammonium oxidation. FEMS Microbiol. Reviews **22**(5), 421-437.

62. Jin R.C., Yang G.F., Yu J.J., Zheng P. (2012) The inhibition of the Anammox process: A review. Chem. Eng. J. **197**, 67-79.

63. Joss A., Derlon N., Cyprien C., Burger S., Szivak I., Traber J., Siegrist H., Morgenroth E. (2011) Combined Nitritation-Anammox: Advances in Understanding Process Stability. Environ. Sci. Technol. **45**(22), 9735-9742.

64. Joss A., Salzgeber D., Eugster J., Koenig R., Rottermann K., Burger S., Fabijan P., Leumann S., Mohn J., Siegrist H. (2009) Full-Scale Nitrogen Removal from Digester Liquid with Partial Nitritation and Anammox in One SBR. Environ. Sci. Technol. **43**(14), 5301-5306.

65. Jung J.Y., Kang S.H., Chung Y.C., Ahn D.H. (2007) Factors affecting the activity of anammox bacteria during start up in the continuous culture reactor. Water Sci. Technol. **55**(1-2), 459-468.

66. Kaelin D., Rieger L., Eugster J., Rottermann K., Bänninger C., Siegrist H. (2008) Potential of in-situ sensors with ion-selective electrodes for aeration control at wastewater treatment plants. Water Sci. Technol. **58**(3), 629-637.

67. Kampschreur M.J., Temmink H., Kleerebezem R., Jetten M.S.M., van Loosdrecht M.C.M. (2009) Nitrous oxide emission during wastewater treatment. Water Res. **43**(17), 4093-4103.

68. Katsogiannis A.N., Kornaros M., Lyberatos G. (2003) Enhanced nitrogen removal in SBRs bypassing nitrate generation accomplished by multiple aerobic/anoxic phase pairs. Water Sci. Technol. **47**(11), 53-59.

69. Koch G., Egli K., van der Meer J.R., Siegrist H. (2000) Mathematical modeling of autotrophic denitrification in a nitrifying biofilm of a rotating biological contactor. Water Sci. Technol. **41**(4-5)**,** 191-198.

70. Kovacic Z., Bogdan S. (2005) Fuzzy Controller Design: Theory and Applications, CRC Press

71. Kreft J.U., Picioreanu C., Wimpenny J.W.T., van Loosdrcht M.C.M. (2001) Individual-based modelling of biofilms. Microbiol. **147**, 2897-2912.

72. Kuai L.P., Verstraete W. (1998) Ammonium removal by the oxygen-limited autotrophic nitrification- denitrification system. Applied and Environ. Microbiol. **64,** 4500-4506.

73. Kuenen J.G. (2008) Anammox bacteria: from discovery to application. Nature Reviews Microbiology **6,** 320-326.

74. Kwak W., McCarty P.L., Bae J., Huang Y.T., Lee P.H. (2012) Efficient single-stage autotrophic nitrogen removal with dilute wastewater through oxygen supply control. Bioresource Technol. **123**, 400-405.

75. Lackner S., Smets B.F. (2012) Effect of the kinetics of ammonium and nitrite oxidation on nitritation success or failure for different biofilm reactor geometries. Biochem. Eng. J. **69**, 123-129.

76. Lackner S., Lindenblatt C., Horn H. (2012) 'Swinging ORP' as operation strategy for stable reject water treatment by nitritation-anammox in sequencing batch reactors. Chem. Eng. J. **180**, 190-196.

77. Lackner S., Terada A., Smets B.F. (2008) Heterotrophic activity compromises autotrophic nitrogen removal in membrane-aerated biofilms: Results of a modeling study. Water Res. **42**(4-5), 1102-1112.

78. Lardon L.A., Merkey B.V., Martins S., Dötsch A., Picioreanu C., Kreft J.U., Smets B.F. (2011) iDynoMiCS: Next-generation individual-based modeling of biofilms. Environ. Microbial. **13**(9), 2416-2434.

79. Lardon L., Punal A., Martinez J.A., Steyer J.P (2005) Modular expert system for the diagnosis of operating conditions of industrial anaerobic digestion plants. Water Sci. Technol. **52**(1-2), 427-433.

80. Lemaire R., Marcelino M., Yuan Z. (2008) Achieving the nitrite pathway using aeration phase length control and step-feed in an SBR removing nutrients from Abattoir wastewater. Biotechnol. Bioeng. **100**(6), 1228-1236.

81. Lindberg C.F., Carlsson B. (1996) Nonlinear and set-point control of the dissolved oxygen concentration in an activated sludge process. Water Sci. Technol. **34**(3-4), 135-142.

82. Luff R., Haeckel M., Wallmann K. (2001) Robust and fast FORTRAN and MATLAB (R) libraries to calculate pH distributions in marine systems. Comput. Geosci. **27**(2), 157-169.

83. Masic A., Eberl H.J. (2012) Persistence in a Single Species CSTR Model with Suspended Flocs and Wall Attached Biofilms. Bull. Math. Biol. **74**(4), 1001-1026.

84. Masic A., Bengtsson J., Christensson M. (2010) Measuring and modeling the oxygen profile in a nitrifying Moving Bed Biofilm Reactor. Math. Biosci. **227**(1), 1-11.

85. Morgenroth E., Wilderer P. (2000) Influence of detachment mechanisms on competition in biofilms Water Res. **34**(2), 417-426.

86. Mulder A., van de Graaf A.A., Robertson L.A., Kuenen J.G. (1995) Anaerobic ammonium oxidation discovered in a denitrifying fluidized-bed reactor. Fems Microbiol. Ecol. **16,** 177-183.

87. Mutlu A.G., Vangsgaard A.K., Sin G., Smets B.F. (2013) Performance and community dynamics during controlled lab-scale start-up of completely autotrophic nitrogen removing SBRs. *In preparation*

88. Mutlu A.G., Vangsgaard A.K., Sin G., Smets B.F. (2013) An operation protocol for facilitating start-up of single-stage autotrophic nitrogen removing reactors based on process stoichiometry. Water Sci. Technol. **68**(3), 514-521.

89. Ni B.J., Yuan Z., Chandran K., Vanrolleghem P.A., Murthy S. (2013) Evaluating four mathematic models for nitous oxide production by autotrophic ammonium-oxidizing bacteria. Biotechnol. Bioeng. **110**(1), 153-163.

90. Ni B.J., Ruscalleda M., Smets B.F. (2012) Evaluation on the microbial interactions of anaerobic ammonium oxidizers and heterotrophs in anammox biofilms. Water Res. **46**(15), 4645-4652.

91. Ni B.J., Chen Y., Liu S., Fang F., Xie W., Yu H. (2009) Modeling a Granule-Based Anaerobic Ammonium Oxidizing (ANAMMOX) Process. Biotechnol. Bioeng. **103**(3), 490-499.

92. Nicolella C., van Loosdrecht M.C.M., Heijnen J.J. (1998) Mass transfer and reaction in a biofilm airlift suspension reactor. Chem. Eng. Sci. **53,** 2743-2753.

93. Nielsen M.K., Persson O., Kümmel M. (1981) Computer control of nitrifying and denitrifying activated sludge process. Water Sci. Technol. **13**(9), 285-291.

94. Nielsen P.H., Mielczarek A.T., Kragelund C., Nielsen J.L., Saunders A.M., Kong Y., Hansen A.A., Vollertsen J. (2010) A conceptual ecosystem model of microbial communities in enhanced biological phosphorus removal plants. Water Res. **44**(17), 5070-5088.

95. Nikacevic N.M., Huesman A.E.M., van den Hof P.M.J., Stankiewicz A.I. (2012) Opportunities and challenges for process control in process intensification. Chem. Eng. Process. 52, 1-15.

96. Olsson G. (2012) ICA and me – A subjective review. Water Res. **46**(6), 1585-1624.

97. Olsson G. (2011) Automation development in water and wastewater systems. Environ. Eng. Research **16**(4), 197-200.

98. Pambrun V., Paul E., Sperandio M. (2008) Control and modelling of partial nitrification of effluents with high ammonia concentrations in sequencing batch reactor. Chem. Eng. Process. **47,** 323-329.

99. Pambrun V., Paul E., Sperandio M. (2006) Modeling the partial nitrification in sequencing batch reactor for biomass adapted to high ammonium concentrations. Biotechnol. Bioeng. **95**(1), 120-131.

100. Park S., Bae W., Rittmann B.E. (2010) Multi-Species Nitrifying Biofilm Model (MSNBM) Including Free Ammonia and Free Nitrous Acid Inhibition and Oxygen Limitation. Biotechnol. Bioeng. **105**(6), 1115-1130.

101. Pellicer-Nàcher C., Sun S., Lackner S., Terada A., Schreiber F., Zhou Q., Smets B.F. (2010) Sequential aeration of membrane-aerated biofilm reactors for high-rate autotrophic nitrogen removal: Experimental demonstration. Environ. Sci. Technol. **44**(19), 7628-7634.

102. Peng Y., Zhu G. (2006) Biological nitrogen removal with nitrification and denitrification via nitrite pathway. Appl. Microbiol. Biotechnol. **73**(1), 15-26.

103. Perry R.H., Green D.W. (1997) Perry's Chemical Engineers' Handbook, 7th edition ed. McGraw-Hill Companies Inc., New York.

104. Picioreau C., van Loosdrecht M.C.M., Heijnen J.J. (1998) Mathematical modeling of biofilm structure with a hybrid differential-discrete cellular automaton approach. Biotechnol. Bioeng. **58**(1), 101-116.

105. Picioreau C., van Loosdrecht M.C.M., Heijnen J.J. (1997) Modelling the effect of oxygen concentration on nitrite accumulation in a biofilm airlift suspension reactor. Water Sci. Technol. **36**(1), 147-156.

106. Pollice A., Tandoi V., Lestingi C. (2002) Influence of aeration and sludge retention time on ammonium oxidation to nitrite and nitrate. Water Res. **36**(10), 2541-2546.

107. Power M. (1993) The predictive validation of ecological and environmental models. Ecol. Modell. **68,** 33-50.

108. Punal A., Rodriguez J., Franco A., Carrasco E.F., Roca E., Lema J.M. (2001) Advanced monitoring and control of anaerobic wastewater treatment plants: Diagnosis and supervision by a fuzzy-based expert system. Water Sci. Technol. **43**(7), 191-198.

109. Pynaert K., Smets B.F., Wyffels S., Beheydt D., Siciliano S.D., Verstraete W. (2003) Characterization of an autotrophic nitrogen-removing biofilm from highly loaded lab-scale rotating biological contactor. Appl. Environ. Microbiol. **69**(6), 3626-3634.

110. Rieger L., Gillot S., Langergraber G., Ohtsuki T., Shaw A., Takacs I., Winkler S. (2013) Guidelines for Using Activaed Sludge Models. IWA Scientific and Technical Report no. 22. IWA publishing, London

111. Rieger L., Langergraber G., Thomann M., Fleischmann N., Siegrist H. (2004) Spectral in-situ analysis of NO2, NO3, COD, DOC and TSS in the effluent of a WWTP. Water Sci. Technol. 50(11), 143-152.

112. Rittmann B.E., McCarty P.L. (1980) Model of steady-state-biofilm kinetics. Biotechnol. Bioeng. 22(11), 2343-2357.

113. Ruano M.V., Ribes J., Sin G., Seco A., Ferrer J. (2010) A systematic approach for fine-tuning of fuzzy controllers applied to WWTPs. Environ. Model. Software **25**(5), 670-676.

114. Ruano M.V., Ribes J., De Pauw D.J.W., Sin G. (2007) Parameter subset selection for the dynamic calibration of activated sludge models (ASMs): experience versus systems analysis. Water Sci. Technol. **56**(8), 107-115.

115. Rush D., Wakeham S.G., Hopmans E.C., Schouten S., Sinninghe Damste, J.S. (2012) Biomarker evidence for anammox in the oxygen minimum zone of the Eastern Tropical North Pacific. Org. Geochem. **53**, 80-87.

116. Saltelli A., Ratto M., Andres T., Campolongo F., Cariboni J., Gatelli D., Saisana M., Tarantola S. (2008) Global Sensitivity Analysis. The Primer. John Wiley and Sons, Ltd, West Sussex

117. Seborg D.E., Edgar T.F., Mellichamp D.A. (2004) Process Dynamics and Control. Second edition, John Wiley & Sons Inc.

118. Siegrist H., Reithaar S., Koch G., Lais P. (1998) Nitrogen loss in a nitrifying rotating contactor treating ammonium-rich wastewater without organic carbon. Water Sci. Technol. **38**(8-9), 241-248.

119. Sin G., Gernaey K.V., Neumann M.B., van Loosdrecht M.C.M., Gujer W. (2011) Global sensitivity analysis in wastewater treatment plant model applications: Prioritizing sources of uncertainty. Water Res. **45**(2), 639-651.

120. Sin G., Gernaey K.V., Neumann M.B., van Loosdrecht M.C.M., Gujer W. (2009) Uncertainty analysis in WWTP model applications: A critical discussion using an example from design. Water Res. **43**(11), 2894-2906.

121. Sin G., Weijma J., Spanjers H., Nopens I. (2008a) Dynamic model development and validation for a nitrifying moving bed biofilter: Effect of temperature and influent load on the performance. Process Biochem. **43**, 384-397.

122. Sin G., De Pauw D.J.W., Weijers S., Vanrolleghem P.A. (2008b) An efficient approach to automate the manual trial and error calibration of activated sludge models. Biotechnol. Bioeng. **100**(3), 516-528.

123. Sin G., Kaelin D., Kampschreur M.J., Takacs I., Wett B., Gernaey K.V., Rieger L., Siegrist H., van Loosdrecht M.C.M. (2008c) Modelling nitrite in wastewater treatment systems: a discussion of different modelling concepts. Water Sci. Technol. **58**(6), 1155-1171.

124. Sin G., Vanrolleghem P.A. (2007) Extensions to modeling aerobic carbon degradation using combined respirometric-titrimetric measurements in view of activated sludge model calibration. Water Res. **41**(15), 3345-3358.

125. Skogestad S. (2003) Simple analytic rules for model reduction and PID controller tuning. J. Process Control **13**(4), 291-309.

126. Sliekers A.O., Derwort N., Gomez J.L.C., Strous M., Kuenen J.G., Jetten M.S.M. (2002) Completely autotrophic nitrogen removal over nitrite in one single reactor. Water Res. **36**(10), 2475-2482.

127. Strous M., Kuenen J.G., Jetten M.S.M. (1999) Key physiology of anaerobic ammonium oxidation. Applied and Environ. Microbiol. **65**, 3248-3250.

128. Strous M., Heijnen J.J., Kuenen J.G., Jetten M.S.M. (1998) The sequencing batch reactor as a powerful tool for the study of slowly growing anaerobic ammonium-oxidizing microorganisms. Appl. Microbiol. Biotechnol. **50,** 589-596.

129. Strous M., van Gerven E., Kuenen J.G., Jetten M.S.M. (1997) Effects of aerobic and microaerobic conditions on anaerobic ammonium-oxidizing (Anammox) sludge. Appl. Environ. Microbiol. **63**(3), 2446-2448.

130. Tay J.H., Tay S.T.L., Liu Y., Show K.Y., Ivanov V. (2006) Biogranulation Technologies for Wastewater Treatment, Waste Management Series 6, Elsevier Science, Oxford.

131. Tchobanoglous G., Burton F.L., Stensel H.D. (2003) Wastewater Engineering, Treatment and Reuse, Metcalf and Eddy. Fourth edition, The McGraw-Hill Companies Inc., New York.

132. Terada A., Lackner S., Tsuneda S., Smets B.F. (2007) Redox-stratification controlled biofilm (ReSCoBi) for completely autotrophic nitrogen removal: The effect of co- versus counter-diffusion on reactor performance. Biotechnol. Bioeng. **97**(1), 40-51.

133. Third K.A., Sliekers A.O., Kuenen J.G., Jetten M.S.M. (2001) The CANON (Completely Autotrophic Nitrogen-removal Over Nitrite) under Ammonium Limitation: Interaction and Competition between Three Groups of Bacteria. Systematic and Applied Microbiology **24**(1), 588-596.

134. Tora J.A., Lafuente J., Baeza J.A., Carrera J. (2010) Combined effect of inorganic carbon limitation and inhibition by free ammonia and free nitrous acid on ammonia oxidizing bacteria. Bioresource Technol. **101**, 6051-6058.

135. Valverde-Perez B., Mauricio-Iglesias M., Sin G. (2012) Control of SHARON reactor for autotrophic nitrogen removal in two-reactor configuration. Conference proceedings from Ecotechnologies for Wastewater Treatment - IWA International conference. Santiago de Compostela.

136. van de Graaf A.A., de Bruijn P., Robertson L.A., Jetten M.S.M., Kuenen J.G. (1996) Autotrophic growth of anaerobic ammonium-oxidizing micro-organisms in a fluidized bed reactor. Microbiol.-UK **142,** 2187-2196.

137. van de Graaf A.A., Mulder A., Debruijn P., Jetten M.S.M., Robertson L.A., Kuenen J.G. (1995) Anaerobic oxidation of ammonium is a biologically mediated process. Appl. Environ. Microbiol. **61**, 1246-1251.

138. van der Star W.R.L., Abma W.R., Blommers D., Mulder J.W., Tokutomi T., Strous M., Picioreanu C., van Loosdrecht M.C.M. (2007) Startup of reactors for anoxic ammonium oxidation: Experiences from the first full-scale anammox reactor in Rotterdam. Water Res. **41**(18), 4149-4163.

139. van Dongen U.G.J.M., Jetten M.S.M., van Loosdrecht M.C.M. (2001) The SHARON-Anammox process for treatment of ammonium rich wastewater. Water Sci. Technol. **44**(1), 153-160.

140. van Hulle S.W.H., Vandeweyer H.J.P., Meesschaert B.D., Vanrolleghem P.A., Dejans P., Dumoulin A. (2010) Engineering aspects and practical application of autotrophic nitrogen removal from nitrogen rich streams. Chem. Eng. J. **162**(1), 1-20.

141. van Hulle S.W.H., Volcke E.I.P., Teruel J.L., Donckels B., van Loosdrecht M.C.M., Vanrolleghem P.A. (2007) Influence of temperature and pH on the kinetics of the Sharon nitritation process. J. Chem. Technol. Biotechnol. **82**(5), 471-480.

142. van Hulle S.W.H. (2005) Modelling, simulation and optimization of autotrophic nitrogen removal processes. PhD Dissertation, Faculty of Bioengineering Sciences, Ghent University, Ghent

143. van Kempen R., Mulder J.W., Uijterlinde C.A., van Loosdrecht M.C.M. (2001) Overview: full scale experience of the SHARON process for treatment of rejection water of digested sludge dewatering. Water Sci. Technol. **44**(1), 145-152.

144. Van't Riet K., Tramper J. (1991) Basic Bioreactor Design. First edition, CRC Press

145. Van't Riet K. (1979) Review of Measuring Methods and Results in Nonviscous Gas-Liquid Mass Transfer in Stirred Vessels. Ind. Eng. Chem. Process Des. Dev. **18**(3), 357-364.

146. Vangsgaard A.K., Mauricio-Iglesias M., Gernaey K.V., Smets B.F., Sin G. (2012) Sensitivity analysis of autotrophic N removal by a granule based bioreactor: Influence of mass transfer versus microbial kinetics. Bioresource Technol. **123**, 230-241.

147. Vanrolleghem P.A., Sin G., Gernaey K.V. (2004) Transient Response of Aerobic and Anoxic Activated Sludge Activities to Sudden Substrate Concentration Changes. Biotechnol. Bioeng. **86**(3), 277-290.

148. Vazquez-Padin J., Fernadez I., Figueroa M., Mosquera-Corral A., Campos J.L., Mendez R. (2009) Applications of Anammox based porcesses to treat anaerobic digester supernatant at room temperature. Bioresource Technol. **100**, 2988-2994.

149. Vlaeminck S.E., De Clippeleir H., Verstraete W. (2012) Microbial ressource management of one-stage partial nitritation/anammox. Microbial Biotechnol. **5**(3), 433-448.

150. Vlaeminck S.E., Terada A., Smets B.F., De Clippeleir H., Schaubroeck T., Bolca S., Demeestere L., Mast J., Boon N., Carballa M., Verstraete W. (2010) Aggregate size and architecture determine microbial activity balance for one-stage partial nitritation and anammox. Appl. Environ. Microbiol. **76**(3), 900-909.

151. Vlaeminck S.E., Cloetens L.F.F., Carballa M., Boon N., Verstraete W. (2009) Granular biomass capable of partial nitritation and anammox. Water Sci. Technol. **59**(3), 609-617.

152. Volcke E.I.P., Picioreanu C., De Baets B., van Loosdrecht M.C.M. (2012) The Granule Size Distribution in an Anammox-Based Granular Sludge Reactor Affects the Conversion – Implications for Modeling. Biotechnol. Bioeng. **109**(7), 1629-1636.

153. Volcke E.I.P., Picioreanu C., De Baets B., van Loosdrecht M.C.M. (2010) Effect of granule size on autotrophic nitrogen removal in a granular sludge reactor. Environ. Technol. **31**(11), 1271-1280.

154. Volcke E.I.P., van Loosdrecht M.C.M., Vanrolleghem P.A. (2007) Interaction between control and design of a SHARON reactor: economic considerations in a plant-wide (BSM2) context. Water Sci. Technol. **56**(9), 117-125.

155. Volcke E.I.P., van Loosdrecht M.C.M., Vanrolleghem P.A. (2006a) Controlling the nitrite:ammonium ratio in a SHARON reactor in view of its coupling with an Anammox process. Water Sci. Technol. **53**(4-5), 45-54.

156. Volcke E.I.P., Gernaey K.V., Vrecko D., Jeppsson U., van Loosdrecht M.C.M., Vanrolleghem P.A. (2006b) Plant-wide (BSM2) evaluation of reject water treatment with a SHARON-Anammox process. Water Sci. Technol. **54**(8), 93-100.

157. Vrecko D., Hvala N., Stare A., Burica O., Strazar M., Levstek M., Cerar P., Podbevsek S. (2006) Improvement of ammonia removal in activated sludge process with feedforward-feedback aeration controllers. Water Sci. Technol. **53**(4-5), 125-132.

158. Wanner O., Eberl H.J., Morgenroth E., Noguera D.R., Picioreanu C., Rittmann B.E., van Loosdrecht M.C.M. (2006) Mathematical Modeling of Biofilms - IWA Scientific and Technical Report no. 18, IWA publishing, London.

159. Wanner O., Gujer W. (1986) A multispecies biofilm model. Biotechnol. Bioeng. **28**(3), 314-328.

160. Wett B., Omari A., Podmirseg S.M., Han M., Akintayo O., Gómez Brandón M., Murthy S., Bott C., Hell M., Takács I., Nyhuis G., O'Shaughnessy M. (2013) Going for mainstream deammonification from bench to full scale for maximized resource efficiency. Water Sci. Technol. **68**(2), 283-289.

161. Wett B. (2007) Development and implementation of a robust deammonification process. Water Sci. Technol. **56**(7), 81-88.

162. Wett B. (2006) Solved upscaling problems for implementing deammonification of rejection water. Water Sci. Technol. **53**(12), 121-128.

163. Wiesmann U. (1994) Biological nitrogen removal from wastewater. Advances in Biochem. Eng. Biotechnol. 51, ed. by A. Fiechter, Springer-Verlag Berlin, New York, 113-154.

164. Wyffels S., van Hulle S. W.H., Boeckx P., Volcke E.I.P., van Cleemput O., Vanrolleghem P.A., Verstraete W. (2004) Modeling and simulation of oxygen-limited nitritation in a membrane-assisted bioreactor (MBR). Biotechnol. Bioeng. **86**(5), 531-542.

165. Xavier J.B., Picioreanu C., van Loosdrecht M.C.M. (2005) A framework for multidimensional modelling of activity and structure of multispecies biofilms. Environ. Microbiol. **7**, 1085-1103.

166. Zhang M., Lawlor P.G., Wu G., Lynch B., Zhan X. (2011) Partial nitrification and nutrient removal in intermittently aerated sequencing batch reactors treating separated digestate liquid after anaerobic digestion of pig manure. Bioprocess Biosyst. Eng. **34**(9), 1049-1056.

167. Zubrowska-Sudol M., Yang J., Trela J., Plaza E. (2011) Evaluation of deammonification process performance at different aeration strategies. Water Sci. Technol. **63**(6), 1168-1176.

168. Åmand L., Olsson G., Carlsson B. (2013) Aeration control – a review. Water Sci. Technol. **67**(11), 2374-2398.

Appendix

Appendix A1

List of publications

Journal articles:

Mutlu A.G., Vangsgaard A.K., Sin G., Smets B.F. (2013). Performance and community dynamics during controlled lab-scale start-up of completely autotrophic nitrogen removing SBRs. *In preparation*

Vangsgaard A.K., Mauricio-Iglesias M., Gernaey K.V., Sin G. (2013). Experimental validation of a novel control strategy for single-stage autotrophic nitrogen removal. *In preparation*

Vangsgaard A.K., Mauricio-Iglesias M., Gernaey K.V., Sin G. (2013). Development of novel control strategies for single-stage autotrophic nitrogen removal: A process oriented approach. Com. Chem. Eng. *Submitted*

Vangsgaard A.K., Mutlu A.G., Gernaey K.V., Smets B.F., Sin G. (2013). Calibration and validation of a model describing complete autotrophic nitrogen removal in a granular SBR system. J. Chem. Technol. Biotechnol. *In press.* DOI: 10.1002/jctb.4060

Mutlu A.G., Vangsgaard A.K., Sin G., Smets B.F. (2013). An operation protocol for facilitating start-up of single-stage autotrophic nitrogen removing reactors based on process stoichiometry. Water Sci. Technol. **68**(3), 514-521.

Vangsgaard, A.K., Mauricio-Iglesias, M., Valverde-Perez, B., Gernaey, K.V. & Sin, G. (2013). pH variation and influence in an autotrophic nitrogen removing biofilm system using an efficient numerical solution strategy. Water Sci. Technol. **67**(11), 2608-2615.

Vangsgaard A.K., Mauricio-Iglesias M., Gernaey K.V., Smets B.F., Sin G. (2012). Sensitivity analysis of autotrophic N removal by a granule based bioreactor: Influence of mass transfer versus microbial kinetics. Bioresource Technol. **123**, 230-241.

Popular science:

Vangsgaard A.K., Gernaey K.V., Sin G., Mutlu A.G., Smets B.F. (2012). Energibesparende biologisk proces til kvælstoffjernelse i spildevand. Dansk Kemi 93(10), 16-18.

Conference contributions:

Mauricio-Iglesias M., Vangsgaard A.K., Gernaey K.V., Sin G. (2013). A fuzzy-logic based diagnosis and control of a reactor performing complete autotrophic nitrogen removal. Computer Application in Biotechnology – IFAC CAB, Mumbai, India. *Accepted for poster presentation*

Vangsgaard A.K., Mauricio-Iglesias M., Mutlu A.G., Gernaey K.V., Smets B.F., Sin G. (2013). Performance of an autotrophic nitrogen removing reactor: Diagnosis through fuzzy logic. 11th IWA conference on instrumentation control and automation, Narbonne, France. *Accepted for poster presentation*

Mutlu A.G., Domingo-Felez C., Vangsgaard A.K., Smets B.F. (2013) Nitrous oxide and nitric oxide emissions from single-stage nitritation/anammox reactors under varying aeration regimes. 86th Annual Water Environment Federation Technical Exhibition and Conference, Chicago, USA. *Accepted for oral presentation*

Vangsgaard A.K., Mauricio-Iglesias M., Gernaey K.V., Smets B.F., Sin G. (2013). Control of a novel energy efficient biological nitrogen removal process. *Poster presentation.* 9th World Congress of Chemical Engineering, Coex, Seoul, Korea.

Vangsgaard A.K., Mauricio-Iglesias M., Gernaey K.V., Smets B.F., Sin G. (2013). Control of a Biological Nitrogen Removal Process in an Intensified Single Reactor Configuration. *Oral presentation.* 23rd European Symposium on Computer Aided Process Engineering, Lappeenranta, Finland.

Mutlu A.G, Vangsgaard A.K., Sin G., Smets B.F. (2013). Driving towards stratified aggregation in single-stage nitritation/anammox reactors by varying aeration regimes. *Poster presentation.* 9th International Conference on Biofilm Reactors, Paris, France.

Vangsgaard A.K., Mutlu A.G., Gernaey K.V., Smets B.F., Sin G. (2012). Calibration and validation of model describing complete autotrophic nitrogen removal in granular sludge. *Oral presentation.* IWA Nutrient Removal and Recovery 2012, Harbin, China.

Vangsgaard A.K., Mauricio-Iglesias M., Valverde-Perez B., Gernaey K.V., Sin G. (2012). pH variation and influence in an autotrophic nitrogen removing biofilm system. *Poster presentation.* IWA Nutrient Removal and Recovery 2012, Harbin, China

Flores-Alsina X., Guerrero J., Vangsgaard A.K., Guisasola A., Baeza J., Jeppsson U., Smets B.F., Sin G., Gernaey K.V. (2012). Recent trends in modelling and simulation of biological nutrient removal systems. *Poster presentation.* IWA Nutrient Removal and Recovery 2012, Harbin, China.

Mutlu A.G., Vangsgaard A.K., Sin G., Smets B.F. (2012). An operation protocol for facilitating start-up of single-stage autotrophic nitrogen removing reactors based on process stoichiometry. *Oral presentation.* IWA World Water Congress & Exhibition, Busan, Korea

Mutlu A.G., Vangsgaard A.K., Jensen M.M., Smets B.F. (2012). Architecture evolution of biomass aggregates in single stage nitritation/anammox reactors. *Poster presentation.* 14th International Symposium on Microbial Ecology, Copenhagen, Denmark

Smets B.F., Mutlu A.G., Pellicer i Nàcher C., Jensen M.M., Vangsgaard A.K., Sin G., Gernaey K.V., Vlaeminck S. (2011). Micro2-Managed Microbial Communities: Next Generation Environmental Bio/Technologies. *Oral presentation.* 1st International Symposium on Microbial resource management in biotechnology: Concepts & Applications, Ghent, Belgium

Vangsgaard A.K., Mauricio-Iglesias M., Gernaey K.V., Smets B.F., Sin G. (2011). Framework for Construction of Multi-scale Models for Biological Wastewater Treatment Processes - Case Study: Autotrophic Nitrogen Conversion. *Poster presentation.* IWA Symposium on Systems Analysis and Integrated Assessment: Watermatex 2011, San Sebastian, Spain

Appendix A2

Individual standardized regression coefficients

The variances of the ten model outputs (the bulk concentration of the five soluble species and the mass fraction of the five particulate species at steady state) obtained from the Monte Carlo simulations have been decomposed, with respect to the 38 parameters considered in the uncertainty analysis, by linear regression for each of the four scenarios (see Table A2.1-A2.4).

Most significant parameters for the bulk concentrations – scenario 1

The most significant parameters for the TAN concentration in the bulk liquid are the AOB oxygen half saturation constant ($K_{O2,AOB}$), maximum growth rate ($\mu_{max,AOB}$), decay rate (b_{AOB}), and growth yield (Y_{AOB}). Also the thickness of the MTBL (L_B) has an impact as the third most important parameter. In Table A2.1, it can be seen that also the nitrogen content of the biomass (i_{NXB}) is a significant parameter and has a negative impact on the TAN bulk concentration, which is because TAN is the assumed nitrogen form that the bacteria use for cell synthesis. For the same reason i_{NXB} does not have an impact on any of the other selected model outputs.

$K_{O2,AOB}$ is also found to be an important parameter for the bulk TNN concentration. However, for TNN the oxygen inhibition constant of AnAOB ($K_{O2,AnAOB}$) is most important. Thus, it is a mixture of AnAOB and AOB related parameters that affect the bulk TNN concentration. It is noteworthy that the diffusivity of TNN has a significant impact on the TNN concentration, as the fourth most important parameter. An increased diffusivity makes TNN more available inside the granule, and thus more is consumed, which leads to a decrease in the bulk concentration.

For the bulk nitrate concentration, the yield of the AnAOB is the most significant parameter, which is because the AnAOB is the only bacterial group producing nitrate since NOB have been outcompeted from the biofilm in all cases. It is also interesting that the HB organic substrate half saturation constant ($K_{S,HB}$) and the anoxic deactivation constant (η_{HB}) are the fourth and fifth most important parameters for the nitrate concentration. This indicates that even if the heterotrophs are present only in very low concentrations, their denitrifying activity is of importance for the effluent nitrate concentration and thus for the overall N removal.

For the bulk N_2 concentration, the same parameters as for TAN are the most important except that AnAOB instead of AOB growth yield is among the most significant parameters. Thus, the results indicate that the oxygen half saturation constant has a significant impact on the

performance. This finding is in contrast with the study by Hao et al. (2002a) who found that the effluent concentrations were insensitive to the half saturation constants.

For the bulk DO concentration, $K_{O2,AOB}$ and $\mu_{max,AOB}$ are the most important parameters. It is also noteworthy that the ammonium affinity constant ($K_{NH3,AOB}$) has an impact. This indicates that anything influencing the growth rate of AOB will also affect the DO concentration, because they are the primary consumers of DO in the biofilm.

Most significant parameters for the microbial composition – scenario 1

For AOB, three out of the five most significant parameters are related to the bacterial group's own kinetic parameters. The reason for the negative effect of the $\mu_{max,AOB}$ on the mass fraction of AOB is due to an increase in the overall growth rate, which entails a higher detachment rate, and the positive effect is thus annulled by the negative side effect. However, the AOB still present in the biofilm have more substrate available and thus a higher activity, which can be seen on the negative impact of $\mu_{max,AOB}$ on the bulk TAN concentration (Table A2.1). The diffusivity of oxygen and the thickness of the MTBL are also found to be significant for the AOB mass fraction. A higher D_{O2} or smaller L_B means that the oxygen will be transported faster or easier, and thus be more available as substrate for the AOB.

For AnAOB, only kinetic parameters are among the five most important parameters. Its oxygen inhibition constant ($K_{O2,AnAOB}$) is most significant, followed by the AOB oxygen half saturation constant and the maximum growth rates of AnAOB and AOB.

For HB, their own kinetic parameters, $K_{S,HB}$ and $\mu_{max,HB}$, are important. Out of the five most significant parameters, the other three relate to AOB kinetics, probably due to the HB growing on decay products originating from AOB. Even if AOB are present in low concentrations, their decay rate is fifty times higher than the decay rate of AnAOB, and thus more organic substrate will be originating from them. Therefore the decay rate of AOB is of great significance as the third most important parameter.

Generally AOB kinetic parameters ($K_{O2,AOB}$, $\mu_{max,AOB}$ and b_{AOB}) are of highest importance for all selected model outputs since the absolute values of the SCRs are above 0.1 in all cases (Table A2.1). The $K_{O2,AnAOB}$ and $\mu_{max,AnAOB}$ are important for the TNN and nitrate bulk concentrations and for the mass fraction of the AnAOB, HB and inerts in the biofilm. Mass transfer affects mainly DO and TNN concentrations among the soluble species, and only the AOB and slightly the AnAOB among the particulates.

Table A2.1 Result of sensitivity analysis of scenario 1. Standardized regression coefficients ($\beta_{k,i}$) of the linearized model for ten selected model outputs. Values abs($\beta_{k,i}$)>0.1 are highlighted in bold.

Output →	**TAN**	**TNN**	**Nitrate**	**N_2 gas**	**DO**	**AOB**	**AnAOB**	**NOB**	**HB**	**Inerts**
R^2	0.98	0.85	0.98	0.98	0.98	0.99	0.93	0.05	0.95	0.94
Parameter ↓										
$\mu_{max,AOB}$	**-0.58**	**-0.23**	**0.29**	**0.54**	**-0.58**	**-0.55**	**-0.32**	-0.08	**-0.29**	**0.34**
$K_{O2,AOB}$	**0.74**	**0.43**	**-0.38**	**-0.70**	**0.72**	**0.62**	**0.56**	-0.03	**0.42**	**-0.58**
$K_{NH3,AOB}$	**0.16**	0.07	-0.07	**-0.15**	**0.17**	**0.15**	0.08	-0.05	0.06	-0.09
$K_{HNO2,AOB}$	0.00	-0.02	0.01	0.00	0.00	-0.01	-0.02	-0.05	0.01	0.02
b_{AOB}	**0.23**	**0.23**	**-0.24**	**-0.17**	**0.13**	**-0.27**	**0.28**	-0.03	**0.37**	**-0.26**
$\mu_{max,NOB}$	0.00	0.00	0.00	0.00	0.00	0.00	0.00	0.00	0.00	0.00
$K_{O2,NOB}$	0.00	-0.04	0.00	0.00	0.01	0.00	-0.02	0.02	-0.01	0.02
$K_{HNO2,NOB}$	0.01	0.02	-0.01	-0.01	0.00	0.02	0.02	0.02	0.01	-0.02
b_{NOB}	-0.01	-0.02	0.01	0.01	0.00	0.00	-0.01	-0.10	0.00	0.01
$\mu_{max,AnAOB}$	-0.06	**-0.38**	**0.13**	0.05	0.02	-0.03	**-0.43**	-0.02	**-0.15**	**0.43**
$K_{O2,AnAOB}$	**-0.11**	**-0.62**	**0.21**	0.08	0.02	-0.07	**-0.69**	0.02	**-0.23**	**0.68**
$K_{NH3,AnAOB}$	0.00	0.01	0.00	0.00	-0.01	0.00	0.01	-0.03	-0.01	-0.01
$K_{HNO2,AnAOB}$	0.04	**0.21**	-0.08	-0.03	0.00	0.02	**0.27**	-0.01	0.08	**-0.26**
b_{AnAOB}	0.05	-0.05	**-0.15**	0.01	-0.01	0.05	**-0.22**	0.02	**0.24**	**0.21**
$\mu_{max,HB}$	0.06	0.02	**-0.18**	-0.02	0.00	-0.05	0.01	0.01	**0.31**	-0.01
$K_{O2,HB}$	-0.05	0.01	-0.11	0.08	0.01	0.00	0.01	-0.04	0.02	-0.01
$K_{S,HB}$	-0.10	0.01	**0.29**	0.04	-0.02	0.08	0.02	0.05	**-0.47**	-0.02
$K_{TNN,HB}$	-0.04	0.00	0.02	0.03	0.00	0.01	0.00	-0.02	-0.06	0.00
$K_{NO3,HB}$	0.01	0.00	0.03	-0.01	0.00	0.01	0.01	0.02	-0.02	-0.01
$K_{TAN,HB}$	0.01	0.00	0.00	-0.01	0.01	0.01	0.00	0.01	0.00	0.00
η_{HB}	0.02	0.00	**-0.29**	0.06	0.00	0.00	0.00	0.02	**0.22**	0.00
b_{HB}	0.01	0.02	0.02	-0.01	0.01	0.02	0.03	-0.03	**-0.10**	-0.02
Y_{AOB}	**-0.16**	0.01	-0.01	**0.16**	0.04	**0.15**	0.01	0.00	0.06	-0.02
Y_{NOB}	-0.01	0.01	0.00	0.01	-0.01	0.00	0.01	0.02	-0.01	-0.01
Y_{AnAOB}	**0.15**	0.07	**0.63**	**-0.37**	-0.01	-0.07	**0.10**	0.00	0.00	-0.09
Y_{HB}	-0.01	-0.01	0.03	0.00	0.01	-0.02	0.00	-0.05	**0.21**	-0.01
f_i	-0.03	0.00	0.08	0.00	0.01	-0.03	-0.06	-0.04	**-0.15**	0.06
i_{NXI}	-0.01	-0.01	0.00	0.00	0.00	0.00	-0.01	0.00	-0.01	0.01
i_{NXB}	**-0.15**	0.06	-0.02	-0.02	0.02	0.02	0.04	0.03	0.01	-0.04
k_H	0.00	-0.01	0.00	0.00	0.00	0.00	0.00	-0.02	0.01	0.00
K_X	-0.01	-0.02	0.00	0.01	0.00	-0.01	-0.02	0.06	0.02	0.02
D_{TAN}	-0.01	-0.01	0.00	0.01	0.00	-0.01	-0.02	-0.02	0.00	0.02
D_{TNN}	-0.01	**-0.35**	-0.01	0.04	0.00	0.02	**0.15**	-0.03	-0.01	**-0.15**
D_{O2}	-0.09	0.00	-0.06	**0.12**	**-0.16**	**0.31**	0.01	-0.02	**0.14**	-0.03
D_{NO3}	0.01	0.01	-0.01	-0.01	0.02	0.00	0.01	0.04	0.00	-0.01
D_{N2}	-0.02	-0.04	0.01	0.02	-0.01	0.00	-0.02	0.09	-0.01	0.02
D_S	0.00	0.00	0.01	0.00	0.00	0.01	-0.01	-0.08	-0.01	0.01
L_B	**0.26**	**0.16**	0.01	**-0.31**	**0.38**	**-0.28**	-0.01	-0.03	-0.03	0.03

Table A2.2 Result of sensitivity analysis of scenario 2. Standardized regression coefficients ($\beta_{k,i}$) of the linearized model for ten selected model outputs. Values abs($\beta_{k,i}$)>0.1 are highlighted in bold.

Output →	**TAN**	**TNN**	**Nitrate**	**N_2 gas**	**DO**	**AOB**	**AnAOB**	**NOB**	**HB**	**Inerts**
R^2	0.86	0.49	0.46	0.78	0.96	0.87	0.89	0.95	0.89	0.83
Parameter ↓										
$\mu_{max,AOB}$	**-0.45**	0.03	0.04	-0.06	**-0.16**	**-0.21**	0.05	-0.09	-0.04	**0.11**
$K_{O2,AOB}$	**0.50**	-0.02	**0.10**	**-0.11**	-0.09	**-0.15**	**-0.11**	**-0.10**	**0.12**	0.05
$K_{NH3,AOB}$	**0.59**	-0.01	-0.06	0.03	**0.16**	**0.21**	-0.09	0.08	0.07	**-0.13**
$K_{HNO2,AOB}$	-0.02	0.01	-0.02	-0.01	0.00	0.02	0.00	0.01	0.00	-0.02
b_{AOB}	**0.27**	0.00	0.03	-0.04	-0.08	**-0.59**	-0.06	**0.35**	**0.10**	0.06
$\mu_{max,NOB}$	0.06	**-0.27**	**0.30**	**0.14**	-0.05	**-0.10**	**0.12**	0.00	**-0.11**	0.05
$K_{O2,NOB}$	-0.04	**0.38**	**-0.40**	**-0.23**	0.03	**0.14**	**-0.21**	-0.04	**0.21**	**-0.19**
$K_{HNO2,NOB}$	0.00	**0.14**	**-0.14**	-0.08	0.01	0.01	**-0.13**	-0.05	**0.13**	0.01
b_{NOB}	0.00	**0.16**	**-0.16**	**-0.10**	-0.01	0.09	-0.07	0.05	**0.10**	**-0.69**
$\mu_{max,AnAOB}$	**-0.20**	**-0.17**	0.00	**0.32**	**0.29**	**0.15**	**0.20**	**0.17**	**-0.22**	**0.12**
$K_{O2,AnAOB}$	**-0.41**	**-0.41**	0.07	**0.66**	**0.54**	**0.24**	**0.38**	**0.29**	**-0.41**	**0.28**
$K_{NH3,AnAOB}$	0.03	0.05	-0.02	-0.07	-0.05	-0.02	-0.07	-0.04	0.08	-0.04
$K_{HNO2,AnAOB}$	0.01	0.02	-0.01	-0.02	-0.01	0.00	-0.01	-0.01	0.01	0.00
b_{AnAOB}	0.00	0.05	-0.04	-0.04	-0.06	**0.11**	**-0.67**	**0.21**	**0.65**	-0.04
$\mu_{max,HB}$	0.01	0.04	-0.05	-0.02	-0.01	-0.01	-0.07	**0.17**	0.07	-0.06
$K_{O2,HB}$	-0.01	-0.04	0.02	0.04	0.02	0.02	0.02	0.08	-0.03	0.08
$K_{S,HB}$	-0.04	0.02	-0.02	-0.01	0.03	0.09	**0.11**	**-0.26**	**-0.11**	0.02
$K_{TNN,HB}$	-0.01	-0.02	0.02	0.02	0.00	0.01	0.04	0.03	-0.04	0.02
$K_{NO3,HB}$	0.03	0.00	0.00	-0.01	-0.01	0.00	-0.02	-0.02	0.02	0.01
$K_{TAN,HB}$	-0.01	-0.04	0.02	0.05	0.03	0.01	**0.12**	0.05	-0.12	0.06
η_{HB}	0.05	0.01	0.01	-0.03	-0.04	-0.06	**-0.17**	-0.04	**0.17**	-0.01
b_{HB}	0.02	0.03	-0.02	-0.03	-0.01	0.02	-0.01	**-0.23**	0.01	-0.01
Y_{AOB}	-0.01	0.01	0.00	-0.03	0.04	**0.19**	-0.02	**0.14**	0.01	-0.03
Y_{NOB}	0.01	-0.06	0.06	0.04	0.01	-0.04	0.02	0.02	-0.03	**0.19**
Y_{AnAOB}	0.07	0.05	0.00	-0.09	-0.05	**-0.10**	0.09	-0.05	-0.08	-0.06
Y_{HB}	0.04	-0.04	0.07	-0.01	-0.03	**-0.11**	-0.07	**0.46**	0.07	0.01
f_i	0.08	0.02	0.05	**-0.10**	-0.06	**-0.22**	**-0.23**	**-0.39**	**0.25**	-0.03
i_{NXI}	0.03	0.00	0.01	-0.01	-0.01	-0.01	0.01	-0.01	0.00	0.01
i_{NXB}	0.01	-0.02	0.03	-0.04	0.00	0.00	-0.02	0.00	0.02	0.02
k_H	-0.02	0.03	-0.03	-0.02	-0.01	0.01	-0.01	-0.01	0.01	0.00
K_X	-0.03	-0.01	0.00	0.02	0.01	0.02	0.02	0.02	-0.02	-0.01
D_{TAN}	-0.03	0.00	-0.04	0.04	0.05	0.09	-0.03	0.05	0.02	-0.07
D_{TNN}	0.00	-0.03	0.04	0.01	-0.01	-0.04	-0.02	-0.02	0.02	0.06
D_{O2}	0.01	0.00	**0.22**	**-0.23**	**-0.44**	**0.26**	**-0.13**	**0.22**	0.08	**0.31**
D_{NO3}	-0.01	0.07	-0.07	-0.05	0.00	0.02	-0.04	-0.01	0.04	-0.04
D_{N2}	-0.04	-0.01	0.00	0.01	0.00	0.01	0.01	0.00	-0.01	0.01
D_S	-0.02	0.01	-0.02	0.00	0.01	0.02	0.03	0.02	-0.03	0.00
L_B	0.09	0.00	**-0.27**	**0.27**	**0.54**	**-0.25**	**0.13**	**-0.19**	-0.09	**-0.21**

Table A2.3 Result of sensitivity analysis of scenario 3. Standardized regression coefficients ($\beta_{k,i}$) of the linearized model for ten selected model outputs. Values abs($\beta_{k,i}$)>0.1 are highlighted in bold.

Output →	**TAN**	**TNN**	**Nitrate**	**N_2 gas**	**DO**	**AOB**	**AnAOB**	**NOB**	**HB**	**Inerts**
R^2	0.98	0.82	0.98	0.98	0.98	0.98	0.95	0.11	0.95	0.95
Parameter ↓										
$\mu_{max,AOB}$	**-0.53**	**-0.21**	**0.27**	**0.48**	**-0.52**	**-0.50**	**-0.30**	-0.03	**-0.30**	**0.32**
$K_{O2,AOB}$	**0.73**	**0.39**	**-0.35**	**-0.67**	**0.70**	**0.61**	**0.53**	-0.01	**0.46**	**-0.56**
$K_{NH3,AOB}$	**0.15**	0.06	-0.06	**-0.14**	**0.16**	**0.14**	0.08	0.01	0.06	-0.08
$K_{HNO2,AOB}$	0.01	-0.01	0.00	-0.01	0.00	-0.01	-0.01	**0.12**	0.02	0.01
b_{AOB}	**0.23**	**0.22**	**-0.24**	**-0.16**	**0.13**	**-0.33**	**0.26**	-0.05	**0.36**	**-0.24**
$\mu_{max,NOB}$	0.00	0.00	0.00	0.00	0.01	0.00	0.00	-0.07	0.00	0.00
$K_{O2,NOB}$	0.00	-0.04	0.00	0.00	0.01	0.00	-0.01	**0.10**	-0.01	0.01
$K_{HNO2,NOB}$	0.01	0.02	0.00	-0.01	0.00	0.01	0.01	0.00	0.01	-0.01
b_{NOB}	-0.01	-0.02	0.01	0.01	0.00	-0.01	-0.01	0.01	0.01	0.01
$\mu_{max,AnAOB}$	-0.06	**-0.38**	**0.12**	0.03	0.02	-0.02	**-0.41**	**0.10**	**-0.14**	**0.40**
$K_{O2,AnAOB}$	**-0.10**	**-0.59**	**0.18**	0.06	0.01	-0.06	**-0.65**	0.04	**-0.20**	**0.63**
$K_{NH3,AnAOB}$	0.00	0.01	0.00	0.00	-0.01	-0.01	0.01	0.04	-0.01	-0.01
$K_{HNO2,AnAOB}$	0.04	**0.25**	-0.08	-0.02	0.00	0.02	**0.29**	**-0.13**	0.08	**-0.29**
b_{AnAOB}	0.06	-0.04	**-0.16**	0.01	-0.01	0.06	**-0.24**	0.02	**0.23**	**0.23**
$\mu_{max,HB}$	0.06	0.02	**-0.19**	-0.01	0.00	-0.05	0.00	0.04	**0.29**	0.00
$K_{O2,HB}$	-0.07	-0.01	**-0.13**	**0.12**	0.01	0.00	0.00	0.03	0.00	0.00
$K_{S,HB}$	-0.10	0.02	**0.30**	0.03	-0.02	0.08	0.03	-0.07	**-0.44**	-0.02
$K_{TNN,HB}$	-0.04	0.01	0.01	0.04	0.00	0.01	0.01	0.00	-0.05	-0.01
$K_{NO3,HB}$	0.00	-0.01	0.03	-0.01	0.00	0.01	0.00	0.00	-0.03	0.00
$K_{TAN,HB}$	0.00	0.00	0.00	0.00	0.00	0.01	0.00	0.01	0.00	0.00
η_{HB}	0.01	0.00	**-0.33**	**0.10**	0.00	0.00	-0.01	0.10	**0.21**	0.00
b_{HB}	0.00	0.00	0.02	-0.01	0.01	0.02	0.02	-0.07	**-0.10**	-0.02
Y_{AOB}	**-0.18**	0.02	-0.02	**0.18**	0.03	**0.16**	0.02	0.08	0.06	-0.03
Y_{NOB}	-0.01	0.01	0.00	0.01	-0.01	0.01	0.01	-0.06	-0.01	-0.01
Y_{AnAOB}	**0.16**	0.07	**0.60**	**-0.40**	-0.01	-0.07	**0.10**	0.03	0.00	-0.10
Y_{HB}	-0.01	-0.01	0.04	-0.01	0.02	-0.02	0.01	0.01	**0.21**	-0.01
f_i	-0.03	0.02	0.09	0.00	0.01	-0.04	-0.06	-0.03	**-0.16**	0.07
i_{NXI}	-0.01	0.00	-0.01	0.00	0.00	0.00	0.00	-0.01	0.00	0.00
i_{NXB}	**-0.15**	0.05	-0.01	-0.02	0.02	0.02	0.03	-0.04	0.01	-0.03
k_H	0.00	-0.02	-0.01	0.00	0.00	-0.01	0.00	-0.03	0.01	0.00
K_X	-0.01	-0.02	0.00	0.01	0.00	-0.01	-0.02	0.07	0.02	0.02
D_{TAN}	0.00	0.00	0.00	0.00	0.00	-0.01	-0.01	0.02	0.00	0.01
D_{TNN}	-0.01	**-0.31**	-0.02	0.04	0.00	0.02	**0.15**	-0.05	0.00	**-0.15**
D_{O2}	**-0.10**	-0.01	-0.08	**0.16**	**-0.20**	**0.30**	0.01	0.05	**0.15**	-0.03
D_{NO3}	0.01	0.01	-0.01	-0.01	0.01	0.00	0.01	-0.07	0.00	-0.01
D_{N2}	-0.02	-0.05	0.01	0.02	-0.01	0.00	-0.01	-0.03	-0.02	0.01
D_S	0.00	0.00	0.01	0.00	0.00	0.01	-0.01	-0.02	-0.01	0.01
L_B	**0.28**	**0.14**	0.03	**-0.35**	**0.45**	**-0.29**	-0.03	-0.07	-0.04	0.04

Table A2.4 Result of sensitivity analysis of scenario 4. Standardized regression coefficients ($\beta_{k,i}$) of the linearized model for ten selected model outputs. Values abs($\beta_{k,i}$)>0.1 are highlighted in bold.

Output →	**TAN**	**TNN**	**Nitrate**	**N_2 gas**	**DO**	**AOB**	**AnAOB**	**NOB**	**HB**	**Inerts**
R^2	0.66	0.58	0.69	0.61	0.93	0.95	0.61	0.09	0.84	0.64
Parameter ↓										
$\mu_{max,AOB}$	**-0.30**	**-0.20**	**0.25**	**0.25**	**-0.58**	**-0.52**	**-0.13**	-0.07	**-0.25**	**0.17**
$K_{O2,AOB}$	**0.51**	**0.42**	**-0.47**	**-0.46**	**0.60**	**0.57**	**0.31**	0.05	**0.31**	**-0.35**
$K_{NH3,AOB}$	0.08	0.06	-0.07	**-0.07**	**0.13**	**0.13**	0.05	-0.01	0.06	-0.06
$K_{HNO2,AOB}$	0.04	0.05	-0.04	-0.04	-0.01	0.02	-0.06	-0.07	-0.02	0.05
b_{AOB}	**0.15**	**0.13**	**-0.17**	**-0.14**	0.07	**-0.20**	**0.18**	0.08	**0.40**	**-0.17**
$\mu_{max,NOB}$	0.00	0.00	0.00	0.00	-0.01	0.00	0.01	0.08	-0.02	-0.01
$K_{O2,NOB}$	0.01	0.01	-0.01	-0.01	0.00	0.01	-0.04	-0.06	-0.03	0.04
$K_{HNO2,NOB}$	-0.05	-0.06	0.05	0.05	0.04	0.00	0.07	0.04	0.06	-0.07
b_{NOB}	0.00	0.00	0.00	0.00	0.01	0.01	0.00	0.08	0.01	0.00
$\mu_{max,AnAOB}$	**-0.24**	**-0.27**	**0.27**	**0.26**	**0.13**	-0.05	**-0.33**	-0.03	**-0.10**	**0.33**
$K_{O2,AnAOB}$	**-0.44**	**-0.50**	**0.49**	**0.47**	**0.22**	-0.08	**-0.47**	-0.04	**-0.14**	**0.47**
$K_{NH3,AnAOB}$	-0.01	-0.02	0.01	0.01	0.02	0.00	0.02	0.08	0.05	-0.02
$K_{HNO2,AnAOB}$	-0.02	-0.02	0.01	0.02	0.00	-0.01	**0.20**	-0.05	0.06	**-0.19**
b_{AnAOB}	0.04	0.03	-0.07	-0.03	-0.01	0.04	**-0.18**	0.02	**0.33**	**0.17**
$\mu_{max,HB}$	-0.01	-0.02	0.00	0.01	0.01	-0.01	0.01	-0.06	**0.11**	-0.01
$K_{O2,HB}$	-0.04	-0.04	0.00	0.04	0.03	0.00	0.04	0.05	0.00	-0.04
$K_{S,HB}$	-0.01	0.00	0.02	0.00	0.00	0.02	0.02	0.01	**-0.19**	-0.02
$K_{TNN,HB}$	0.02	0.02	-0.01	-0.02	0.01	0.02	-0.02	0.03	**-0.13**	0.02
$K_{NO3,HB}$	0.04	0.04	-0.03	-0.04	0.00	0.01	-0.04	-0.02	-0.03	0.04
$K_{TAN,HB}$	0.04	0.05	-0.04	-0.04	0.00	0.02	-0.03	0.05	-0.02	0.03
η_{HB}	-0.02	-0.02	-0.03	0.03	0.00	-0.02	0.00	-0.08	**0.37**	-0.01
b_{HB}	-0.02	-0.02	0.02	0.02	0.01	0.00	0.02	0.02	-0.08	-0.02
Y_{AOB}	-0.03	0.00	-0.01	0.02	0.07	**0.16**	0.04	-0.01	**0.11**	-0.05
Y_{NOB}	0.01	0.01	0.00	-0.01	-0.02	-0.01	-0.02	-0.04	0.01	0.02
Y_{AnAOB}	0.07	0.05	**0.19**	-0.08	-0.05	-0.08	0.08	-0.04	-0.05	-0.07
Y_{HB}	0.00	0.00	0.01	0.00	0.01	0.00	0.01	0.07	**0.30**	-0.02
f_i	0.03	0.04	-0.01	-0.03	0.00	0.00	-0.08	0.02	**-0.17**	0.08
i_{NXI}	0.01	0.01	-0.01	-0.01	0.00	0.00	-0.02	0.08	-0.02	0.02
i_{NXB}	-0.04	-0.01	0.01	0.01	0.06	0.04	0.04	0.04	0.03	-0.04
k_H	0.01	0.01	-0.01	-0.01	0.01	0.01	0.01	0.05	0.03	-0.01
K_X	0.01	0.01	-0.01	-0.01	0.01	0.01	0.00	0.02	-0.01	0.00
D_{TAN}	-0.03	-0.04	0.03	0.03	0.01	0.00	0.03	-0.04	-0.02	-0.03
D_{TNN}	0.00	0.00	-0.01	0.00	0.00	0.01	0.08	-0.01	-0.04	-0.08
D_{O2}	-0.02	0.00	-0.01	0.02	**-0.16**	**0.33**	0.00	-0.06	**0.13**	-0.03
D_{NO3}	-0.05	-0.05	0.04	0.05	0.00	0.00	0.06	-0.02	0.03	-0.06
D_{N2}	-0.01	-0.01	0.01	0.01	0.00	-0.01	-0.02	-0.04	-0.02	0.02
D_S	0.01	0.01	-0.01	-0.01	-0.01	-0.01	-0.02	0.01	0.00	0.02
L_B	0.02	-0.03	0.03	0.00	**0.34**	**-0.38**	-0.03	-0.03	-0.06	0.06

This PhD-project was carried out at CAPEC, the Computer Aided Product-Process Engineering Center.
CAPEC is committed to research, to work in close collaboration with industry and to participate in educational activities. The research objectives of CAPEC are to develop computer-aided systems for product/process simulation, design, analysis and control/operation for chemical, petrochemical, pharmaceutical and biochemical industries. The dissemination of the research results of CAPEC is carried out in terms of computational tools, technology and application. Under computational tools, CAPEC is involved with mathematical models, numerical solvers, process/operation mathematical models, numerical solvers, process simulators, process/product synthesis/design toolbox, control toolbox, databases and many more. Under technology, CAPEC is involved with development of methodologies for synthesis/design of processes and products, analysis, control and operation of processes, strategies for modelling and simulation, solvent and chemical selection and design, pollution prevention and many more. Under application, CAPEC is actively involved with developing industrial case studies, tutorial case studies for education and training, technology transfer studies together with industrial companies, consulting and many more.

Further information about CAPEC can be found at www.capec.kt.dtu.dk.

Computer Aided Process Engineering Center
Department of Chemical and Biochemical Engineering
Technical University of Denmark
Søltofts Plads, Building 229
DK-2800 Kgs. Lyngby
Denmark

Phone: +45 4525 2800
Fax: +45 4525 4588
Web: www.capec.kt.dtu.dk

ISBN : 978-87-93054-12-7